COAL FLY ASH AND ACID MINE DRAINAGE BASED, HETEROGENEOUS Fe CATALYSTS FOR THE FRIEDEL-CRAFTS ALKYLATION REACTION

By:

TAPIWA HLATYWAYO

MSc. CHEMICAL SCIENCE

UNIVERSITY OF THE WESTERN CAPE

A thesis submitted in fulfilment of the requirements for the degree of Doctor of Philosophy in Chemistry

Department of Chemistry
University of the Western Cape

Supervisor: Prof. L.F. Petrik

Co-supervisor: Dr. B. Louis

February 2020

CFA &AMD based, heterogeneous Fe catalysts for the FC alkylation reaction

KEYWORDS

Acid leaching

Acid mine drainage

Benzene

Catalysis

Characterisation

Coal fly ash

Friedel-Crafts alkylation

HBEA

Hydrothermal

Ion exchange

MCM-41

Physico-chemical properties

Silica extraction

t-butylbenzene

 t-butylchloride

Wet impregnation

DECLARATION

I declare that "*COAL FLY ASH AND ACID MINE DRAINAGE BASED, HETEROGENEOUS Fe CATALYSTS FOR THE FRIEDEL-CRAFTS ALKYLATION REACTION"* is my own work, that it has not been submitted for any degree or examination in any other university, and that all the sources I have used or quoted have been indicated and acknowledged by complete references.

1. **TAPIWA HLATYWAYO February 2020**

Signed…………………………………

ABSTRACT

The catalytic support materials used in the present study are zeolite HBEA and MCM-41. These high silica zeolites were synthesised from coal fly ash (CFA) waste via a novel approach that involved a fusion step, acid assisted silica extraction and removal of Al, Ca and Na from the silica by treatment with oxalic acid. The generated silica was converted to HBEA and MCM-41 via conventional hydrothermal treatment. The metal incorporation onto HBEA was done via two approaches namely; liquid phase ion exchange (LIE) and wet impregnation (WI) while the loading on MCM-41 was only done via WI since the material does not possess exchange sites. The metal solution precursors were AMD and Fe extracted from CFA (FeAsh) via acid leaching followed by pH regulation by concentrated NaOH. This is the first time these solutions were tested as possible metal precursors in catalyst synthesis.

The prepared catalysts were subjected to a range of characterisation techniques namely; XRD, SEM, HRTEM, SAED, ICP-OES and N_2 adsorption analysis. From the XRD, SEM and HRTEM analyses it was found that the crystallinity and morphology of the parent materials were retained upon metal loading from AMD or FeAsh using ion exchange or wet impregnation. The ICP-OES data also revealed that the theoretical metal loading and the actual metal loading achieved were comparable, leading to the conclusion that the two metal loading approaches applied in the study can be tailored to achieve desired metal wt % loadings.

When wet impregnation is applied with AMD as metal precursor it leads to polymetallic catalyst systems. The major ion in the AMD used was Fe, however there were other metals in significant quantities and these include; Ca, Na. Mg, Mn and Ni. The presence

of these metals had significant effects on the overall catalytic activity of the resultant materials. The activity of the prepared catalysts was tested on the Friedel-Crafts alkylation of benzene with t-butyl chloride. The reaction was carried out in a batch reactor under reflux conditions at a temperature of 45 $^\circ$C and a total 38 catalysts were tested.

Generally, the conversion over the HBEA catalysts was higher relative to the conversions achieved over the MCM-41 supported catalysts. This was due to the presence of both Brønsted and Lewis acidity in HBEA whereas only Lewis acidity was responsible for the activity observed over the MCM-41 supported catalyst series. The pristine MCM-41 was found to be inactive. Of the HBEA supported catalysts higher conversions were obtained over the wet impregnated samples than on the ion exchanged samples. The ion exchanged samples were composed of only Fe as the active metal while the wet impregnated samples contained Ni which was found to enhance the conversion. The AMD based catalysts were more active relative to the FeAsh based catalysts.

In all the reactions studied, the primary product was the desired monoalkylated product. The 1,4 di-tertiary butyl benzene and the 1,3 di-tertiary butyl benzene were also detected in the product mixture. The 1,2 di-tertiary butyl benzene and the tri alkylated product were not detected in the product mixture. The research proved that fly ash can be used as a feedstock in the preparation of green catalysts for use in the Friedel Crafts alkylation reaction as both source of zeolite synthesis and source of metal. Again AMD can be used as a metal precursor in catalyst synthesis. The catalysts prepared using AMD as metal precursor showed activity that was higher than that of catalysts prepared using commercial salts. The catalysts prepared using FeAsh also had good activity that was comparable to that obtained over commercial catalysts.

<ins>DEDICATION</ins>

https://thelifebridgechurch.com/dry-bones/

Dry bones

Will these dry bones rise again
Will these ashes turn to beauty
Will this grass transform to grace
Will waste convert to wealth
Will these rags turn into a coat of many colours
Will garbage at least give cabbage
Will nonSense ever make Sense

Diaries of a world of limited resources
Murmurs of a world at the brink of collapse
Cries of a world constantly being polluted
Yawnings of a world in need of new approaches
Pangs of a world hungry for change
Lamentations of a world that needs healing
Supplications of a world that pants for redemption

(Tapiwa Hlatywayo)

This research project is centred on the conversion of waste materials to valuable green by-products. It is therefore dedicated to those who practically endeavour to preserve the world, keeping the consciousness that we owe it to the next generation. In this era of limitedness, waste utilisation is the new renaissance.

ACKNOWLEDGEMENTS

Innumerable clement souls have taken out precious time from their respective busy schedules dedicating it to seeing that this research project is transformed into a tangible reality. Most worthy of acknowledging are my supervisor and co-supervisor Prof. Leslie F. Petrik and Dr. Benoit Louise respectively. These have been my light in the dark and my tower in which I took refuge in seasons of academic storms. They have walked on the burning charcoals of academic pursuit way before me, and later showed me how to do the same. I sincerely appreciate.

It would be remiss of me not to mention the Environmental and Nanosciences (ENS) group members whom to me at first were mere academic associates but became family, what I will be without you…I tend to wonder. Words have a tendency of failing to effectively reflect profound emotions, and on considering the unwavering all-weather support I received from Vanessa Kellerman and Theresa Onwordi, I decide not to put it in words, but leave it to the powers beyond me.

It would be a wild goose chase if not an impeccable futile attempt to carry out a study of this nature without making reference to the works of others. It is in this vain that I find it worthwhile to acknowledge all the authors and publishers of the studies cited in this thesis. I further need to extend my sincere gratitude to the technical assistance I received from Ilse Wells (UWC) ICP-OES, N_2-adsorption, Timothy Lesch (UWC) GC, Adrian Josephs (UWC) SEM, Subelia Botha (UWC) HRTEM, Remy Bucher (iThemba LABS) XRD. I also desire to convey my sincere gratitude to Eskom Holdings for providing funding to meet the research costs.

Lastly but mostly, the Most high in whom I trust….I sleep, He does not. He has been forever watchful throughout this entire academic pilgrimage and leading me by the hand. Praise be unto Thee.

Table of Contents

https://etd.uwc.ac.za

https://etd.uwc.ac.za

https://etd.uwc.ac.za

LIST OF FIGURES

LIST OF TABLES

https://etd.uwc.ac.za

LIST OF ABBREVIATIONS

AMD   Acid Mine Drainage

BET   Brunauer – Emmett -Teller

CFA   Coal Fly Ash

DWS   Department of Water and Sanitation

EDS   Energy Dispersive Spectroscopy

FC   Fridel-Crafts

FeAsH   Iron extracted from coal fly ash via acid leaching

HRTEM   High Resolution Transmission Electron Microscopy

ICP-OES   Inductive Coupled Plasma -   Optial emission spectrometry

IE   Ion – Exchange

MCM   Mobil Composition of Matter

SAED   Selected Area Electron Dispersion

SDA   Structure Directing Agent

SEM   Scanning Electron Microscopy

t-BB   *t*-butylbenzene

t-BC   *t*-butylchloride

WI   Wet Impregnation

wt %   Weight Percentage

XRD   X-Ray Diffraction

CHAPTER 1

1.0   Introduction

This chapter presents an introduction and background of zeolites and their synthesis from coal fly ash. It further presents the generation of acid mine drainage from abandoned former coal mines and their associated waste dumps. The possibility of using acid mine drainage as a metal precursor in the synthesis of iron loaded zeolite catalysts is also presented. A brief review on the applications of iron loaded zeolites in organic and inorganic reactions is also outlined. The present work focuses on synthesising iron loaded zeolites for application in organic synthesis, and the Friedel-Crafts alkylation reaction was studied as a probe reaction. The general background of the reaction is highlighted. The chapter goes on to outline the problem statement, research questions, motivation of study, research approach, scope and delimitation and finally the thesis layout.

1.1   Zeolites and mesoporous silica materials

Zeolites are defined as inorganic crystalline hydrated aluminosilicates generated from an infinite three-dimensional network of AlO_4 and SiO_4 tetrahdra linked to one another by sharing of the oxygen atom (Georgiev et al., 2009). They have regular, structured microspores which are of molecular dimensions. This unique character of zeolites gives them adsorption, catalytic and ion exchange properties (Sebastian et al., 2009). In catalysis, zeolites are a choice material due to their ability to perform shape selective reactions. The principle of shape selectivity is the phenomena in which the pore cavity system of the zeolite restricts the entrance of reactant molecules, the exit of product molecules or the formation of transition states within the zeolite pore channels (Csicsery, 1984). Some of the most prominent industrial applications of zeolites include fluid catalytic cracking (FCC), hydroxylation, alkylation, oximation, epoxidation, hydrocracking, catalytic dewaxing, conversion of methanol to gasoline (MTG) and xylene isomerisation (Yilmaz & Müller, 2009).

Certain zeolite types occur in nature and the first discovery of natural zeolites was in the year 1756. Upon the discovery of zeolites, efforts were made to synthesise them and the first reported success was in 1862. The synthesis was based on mimicking natural conditions under which zeolites form i.e. high temperatures above of 200 °C and high pressures of above 100 bar. Industrial production of zeolites started in the late 1940s and the synthesis was carried out at temperatures below 100 °C under autogenous pressure. The feed stock used were alkali-metal hydroxides and reactive forms of silica such as sodium silicate, colloidal silica, fumed silica and amorphous silica. The silica and the alkali-metal hydroxide were mixed with water and an alumina source to form the synthesis gels. The most commonly used sources of alumina were aluminium hydroxide and aluminium sulphate (Davis & Lobo, 1992). However, producing zeolites from commercial sources is still very expensive and a lot of research in zeolite synthesis has been centred on using waste materials such as coal fly as a feedstock (Georgiev, 2009; Ojha et al., 2004; Querol et al., 2002; Sutarno et al., 2007).

1.2   Coal fly ash

Coal fly ash (CFA) is the resultant solid residue generated in the combustion of pulverised bituminous coal in power stations. The CFA is made up of non-combustible mineral matter found in coal and it is mostly composed of silica, alumina and iron oxides (Sear, 2001). The fine ferroaluminosilicate material is composed of hollow, glassy particles enriched with Ca, K, Na and several other trace elements such as As, B, Mo, Se and Sr (Sajwan, 2003). The particle size of the CFA is usually in the range 10 – 100 microns and hence are collected using electrostatic precipitators or mechanical filter fabric bag houses. The heavier particles, referred to as bottom ash, are collected using mechanical cyclones (Rafalowski, 2003; Sear, 2001).

Coal fly ash has considerable human health and environmental implications. The dry particulate coal fly ash can get airborne and migrate into surrounding areas causing health ailments such as allergic bronchitis, asthma, silicosis among others. The CFA also contaminates surface water hence impacting negatively on aquatic life as it gets into vicinal water bodies. The disposal of CFA requires vast tracts of land and this causes enormous land degradation (Dayal & Sinha, 2005). These environmental concerns have

stimulated the recognition of proper CFA collection, handling, disposal and effective utilisation.

1.2.1   Fly ash: The South African case

The economy of South Africa largely rests on the mining industry, which is energy intensive. On the other hand, population growth results in increased domestic demand for electricity. At the present moment 77 % of the power produced by the country's power utility, Eskom, is generated from coal powered stations. Eskom also produces power that is exported to neighbouring countries such as Lesotho, Zimbabwe, Swaziland, Botswana, Mozambique and Namibia. Globally the country is rated as the 7th electricity producer and ranked 5th as a coal producing country. The power utility produces about 95 % of all the power used in the country and two thirds of all the power produced in the whole continent of Africa. The dependence on coal as a source of power is estimated to continue for a considerable time in the future considering that the country has limited power generating options such as hydro-electric and nuclear. On the other hand, the country has well established infrastructure for coal fired power stations. The country also boasts of large coal reserves which are estimated to be around 53 billion tonnes and, with the current consumption rate, this volume of coal may last for the next 200 years (Eskom 2017; Oxford Buss. Grp., 2008).

Considering the power demand in South Africa it is not possible at present to abandon the use of coal as a source of power generation. However, the use of coal in power generation creates a perpetual accumulation of coal fly ash at the power stations. This scenario necessitates the conversion of coal fly ash into useful products to ease disposal constraints as well as improve waste utilisation. The problem with the use of coal does not end with the accumulation of coal fly ash alone, but it also brings about another environmental challenge in the form of acid mine drainage (AMD). The source of the AMD is mostly from abandoned former coal mines and their associated waste dumps. The greatest problem that arises from AMD is that it spreads far beyond the immediate surroundings and eventually ends up in natural water ways (Mjimbo et al., 2017).

1.3   Acid mine drainage

South Africa is already a water-poor country and the release of acid mine drainage (AMD) into water sources has resulted in high salinities of water which consequently has brought about an unacceptable degradation in water quality (Yanful, 2009). AMD has serious negative ecological impacts and it is also a major threat to the river systems in areas where it is produced (Merkel & Schipek, 2011). The acid produced mobilises metals that may be contained in the associated rock. The resultant drainage contains metals such as Fe, Cd, Zn, Al and Mn. These metals are toxic to aquatic organisms. Zeolites have been used in the removal of toxic metals from AMD (Motsi et al., 2009). However, there is little work reported in literature that focuses on the conversion of the metal impregnant zeolite to a useful material such as a catalyst for various reactions. Since the removal of these metals from AMD are based on the same principals as the loading of metals on zeolites in catalyst synthesis it would be of interest to test the catalytic feasibility of the material generated upon contacting zeolites with AMD. In addition, CFA contains significant amounts of Fe, which can be leached out and used for the synthesis of Fe-loaded zeolites.

1.4   Iron loaded zeolite catalysts

Iron containing zeolites have proved to be versatile catalysts and have been applied in both liquid phase and gas phase reaction transformations. Some of the reactions include: oxidation of benzene to phenol, dehydrative aromatisation of furans to aromatics, selective catalytic reduction of nitrogen oxides, hydrogenation of CO_2 into hydrocarbons, fenton and photo-fenton oxidation among others (Meng et al., 2017; Patet et al., 2017; Ingole et al., 2017; Yang et al., 2017; Velichkova et al., 2016). Zeolite supported iron catalysts have recently gained much attention in the Friedel-Crafts alkylation reaction, replacing traditional mineral acids and Lewis acid previously used for the reaction. Bidart et al. (2001) reported a high conversion of 100 % in the Friedel-Crafts (FC) alkylation of benzene with *t*-butylchloride under mild conditions using iron supported on zeolite Y.

Apart from acting as the primary catalyst, iron supported on zeolites can also act as a promoter in certain reactions. Some of the notable reactions in which iron acts as a promoter are; the Pt-Fe bimetallic system for application in oxygen reduction in fuel cells, Pt-Fe bimetallic catalysts in the selective oxidation of CO to CO_2, the Ni-Fe system in the CO methanation (Wang et al., 2009; Watanabe et al., 2003; Tian et al., 2012). In all these cases Fe induced the promoting effect by modifying the electron density of the primary

metal catalyst. One of the most studied reactions that applies the use of the Pt-Fe bimetallic system supported on zeolites is the selective hydrogenation of cinnamaldehyde (SHC). When Pt alone is used there is a tendency of formation of hydrocinnamaldehyde and not the unsaturated alcohol, cinnamyl alcohol. However, the introduction of Fe to the Pt-zeolite catalyst greatly enhanced the selectivity towards the formation of the unsaturated alcohol (Yan et al., 2010).

1.5   Friedel-Crafts alkylation

The Friedel-Crafts (FC) alkylation of aromatic compounds is one of the bedrock reactions in organic synthesis. It was first reported in 1887 based on the work done by Charles Friedel and James Mason, and in their ground-breaking discovery the alkylation of benzene was catalysed by $AlCl_3$ ((Olah, 2003; Bandini et al., 2009). The FC alkylation reaction can be described as an electrophilic substitution reaction of an aromatic compound with an alkylating agent such as alkene, alcohol or alkyl halide, with the resultant product being an alkylated aromatic compound (Wasserscheid & Joni, 2010). It is worth mentioning that a third of worldwide organic chemical production is based on aromatic compounds and hence their synthetic manipulation has attracted much attention over the years (Bandini et al., 2009). As with most discoveries in organic synthesis, the FC reaction has evolved from the days of its discovery to date, and vast research activities centred on the transformation have been reported. Around the 1960's, the generally accepted classification of the FC alkylation reaction was, any organic reaction that involves isomerisation, elimination, cracking, polymerisation or addition, that takes place under the catalytic influence of either a Lewis acid or a Brønsted acid. In recent times the widely acceptable classification of the FC alkylation reaction is any reaction that involves the introduction of an alkyl group on the aromatic ring. This is commonly performed by alkylating the aromatic compound with an alkyl halide in the presence of $AlCl_3$ (McMurry, 2012).

On a large scale the FC alkylation reactions are carried out using either homogeneous or heterogeneous catalyst systems. The widely applied industrial approach known as the Monsanto/Kellog technology exploits the use of $AlCl_3$ under a homogeneous catalytic system. In this approach, water or basic aqueous solutions have to be added to the reaction

mixture to facilitate product isolation. This addition results in irreversible hydrolysis of the catalyst which consequently gives rise to the formation of toxic waste, mostly water contaminated with organic substances, alongside corrosive gas emissions (Wasserscheid & Joni, 2010). In recent years there has been a growing advocacy for green chemistry and much interest has been invested in the employment of eco-friendly approaches which minimise the production of hazardous waste as well as promote the application of green catalysts. However, these approaches ought to be economically sustainable and able to present elevated positional selectivity (Bandini et al., 2009; Wasserscheid & Joni, 2010). It is against this background that acid zeolites become a viable alternative as catalyst in the FC alkylation reactions.

1.6   Problem statement

Traditionally, the most applied industrial catalysts for the Friedel-Crafts alkylation of benzene to produce alkyl benzenes are Lewis acids and strong mineral acids. These catalysts pose a number of constrains, for instance Lewis acids do not require the use of stoichiometric quantities, and catalyst recovery upon reaction completion is not feasible. Another challenge associated with these acids is that of separation constraints and in the process of separation there is liberation of HCl alongside high amounts of aqueous and salt waste (Bidart, 2001). Separation constraints are also a characteristic feature when strong mineral acids are employed. They are also corrosive to industrial equipment as well as posing handling problems (Harmer, 2001).

Considering these challenges, it is inevitable to pursue new routes of developing efficient, sustainable and eco-friendly catalysts for the Friedel-Crafts alkylation of benzene. The catalysts also ought to be easily separable from the product matrix. In this light heterogeneous catalysts supported on zeolites have proved to be a viable alternative. It has to be noted that the sustainability of any large scale production of any synthetic product should be economically viable and commercial zeolites are a bit expensive (Georgiev, 2009). However, numerous zeolites of high quality can easily be produced from coal fly ash with good reproducibility and several research activities have proved this (Ojha et al., 2004, Querol et al., 2002, Sutarno et al., 2007).

South Africa's electricity is mostly produced from coal fired powers stations. The combustion of coal in these stations results in production of high volumes of coal fly ash. The accumulation of the fly ash poses a disposal constraint and its use in zeolite synthesis will solve two problems, namely disposal challenges as well as providing a cheap starting material for zeolite synthesis. A detailed background of coal fly ash is presented in Chapter 2.

On the other hand, South Africa is also faced with another problem with regard to the release of Acid Mine Drainage (AMD) from former gold and coal mines. The AMD has significant environmental concerns and it poses a threat to the vicinal aquatic systems, since it is acidic and also contains a variety of toxic metals (Taylor, 2008; Yanful, 2009)). According to United States Environmental Protection Agency (USEPA), the ramifications of AMD can be rated as second to that of ozone depletion and global warming (Mandrees, 2009). Details with regard to AMD are presented in broader terms in Chapter 2. The use of AMD as a source of iron to load zeolites can also ease the problem in two ways, firstly removing the pollutants in AMD and secondly the potential creation of a cheap and green, iron loaded catalyst.

In the event that the presented problems are solved it would bring relief to both the environment as well as industry since a cheap, sustainable and environmentally eco-friendly catalyst would have been created for application in the FC alkylation reaction. Furthermore, the catalysts would have been created primarily from waste materials i.e. CFA and AMD.

1.7   Broad Aim

The broad aim of the study is to synthesise active supported metal catalysts for application in the Friedel-Crafts alkylation using waste materials via green chemistry approaches.

1.8   Specific objectives

- To synthesise high silica zeolite HBEA and MCM-41 from South African Fly ash collected from Arnot power station.
- To load Fe on HBEA via ion exchange and wet impregnation using Fe extracted from coal fly ash and acid mine drainage as metal solution precursors.

- To load Fe on MCM-41 via wet impregnation using Fe extracted from coal fly ash and acid mine drainage as metal solution precursors.

- To characterise the supported metal catalysts by XRD, HRTEM, SAED, SEM, ICP-OES, and N_2-adsorption.

- To test the catalytic activity of the Fe loaded coal fly ash based supports in the Friedel-Crafts alkylation of benzene with *t*-butylchloride.

- To determine the effect of other metals found in AMD (Ni, Mn, Ca, Na and Mg) on the catalytic activity of the resultant catalysts on the Friedel-Crafts alkylation reaction.

- To determine the effect of Brønsted acidity of the support material on the Friedel-Crafts alkylation of benzene.

The present work endeavours to establish a variety of issues with regard to the possibility of using South African coal fly ash as a starting material in the synthesis of porous support materials for use in the Friedel-Crafts alkylation reaction. The work also explores the feasibility of using Fe extracted from CFA via acid leaching and acid mine drainage as a metal solution precursors in the preparation of metal loaded porous material for application in the aforementioned reaction. It is against this background that the following questions were coined and this study presents answers to their feasibility.

- Is South African coal fly ash usable as a starting material for the synthesis of high silica zeolite HBEA and MCM-41 and how reproducible are the synthesis outcomes?

- Are the fly ash based support materials under study; MCM-41 and zeolite HBEA, suitable substrates for the Friedel-Crafts alkylation reaction?

- Can Fe extracted from CFA be used as a metal solution precursor in the preparation of Fe-Loaded zeolites for application in the FC alkylation reaction?

- Can Fe from AMD be easily incorporated on high silica zeolite HBEA and MCM-41 via liquid phase ion exchange or wet impregnation and retain the crystallinity of the parent support materials upon metal loading?

- What effect do the other metals found in AMD have on the overall catalytic activity of the resultant metal loaded supports on the Friedel-Crafts reaction?

- Does acidity have any marked influence in determining the percentage conversion as well as the product selectivity, when applied in the test reaction?

1.9   Motivation of Study

The current study is motivated by a number of hypotheses on which the hope of bringing to life the set objectives is based on. The overall intention being to provide an alternative green synthesis route in the Friedel-Crafts alkylation reaction by using fly ash based porous materials as metal supports. Porous zeolitic materials have been extensively employed as metal support in the preparation of green metal loaded catalysts for application in organic synthesis. On the other hand, a lot of low silica zeolites have been successfully synthesised using coal fly ash as a starting material. Querol et al., (2002) presents a comprehensive review on numerous studies that have been carried out by different researchers with regard to low silica zeolite synthesis from coal fly ash. In addition, CFA contains significant amounts of Fe, which can be extracted via acid leaching to form a Fe solution. The feasibility of using the solution as a metal precursor is to be explored in the present work.

Furthermore, zeolites have been applied in the remediation of AMD, and the adsorption studies carried out indicated that the selectivity towards the removal of Fe from AMD using zeolites was the highest compared to that of the other metals (Motsi et al., 2009). Considering the fact that commercial Fe loaded zeolites made from pure chemicals have catalytic properties and have been employed in various reactions, the present study aspires to test the feasibility of synthesising Fe loaded on coal fly ash based supports and testing the activity of the resultant catalysts in the Friedel-Crafts alkylation reaction.

1.10   Research Approach

In a bid to convert the set objectives into tangible realities, a series of experiments were carried out. The first step was the synthesis of high silica zeolite HBEA and MCM-41 from South African coal fly ash collected from Arnot power station. The starting stage in the zeolite synthesis involved the extraction of silica from coal fly ash using citric acid. The extracted silica was then mixed with sodium aluminate to an appropriate Si/Al ratio to obtain zeolite HBEA. In the case of MCM-41 there was no addition of the aluminate. The synthesis was done via a hydrothermal approach for both materials. Upon crystallisation the synthesised materials were calcined in air at a temperature of 550 °C to remove the template.

Metal incorporation on zeolite HBEA was done via two conventional approaches namely liquid phase ion exchange and wet impregnation. The ion exchange approach was not applicable to the MCM-41 support since it does not contain exchange sites, so only wet impregnation was used with MCM-41. The metal precursor used in all cases was either Fe extracted from CFA via acid leaching or Fe from acid mine drainage. The resultant catalysts obtained via wet impregnation contained mostly iron since it is the major element found in AMD. There were traces of other metals such as Ni, Mn, Ca, Na, Cr and Mg. With the catalysts prepared via ion exchange the catalyst consisted of mostly Fe and very little, if any of the other metals found in AMD were incorporated onto the porous materials. This is due to the high selectivity that the zeolite has toward Fe relative to the other metals (Motsi et al., 2009). With the catalysts prepared using Fe extracted from CFA the catalysts contained only Fe and Na. The Fe solution from acid leaching had a very low pH, it was adjusted using concentrated NaOH, this gave rise to the presence of Na ions in the precursor solution. Another series of catalysts supported on both HBEA and MCM-41 was prepared via wet impregnation again using the Fe extract and AMD as source of Fe.

The synthesised catalysts were subjected to a range of material characterisations. The crystallinity and mineralogical identity of the respective catalysts was done via X-ray diffraction (XRD). This enables the determination of whether the integrity of the pristine material is retained upon metal loading as well as investigating whether large metal crystallites are formed on the zeolite surface. The nature of the metal dispersion has a great influence on the resultant catalytic activity. Determination of the catalyst morphology was done via scanning electron microscopy together with high resolution transmission electron microscopy. The objective of undertaking the fore mentioned analysis was to assess whether the integrity of the parent material was maintained after metal incorporation. The surface area of the prepared catalysts was analysed using N_2-adsorption and compared to that of the parent material. Further catalyst characterisation was done by selected area electron dispersion (SAED). The intent was to investigate the crystal structure and the degree of polycrystallinity of the catalysts. Evaluation of the acidity of the catalysts was done via NH_3-TPD. The catalyst acidity impacts greatly on the overall activity.

The Fe loaded catalysts were tested for their activity using a probe reaction, the Friedel-Crafts alkylation of benzene with t-butylchloride. The reaction was chosen as a probe for comparative purposes. The alkylation reaction was carried out in a batch reactor at a temperature of 45 ^{0}C over a time interval of 5 h. The reaction progress was followed by taking samples at fixed time intervals and analysis by gas chromatography. The chromatograms generated enabled the calculation of the extent of t-butylchloride conversion, selectivity towards formation of t-butylbenzene, product distribution and percentage yield of the produced t-butylbenzene.

1.11   Scope and Delimitation of Study

The present study aimed to present green, effective but cheap Fe supported catalysts for application in various inorganic and organic reactions, with the Friedel-Crafts alkylation of benzene with t-butylchloride used as a probe reaction. The focal point was to use waste materials to prepare the said catalysts. In the present work the catalyst support materials HBEA and MCM-41 were synthesised from coal fly ash while acid mine drainage and Fe extracted from coal fly ash were used as metal precursors. The major difference that exists between the choice of supports investigated is mainly the presence of Brønsted acidity present in HBEA but absent in MCM-41. Thus the effect of Brønsted acidity was investigated. The catalytic activity of the catalysts tested was also compared to catalytic activity of other catalysts tested under comparable conditions and presented in open literature. The alkylation of benzene with t-butylchloride is accompanied by the formation of HCl and this changes the pH of the reaction mixture. However, in the present study the pH was not controlled. Furthermore, the reaction kinetics and mechanism were not studied, as they are well known. The reaction conditions were adopted from standard methods available in open literature and this work did not look into the reaction condition optimisation as this was a probe reaction used for comparsion with literature. Only the effect of the major elements immobilised on the supports was studied and the effect of the traces was not investigated. It should however be noted that the trace elements might have had an impact on the catalytic activity obtained in the reactions presented in the study.

1.12   Thesis Outline

https://etd.uwc.ac.za

This thesis is divided into seven chapters, and this section presents the chapter chronology, outlining the main features of each respective chapter.

Chapter 1: The chapter covers a brief introduction and background of zeolites and their synthesis from waste materials such as coal fly ash. It further highlights the environmental and human health hazards associated with CFA and the advantages of using CFA as a feedstock in zeolite synthesis. It presents the possibility of using Fe extracted from CFA or AMD as metal solution precursors in the preparation of Fe-loaded zeolites for use in organic synthesis. The probe reaction in this work is the Friedel-Crafts alkylation of benzene, and its background is presented as well in the chapter. The research's broad aim, specific objectives, problem statement, research questions, motivation of study, research approach, scope and delimitation and the thesis layout are presented.

Chapter 2: The chapter presents a detailed account of zeolite physico-chemical properties as well as the most common applications of zeolites. The effects of various zeolite synthesis parameters are reviewed alongside the use of CFA as a feedstock in low and high silica zeolite synthesis. Furthermore, the chapter highlights the formation of AMD and its associated hazards, together with its potential use as a source of metal precursor in Fe-loaded zeolite catalysts. Different zeolite metal loading approaches are presented with more emphasis on ion exchange and wet impregnation. The background, mechanism, thermodynamics and catalysts applicable to the Friedel-Crafts alkylation reaction are also reviewed.

Chapter 3: The chapter presents a list of the materials and equipment used in the present work. It further goes on to present the synthesis conditions applied in the MCM-41 and HBEA preparation. The experimental conditions and reagent proportions used during metal loading are also presented. The different characterisation techniques applied on the prepared catalysts together with the respective instrumental set up conditions assumed during characterisation are also highlighted. The final sections of the chapter present the experimental details with regard to catalytic evaluation on the Friedel-Crafts alkylation reaction alongside the product identification and quantification.

Chapter 4: The chapter presents the characterisation outcomes generated on the pristine and metal loaded supports. Appropriate facts and postulations responsible for the observed outcomes are made on respective characterisation data. The data is also compared to that generated from related research activities found in open literature. Discussion is made on the differences and similarities obtained, and rational attributes are presented. The characterisation techniques undertaken and discussed in the chapter are; XRD, HRTEM, SAED, SEM, ICP-OES, and N2-adsorption.

Chapter 5: The chapter focuses on the catalytic evaluation of the catalysts prepared using AMD as a metal precursor. The series of catalysts contain a host of metals other than Fe. The focal point is to study the effect of these other metals on the overall activity. The effect of; Ni, Mn, Ca, Na and Mg, in the presence of Fe are studied and discussed in the chapter. Again, the evaluation is based on percentage conversion, selectivity, product distribution and yield. Discussion on how the activity is corroborated by the catalysts' properties, generated via different characterisation techniques is also presented.

Chapter 6: This chapter presents the catalytic evaluation of the Fe-loaded supports (MCM-41 and HBEA) prepared using Fe extracted from CFA on the Friedel-Crafts alkylation of benzene with t-butylchloride. Evaluation is made based on the percentage conversion of t-butylchloride, selectivity towards formation of t-butylbenzene, yield and product distribution. The outcomes are compared and discussed against similar research activities done using commercial catalysts. Comparison is also made on the effect of the loading approaches applied (ion exchange and wet impregnation). The effect of the pore system, acidity, reaction time and metal wt % loading are also discussed.

Chapter 7: The final chapter provides a general conclusion on the characterisation and catalytic activity. The chapter goes on to present the significance of the study, the novelty and recommendations based on the research findings.

CHAPTER 2

2.0   Literature review

This chapter gives a general background of zeolites and their physicochemical properties, alongside their various applications. It further goes on to present a review on zeolite synthesis from both commercial and waste materials. Emphasis is given on the use of coal fly as a feedstock in zeolite synthesis. A review on coal fly ash properties and its environmental hazards are also presented. Different metal loading approaches are highlighted with much emphasis on ion exchange and wet impregnation. Additionally, the potential use of acid mine drainage (AMD) as a metal precursor solution in preparation of metal loaded zeolites is featured. This is followed by the chemistry of AMD, its environmental hazards and application of iron-loaded zeolites for the Friedel-Crafts (FC) alkylation reaction. The final section of the chapter presents the background of the FC alkylation reaction, its kinetics, thermodynamics, catalysts used, and the different alkylating agents.
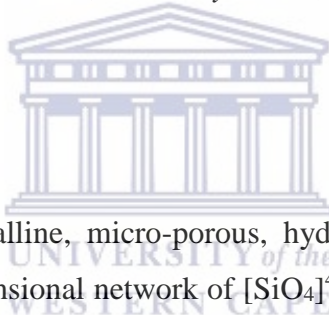
2.1   Zeolites

Zeolites are defined as crystalline, micro-porous, hydrated aluminosilicates that are constructed from a three-dimensional network of $[SiO_4]^{4-}$ and $[AlO_4]^{5-}$ tetrahedra linked to each other by shared oxygen atoms. They are considered to be inorganic polymers with channels or cavities (Subbulekshmi & Subramanian, 2016).

2.1.1   *Historical background of zeolites*

The history of zeolites goes back to 1756, when Baron Axel Fredrik Crønstedt, a Swedish mineralogist coined the term to describe the peculiar property of minerals found in a copper mine in Svappavaara (Lapland, Sweden). When the minerals were heated in a blow-pipe flame they appeared to boil, a behaviour not exhibited by any known minerals at the time. Based on this distinctive character, Crønstedt coined the term "zeolites" from a combination of two Greek terms; '*zein*', meaning "to boil" and '*lithos*', meaning "stone". Subsequently, various other zeolites were discovered and their basic properties reported. One of the most ground-breaking discoveries regarding zeolite properties was reported in 1857 by Alexis Damour. He observed that crystals of various natural zeolites

(such as harmotome, brewsterite, faujasite, chabazite, gmelinite, analcime and levyne) desorb water without perceptible change to their transparency or morphology. A short time later in 1858, Eichhorn discovered that natural zeolites natrolite and chabazite exhibited the ability to undergo ion exchange when contacted with ammonium salts (Millini & Bellussi, 2017).

Work done by William Taylor and by Linus Pauling in the 1930s helped define some of the main characteristics of zeolites. The crystal structure of zeolites was described as a tridimensional framework built up of corner-sharing SiO_4 and AlO_4 tetrahedra. The zeolites have regular channels that vary from zeolite to zeolite but generally fall within the range of 3 – 12 Å. The SiO_4 tetrahedra are neutral, whilst the AlO_4 tetrahedra carry a negative charge that is usually balanced by either group 1A or 2A metals (such as Na, K, Ca, Mg, Sr and Ba). These cations occupy the interconnected void channels in the zeolite, and are exchangeable by other cations (Inglezakis & Poulopoulos, 2006). The first definition of zeolites was proposed by Joseph Victor Smith in 1963 as '*an aluminosilicate with a framework structure enclosing cavities occupied by large ions and water molecules, both which have considerable freedom of movement, permitting ion exchange and reversible dehydration*', (Millini & Bellussi, 2017).

Commercial production of zeolites for industrial use begun in 1954 by Union Carbide, for gas separation, purification and the drying of natural gas. A few years later the same company initiated the use of synthetic zeolites in the separation of normal-isoparaffins. In 1962, Mobil Oil introduced zeolite X for use as a cracking catalyst (Mayoral et al., 2015).

2.1.2   *Zeolite composition and structure*

The enthralling properties of zeolites arise from their unique structures. Zeolite composition is generally expressed by the following formula.

$$\mathbf{M}_{x/n}[\mathbf{AlO_2})_x(\mathbf{SiO_2})_y].m\mathbf{H_2O}$$

where M is the cation of valence *n*, which counter-balances the negative aluminosilicate framework. The term *m* defines the number of water molecules, whilst *x* and *y* are the stoichiometric ratios of Al and Si in the respective unit cell. The primary building blocks of zeolites are the $[SiO_4]^{4-}$ and the $[AlO_4]^{5-}$ tetrahedra which form oxygen bridges by

corner sharing. The –O– bridges are not usually linear, however they are flexible, and bridge angles may vary from 120 º – 180 º. The SiO_4 tetrahedra are electrically neutral when connected together in a three dimensional array, while the AlO_4 tetrahedra are negatively charged and require charge balancing by exchangeable cations (Smart & Moore, 2012). This implies that the more Al atoms in the lattice structure of the zeolite, the greater the ion exchange capacity and hydrophilicity. On the other hand, increased Si results in the formation of surface silanol groups and hydrophobicity. During zeolite synthesis, the ratio of Si/Al can be tailored to effectively generate a high field density and polarity, depending on the targeted application. The zeolite surface chemistry can also be modified at will by isomorphous replacing the framework with elements as Ga, Fe, P and Ge. The high electronegativity of these elements relative to Al provides decreased acid strength of the Brønsted centres. The SiO_4 and AlO_4 tetrahedra are referred to as the T-atoms and can be arranged in numerous variations giving a diverse range of channel systems (Breck, 1974). Figure 2.1 shows a typical arrangement of the T-atoms in zeolite A.
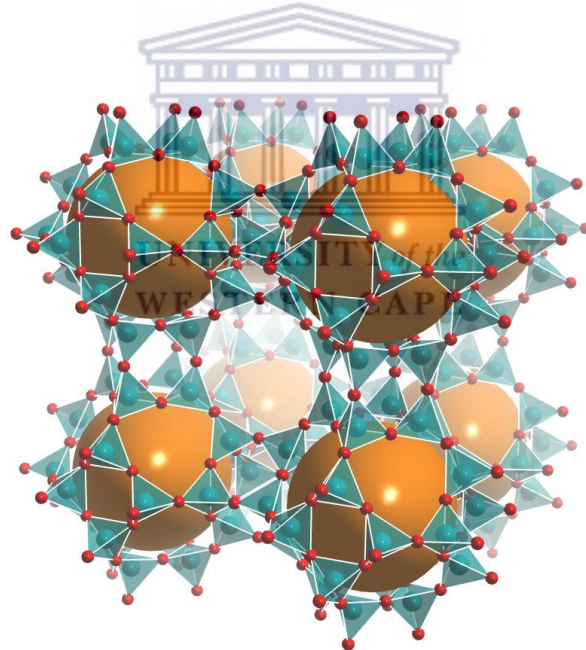
Figure 2. 1: Zeolite crystal framework structure of zeolite A: Silicon atoms are teal, oxygen atoms are red and the sodalite cages are the orange spheres that fill the voids (https://chemicalstructure.net/portfolio/linde-type-a)

Figure 2.1, shows how the T-atoms link in zeolite A to form a sodalite cage. The T-atoms are referred to as the primary building units (PBUs) and can link by sharing 2, 3 or all the 4 corners giving variation of three dimensional frameworks or lattice structures (Wagner & Davis, 2000).

2.1.3 Properties and applications of zeolites

Zeolites can be used in numerous scientific and industrial applications depending on both their intrinsic properties and the synthesis routes applied. The most basic intrinsic properties of zeolites include their acid-base characteristics, pore size and channel geometry as well as their framework stability.

Zeolites are unique materials, due to their adsorbent quality, ion exchange capacity, and molecular sieve properties. Molecular sieves are defined as materials that can selectively adsorb molecules based on their size, shape or electrical charge, and are widely used in industry for the separation of straight chain from branched chain hydrocarbons. They are also used in chemical sensors for industrial process control. Other applications of zeolites include: environmental indoor air quality monitoring, effluent treatment, exhaust control, gas separation, catalysis and removal of toxic metals from waste water (Moshoeshoe et al., 2017).

2.1.4 Zeolites in waste water treatment

The absorbant character of zeolites enables them to be applied in wastewater treatment for the removal of various pollutants. Industrial waste water often contains significant amounts of cation metals such as Sb, Cr, Cu, Pb, Zn, Co, and Ni. These metals have well known negative environmental and health effects, and industrial waste water that contains these ions cannot be discharged into the ecosystem (Moshoeshoe at al., 2017). Zeolites can be used in waste water treatment to remove cations, and can also be modified to remove anions. This surface modification can be performed using inorganic salts or organic surfactants, which are adsorbed on the zeolite surface, leading to the creation of positively charged oxihydroxides or surfactant micelles. Upon this modification, the zeolite surface can then bind to anions, like arsenates or chromates, in stable or less stable complexes. The advantage that zeolites have over other ion exchange materials commonly used in waste water treatment, such as organic resins, is that they are relatively cheap and have very high selectivity for different cations. In addition, the exchange occurs at low temperatures (Margeta et al., 2013)

Zeolites have also been successfully employed in the removal of radioactive fission products from industrial waste water. Fang et al. (2016) used zeolite 4A to remove the simulated radionuclides Sr^{2+}, Cs^+, and Co^{2+} from water under ambient conditions and

reported an adsorption rate of almost 90 %. An adsorption rate of 98.7 % was achieved under alkaline conditions. The adsorptive property of zeolites can also be exploited in the removal of odours from waste water. Adelodun et al. (2017) reports that, 16 offensive odours comprising reduced sulphur compounds, nitrogenous compounds, volatile fatty acids and phenol/indoles were successfully reduced to acceptable limits in waste water.

2.1.5   *Zeolites in gas purification*

Zeolites have emerged as the preferred inorganic fillers in the production of mixed matrix membrane (MMM) used in gas separation. This is due to their high porosity, uniform pore system, as well as their good chemical and thermal stability (Ahmad et al., 2016). Silicoaluminophosphate (SAPO) zeolites have been applied in the separation of CO_2 from CH_4, a process that can be greatly improved by the incorporation of ionic liquids on to the zeolite. Ahmad et al. (2016) immobilised imidazolium ionic liquid on to SAPO-type zeolites, reporting a 110 % improvement in separation performance with respect to the unmodified zeolites.

The separation of ethylene from ethane has been traditionally done via cryogenic distillation. However, Bereciartua et al. (2017) reported the successful use of small pore zeolite ITQ-55 as a viable and cheaper alternative for this particular separation. Industrial purification of oxygen by pressure swing adsorption has also been performed using zeolite LiX and zeolite 5A (Hamed, 2015).

2.1.6   *Medical applications of zeolites*

Many biochemical processes occur via adsorption, ion exchange, catalysis or processes that are closely linked to them, and the intrinsic properties of zeolites can be manipulated to facilitate these mechanisms (Moshoeshoe et al., 2017). In addition, zeolites are stable in biological environments, and when used in drug delivery systems, there is no hindrance in the drug's pharmacological effect. The most established zeolite applications in medicine include: the enrichment and identification of low abundance peptides, enzyme immobilisation in bio-sensing, processes in magnetic resonance imaging in wound treatment, as well as in various drug delivery systems. Amorim et al. (2012) reported the successful application of zeolite A and zeolite Y as drug delivery systems in the treatment of cancer. In the study the zeolites were employed as hosts for the encapsulation of α-cyano-4- hydroxycinnamic acid (CHC), an anti-cancer drug. The encapsulated CHC was

found to inhibit cell viability up to 585 times relative to the non-encapsulated drug. Mechanically activated clinoptilolite was also discovered to have anti-cancer therapeutic effects in in vivo animal and tissue studies. The local application of clinoptilolite on dogs suffering from skin cancer was found to significantly reduce the cancerous tumours on the dog's skin. In addition, the oral administration of the zeolite to both mice and dogs suffering from a variety of tumours resulted in an improvement in the general health of the animals, reduced tumour sizes and prolonged life (Moshoeshoe et al., 2017).

2.1.7   *Zeolites as detergent builders*

Industrial production of soap and detergents is based on the combination of six major components: surfactants, builders, enzymes, fillers, bleaching agents and other minor additives such as dispersing agents, fabric softening clay, dye-transfer inhibiting ingredient, and optical brighteners. Out of these components, builders constitute about 30 %, of the final product and in most cases these builders are made from phosphate-containing compounds like sodium tripolyphosphate. The role of the phosphate in detergents is to sequester water hardening alkaline earth ions such as calcium and magnesium. However, there are concerns over the use of polyphosphates as builders since phosphates are associated with eutrophication, and therefore their use has been discouraged. Zeolite A and zeolite P have emerged as alternative and efficient builder replacements. The ability to exchange ions coupled with the high cation exchange capacity of zeolites, renders them a suitable substitute, since they can easily sequester alkaline earth metals from water, as well as enhance solubilising, emulsifying and suspending action in the detergent (Ayele et al., 2016).

2.1.8   *Zeolites in agriculture and food production*

Food security has become an important issue in many parts of the world. As a result of climate change and depreciation of the quality of the soil resources, farming with zeolites has gained momentum in recent times. Large porosity, cation exchange capacity, and selectivity for ammonium and potassium ions enables zeolites to be used as nutrient carriers. The reversible hydration property of zeolites enables them to be used as fertilisers, stabilisers and chelators. Zeolites additionally allow the slow release of nutrients by both inorganic and organic fertilisers, giving them a major application in agriculture in terms of nitrogen capture, storage and slow release (Sangeetha & Baskar, 2016). Their application in agriculture is expected to rise significantly due to the fact that

they are classified as non-toxic by the International Agency for Research on Cancer and safe for human consumption by Food and Drug Administration (Eroglu et al., 2017).

2.1.9   Zeolites as solar thermal collectors

Due to the rise in demand for energy and the rising cost of fossil resources coupled with their imminent depletion, there has been widespread attention in the quest to search for renewable energy sources, such as solar power. Solar power suffers from a mismatch between sunny and dark periods, necessitating the creation of efficient heat storage technologies. Zeolites have been explored as possible solar thermal collectors due to their adsorption properties (Tatsidjodoung et al., 2016). Working on an experimental open thermal collector prototype and using zeolite 13X as the adsorbent, Johannes et al. (2015) reported that 2250 W of power was discharged in a space of 6 h which would convert to 27 W kg^{-1} of zeolite. Using zeolite 13X, Tatsidjodoung et al. (2016) reported the outcomes obtained from an open-cycle prototype thermal collector composed of 80 kg of dry zeolite. The report concludes that the storage system may significantly contribute in the share of solar energy to cover a building's needs for over a year.

2.1.10   Zeolites in catalysis

The unique properties of zeolites, such as their large surface area, crystallinity, thermal stability, as well as their unique and uniform channel system, make them attractive materials for application in homogenous catalysis. The pore system of zeolites can be tuned in synthetic zeolites and improve catalytic activity for a specific reaction. Their ion exchange ability enables them to function as Brønsted acids in catalytic transformations (Moshoeshoe et al., 2017). Their use in catalytic reactions is one of the major application of zeolites, and over recent decades, they have been replacing homogeneous catalytic systems based on the use of mineral acids and chloro-derivatives as they have superior economic and environmental benefits. In addition, they are easily separated from reaction products, are regenerable with a considerable working life, and are also easy to handle (Millini & Bellussi, 2017).

The most important commercial catalytic applications of zeolites are in Fluid Catalytic Cracking (FCC) and Hydro-Cracking (HC). They are also applied in other processes in oil refining, such as isomerisation, alkylation, dewaxing and reforming. Zeolite-based catalysts are core for the production of cumene and ethylbenzene, as well as in the

isomerisation of xylenes. Of late zeolites have also been extensively applied in methanol-to-hydrocarbons (MTH) processes, which result in the production of gasoline, aromatics and olefins. Zeolite-based catalysts have also been applied in the oxidation and reduction of gases: for instance, Fe-loaded zeolite ZSM-5 and HBEA have been used in NOx reduction, while Cu-loaded zeolites have been applied in the oxidation of NH_3 (Weckhuysen & Yu, 2015; Xu et al., 2007).

2.1.11 Natural zeolites

Natural zeolites are hydrated aluminosilicate minerals classified as tectosilicates. They form via the interaction of glass-rich volcanic rocks with fresh water or seawater (Shaheen et al., 2012), or when volcanic rocks and ash react with alkaline groundwater. There is a strong correlation between the mineral formations of the zeolite sedimentary rocks with the host rock in terms of silica composition and water chemistry of the depositional and post-depositional environment. The age and burial depth also affects the nature of the zeolite formed. The salt content of the water is also significant since it favours the conversion of volcanic glass into zeolites. There are numerous known natural zeolites but the most common ones include chabazite, clinoptilolite, mordenite, heulandite, laumontite, analcime, natrolite, thomsite, and stilbite. Since natural zeolites form under diverse conditions, they differ in their physical and chemical composition. These compositional variations are expressed as the ratio R=Si:(Si+Al+Fe) (Iijima, 1980)

2.1.12 Natural versus synthetic zeolites

Natural zeolites are abundant and can be procured at relatively low cost. Natural zeolites, such as chabazite and clinoptilolite, have proved to be effective and efficient relative to synthetic zeolite Y when applied in the catalytic cracking of heavy molecules into lighter ones. However, natural zeolites are seldom pure due to the diverse conditions under which they form, and are usually contaminated by other elements (Montalvo et al., 2012). The cation exchange capacity of natural zeolites is also limited, relative to synthetic ones. Natural zeolites furthermore, do not show appropriate ion affinity towards Cu, Cs, Co and Ur ions. Due to these limitations, artificial zeolites are more often commercially employed than natural ones. By contrast, the advantage synthetic zeolites have is that they can be tuned with a wide variety of physical and chemical properties, giving them specific pore sizes and high thermal stability (Georgiev et al., 2009).

Natural zeolites are characterised by a low Si/Al ratio and therefore tend to be more hydrophilic, due to the interaction of the dipole of the H_2O molecule with the electrostatic fields of the anionic aluminosilicate zeolite framework. On the other hand, zeolites with high Si/Al ratio are hydrophobic. The ratio of the Si/Al can be engineered in synthetic zeolites to create a high presence of Si. High silica zeolites have a more homogenous surface, with high hydrophobicity. The latter have been successfully used in the direct esterification of acetic acid with n-, iso-, and tertiary-butyl alcohol. These reactions would otherwise fail if they were carried out using natural zeolites, since the produced water would poison the natural zeolite catalyst (Moshoeshoe et al., 2017).

It was previously thought that zeolites require high temperatures and pressures to form. However, it was later discovered that it was not the case since zeolites form in sedimentary rocks. This discovery formed the basis of hydrothermal synthesis, which is a widely applied approach in the synthesis of artificial zeolites.

2.2   Zeolite synthesis

The synthesis of crystalline materials such as zeolites is usually carried out via two main approaches, solid-state and liquid-state reactions. The solid-state reactions require temperatures above 300 ^{0}C to overcome reactant transportation to the reaction site. Synthesis in solution occurs at lower temperatures, since molecular transportation is much easier. Liquid phase synthesis of zeolites is referred to as solvothermal, however in most zeolite synthesis procedures water is used as the solvent and hence the approach is referred to as hydrothermal synthesis (Cejka & Zones, 2010).

2.2.1   Hydrothermal synthesis

The hydrothermal synthesis approach is one of the earliest methods applied to zeolite synthesis. It is a multiphase reaction-crystallisation process, involving at least one liquid phase and both crystalline and amorphous solid phases. The hydrothermal method is described as an in-situ reaction occurring above room temperature in an aqueous solution under pressure. It is carried out using water as a solvent, and a base solution as mineraliser, within a temperature range of 90 – 180 ^{0}C. In certain cases, a structure-

directing agent (SDA) is added to the starting solution, forming a slurry, which is stirred to form a homogeneous gel. The role of each of components is presented in Table 2.1, and will be expanded upon in the following sections.

Table 2.1: Chemical components and their respective roles in hydrothermal zeolite synthesis.

Source	Role
SiO_4^{4-}	Primary building unit(s) of the framework
AlO_4^{5-}	Primary building unit(s) of the framework
	Charge difference origin in the framework
OH^-	Mineraliser and provider of basic media
M (alkali cation), template	Counter-ion of the framework charge, guest molecule, pore stabiliser
H_2O	solvent, guest molecule inside the framework

The hydrothermal approach has the advantage of: high reactant reactivity, low energy consumption, low air pollution, easy control of the solution, formation of metastable phases and unique condensed phases (Abdullahi et al., 2017). The resultant zeolite structure is dependent on initial synthesis conditions such as: temperature, pressure, water content, synthesis duration, the cations present in the synthesis gel, and the Si/Al ratio. The synthesis progresses via three main stages: The first stage involves the synthesis solution reaching supersaturation as the aluminosilicate species increase. The second stage is nucleation of the species- initially forming amorphous solids, which later slowly become more ordered. The final stage is crystal growth, when nuclei have reached a critical size. Species from the solution attached to the nuclei, forming the zeolite crystal surface (Lobo, 2012). The stages are depicted in Figure 2.2.
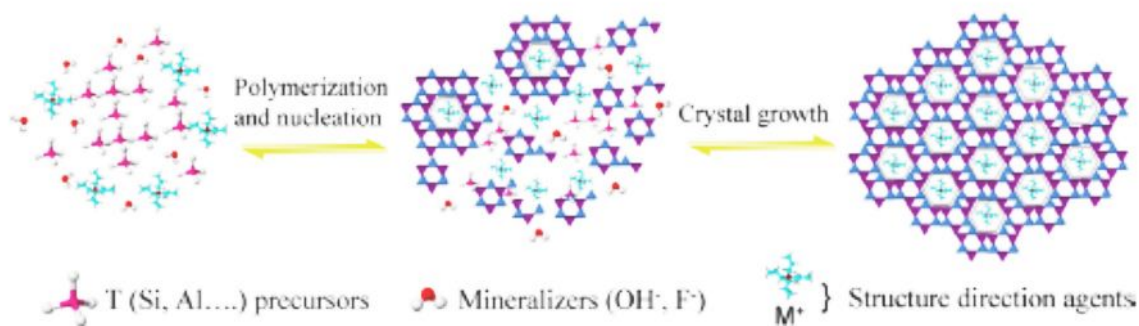
Figure 2. 2: Stages in hydrothermal zeolite synthesis (Zaarour et al., 2014)

2.2.2   Silica and alumina role and their sources

Silica and alumina are the primary zeolite building blocks, and therefore are crucial components in zeolite synthesis. The source of silica is known to influence the crystal size, morphology, nucleation, and crystallisation rate, as well as the chemical properties of the resultant zeolite. This is because different silica sources differ in reactivity and solubility (Eskandari et al., 2015). The most commonly used commercial sources of silica are: Ludox AM-30, fumed silica, and water glass. In cases where low Al content zeolites are desired, colloidal silica such as Ludox are preferred. The purity of the silica source is also of paramount importance, for instance the presence of Al^{3+} ions cause formation of hydroxylated anions of the $[HO\text{-}(SiO_3)m\text{-}AlO_2\text{-}(SiO3)_n\text{-}OH]^{2m+2n+1}$ type in active silica. When a silica source is contaminated with these Al^{3+} ions, the hydroxylated ions go into solution and form nuclei onto which zeolite crystal growth is initiated. Thus, a silica source with high Al^{3+} ions tends to have a higher specific number $\tilde{N}$. of crystals in the final zeolite product. The higher the nuclei number the less the time required for the complete transformation of the amorphous aluminosilicate gel species into crystal products (Krznaric et al., 2003). Both the silica and alumina ought to be dissolved to form a gel prior to nucleation and crystallisation. The mineraliser brings about this dissolution, and therefore its nature and concentration vital in zeolite synthesis.

2.2.3   Effect of mineraliser

The most commonly employed mineraliser in zeolite synthesis is the hydroxyl ion, whose source is usually KOH or NaOH. High concentrations of the ion are used to mineralise the alumina and silicate species in the reaction gel. The silica is dissolved in such a way that the amorphous particles are depolarised, forming oligomer species. However, the hydroxyl ion concentration ought to be carefully chosen, since there is an equilibrium

between the solution species and the solid species. Too high a concentration shifts the equilibrium towards the solution and hinders crystallisation. On the other hand, too low a concentration compromises the solubility, and consequently the silica alumina species' transportation is hindered. Limitations to species transport results in formation of amorphous product. The OH$^-$ concentration may also affect the transformation of the desired metastable phase to more dense phases such as zeolite P, sodalite, analcime and quartz (Strohmaier, 2010). During crystallisation, it is the metastable (desired) phase that crystallises out first, and prolonged crystallisation time transforms the metastable phase to the dense phases. A typical example is reported by Strohmaier (2010), in which the effects of the hydroxyl ion concentration on the resultant zeolite type was investigated using 1,4-bis(N-methylpyrrolidium) butane as a structure directing agent. In the investigation, a constant Si/Al ratio of 30 was maintained and ZSM-12 was obtained with gels that had a OH$^-$/Si ratio of $\leq$ 0.6. TNU-9 was obtained with OH-/Si ratio of 0.79, while a further adjustment to 1.0 resulted in the formation of STI.

Although the hydroxyl ion is the most common mineraliser, the fluoride ion (F$^-$) can also serve as a mineraliser. The use of the F$^-$ ions allows for the synthesis of zeolites in slightly acidic media (pH~5). At such pH values the solubility of the silica is significantly increased, due to the formation of hexafluorosilicate SiF_6^{2-} species. The most commonly used sources of F$^-$ are NH_4F, NH_4HF_2 and HF. Zeolites synthesised using F$^-$ as mineraliser can be easily converted to the hydrogen-form upon calcination (Kessler, 2001).

2.2.4 *Effect of ageing*

Ageing time affects nucleation and crystal growth kinetics. The seed nuclei required for crystal growth are formed during the ageing process. Ageing increases the nucleation rate, and reduces the stimulation period and length of crystallisation. It furthermore reduces the crystal size and increases the crystal population (Abdullahi et al., 2017). Grecco et al., (2014) studied the influence of the ageing period on the properties of zeolite BEA and MCM-41. In their study, increasing the ageing time from 24 to 192 h was found to diminish the crystallinity and favour formation of bigger crystals. With BEA zeolite, an increase in ageing time led to an increase in the zeolite acidity. It was concluded that the ageing time could be optimized to produce zeolites with specific acidity, depending on the intended purpose of the final material. In a different study by Kovo and Holmes

(2010), on the effect of ageing time on the synthesis of zeolite Y, it was found that the surface area of the zeolite increased while raising the ageing time.

2.2.5   *Structure directing agents*

Structure directing agents (SDA) - also known as capping agents, templates, or solution-phase additives also influence the nature of the resultant zeolite. These molecules have multiple functions in shape selective synthesis, and are added to the reaction matrix to guide the organisation of the anionic building blocks of zeolites. In zeolite synthesis, the most commonly used SDAs are inorganic cations like Na^+, Li^+, Cs^+, K^+, Rb^+, Ca^{2+} and Sr^{2+}. However, the use of these inorganic cations results in the formation of low silica zeolites, unless there is the presence of large amounts of seed crystals to allow high silica zeolites to form (Moliner et al., 2013). In most cases when a high silica zeolite is desired, usually the selected SDA would be an organic moiety such as tetra-alkyl-ammonium cations (TMA^+, TEA^+, TPA^+), dihydrozyethyldimethylammonium, dialkyl and trialkyl amines, and phosphonium compounds. Indeed, larger organic moieties introduce a lower number of positive charges in the zeolite cavities relative to small inorganic cations, thus reducing the number of charge balancing anions (AlO_4^-). In essence, the size of the SDA determines the concentration of the trivalent elements in the zeolite framework. An appropriate SDA should have very weak interactions with the solvent to avoid formation of complexes. Furthermore, it should be able to fill in the zeolite cavites with as many van der Waals forces as possible but with limited deformation (Corma et al., 2004).

Early synthesis of nanosized zeolite BEA was based on the use of tetraethylammonium (TEA) as a template. However, this synthesis approach is characterised by low yields. Gallego et al., (2017) report on the synthesis of high silica zeolite BEA and ZSM-5 (Si/Al~ 10–30) with small particle sizes (~50–100 nm) and increased solid yields (above 80%). These outcomes were achieved using 4,4-trimethylenebis(*N*-methyl,*N*-benzyl-piperidinium) and   3,10-diazoniabicyclo[10.2.2]hexadeca-12,14,15-triene-3,3,10,10-tetramethyl-dichloride, or polydiallyldimethylammonium chloride.

2.2.6   *The effect of pH*

The pH controls crystallisation, and hence determines the composition and type of the resultant zeolite. It influences the solubility of the aluminosilicate species, and promotes

supersaturation for nucleation and crystal growth. In cases where the mineraliser is a hydroxide, the pH value of the synthesis gel is determined by the total alkali content and the buffering action of the species in the synthesis solution. The synthesis solution composition can be described by the following expression:

$$MAlO_2 n[M_m H_{4-m} SiO_4]pH_2O$$

Where m is the excess alkalinity (the difference between total alkalinity MOH and the alkali aluminate $MAlO_2$ per mol of SiO_2)

$$\text{and } n = (MOH\text{-}MAlO_2)/SiO_2$$

In studies focusing on the effect of pH on the Si/Al ratio, m is considered a critical parameter. Different zeolites with different Si/Al ratios form at different pH values. For instance, FAU crystallises at a pH range of 12.3 – 13.8, NaY at around pH 11 and MOR at a pH range of 11.3 – 12.7 (Lechert, 2001).

2.2.7   The effect of water content

Zeolite formation is dependent on the degree of supersaturation of the synthesis gel. An increase in the water amount will decrease supersaturation, and consequently nucleation and growth will also decrease (Maghsoodloorad et al., 2011). In a study investigating the effect of water content on the formation of ZSM-39, ZSM-48 and KZ-1, Martens and Jacobs (1988) found that changing the H_2O/SiO_2 ratio from 20 to 80 shifted the structure of the zeolite produced. In low water and high SiO_2/Al_2O_3 ratios, ZSM-39 was formed, while in Al rich gels KZ-1 was formed. ZSM-48 was observed to crystallise in dilute solutions. Generally, an increase the water content tends to prolong crystallisation.

2.2.8   Effect of Time and Temperature

The crystallisation temperature and time influence the nucleation and crystal growth mechanism (Abdullahi et al., 2017). It is well understood that a reduction in the crystallisation temperature results in the formation of a larger number of crystals and smaller particle size. The rate of zeolite crystallisation decreases with a fall in temperature (Otterstedt & Brandreth, 1998). The crystal linear growth rate (K) and crystal size (l) are described by the following equation:

$$DN/\delta t = A[exp(E_t)^{-1}]; \quad R = Kt$$

where K is the linear crystal growth rate coefficient, and A and E are rates of nucleation coefficients. The coefficients K, A and E all increase with increasing temperature. The equation implies that the crystallisation of zeolites should increase with prolonged time. However, since zeolites are thermodynamically metastable phases, the Ostwald's law of successive reaction oversteps the synthesis process such that the metastable phase forms first and is later replaced by more dense phases. Zeolite formation is hence not limited by thermodynamics alone, but kinetics of crystallisation ought to be considered too (Abdullahi et al., 2017). The formation of more dense phases can also be explained by the fact that, as the temperature increases, the water filling the pores is significantly reduced, leading to the formation of dense phases. It is however possible to synthesise zeolites at high temperatures if non-volatile pore space fillers are used.

During zeolite synthesis, the heating is usually done by placing the crystallisation solution into an autoclave. In certain cases, the solution is heated up using a heating mantle. This approach however, results in inhomogeneous heat distribution. Another option is microwave heating, an approach that is associated with homogenous heat distribution and rapid crystal growth (Byrappa & Yoshimura, 2001).

2.2.9   *Effect of pressure*

Generally, pressure variations do have an effect upon zeolite synthesis, since the crystallisation is performed under autogeneous pressure (Weitkamp and Puppe, 1999). In cases where synthesis is carried out in the presence of volatile reagents such as ammonia and methane, pressure changes ought to be carefully monitored. High-pressure synthesis may influence specific parameters such as synthesis solution viscosity, which has a great impact on crystallisation kinetics (Nagy et al., 1998).

2.2.10 *Effect of stirring*

Stirring or agitation during zeolite synthesis influences crystallisation kinetics, particle size, particle size distribution, and the final Si/Al ratio of the resultant zeolite. Agitation facilitates the rapid transport of reactive species from the synthesis solution to the surface of the growing crystals. In addition, agitation ensures homogeneous heat distribution and keeps the crystals in suspension during zeolite crystallisation. However, agitation also accelerates the dissolution of viable nucleus or zeolite crystals, and consequently may

reduce the rate of crystallisation and crystal growth. The effects of agitation become more critical when the rate of viable nucleus formation approaches the rate of nucleus dissolution (Derewinski & Machowska, 2004).

Hydrogels that are poorly mixed tend to produce impure zeolite phases, with the amount of impurities decreasing with increased mixing. In the synthesis of zeolite BEA and TS-1, the effect of stirring was studied and it was found that stirred samples gave rise to smaller crystals while larger crystals were obtained from unstirred samples (Camblor et al., 1991). The product crystal size is also affected by stirring, for instance in the synthesis of zeolite beta and TS-1, stirred samples gave rise to smaller crystals, while unstirred samples produced much larger crystals (Camblor et al., 1991). This observation can be described by the general tendency of zeolites to form large crystals in viscous systems where convective motion is hindered and mass transfer is diffusion controlled. Derewinski and Machowska (2004), investigated the effect of stirring in the synthesis of zeolite MEL and TON using 1,8- diaminooctane as template, with a gel of Si/Al (25-45). It was found that unstirred sample gave out a pure phase MEL characterised by large crystals. When the same gel was used under the same conditions but in rotating autoclaves (56 rpm), the product was pure TON with 100 % selectivity.

2.2.11 *Crystallisation and nucleation*

Nucleation and crystallisation are basic steps upon which zeolite synthesis is based. Nucleation is the rate determining step, and is defined as the process in which minute precursor aggregates form germ nuclei. Nucleation precedes crystallisation and occurs on the interface between solution and gel via adsorption and rearrangement of the soluble precursor species. Crystal growth can only occur when the nucleus has grown to a specific critical size.

The process of nucleation is generally divided into two main categories, namely primary and secondary nucleation. Primary nucleation occurs either within the solution itself (homogeneous nucleation) or via the catalytic activity of extraneous material in the solution (heterogeneous nucleation). Secondary nucleation is catalysed by the presence of parent crystals, and has lower activation energy relative to that of primary nucleation. The parent crystals can either be added at the beginning of the synthesis as seed crystals or can grow within the unseeded starting synthesis gel (Thompson, 2001; Xu et al., 2007).

In synthesis that involves the use of a hydroxide as mineraliser, the precursor species are initiated by hydrolysis, resulting in the formation of M – OH groups. This is followed by condensation, in which M-O-M bonds are formed. Condensation is caused via two mechanisms, olation and oxolation, according to the following reaction schemes (Livage, 1994):

$$\text{M-OH}^{\partial -} + \text{M}^{\partial +}\text{-OH}_2 \rightarrow \text{M-OH-M}^{\partial +}\text{-OH}_2{}^{\partial +} \rightarrow \text{M-OH-M} + \text{H}_2\text{O} \ (olation)$$
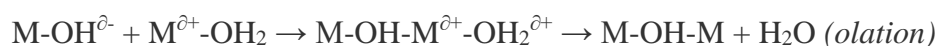
Olation is enabled by the nucleophilic addition of positively charge hydrated metal cations, while oxalation is enabled by condensation of two metal hydroxides, as presented in the following equation:

$$\text{M-OH} + \text{HO-M} \rightarrow \text{M-O-M} + \text{H}_2\text{O} \ (oxolation)$$

Nucleation and crystallisation can be described in four stages: formation of simple and polymeric aluminosilicates (evolution), formation of embryo from the aggregation of aluminosilicates (agglomeration and nucleation), formation of primary particles (well-ordered micelle formation-crystal growth by agglomeration), and aggregation of primary particles by oriented aggregation (crystal growth). The processes are described in Figure 2.3 below:
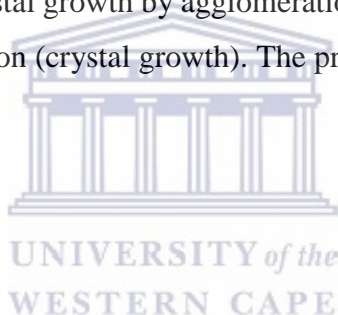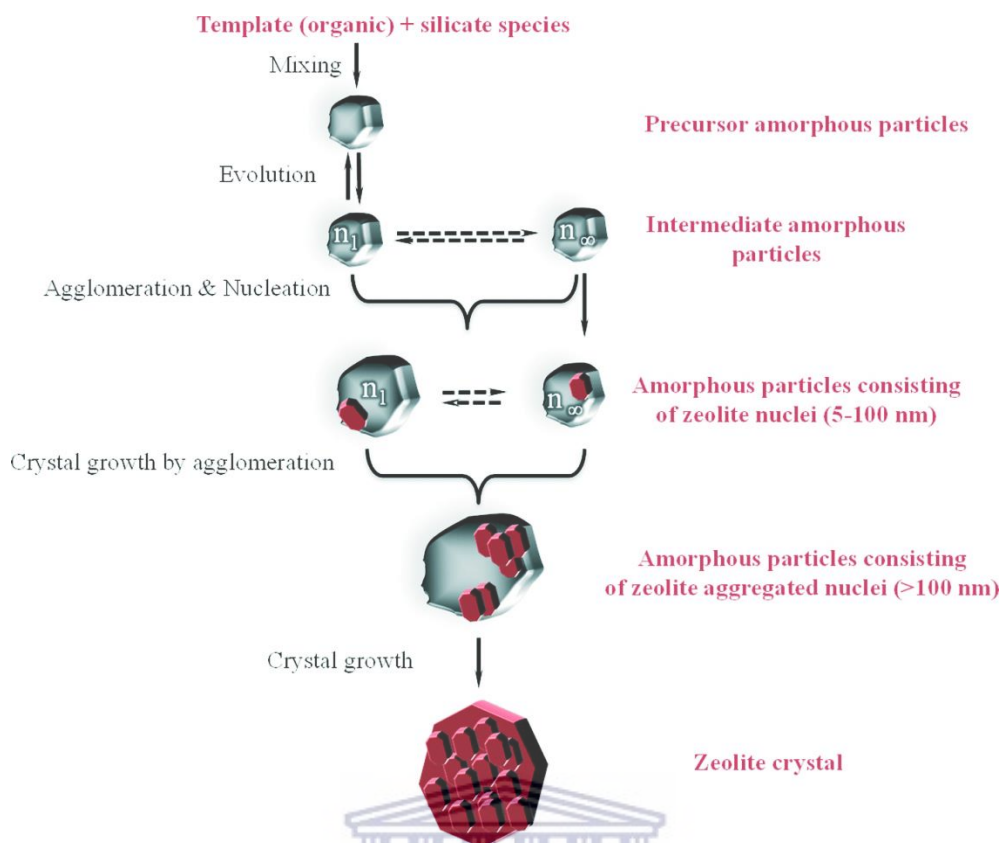
Figure 2. 3: Zeolite nucleation and crystallisation steps (Grand et al., 2016)

Although crystallisation is much faster than nucleation, the process is dependent on several reaction conditions: temperature, stirring/agitation, seeding, gel ageing, pH, water content, ratio and concentration of framework forming elements and template concentration. A typical crystallisation curve plotting the nucleation rate and crystal growth is presented in Figure 2.4.

(a) Nucleation rate

Gel diffusion to equilibrate composition | Nucleation process | Crystal growth

(b) Crystal growth rate

Time

(c)

Polymerisation & nucleation

Crystal growth

T (Si, Al, Ti,….) Precursors   Mineralizers (OH⁻, F⁻)   Structure directing agents
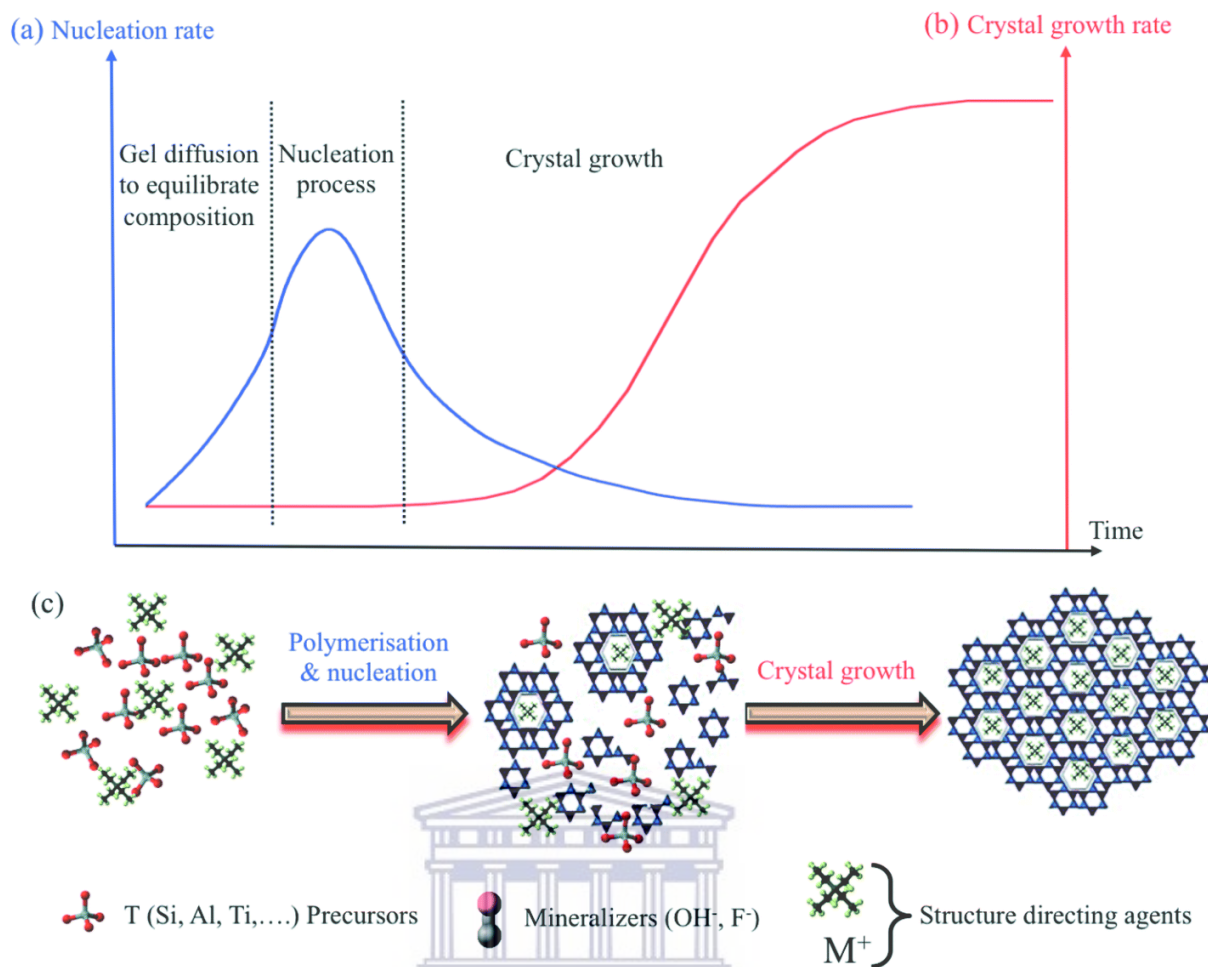
Figure 2. 4: Evolution of nucleation and growth rates as well as supersaturation, as a function of synthesis time (Grand et al., 2016)

With time, the rate of nucleation rises to a threshold value at which crystallisation starts. Once crystallisation has begun, the growth rate increases until a steady state is achieved, and the reactant ingredients are depleted.

2.2.12 Recent developments in zeolite synthesis

The increased need to control zeolite properties and structure has necessitated the evolution of zeolite synthesis over the years. Conventional synthesis approaches have been modified by alteration of synthesis parameters and replacement of reagents with others which provide the desired chemical and physical properties to the resultant zeolite. Methods have been designed that target the preparation of particular zeolite catalysts for specific reactions by using SDA's that mimic the transition state of the target reaction. These approaches have enabled the commercial synthesis of once 'exotic' materials.

Notable recent advances in zeolite synthesis include: solvent-free synthesis, ionothermal synthesis, and computer aided synthesis.

(i) Solvent-free synthesis: Traditionally zeolites have been prepared from solvothermal synthesis in which water or alcohols are used as solvents in closed autoclaves under autogeneous pressure. However, these solvents tend to occupy a large volume of space in the autoclaves and consequently reduce the zeolite yield. In addition, the use of solvents generates significant amounts of waste pollution. Recently researchers have put much attention in solvent-free synthesis, since the approach is environmentally friendly, uses less energy, and is much safer as the synthesis is carried out at low pressure (Wu et al., 2018). The earliest solvent-free approaches were dry gel conversion (DGC) and vapour-phase transport (VPT). In these methods, solid aluminosilicate gel of appropriate composition is suspended over vapours of amines and water, or water alone. The role of the amines is to regulate the pH. Wu et al. (2017) in the synthesis of ITQ-12, ITQ-13, and ITQ-17 zeolites via a solvent free approach, reported that the zeolite yield was very high, with a short crystallisation time compared to conventional approaches. The synthesis was carried out at temperatures comparable to those used in conventional hydrothermal synthesis (140-180 ^{0}C). Rao et al., (1998) and Xu et al., (2007) successfully prepared zeolite BEA in the form of self-bonded pellets and zeolite ZSM-5 using the solvent-free approach.

(ii) Low water and non-aqueous syntheses: Conventional hydrothermal synthesis of zeolites requires significant amounts of water (of ratio $H_2O : SiO_2 > 25$) to enable homogenisation as well as synthesis gel handling. However, the introduction of fluoride media in zeolite synthesis has enabled low water synthesis ($H_2O/Si = 2–14$) to be practical. Fluoride media has allowed the synthesis of all-silica compositions of zeolite beta and chabazite. Hydroxide mediated synthesis is characterised with high SDA : Si which results in elevated concentrations of siloxy/silanol defects in the resultant zeolite framework, thus making it impossible to synthesise highly open all-silica frameworks. In addition, the fluoride can coordinate with silicon to form a pentacoordinated complex SiO_4F^- that counter-balances the positive charge on the SDA cation without presenting siloxy/silanol defects in the framework (Burton, 2018). Successful low water synthesis ($H_2O : SiO_2 < 10$) of zeolite BEA in fluoride media was noted in a review by Strohmaier (2010). The same review mentioned the synthesis of MFI, ZSM-39, ZSM-48 using

ethylene glycol, butanol, glycerol as solvents. Li et al., (1992) reported the successful synthesis of Fe-ZSM-48 in non-aqueous media. The synthesis involved isomorphous substitution of the metals in the framework by Fe in mixed (ethylenediaminetriethylamine) solution.

(iii) Ionothermal and deep eutectic mixtures syntheses: In ionothermal synthesis, ionic liquids (IL) are used as both solvents and structure directing agents. Ionic liquids are a distinct group of organic solvents, ILs are composed of a bulky organic cation (such as imidazolium, pyridinium, piperidinium or pyrrolidinium with alkyl side chains) and an organic or inorganic anion. ILs are considered more environmentally friendly relative to the commonly-used organic solvents. They are characterised by low volatility, excellent solvating properties and high thermal stability (Parnham & Morris, 2007; Nikinmaa, 2014). Deep eutectic mixtures are a peculiar class of ILs usually made by complexing an ammonium halide salt with hydrogen bond donor molecules. This complexing suppresses the glass transition temperature at the eutectic molar ratio. Properties of the solvent, such as hydrophobicity, can be altered by changing either the salt or hydrogen bond donor (Hammond et al., 2017). Cooper et al., (2004) reported the first successful synthesis of zeolites using ILs. In the study 1-ethyl-3-methylimidazolium bromide, was used to synthesise SIZ-1, SIZ-2, SIZ-3, SIZ-4, SIZ-5, SIZ-8 and SIZ-9 zeolites. ILs have also led to the synthesis of new zeolites such as HPM-1, in addition to already known zeolites such as ZSM-5 (Rojas et al., 2013; Mignoni et al., 2010). Wheatley et al., (2010) also reported on the successful synthesis of TON and MFI zeolites using 1-butyl, 3-methyl imidazolium based ionic liquids with bromide-hydroxide counter anions.

(iv) Computer aided synthesis: Computational-based approaches in zeolite synthesis have proved to be highly useful in determining suitable synthesis parameters as well as the nature and ratios of starting materials. Approaches based on interatomic potentials have successfully been used in modelling bulky crystalline structures, as well as the metal atoms both in framework and extra-framework sites. These techniques have allowed the development of new framework structures by providing new templates/SDAs from a library of suitable molecular fragments (Lewis et al., 1997). Wilson (2001) reports on the successful synthesis of zeolites ZSM-5, ZSM-11 and SSZ-33 using computer-based host/guest stabilities. The author also reports on the application of a computer programme, "ZEBEDDE," in the synthesis of an aluminophosphate with CHA structure,

using 4-piperidinopiperidine as template. Khan et al., (2015) successfully applied the Parallel Tempering Monte Carlo simulations (PTMC) to determine the final crystalline structure of microporous silica materials based on SDA concentration and interaction strength with silica polymerisation around the SDA. Efforts should be pursed to ensure that the synthesis is eco-friendly, with minimal waste generation, and sustainable material use (Millini & Bellussi, 2017).

2.3   Zeolite synthesis from coal fly ash

Coal fly ash (CFA) is a complex mixture of small particulate materials generated when pulverised coal is combusted in powers stations. The CFA is mainly composed of silica and alumina (60–70 and 16–20 wt. %, respectively) which are essential ingredients in zeolite synthesis and hence CFA has been used as a feed stock (Hui & Chao, 2006). Recently the conversion of CFA to zeolites is viewed as a techno-economically viable application.

2.3.1   Environmental hazards and chemical composition of fly ash

When CFA is released into the environment, it presents a hazard to human and environmental health, both directly and indirectly. The CFA particle size is less than 1 μm and can easily be inhaled and deposited in the lungs (Speight, 2013). From epidemiological studies, pollution particles of less than 2.5 μm have been associated with: Alzheimer's disease, lung cancer, stroke, cardiovascular disease, lung inflammation and diabetes, reduced renal function in older males, morbidity and premature mortality, decreased male fertility, low birth weight, and onset of asthma (Herndon & Whiteside, 2017). Inhalation of CFA can cause hazards to exposed persons by leaching genotoxic compounds, and via causing immunological alterations. CFA is composed of four main components: silica, alumina, iron and calcium. Other trace elements include Ni, Al, Cr, Pb, As and Cd, together with radioactive metals such as thorium and uranium (Borm, 1997). Chemically mobile aluminium is associated with neurological diseases such as Autism, Parkinson's and Attention Deficient/ Hyperactivity Disorder (Belluck & Benjamin, 2001). In addition, the CFA also contains significant amounts of toxic organic compounds such as: phenanthrene, anthracene, pyrene, benz[a]anthracene, chrysene and benzo[a]pyrene. These toxic organic compounds are photochemically non-degradable, and hence will be available for uptake by living organisms (Belluck & Benjamin, 2001).

2.3.2   Coal Fly ash: The South African case

The economy of South Africa is largely anchored on mining, an energy intensive industry which creates huge demands in power generation. The country's power utility ESKOM currently generates 77 % of its power from coal-fired stations. The country also has an increasing population and thus a growing demand for domestic power. Growth in manufacturing industries also puts a further burden on the electricity supply. In the period 2014-2015, ESKOM combusted 120 Mt of coal across 13 power stations, producing 35 000 MW of electricity, together with 34.4 Mt of CFA as waste. Of the large volume of CFA produced, only 7 % was sold from 6 powers stations, while the rest remains stored on site. Most power stations are gradually running out of storage space. The further accumulation of CFA in South African power staions may require more sophisticated and expensive storage facilities.

CFA utilisation may possibly avoid such or at least reduce expenditure (Reynolds-Clausen & Singh, 2017). There are several possible ways in which CFA can be utilised and reduce storage constraints. It has been used as a filler in plastic and rubber manufacturing, fillers in road surface applications, amelioration of poor quality agricultural land, acid mine drainage treatment, synthesis of geopolymers, and production of bricks, cement and concrete. The chemical composition of CFA has also enabled it to be used as a feed stock in zeolite synthesis (Rycrof, 2017).

2.3.3   Coal fly ash conversion to zeolites

Since CFA is largely composed of Si and Al, it can be used as a Si and Al source in zeolite synthesis. The first reported conversion of CFA to zeolites was reported by Holler and Wirsching (1985), and since then numerous publications and patents have reported on the conversion of CFA to various zeolites (Bukharia et al., 2015). However, while the use of CFA in zeolite production may not necessarily consume the vast amount of it produced by power stations, it will definitely produce a value-added material. There are numerous reports on zeolite synthesis from CFA at laboratory, pilot and industrial scale. Wdowin et al., (2014) reports on the successful conversion of 20 kg of CFA to zeolite NaP1 with a high purity of 81 %. Different researchers have worked on the conversion of CFA to various zeolites such as analcime, chabazite, cancrinite, gmelite, ZSM-28, ZSM-5, NaX, BEA, philipsite and sodalite (Adamczyk & Białecka, 2005; Murayama et al., 2005; Kasture et al., 2005; Franus, 2012; Missengue et al., 2017).

2.3.4   Zeolite synthesis approaches from coal fly ash

Synthesis of zeolites from CFA is usually achieved by the dissolution of amorphous aluminosilicate in the reaction mixture. The dissolution determines both the percentage conversion as well as the conversion rate. CFA samples from different origins vary in their Si and Al contents, and if a particular zeolite has to be synthesised necessary adjustments ought to be made by adding the deficient constituent. The presence of certain cations in the CFA may also supress or enhance the crystallisation process. The presence of trace oxides of Ti, Mn, Mg, Na and K alongside anions such as carbonate and sulphates tends to promote nucleation and crystallisation. The presence of CaO tends to reduce the formation of mullite and give higher conversion. Furthermore, the presence of these cations affects the type of zeolite that can be formed from a specific sample of CFA (Bukhari et al., 2015). Numerous synthesis approaches are used in the conversion of CFA to zeolites, the most common being; conventional hydrothermal, fusion and hydrothermal, microwave assisted hydrothermal, and the molten salts approach. The following table gives a summary of these methods (Jha & Singh, 2011).

Table 2.2: A summary of the common methods employed in synthesis of fly ash based zeolites (Jha & Singh, 2011)

Method	Reagent	Temp. (^{0}C)	Time (h)	Zeolites	Remarks
Conventional hydrothermal	NaOH KOH Na$_2$CO$_3$	90 - 150	24 - 96	chabazite Na-P1 Phillipsite Sodalite Zeolite KH 4A, A, P Zeolite X, Y	Low yield, low purity, structural heterogeneity
Microwave assisted hydrothermal	NaOH	100	0.25 - 2	Na-P1	Less synthesis time
Fusion and hydrothermal	NaOH or sodium aluminate	500 - 650	1 - 2	Faujasite, Na-A, NaX or zeolite X	More yield
	water	90 - 100	6		
Molten salt	KOH KNO$_3$ NaOH NaNO$_3$ NH$_4$F NH$_4$NO$_3$	350	3 - 6 24	Sodalite Cancrinite	No addition of water Irregular mophology

Fusion followed by hydrothermal treatment: Numerous studies in the processing of CFA have revealed that the most challenging step is digesting the mullite (a mineral found in fly ash of composition Al$_6$Si$_2$O$_{13}$ to Al$_4$SiO$_8$). Mullite is insoluble in either acidic or alkaline media under atmospheric pressure. However, fusing the mullite at high temperature with alkali allows the mineral to form water-soluble silicate and aluminate compounds. In this approach, the alkali fusion step is performed prior to hydrothermal treatment and this increases the zeolite yield (Shoppert et al., 2017; Ozdemir & Piskin, 2017). Shigemoto et al. (1993) reported the first successful conversion of CFA to zeolite NaX using this approach, after which numerous other researchers reported the application

of this method in preparation of various zeolites. Bukari et al. (2015), notes that zeolites that have been prepared according to this approach include NaP, NaA, NaX and SOD.

Conventional hydrothermal synthesis: The direct hydrothermal synthesis method involves the dissolution of CFA in an alkaline solution, such as NaOH or KOH, to extract the aluminosilicate. After dissolution, hydrothermal treatment is used to generate zeolite crystals from the reaction mixture. Adjustment of the Si/Al ratio is achieved by addition of an aluminate or silicate compound. In a review by Bukari et al. (2015) several zeolites are reported to have been successfully produced from CFA via this approach including: Zeolite X, A, analcime, chabazite and hydrosodalite. As with zeolite synthesis from commercial salts, the nature of the resultant zeolite product is dependent on synthesis parameters such as temperature, pressure, reaction time, Si/Al ratio, alkaline solution, pH and seeding. However, the approach is characterised by relatively lower yield for instance Hollman et al. (1999) synthesised zeolite Na-P1 from CFA using the approach and the highest yield obtained was 85 g per kg of CFA.

Microwave assisted hydrothermal: The first successful report on the synthesis of zeolites from CFA was by Querol et al. (1997). In this work, zeolite A was produced from CFA with a Si/Al ratio of 1.85 using NaOH and KOH as the alkaline agents. It was found that the conventional hydrothermal and microwave assisted approaches both produced similar zeolite types. However, the microwave method greatly reduced the activation time from between 24 to 48 h to only 30 min. The most commonly reported zeolites synthesised from this approach include KM, phillipsite, Na-P1, and NaA (Bukhari et al., 2015).

Synthesis from molten salt: Park et al. (2000) reported on the first successful zeolitisation of waste materials, including coal fly ash, using the molten-salt approach. The method involves thermal treatment of the molten states of salt mixtures, without addition of water. Various salt combinations have been used, with NaOH, KOH, or NH_4F used as mineralisers and $NaNO_3$, KNO_3, or NH_4NO_3 used as stabilisers. The molten salt mixtures act like water in hydrothermal synthesis. Zeolites such as cancrinite and sodalite can be crystallised from the mixture of NaOH and $NaNO_3$ over activation times of 3-6 hours and 24 hours respectively, at temperatures of 350 ± 5 °C. However, one drawback associated with the approach is that low temperatures and insufficient contact with the NaOH can lead to incomplete zeolitisation (Jha & Sing, 2011).

2.3.5   Zeolite synthesis from other silica and alumina sources

Besides coal fly ash and commercial sources, zeolites can be produced from other sources of silica and alumina. Commonly used sources include kaolinite, blast furnace slag, rice husk, bagasse ash and oil palm ash. There is vast amount of work available in open literature describing the use of these materials in the synthesis of a wide range of zeolites.

Kaolinite: Kaolinite is a layered silicate clay mineral with the formula Al_2O_3 $2SiO_2 \cdot 2H_2O$. It has a 1:1 uncharged dioctahedral layer, with each layer consisting of single silica tetrahedral sheet and single alumina octahedral sheet. The synthesis of zeolites from kaolinite is based on two approaches: metakaolinisation (the chemical activation of kaolin to metakaolin) and zeolitisation (the aqueous treatment of metakaolin to produce zeolites) (Abdullahi et al., 2017). Numerous studies available in open literature report on the synthesis of various zeolites from kaolinite: Johnson & Arshad (2014); Belviso et al. (2015); Ayele et al. (2016); Ayoola et al. (2017); and Ayoola et al. (2018).

Blast furnace slag: Blast furnace slag is waste produced in steel production and is mainly composed of SiO_2, Al_2O_3, CaO and MgO. Studies reporting on the use of slag in the synthesis of various zeolites include: Kuwahara et al. (2008); Wajima (2014); Guo et al. (2017).

Rice husk ash: Rice husk ash (RHA) is an agricultural waste produced when rice husk is partially burnt in milling plants. When rice husk is burnt at controlled temperatures below 800 ºC, the resultant ash produced is high in silica (98 %). The RHA has been used considerable as a feedstock in zeolite synthesis, as reported by: Bhavornthanayod & Rungrojchaipon (2009); Habeeb & Mahmud (2010); Mohamed et al. (2015); and Gargiulo et al. (2018).

Oil palm ash: Oil palm ash is the residue produced after the combustion of oil palm biomass. The biomass is used as a fuel in palm oil processing plants (Ooi et al., 2014). Numerous zeolites including zeolite gismondine, A, X and ZSM-5 have been synthesised from oil palm ash: Pa et al. (2015); Khanday et al. (2016); and Aman et al. (2017).

2.4   Zeolitic structures and synthesis from coal fly ash

The present work is focused on synthesising zeolite BEA and MCM-41 from coal fly ash via a silicon extraction step followed by hydrothermal treatment and application of as-

synthesised materials either as catalysts or catalyst supports in the Friedel-Crafts alkylation reaction. This section presents the framework topologies and their respective synthesis routes from coal fly ash.

2.4.1   Zeolite BEA framework

Zeolite beta (BEA) is a disordered intergrowth of three polymorphs: A, B and C. These polymorphs are generated by different stacking of the same building layer as depicted in Figure 2.5. The stacking of neighbouring layers occurs in a random manner resulting in a faulted zeolite structure.
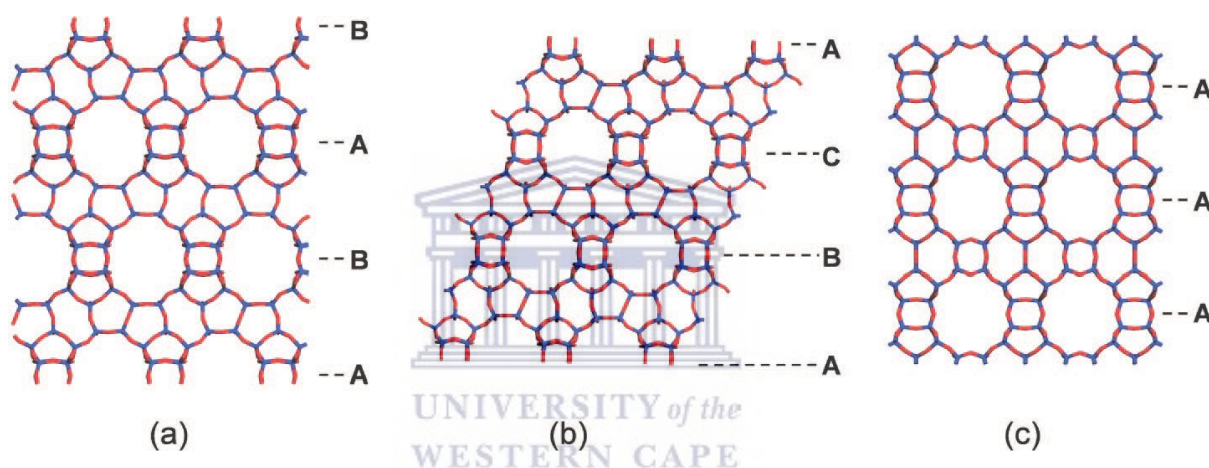
Figure 2. 5: Framework structures of the three zeolite beta polymorphs (a) polymorph A (b) polymorph B and (c) polymorph C (Corma et al., 2008)

The final structure resulting from the stacking of the polymorphs builds a 3-dimensional structure containing 12 membered ring pores in the a- and b- axis, independent of the stacking sequence in the c-axis (Newsam et al., 1988). The pore channel diameters are sized 5.6 x 5.6 Å and 7.7 x 6.6 Å (Bárcia et al., 2005). Figure 2.6 shows the BEA structure as viewed along the b-axis.
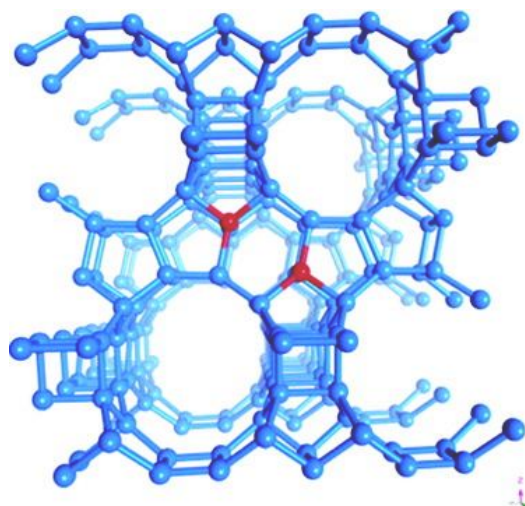
Figure 2. 6: Structure of the BEA zeolite as viewed along the b-axis (the O atoms are not shown for clarity) (Bare et al., 2005).

2.4.2   *Zeolite BEA synthesis from coal fly ash.*

Zeolite BEA was first synthesised in 1967 by researchers at Mobil using pure commercial Si and Al sources with tetraethylammonium hydroxide as a template. Newsam et al., (1988) later determined the structure of BEA. Synthesis of zeolite BEA is performed via the hydrothermal approach. Numerous researchers have reported the successful conversion of coal fly ash to zeolite BEA with various modifications including the use of different SDAs and microwave heating. Synthesis from CFA usually involves fusion followed by hydrothermal treatment, as reported by: Tong et al. (2015); Muñiz et al. (2010); Kasture et al. (2005). Alternatively, Devaki & Priya (2016) used the molten-salt approach to convert CFA to zeolite BEA. The salt mixture was composed of $NaNO_3$ and NaOH, with TEAOH as SDA. Apart from TEAOH, other SDAs have been successfully used and these include: tetrapropylammonium bromide (TPAB), tetrapropylammonium hydroxide (TPAOH), N,N-dimethyl-2,6-cis-dimethylpiperdinium hydroxide (DMPOH), dimethyldipropylammonium hydroxide (DMDPOH), N,N,N-trimethylcyclohexanaminium hydroxide (TMCHOH), and N-ethylN,N-dimethylcyclohexanaminium hydroxide (EDMCHOH) (Muñiz et al., 2010; Tong et al., 2015). However, the direct conversion of CFA to zeolite BEA takes a longer crystallisation time relative to conversion when pure starting materials are used, and hence the silica extraction step from the CFA (as will be shown) prior to hydrothermal

synthesis is more advantageous. In addition, extraction of the silica removes the other elements in the CFA and hence giving a pure BEA phase.

2.4.3   MCM-41 framework

MCM-41 is a mesoporous material characterised by a high surface area of up to 1200 m^2 g^{-1}, and one dimensional cylindrical pores indexed in the space group *p6m*. It belongs to a family of mesoporous materials known as M41S (Dai et al., 2002). These materials were developed and first reported by Mobil Oil Research and Development in 1992. The pore size of MCM-41 ranges from 2.0 – 4.0 nm and can be easily adjusted by using an appropriate SDA. Due to its high specific area, high thermal stability, hydrophobicity and acidity, MCM-41 has found many applications in shape-selective catalysis, adsorption of gases and liquid, biomolecular immobilisation, separation, liquid phase oxidation reactions and preparation of linear alkyl benzenes, among many others (Hui & Chao, 2006). Figure 2.7 presents the framework structure of MCM-41.
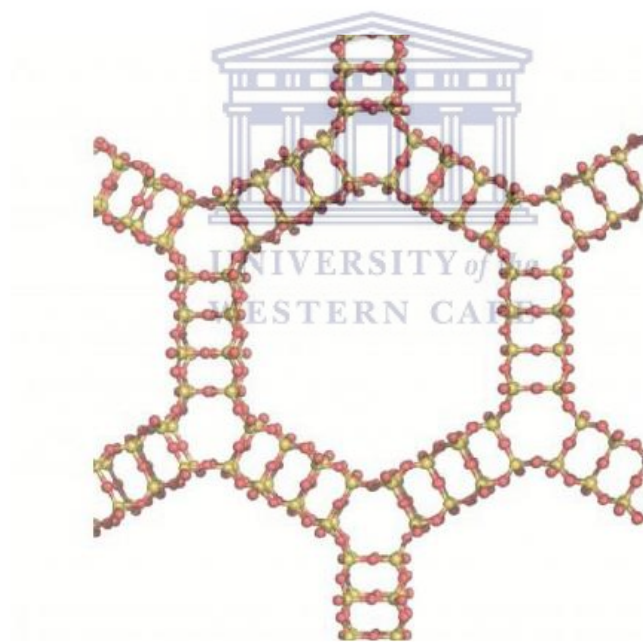
Figure 2. 7: Framework structure of the mesoporous MCM-41 (Lehman & Larsen, 2014)

2.4.4   MCM-41 synthesis

The synthesis of MCM-41 is traditionally carried out starting with the formation of micellar species in alkaline aqueous solution, which is then followed by polycondensation of an organic matrix, and finally, the removal of the organic SDA/template. The physico-

chemical properties of the resultant mesoporous materials are influenced by the interaction of the organic surfactant, and the inorganic matrix. This interaction is dictated by reagent ratios, as well as synthesis conditions like temperature, crystallisation time and ageing. The acidity, ion exchange capacity and catalytic activity of the MCM-41 can be modified by the incorporation of different elements into the silica framework, during synthesis or post-synthesis. The most commonly applied surfactants are trialkyl ammonium halides, such as n-hexadecyltrimethylammonium Bromide (CTAB) (Hui & Chao, 2006). Other surfactants that have been successfully used in the synthesis of MCM-41 include: n-dodecyltrimethylammonium bromide, n-tetradecyltrimethylammonium bromide, n-hexadecyltrimethylammonium bromide, n-hexadecylpyridinium chloride monohydrate and n-octadecyltrimethylammonium bromide (Grüna et al., 1999). Zhu et al. (2017a) successfully synthesised MCM-41 using a mixed template system composed of CTAB, Triton X-100 (TX-100), triethylolamine (TEA), and non-ionicpolyethylene glycol, with molecular masses of 200, 400, and 6000 (PEG200, PEG400, PEG6000) respectively. In their study fumed silica was used as the silica source.

Generally, MCM-41 is synthesised using tetraethylorthosilicate (TEOS) and silicon alkoxides such as sodium silicate (Hui & Chao, 2006). However, TEOS is an expensive reagent and sodium silicate is traditionally obtained from quartz and sodium carbonate at high temperatures of around 1300 ºC, thus requiring high energy. Apart from the fact that these silicon sources are expensive, they also cause considerable environmental pollution (Shah et al., 2017). This motivates the synthesis of MCM-41 from cheap silica sources such, as rice husk ash or CFA. Conventional synthesis is usually performed via hydrothermal treatment involving a liquid templating mechanism and, in some cases, a pH regulator such as ethyl acetate. After crystallisation and filtration, the template is removed, either by ion exchange or calcination at temperatures between 500 – 550 °C (Panek et al., 2017). Modification to conventional hydrothermal synthesis, such as microwave and ultrasonic-assisted synthesis, have been applied successfully in the preparation of MCM-41 from CFA. Numerous studies have reported on this including: (Run et al., 2004; Yılmaz et al., 2011; Zhu et al., 2017b). However, the synthesis of MCM-41 from CFA via a silica extraction step has not been attempted.

2.5   Preparation of zeolite supported metal catalysts

Numerous preparation routes for metal-loaded zeolite catalysts exist, and are categorised into three main groups, namely: *chemical* (wet impregnation, co-precipitation, deposition-precipitation, atomic layer deposition and electrochemical reduction); *physical* (sonochemical, microwave-irradiation, laser-ablation and supercritical fluid); and *physico-chemical* (sonoelectrochemistry, and flame spray pyrolysis) methods (Zahmakiran & Ozbar, 2013). The main aim in catalyst design is to create a catalyst that is stable, active and selective in the targeted reaction. A preparation approach is chosen that gives sufficient high surface area, good porosity and suitable thermal and mechanical strength. High surface area is an essential characteristic, since it allows reactants to access the active site, thus increasing the turn over frequency (TOF) of the catalyst (Schwarz et al., 1995). The most commonly applied methods are incipient wetness impregnation and ion exchange, due to their simplicity.

2.5.1   Impregnation

There are two main techniques applied in the preparation of supported metal catalyst via impregnation namely; incipient wetness impregnation (IWI) and wet impregnation (WI). IWI involves covering a porous support material, such as zeolites with an amount of metal solution precursor that does not exceed the support's pore volume. The most commonly used precursors are metal salts, such as sulphates, carbonates, chlorides, nitrates, acetates and acetylacetonates. Water is the most widely used solvent, although in some instances organic solvents are used, especially when the precursor choice is organometallic. The amount of metal that can be loaded onto the support is also dependent on its solubility in the solvent. The solution uptake into the pore system of the support is via capillary pressure difference (Δp) across the hemispherical meniscus of pore radius r_P in accordance to the Young-Laplace equation, which is expressed as follows:

$$\Delta p = (2\gamma_{lv}/r_P) \cos \theta$$

Where γ_{lv} is the surface tension between the liquid and vapour interface, and θ is the wetting angle between the solid and the liquid (Munnik et al., 2015). It should however be noted that certain salts, at high concentrations, may alter the pH of the solution. For example, a high concentration of $Ni(NO_3)_2$ reduces the pH, which may result in structural distortions of the support material (Schwarz et al., 1995). Solvent is removed from the

support by evaporation, which is then followed by calcination. If the catalyst required is the oxide form, then calcination in air is performed in order to convert the metal to oxide (Pinna, 1995).

The major difference between IWI and WI is that, the later uses an excess of solvent and the mobilisation of metal ions onto the support is not necessarily influenced by capillary action but diffusion, consequently the loading of metals via WI takes longer time relative to that taken when IWI is applied (Munnik et al., 2015).

2.5.2   *Ion exchange*

In zeolites, the negatively-charged AlO_4^- ion in the zeolite framework creates a deficiency of positive charge. These negatively-charged centres allow single- or double-charged positive ions to enter the pores of the zeolite and counter balance the charge in the framework. These ions can be replaced with others through an approach known as ion exchange. The amount of exchangeable ions depends on the zeolite charge density, which in turn is dependent of the Si/Al ratio of the zeolite. The higher the Si/Al ratio, the lower the charge density. The rate of ion exchange depends on two factors: the concentration of the metal solution, and the size of the metal ion. In the case where water is used as the solvent, the size of the hydration shell on the metal ion determines the ease which allows the ion penetrating the zeolite pore system (Kuhl, 1999).

The most common application of ion exchange is the preparation of the H-form zeolite. After synthesis, the Na-zeolite form undergoes ion-exchange with an ammonium salt. Calcination then converts to its H-form. In some cases, the H-form itself is used as a catalyst without further modification. However, this approach may not be applicable to all zeolite forms, for instance ammonium-exchanged zeolite A and X are known to collapse upon calcination (Townsend & Coker, 2001). In addition, certain metals when present in aqueous solution tend to have a very low pH, which may cause structural collapse of the zeolite. Canfield et al. (2010) reported on the collapse of zeolite X following ion exchange with three different metals: Mn^{2+}, Fe^{2+}, and Co^{2+}. In order to circumvent the structural damage, poly(ethylene glycol) oligomers were used as solvents instead of water, preserving the structure of the zeolite upon metal loading.

2.5.3   Adsorption

Introduction of metals onto zeolite supports via adsorption is effective when low metal loadings are required. The approach is based on electrostatic adsorption, which is mainly governed by the solution pH and the point of zero charge (PZC). The mode of metal deposition on porous supports via adsorption occurs by either outer or inner sphere complex formation. With outer sphere complex formation, metal adsorption occurs by electrostatic interactions such that a layer of charged metal ion complexes counterbalances the support surface charge. Inner sphere complex formation occurs when the zeolite surface groups become directly involved in the binding complex, for instance when surface oxygen or hydroxyl groups enter the first coordination sphere of the metal complex (Munnik et al., 2015). When a host for the metals is involved, selectivity comes into play. In the case of a metal rich effluent such as acid mine drainage, several studies have been carried out to investigate the metal selectivity for the zeolite. Other parameters that govern selectivity include temperature and pH of solution (Motsi et al., 2009). Metal adsorption from waste waters using zeolites has been well studied, however a practical application for the metal-impregnated zeolite after adsorption has not been found.

2.5.4   Other metal loading approaches

Solid-state ion exchange: This involves mixing the zeolite with a metal salt and heating the mixture to temperatures within the range 700 – 800 ºC. The heating facilitates the formation of metal ions, which then diffuse into the pore channels of the zeolite (Chen et al., 2016).

Chemical vapour deposition: This involves flowing a gas precursor into a chamber containing the support. The approach is undertaken at temperatures of about 1000 ºC, and the metal is deposited on the zeolite surface as a thin film (Yan & Xu, 2010).

Deposition-precipitation: This involves the transformation of the metal precursor into an insoluble form, which upon precipitation is deposited exclusively onto the zeolite (Schwarz et al., 1995).

Co-precipitation: It involves the simultaneous precipitation of a soluble component with a macro-component from the same solution by the formation of mixed crystals, by adsorption, occlusion or mechanical entrapment. This is achieved by adjusting the

precursor solution pH from low to higher values. As the pH increases one of the metals precipitates, the pH is further increased until the point where the second metal precipitates too. At this point, the first metal re-dissolves and precipitates together with the second metal (McNaught & Wilkinson, 1997).

Since most of the metal loading approaches employ the use of metal precursor solutions, the potential use of acid mine drainage, as a metal precursor solution in catalyst preparation could be a viable option. The following section presents a brief background of acid mine drainage and its environmental hazards.

2.6   Iron loaded zeolites

A brief overview of the applications of Fe-loaded zeolites in catalysis is presented in Section 1.4. In most of these reactions, the catalysts are prepared from commercial sources. However, CFA contains significant amounts of Fe and numerous approaches of metal extraction from CFA are available in open literature. In a review paper, Prafulla et al. (2016) presents various methods applicable to metal recovery from CFA among which are; magnetic separation followed by acid leaching, high temperature chlorination, alkaline leaching followed by electrolysis. It is against this background that Fe extracted from CFA can be used as a metal precursor in preparation of Fe-loaded catalysts. On the other hand, acid mine drainage contains significant amount of Fe and zeolites have been used for its remediation. This stimulated the idea that AMD or Fe extracted from CFA could also be used as a metal solution precursor in catalyst preparation. A review of AMD is given in the following sections.

2.7   Acid mine drainage

Acid mine drainage (AMD) is caused by mining activities, where the excavation below the natural ground water level exposes pyrites or sulphur-bearing compounds to oxygen and water (McGinness, 1999). AMD is considered as the most severe and long-term problem associated with mining sulphide-containing ores (Warhurst, 1994). In general, most mining areas are rich in sulphide-bearing compounds, usually in the form of iron sulphide pyrites (Murcott, 2012). Iron sulphide (FeS_2) in particular is a major cause of water pollution from mining activities (Strydom & King, 2009). When the sulphide bearing ores are exposed to water and oxygen they oxidise via a series of autocatalytic

reactions, giving rise to elevated concentrations of dissolved sulphates (Murcott, 2012). Since the oxidation reactions involved are autocatalytic, it makes it very difficult to control the pollution generated (Warhurst, 1994). This oxidation results in the formation of sulphuric acid, iron oxides and hydroxides, which may be further intensified by bacterial (mostly *Thiobacillus ferroxidans*) activity, which causes the pH to fall to levels as low as 1.5. In general, the oxidation reactions are presented according to the following scheme.

$$2FeS_2 + 7O_2 + 2H_2O = 2Fe^{2+} + 4SO_4^{2-} + 4H^+ \tag{2.1}$$

$$Fe^{2+} + \frac{1}{4}O_2 + H^+ = Fe^{3+} + \frac{1}{2}H_2O \tag{2.2}$$

$$Fe^{3+} + 3H_2O = Fe(OH)_3\,(s) + 3H^+ \tag{2.3}$$

$$FeS_2\,(s) + 14Fe^{3+} + 8H_2O = 15Fe^{2+} + 2SO_4^{2-} + 16H^+ \tag{2.4}$$
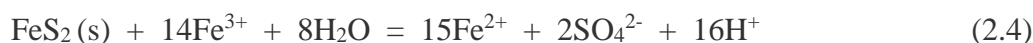
Reaction (2.1) initiates the fundamental oxidation reaction, producing ferrous iron and acid. Reaction (2.2) describes the oxidation of ferrous iron to ferric iron, while reaction (2.3) shows the conversion of ferric iron to ferric hydroxide, with production of more acid. Reaction (2.4) becomes primary, once enough Fe^{3+} is produced. Once the acid generating material has been exposed to the atmosphere, there is no need for a constant supply of oxygen (McElfish & Beier, 1990).

The oxidation brings about a reduction in the solution pH and an increase in the concentration of dissolved ions, especially Fe. The rate of oxidation in the presence of bacteria can be 20 – 100 times faster than normal oxidation in air alone (Warhurst, 1994).

The sulphate solution produced via the oxidation process increases the solubility of As, Co, Fe, Mg, Ni and U, so in most cases AMD has a host of metals in it. When the AMD evaporates the metal- and metalloid-containing salts re-dissolve with the next watering, releasing metals and acids into solution. This gives rise to seasonal sharp concentration increases of metal and metalloids in water systems (Murcott, 2012).

The surface area of mine tailings is much larger compared to that of the ore underground, meaning when mine tailings are brought above ground they have a much higher chance of forming AMD. Naturally, minerals do produce acid, but at such a slow rate that water

can easily buffer the acid formed. Unfortunately, the rate of acid formation from mine tailings is so high that the natural buffering effect is outpaced (Strydom & King, 2009).

2.7.1 *Environmental Hazards of AMD*

AMD has been shown to have serious negative environmental impacts, and is a major threat to water bodies (rivers, lakes and ground water) in areas where it is produced (Ramontja et al., 2011). Its high acid content mobilises metals that may be contained in adjacent rock and sediment, with the resultant drainage containing toxic metals such as Fe, Cd, Zn, Al and Mn. These toxic metals are harmful to aquatic organisms, and when absorbed by fish through their gills, may result in chronic or acute toxicity, and impaired respiration. Fish may also be affected via ingestion of contaminated sediments and food sources. When fish are affected, toxic metals can eventually find their way into the human food chain (Strydom & King, 2009).

Aluminium is generally harmless to plants in neutral soils, but in acidic soils can hamper plant growth (O'Shea, 2005). Aluminium binds to inorganic phosphorus (a macronutrient required for plant growth), reducing its bioavailability. The metal can also be taken up by hyperaccumulative species and can concentrate to levels toxic to herbivores (Sparling & Lowe, 1996). In humans, Al has been exposed as playing a role in Alzheimer's disease (Tomljenovic., 2011).

Manganese is vital for physiological function in both humans and animals. However, chronic exposure leads to a condition known as Manganism, and to Parkinson's disease. This is characterised by visual impairments, eye-hand coordination, hand unsteadiness, lethargy, tremors and psychological disturbances. It is also associated with respiratory effects, impotence and loss of libido (Singh, 2005; O'Shea, 2005).

Iron is also essential to all living organisms, but when it is taken in excess it becomes toxic. Organisms uptake iron via ingestion of water and food. High levels of iron may lead to reduced uptake of nutrients, due to the formation of iron hydroxide encrustment on the gut lining. Excess iron intake may also lead to DNA and membrane damage. When iron is in domestic water it may induce rusting of plumbing fixtures and staining of laundry, and may also give a metallic taste to water (Vuori, 1995; O'Shea, 2005). Apart from Fe, Al and Mn, AMD contains a host of other toxic metals, which in general are

associated with severe detrimental effects to both fauna and flora at low concentrations. The effects are usually long lasting (Strydom & King, 2009).

2.7.2   AMD in South Africa

In the South African context, the issue of AMD has received much attention as an environmental pollutant (Ramontja et al., 2011). South Africa is already a water-poor country. With increasing industrialisation and population growth, the demand for clean water is on the rise. The release of AMD into the water sources has resulted in high salinities of water which consequently has brought about an unacceptable degradation in water quality (Vermeulen & Usher, 2009). The AMD is generated from present and former gold and coal mining areas. Gold mining in the Witswatersrand in Gauteng province commenced more than a century ago in 1886 and is still going on in many areas. The voids left by the exercise and the surface mining deposits resulting from mining, milling and ore processing are responsible for the formation of AMD in these areas. Since most mines have closed or have scaled down mining activities the practice of pumping water from underground to arrest the massive formation of AMD has stopped in some places. In September of 2002 the water in the void day lighted in the West Rand Gold Fields. This has presented severe ecological impacts. The water levels in Central and East Rand Gold Fields continue to rise, posing a possible catastrophe (Ramontja et al., 2011).

When the water level is rising the water reacts with oxygen and sulphide ores to produce AMD and in certain instances the AMD produced on the surface may seep underground and recharge the mine voids resulting in an increase in the AMD generated underground (Strydom & King, 2009: Ramontja et al., 2011).

Apart from gold mining areas, coal mining areas have also been cited as sources of AMD. Coal is the primary source of electricity generation in South Africa (Eskom, 2018). Coal mining activities take place mostly in the Mpumalanga province with other activities going on in Kwa-Zulu Natal, and the eastern and southern parts of Gauteng, and also in the northern parts of the Eastern Cape (Ramontja et al., 2011). Coal mining in the Mpumalanga coalfields has been going on for over a century and is done via two approaches namely the open cast and the underground methods. The depth of these mines range from 10 m to over a 100 m. In such circumstances when the mine is closed the water flows on the mine seam floor and accumulates in the low lying areas resulting in

the voids in those places filling up. This then creates a hydraulic gradient forcing the water to either rise to the surface or move to adjacent mine voids, a phenomenon referred to as intermine flow. In the case where the water rises to the surface it reacts with oxygen and sulphide bearing ores creating AMD (Vermeulen & Usher, 2009).

AMD has been cited as a major pollutant in the Vaal River and the Olifants River. The Vaal River is a source of water to many urban, industrial and farming areas (Ramontja et al., 2011). It supplies most of Gauteng province, Eskom power stations and the Sasol petrochemical plants in Mpumalanga, the North-west and the Free State goldfields, Kimberly and numerous small towns and communities along the river course. It is also the source of water for the Vaalharts Irrigation scheme (Van Wyk et al., 2010).

In the case of South Africa there are three main sources of AMD that are common in former and present mining areas. These are (Xu & Usher, 2006):

- *Spoil heaps*:   these are associated with former mining areas in the West Rand group of   mines.

- *Rock Dumps*: these are coarse rock waste created due to off-reef developments such as underground access routes. Although the rocks do not contain much in terms of mineral they do however contain significant amounts of pyrites.

- *Slimes dams*:   the fine metallurgical waste is deposited wet and the resulting dams have great potential for producing AMD that may seep underground.

From the predicament that South Africa is placed in with regard to the issue of AMD it is apparent that there is a need to get rid of the possible catastrophe that may befall the already compromised water resources. Treatment of AMD is a complex matter but if a way to utilise it for creating a beneficial material can be devised this may act as a sort of waste utilisation as well as providing a cheap metal precursor for various purposes in catalysts synthesis. In the next section, the Friedel-Crafts alkylation reaction is reviewed. The reaction has been studied over numerous catalytic systems, among which is Fe loaded zeolites.

2.8   Friedel Crafts alkylation of benzene

The general background of the Friedel-Crafts (FC) alkylation of benzene alongside the respective applications of the products of the reaction is presented in Chapter 1. The FC alkylation involves the formation of new C-C bonds via an electrophilic aromatic substitution (S_EAr) in the presence of either a Lewis acid or a Brønsted acid catalyst.

2.8.1   Alkylation of arenes

The FC-alkylation of arenes was initially thought to be a simple and straightforward reaction upon its discovery. However, further study has shown that the reaction is complex, and is usually accompanied by isomerisation and polyalkylation. In certain cases, the reaction is characterised by the formation of by-products from dealkylation, transalkylation and the formation of saturated hydrocarbons. Arene alkylation is not limited to benzene alone, but occurs with other benzene homologues such as naphthalene, indene, phenanthracene and anthracene. It is also possible for fused polycyclic rings such as tetraphenyls, bibenzyl, diphenyl methane and biphenyl to be alkylated in the same manner. These include compounds such as biphenyl, diphenyl methane, bibenzyl and tetraphenyls. However, the polycyclic aromatics usually give low yields due to their own high reactivity under the FC operation conditions. Alkyl groups attached to the benzene ring are expected to be ortho- and para-directing to the incoming substituents. However, it was established that it is possible to have a meta-substitution in the event that the alkylbenzenes are monoalkylated.

2.8.2   Alkyl benzenes

The term alkyl benzene is used to refer to a single ring aromatic hydrocarbon with a range of aliphatic side chains attached to the ring. These liquid compounds are characterised by low boiling points, and are used as solvents and as intermediates in synthetic chemical processes. Some of their most popular applications include their use in the manufacture of plastics, and as an additive to gasoline, replacing Pb as an anti-knock agent. They are also used as blending stocks to increase octane number in fuels (Snyder, 1981), as well as in detergent manufacture, where they are used as intermediates. When a branched chain alkyl group is employed, the resulting product is a hard non-degradable alkylate (branched alkyl benzene (BAB)), while when a straight chain alkyl group is used, a soft, degradable, linear alkyl benzene (LAB) is produced. Due to the non-degradability of BABs, most industrial surfactants are based on LABs - for instance, Unilever has since

the 1960's replaced BABs with LABs (Dutilh, 1998). The liquid phase production of LABs employs the use of linear mono-olefins or alkyl chlorides using liquid HF and $AlCl_3$ respectively as catalysts (Riegel, 2003). To date, LABs are still the most preferred raw materials in worldwide surfactant production. They have since replaced soap as industrial surfactants due to the shortage of natural oils and fats that are essential raw materials in soap production (Adami, 2009). The robust characteristics of alkyl benzenes - such as low temperature fluidity, low pour points and stability against oxidation, high temperature decomposition and hydrolysis - have found them favourable for use as lubricants and refrigerants (Michels & Sienel, 2003). These applications have given alkyl benzene economic importance.

Conventionally, the alkylation of benzene to produce alkyl benzenes via the Friedel-Crafts alkylation reaction is catalysed by homogeneous Lewis acids (such as $AlCl_3$) or strong Brønsted acids (such as HF), which are both toxic and corrosive (Devassy et al., 2005). When an alkyl halide is treated with $AlCl_3$, there is formation of an electrophilic carbocation. The $AlCl_3$ forms a complex with the Cl in the alkyl halide resulting in the weakening of the C-Cl bond and consequently inducing charge separation in accordance with the following scheme:

Reaction scheme 1.1: Dissociation of alkyl halide by $AlCl_3$

The electrophilic carbocation formed is attracted to the π electron cloud of the benzene ring and takes two electrons from the electron cloud, forming a σ C-C bond. This is the rate-determining step, and results in the formation of a carbocation intermediate/arenium ion, called Wheland intermediate. The arenium ion goes on losing a proton, forming a neutral alkylated ring (R-Ph) together with HCl, and the AlCl3 is regenerated (McMurry, 2012; Fox et al., 2004).

2.8.3   *Mechanistic aspects of aromatics alkylation*

The (S_EAr) reaction by which the alkylation of aromatics is performed is one of the most well-studied mechanisms in organic synthesis. The reaction has more than 20 distinctly

different types of substitutions, but all are characterised by a common overall mechanism, which involves interaction of the electrophile with the π-system of the aromatic ring (Klumpp, 2016). Usually the commonly employed electrophiles in the FC-alkylation reaction are alkyl halides. The reaction mechanism is generally described by three steps as depicted in the following scheme:
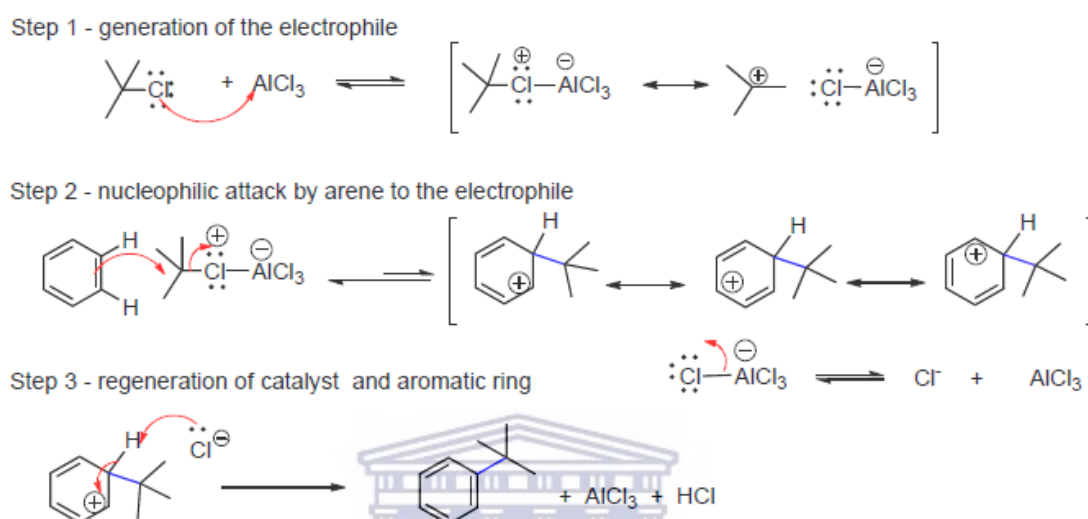
Reaction scheme 1.2: Mechanism of benzene alkylation in the presence of AlCl₃ (Rueping & Nachtsheim, 2010)
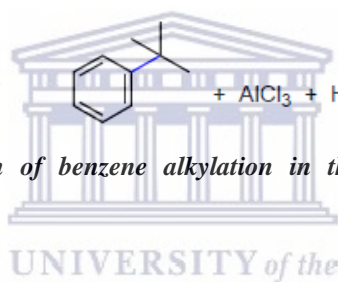
In step 1, the reaction of the tertiary chloroalkane and $AlCl_3$ forms a coordination complex which further breaks down to form a carbocation and $[AlCl_4]^-$. The rate of formation of the coordination complex is dependent on the stability of the carbocation. The stability of the carbocations follows the order: tertiary > secondary > primary, thus tertiary carbocations are more rapidly formed from the coordination complex than the secondary or primary. Secondary and tertiary carbocations are strong electrophiles and in step 3 there is movement of two electrons from the aromatic ring to the carbocation, resulting in the formation of the alkyl benzene alongside HCl, while the $AlCl_3$ catalyst is regenerated (Burrows et al., 2013). When a primary chloroalkane is used in the reaction, it forms a primary carbocation which is less stable and will rearrange to form more stable carbocations. For example, $[CH_3CH_2C^+H_2]$ rearranges to form the corresponding secondary carbocation via a hydride $[H^-]$ shift. Due to the rearrangement associated with primary chloroalkanes, it becomes difficult to predict the way a particular carbocation

will rearrange, but generally the more stable carbocations are preferred. A secondary carbocation, when formed, can only rearrange to form a tertiary carbocation and not a primary one. The rearrangements of the carbocations in the preparation of alkyl benzenes from alkyl halides means that producers face the problem of receiving a mixture of products, and potentially not even the desired product (Taylor & Gagan, 2007). An example of a possible outcome can be depicted by the reaction of 1-chlorobenzene with benzene over AlCl$_3$ as catalyst. The reaction is presented in the following scheme:
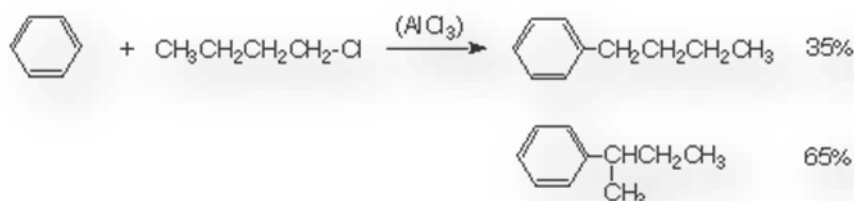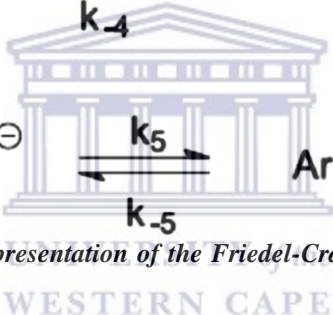
Reaction scheme 1.3: Alkylation of benzene with 1-chlorobutane over AlCl$_3$ (Klumpp, 2016).

Apart from alkyl halides, several other alkylating agents can be employed in the FC alkylation of benzene, the most common including: alcohols, alkenes, olefins, ethers, highly strained cyclo-paraffins and esters. There are also numerous catalysts that are being applied in the FC alkylation reaction, both at laboratory and industrial scale. Commonly employed catalysts include: FeCl$_3$, SbCl$_5$, BF$_3$, ZnCl$_2$, TiCl$_4$, HF, H$_2$SO$_4$, H$_3$PO$_4$ and P$_2$O$_5$ (Adams, 1946). Recently, superacids such as HF•SbF$_5$ and HSO$_3$F•SbF$_5$ have also been employed in the FC reaction. However, these catalysts are associated with a number of challenges, including handling, storage, high wastage and the lack of good product selectivity (Rueping & Nachtsheim, 2010).

Product selectivity in FC alkylation of benzene with alkyl halides can greatly be improved by the use of supported acid catalysts. Apart from improving the selectivity, supported acid catalysts are much easier to separate from the products, compared to traditional mineral acids (Harmer et al., 2001). In research carried out by Birdat et al. (2006) Fe-loaded zeolite Y was used in the alkylation of benzene with alkyl halides. A high selectivity of 98 % towards the formation of the mono alkylated product was achieved. This was alongside an alkyl halide conversion of 96 %. The FC alkylation of benzene

over Fe-loaded zeolites progresses via the steps presented in the following scheme (Birdat 2006):

$$RCl + Fe^{3+}Z \underset{k_{-1}}{\overset{k_1}{\rightleftharpoons}} RCl^{\dot{+}} + Fe^{2+}Z$$

$$RCl^{\dot{+}} + Fe^{2+}Z \underset{k_{-2}}{\overset{k_2}{\rightleftharpoons}} R^{\oplus} + Fe^{2+}Z + Cl\cdot$$

$$R^{\oplus} + Fe^{2+}Z + Ar\text{-}H \underset{k_{-3}}{\overset{k_3}{\rightleftharpoons}} Ar\overset{\oplus}{<}\begin{smallmatrix}H\\R\end{smallmatrix} + Fe^{2+}Z$$

$$Cl^{\bullet} + Fe^{2+}Z \underset{k_{-4}}{\overset{k_4}{\rightleftharpoons}} Cl^{\ominus} + Fe^{3+}$$

$$Ar\overset{\oplus}{<}\begin{smallmatrix}H\\R\end{smallmatrix} + Cl^{\ominus} \underset{k_{-5}}{\overset{k_5}{\rightleftharpoons}} Ar\text{—}R + HCl$$
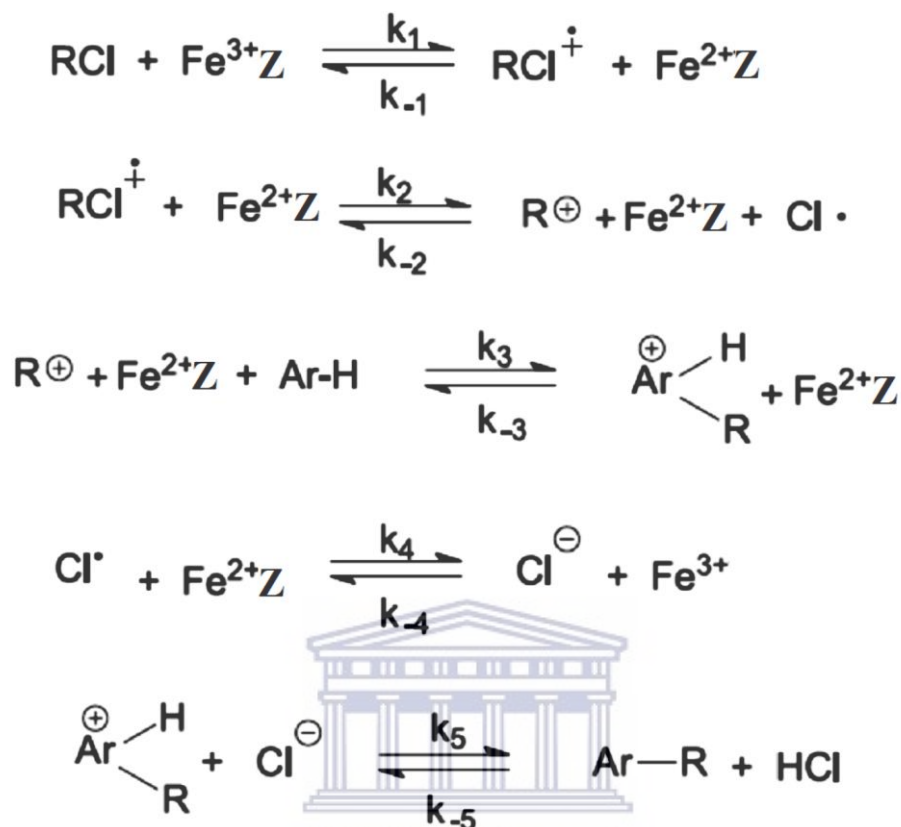
Reaction scheme 1.4: Mechanistic presentation of the Friedel-Crafts alkylation of benzene with alkyl halides over iron loaded zeolites.

In FC alkylation of benzene with alkyl halides over Fe-loaded zeolites, the first step involves a single electron transfer between the alkyl halide and the iron species to generate a cation radical. The resulting radical then goes on to interact with the reduced iron species (Fe^{2+}), forming a carbocation and a chlorine atom. The carbocation, which will go on to alkylate the aromatic ring, can either be free, or bonded to the zeolite framework. The kinetics and mechanism of the reaction is dependent on the nature of the iron species, thus the nature of the iron may alter both the kinetics and the rate determining step (Birdat, 2006).

2.8.4 Kinetics and thermodynamics

Although FC alkylation is one of the most studied reactions, there are only limited reports available in open literature on the kinetics of the reaction (Carey & Sundberg, 2007). In the alkylation of benzene with ethyl bromide in the presence of $GaCl_3$ as catalyst, the reaction is first order with respect to each reactant. However, when the catalyst is changed to $AlCl_3$ the kinetics changes with time, this phenomenon being ascribed to the heterogeneity of the reaction matrix. The initial rate of the reaction is described by the following expression:

$$\text{Rate} = k \, [\text{EtBr}][\text{benzene}][\text{AlBr}_3]^2$$

The alkylating agent also has a significant impact on the kinetics of the reaction. Considering the aforementioned reaction, replacing ethyl bromide with t-butyl benzene and using $AlCl_3$ as catalyst, the reaction rate follows third order kinetics as presented in the following expression:

$$\text{Rate} = k[\text{AlCl}_3][t\text{-butylchloride}][\text{benzene}]$$

The kinetics of a particular FC reaction can only be determined after taking into consideration the three fundamental factors that govern FC alkylation kinetics, namely:

- The complexation of the alkylating agent and the Lewis acid (in certain cases the ionisation of the complex results in the formation of a discrete arenium ion).
- Electrophilic attack on the aromatic ring.
- Disproportionation.

The rearrangement commonly witnessed in the alkyl halide is attributed to the formation of the arenium ion. The rearrangement happens in such a way that the most stable cation is formed and it follows the order tertiary > secondary > primary (Smith & March, 2007). The rearrangement of the carbocation can however be avoided if a transition metal based catalyst is employed. This is due to the fact that the intermediate complexes are less reactive than uncomplexed arenium ions. Alkyl halides that have the halogen bound to the leaving groups (positions where the carbocation would be stabilised) are electrophilic,

and if the alkyl halide concentration is low, the aromatic ring may undergo acid-catalysed oxidative dimerisation rather than alkylation. This phenomenon is observed mostly with electron rich arenes, such as phenols and anilines (Dorwald, 2014).

The rearrangement of the alkyl halide occurs via the relocation of smaller groups to the adjacent carbon atom. This phenomenon makes it more challenging to introduce a primary alkyl halide onto the arene. A typical example is the alkylation of benzene with *n*-propyl bromide. In this particular reaction the product mixture is comprised mostly of isopropyl benzene and minimal amounts of *n*-propyl benzene. Based on this limitation, the preparation of *n*-alkyl benzenes is usually achieved via a step reaction begun with acylation, and followed by reduction (Smith & March, 2007). In most cases the rearrangement is associated with isomerisation, and proceeds either via a 1,2 shift, or via a dissociation to cation and subsequent readdition. Smith (1946) reported that when *sec*-butylbenzene was exposed to a mixed acid (HF-BF$_3$), the product mixture was composed of 36.7 % benzene, 10.9 % *n*-butylbenzene, 21.8 % of *sec*-butylbenzene and 30 % of di-*sec*-butylbenzene. The same work also reported on a related reaction in which *n*-butylbenzene was heated with AlCl$_3$ at a temperature of 100 ºC, for a period of 3 hours, obtaining a product mixture of composition: 45.2 % butylbenzene (> 99.4 % *n*-butylbenzene and 0.6 % *sec*-butylbenzene) 15.2 % benzene, 27.7 % di-butylbenzene (> 90 % meta), and 11.9 % of polyalkylated benzene products. These results lead to the conclusion that Lewis acid-induced isomerisation of dialkylbenzenes favour the formation of the meta isomer relative to the ortho- and para-isomers. This is due to the fact that the meta isomer is more thermodynamically stable, relative to the others.

In the FC alkylation of benzene with t-butyl chloride over AlCl$_3$ catalysts, a 1:1 mole ratio of benzene to alkylating agent produces the di-alkylate as the major product with relatively lower amounts of monolakylate. This outcome is due to the fact that the monoalkylated product is more active than benzene itself, hence easily leading to the second alkylation, and formation of the dialkylate. To suppress formation of dialkylkated product, an excess of benzene can be used (McMurry, 2012). The use of zeolites on the FC alkylation reaction has significant impact on the product selectivity. The following schematic diagram depicts how the zeolite pore system affects product selectivity.
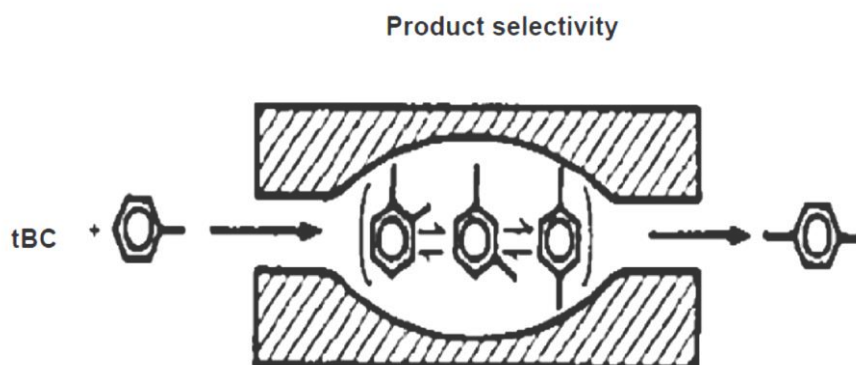
Figure 2. 8: A schematic presentation of the product selectivity through the zeolite channel system in the second alkylation off benzene by t-butylchloride (tBC)

Application of zeolites, such as HBEA, H-ZSM-5, H-CIT, H-MCM-22, H-SSZ and H-SAPO-5, tend to favour the formation of the para isomer relative to the meta isomer, due to the product shape selective ability of the zeolite pore system. This occurs despite the fact that the meta isomer is more thermodynamically stable. However, the acid site on the external surface of the zeolite can allow the formation of the meta isomer but the concentration of the meta isomer will be relatively small in comparison to the amount of the para isomer. A typical example is the dialkylation of biphenyl with propylene, in which the para isomer is selectively formed inside the zeolite pore channels. The same occurs in the dialkylation of benzene, the para isomer is selectively formed (Birdat, 2006).

2.8.5   Catalysts used in the FC reaction

As previously mentioned, the FC alkylation reaction is a major route for the synthesis of alkylated aromatics, and since its discovery numerous catalysts have been applied to facilitate the transformation. The following table presents a summary of the most commonly used catalysts for the reaction:

Table 2.3: Common acid catalysts used in the Friedel-Crafts alkylation reaction (Wasserscheid, & Joni, 2010)

catalyst groups	Examples	Acid type
Metal halide	$AlCl_3$, $AlBr_3$, BF_3, $ZrCl_4$, $FeCl_3$	Lewis acid
Metal alkyles and Alkoxides	AIR_3, BR_3, ZnR_2, $Al(OPh)_3$	Lewis acid
Protonic acids	H_2SO_4, HF, H_3PO_4, HCl	Brønsted
Acidic oxides/sulphide	Zeolite, BeO, Cr_2O_3, P_2O_5, TiO_2, $Al_2O_3SO_3$	Brønsted/Lewis acid
Supported acids	H_3PO_4-SiO_2, BF_3-Al_2O_3	Brønsted/Lewis acid
Cation exchange resins	Permutit Q, Amberlite IR 122, Dowex 50, Nafion-Silica, Deloxan	Brønsted acid

The advocacy for green synthesis routes in organic chemistry has drawn attention to the use of solid acid catalysts in the FC reaction. Heterogeneous catalysts such as clay minerals and zeolites have been studied and the outcomes obtained prove that these materials are effective alternatives as catalysts in the FC reaction. The most commonly used zeolites and clays include BEA, MMT, ERB, ZSM-12, KIT, MOR, FAU, ZSM-5, TNU-9, SSZ-33, ZSM-12, MCM-22, MCM-41 and MFI (Caeiro et al., 2006; Perego, et al., 1996; Degnan et al., 2001; Emana & Chand, 2015; Jun & Ryoo, 2000; Shinde & Rode, 2018).

In the FC alkylation of aromatics, the zeolites are usually modified by metals, which alters the Brønsted acidity as well as the metal state. These alterations bring about changes in the metal site density and acid strength distribution. In addition, the zeolite support influences the metal dispersion, which consequently changes the overall reaction mechanism as well as adsorption on the active sites. In the design of an efficient FC alkylation catalyst there is need for the optimisation of both the chemical and physical factors of the catalyst to obtain optimum reaction kinetics and selectivity (Dimian & Bildea, 2008).

Zeolite modification in the design of FC alkylation of aromatic catalysts can be achieved with a range of metals. In a review of the metal catalysts applied in the FC alkylation reaction, Rueping and Nachtsheim (2010) present a list of transition metals and lanthanides that are able to catalyse the alkylation of aromatics, when supported on

zeolites or attached to organic ligands. The following figure depicts the range of these metals:

Figure 2. 9: Commonly used metal salts for the catalytic alkylation of aromatics (Rueping & Nachtsheim, 2010).

Apart from transition metals and lanthanides, alkali and alkali earth metals have also proved to be effective in the catalysis of aromatics by the FC reaction. Yashima et al. (1972) successfully loaded alkali metals (Li, Na, K, Rb and Cs) on zeolite X and zeolite Y, and applied the catalysts to the alkylation of toluene with methanol. All the alkali metals proved to be active, although having different activities.

Alkali earth metal such as Ca and Mg have also been applied with good success. Iliuta et al. (2001) reported on the successful application of Ca modified zeolite Y on the FC alkylation of benzene with propylene. A bimetallic catalyst composed of B and Mg supported on HZSM-5 was also used with success for the alkylation of benzene with ethanol (Emana & Chand, 2015).

On the basis that a range of metals can effectively facilitate the alkylation of aromatics by the FC alkylation reaction, the use of acid mine drainage as a metal precursor is therefore thought to be a feasible approach in the designing of FC alkylation catalysts,

since AMD contains a range of metals from alkali, earth alkali, transition and lanthanide elements.

2.7.6   *Effect of arene/alkyl alkylating agent molar ratio*

When traditional Lewis acid or homogenous catalytic systems are employed in the FC alkylation, the molar ratio of aromatic compound to alkylating agent plays a significant role in determining which by-products are formed. Alam et al. (2015) studied the effect of molar ratios in the alkylation of phenol with benzyl alcohol in the presence of p-toluenesulphonic acid, and found that as the phenol to benzyl alcohol ratio increased there was a marked increase in the yield of benzylphenol. The lower the molar ratio, the lower the reacting species for the benzyl group of benzyl alcohol, in turn resulting in lower amounts of reaction product. In a related study carried out by Cai and Wang (2015), in which a range of aromatic compounds (phenol, anisole, acetanilide and toluene) were alkylated using *t*-butylalcohol and bromoethane in the presence of imidazolium-based ionic liquid, it was reported that as the amount of alkylating agent relative to that of aromatic compound resulted in an increase in conversion up to a maximum before starting to decline. The lower conversions that were achieved at higher alkylating agent concentration were ascribed to the dilution of the active carbenium ion, which consequently weakened the alkylation and hence the reduced conversion.

However, if alkylation reactions are carried out over metals immobilised upon zeolites, the product selectivity is independent of the reactant molar ratios. This is due to the fact that the reaction occurs within the zeolite pore system and the channels are responsible for determining the product selectivity. However, there are chances of compromising the selectivity, in cases where the metals on the external surface catalyse the reaction (Bidart et al., 2006).

2.8.7   *Effects of temperature*

Reaction temperature has a marked influence on both the thermodynamics and kinetics of a reaction. The FC alkylation of aromatics reaction is exothermic, hence high temperatures impede the formation of the desired product from a thermodynamics perspective. However, lower temperatures usually slow down the reaction rate, and therefore there is a need to compromise between thermodynamic and kinetic factors, when choosing an operating temperature for the reaction (Sun & Zhao, 2006; Cai et al.,

2008). In a study carried out by Bidart et al. (2001), in which the alkylation of benzene using various alkyl halides over Fe supported on zeolite Y was performed, it was found that for primary alkyl halides the increase in temperature had no significant effect on the yield of the monoalkylated product. However, a slight increase in yield with increasing temperature was noted with both secondary and tertiary alkyl halides. The reactions were conducted at moderate temperatures of less than 100 ^{0}C. Cai et al. (2008) studied the alkylation of benzene with dichloromethane over acidic ionic liquids catalysts. As the temperature was increased there was an increase in the conversion of the benzene, reaching a maximum of 83.8 % at a temperature of 80 ºC. Further increase in temperature resulted in a decrease in the conversion, with the conversion dropping to 68 % at 90 ºC. One can infer that the reaction changed from being kinetically controlled to thermodynamically controlled.

2.8.8   *Effect of reaction time*

The general trend in the FC alkylation of aromatics is such that there is an initial increase in the conversion at the beginning of the reaction, but after a period of time the conversion levels off and remains constant. This is a general trend with most reactions, however reaction time has a unique effect on the FC alkylation reaction product selectivity. Prolonged reaction times tend to favour the formation of the thermodynamically stable isomers in cases of di or polyalkylation. In the alkylation of benzene by alkyl halides over Fe loaded zeolilte Y, Bidart et al. (2001) found that times of over 3 hours favoured the formation of the meta isomer, relative to the ortho and para dialkylated products. The meta isomer is more thermodynamically stable, relative to the two counterparts. However, this trend is not necessarily the same with homogenous catalytic systems. In a related study in which benzene was alkylated using dichloromethane over ionic liquid catalysts by Cai et al. (2008), it was found that the selectivity to diphenylmethane remained unchanged with time. This outcome is ascribed to the fact that the product is immiscible with the ionic liquid catalyst used, hence once formed it would rapidly diffuse into surrounding benzene, hence avoiding any further interaction with the catalyst, and suppressing the chances of further reactions.

2.8.9   *Effect of catalyst loading*

The amount of catalyst loaded plays a significant role on both the conversion and product selectivity. An increase in the catalyst charge leads to an increase in the conversion, but

in case of zeolite supported catalyst, a very high catalyst charge allows for the reaction to occur on the external surface, consequently altering the product selectivity. Alotaib et al. (2017) reported that when benzene was alkylated by propane over Pd-acid catalysts, the conversion of the benzene increased with Pd loading, levelling off at about 2 % Pd loading. In a related study by Hlatywayo (2014), in which benzene was alkylated with t-butylchloride over Fe modified zeolite HBEA, the same trend was observed: increase in Fe-loading from 0 – 10 % resulted in a similar increase in conversion.

2.8.10 Recent Advances in the FC reaction

Traditionally, the FC alkylation reaction has always been characterised by the release of acid when alkyl halides were used as alkylating agents. The need for stoichiometric or super stoichiometric amounts of Lewis acid or Brønsted acid to catalyse the reaction has also been a major drawback. Recent advocacy for green synthesis routes in organic chemistry have highlighted the need to consider more environmentally-friendly approaches. These calls have generally translated into a search for sustainable and green catalysts, as well as alkylating agents. When alcohols are used as alkylating agents, they produce water, resulting in increased attention in the use of alcohols in the FC reaction. Another advantage alcohols have is that they are readily available, cheap and of low toxicity (Rueping & Nachtsheim, 2010). Bandini and Tragni (2009) successfully carried out the alkylation of various aromatic compounds using π-activated alcohols over different metal complexes catalysts. Unfortunately, this approach is limited when using solid acid catalysts, since the evolution of water from the reaction deactivates the FC catalysts. The deactivation occurs via an irreversible coordination to the hydroxyl group or via hydrolysis of the water involved. This implies the need for large amounts of additives being used.

Apart from the alkylating agents used in the FC reaction, focus has been put on the nature, sustainability and efficiency of the catalysts applied for the transformation, with organometallic complexes emerging as catalysts with good potential. Bhattacharya et al. (2017) investigated the use of iron triflate as a catalyst for the FC alkylation of arenes with cinnamic acid ester derivatives to yield 1,1-diarylalkanes. The iron triflate proved to be a robust catalyst in the FC alkylation, with α,β-unsaturated carbonyl compounds.

The reaction gave good yields of β,β-diaryl carbonyl in the range of 65 - 95 %, with outstanding regioselectivity.

Another range of emerging green catalysts for the FC reaction are ionic liquids. In a review, Qureshi et al. (2013) presented numerous successful outcomes of arene alkylation using different ionic liquids. While the major drawback associated with homogenous catalytic systems is product separation, Joni et al. (2009) report on the successful immobilisation of ionic liquids onto solid silica support. The silica was coated with acidic chloroaluminate ionic liquid, and proved to be active and selective in the FC alkylation of cumene.

Zhu et al. (2015) report on the successful development of a novel and facile method for the FC alkylation of naphthols with β-haloketones in aqueous solvent without the use of any Lewis acid. In a related study by Halimehjani et al. (2009) a catalyst-free FC alkylation of naphthols with nitrostyrenes in the presence of water is reported. From the investigation, the conversion and yields obtained were very high.

Despite significant strides made in homogeneous FC catalytic systems, the use of solid supports still holds the advantage of easy product separation. Several solid materials have been successfully employed as catalyst support for the FC reaction. In a review, Perego & Ingallina (2002) present various solid support materials that have been applied with good success in the FC reaction. These include zeolites, clays, heteropolyacids and sulphated zirconia. Recently Rahmani and Rahmani (2018) investigated the use of Al and Li supported on metal organic framework MIL-53, in the FC alkylation of benzene with ethanol, which achieved a conversion of 100 % over the bimetallic Al/Li- MIL-53.

2.9 Chapter summary

The literature reviewed in the present work has given a background on zeolite properties, application and synthesis. The effect of various synthesis parameters such as mineraliser, aging time, structure directing agent, pH, crystallisation time and agitation time were reviewed. The evolution of zeolite synthesis approaches was presented ending up with the recent advances include the solvent-free synthesis, low water and non-aqueous

syntheses, ionothermal and deep eutectic mixtures syntheses and finally computer assisted synthesis. However, these approaches require expensive feedstocks. The synthesis of zeolites from waste materials was presented with emphasis on the use of coal fly ash as a feedstock in zeolite synthesis. The environmental and health hazards associated with coal fly ash were also presented. Since the present work is focused on the synthesis of zeolite HBEA and MCM-41, these materials were reviewed focusing on their structure, properties and synthesis from coal fly ash. The approaches traditionally applied in the synthesis of these materials involve a fusion step followed by a hydrothermal treatment. The approach results in the formation of zeolites with considerable impurities from the coal fly ash. It is in this vein that the present work proposes to synthesise the materials via a novel approach that involves acid assisted silica extraction from the coal fly ash after fusion. The extracted silica will further be treated with oxalic acid to remove any residual metal ions such as Ca, Al and Na. This is done to ensure that the silica is almost 100 % pure and the resultant zeolite synthesised would be of high purity. For the first, time the work reports on the synthesis of these materials using this approach.

The preparation of metal loaded zeolites can be undertaken via numerous approaches, and these were reviewed with much emphasis on two conventional approaches used in the present work namely, ion exchange and wet impregnation. In the case when a metal precursor solution such as AMD whose metal ion concentration is usually in the ppm range, wet impregnation is more appropriate since to achieve a high metal loading a larger volume of metal solution precursor is required. The suitability of these approaches in the preparation of Fe loaded porous supports was highlighted. The chapter further reviewed the different applications that employ the use of Fe loaded zeolites in catalysis, both in organic and inorganic synthesis reactions. Considering the importance of Fe loaded zeolites in catalysis, it then became interesting to explore the possibility of using acid mine drainage or Fe extracted from coal fly ash as precursor metal solutions. Acid mine drainage contains a host of metal ions with Fe being the major ion. Furthermore, one of the treatment approaches applied in AMD remediation is adsorption and ion exchange over zeolitic materials. The capacity of zeolites to act as adsorbents and to ion exchange makes them attractive materials in these processes. Since metals from AMD can be adsorbed onto zeolites, it became interesting to investigate the feasibility of using AMD as a precursor solution in catalyst synthesis. It is again for the first time that the application

of AMD and Fe extracted from coal fly ash are used as precursor solutions in the synthesis of heterogeneous Fe catalysts.

Considering the fact that Fe loaded zeolites have vast applications in catalysis, a probe reaction was chosen for the investigation of the activity of the Fe catalysts prepared from AMD and Fe extracted from coal fly ash. The probe reaction selected was the Friedel-Crafts alkylation of benzene with tertiary butyl chloride as it is well known and comparisons can be made with literature. The mechanistic aspects, kinetics and thermodynamics of the reaction were presented as well as the different industrial processes based on the alkylation of benzene. The effects of various reaction parameters on the reaction such as reaction temperature, time and catalyst dosage were reviewed. The final section of the chapter focused on the recent advances in the Friedel-Crafts alkylation reaction. An overview of the different metal catalysts applicable and other homogenous catalytic systems applicable to the reaction were presented. Most transition metals are reported to be active in the Friedel-crafts alkylation of benzene. On the other hand, alkali and earth alkali metals have a significant effect on the Friedel-Crafts alkylation especially on the selectivity. Transition metals, alkali metals and earth alkaline metals are found in AMD. This makes AMD a much interesting choice as precursor solution. Generally, polymetallic catalysts have enhanced activity because when different metals are in close proximity of each other they affect each other's electron density and hence modifying their catalytic properties.

Based on the literature survey undertaken it was found interesting to investigate the possibility of synthesising both zeolite HBEA and MCM-41 from coal fly ash via a silica extraction step and using AMD and Fe extracted from coal fly as precursor solutions in heterogeneous Fe catalyst preparation. Furthermore, the presence of other metal in addition to Fe in AMD instigated a further exploration into the effect of these metals on the overall activity of the resultant catalysts in the Friedel-Crafts alkylation of benzene with tertiary butyl benzene. The effect of Ca, Mg, Mn, Na and Ni was investigated and this is another new exploration since most catalyst applied in the Friedel-Crafts alkylation reaction are either monometallic or bimetallic systems. The use of AMD as precursor solution brings about a new polymetallic system whose activity is unknown at present.

CHAPTER 3

3.0   Experimental details

The chapter presents detailed methodologies of the experimental activities undertaken in catalyst preparation, characterisation and catalytic activity testing. The first section of this chapter focuses on the synthesis of MCM-41 and HBEA from coal fly ash. The second section of the chapter presents details on the metal loading methods on the two supports using iron extracted from coal fly ash or acid mine drainage as metal solution precursors. This is followed by the protocols for characterisation of the prepared catalyst together with the procedures for post synthesis modification undertaken. The final section focuses on the protocols for testing of the prepared catalysts using the Friedel-Crafts alkylation of benzene with tertiary butylbenzene as a probe reaction. A schematic flow diagram presented in Figure 3.1 summarises the experimental details.

Synthesis of MCM-41 and HBEA from coal fly ash

Metal loading MCM-41 and HBEA using Fe extracted from coal fly ash or acid mine drainage as metal solution precursors

Wet impregnation	*conventional ion exchange*
• zeolite HBEA – coal fly ash based • MCM-41 – coal fly ash based	• zeolite HBEA – coal fly ash based

Characterisation XRD, SEM, HRTEM, SAED, ICP-OES N$_2$-adsorption

Catalytic activity testing alkylation of benzene with *t*-butyl chloride

Figure 3. 1: Schematic flow of experimental activities

3.1 Reagents and materials used

The MCM-41 and zeolite HBEA were synthesised using coal fly ash obtained from Arnot power station. The set of equipment and reagents used in the catalyst support (MCM-41 and HBEA) synthesis, catalyst preparation and catalytic activity on the Friedel-Crafts alkylation of benzene with tertiary butyl benzene are presented in sections 3.1.1 and 3.1.2 respectively. The synthesis procedure for MCM-41 and HBEA are outlined in sections 3.2 and 3.3 respectively.

3.1.1 Equipment used in this study

The laboratory equipment used is presented in Table 3.1.

Table 3. 1: Laboratory equipment, brand names and specifications.

Laboratory instrument	Brand name and specifications
Water de-ioniser	Purelab UHQ de-ionizer: ELGA
Muffle furnace	Gallenkamp
Tube furnace	Labofurn (Maximum T=1000 °C)
Rotary evaporator	Buchi R 114
Magnetic stirrer plate and magnetic bar	Lab Smart MS-H-Pro
Oven	Scientific, Series 2000 (Maximum T=250 °C)
pH meter	Hanna HI 8424
Hot plate	Lab Smart MS-H-Pro (Maximum T=340 °C)
30 & 100 mL Teflon lined stainless autoclaves	Parr bomb

The laboratory equipment presented in Table 3.1 were used alongside standard laboratory equipment including polypropylene beakers, mortar and pestle, overhead stirrer, centrifuge, Teflon bottles, Erlenmeyer flask and Buchner funnel, and porcelain dishes.

3.1.2 Reagents

The reagents, supplier and percentage purity are presented in Table 3.2

Table 3. 2: Reagent, supplier and purity.

Reagent	Supplier	Purity/%
Sodium hydroxide	Kimix (SA)	99
Cetyltrimethylammonium bromide	Sigma Aldrich (SA)	99
Tetramethylammonium hydroxide pentahydrate	Sigma Aldrich (SA)	97
Ammonium nitrate	Kimix (SA)	99.9
Sulphuric acid	Merck chemicals (SA)	99
Hydroflouric acid	Merck chemicals (SA)	48
Oxalic acid	Kimix (SA)	99
Nitric acid	Merck chemicals (SA)	65
Hydrochloric acid	Merck chemicals (SA)	37
Benzene	Sigma Aldrich (SA)	99
t-butylchloride	Sigma Aldrich (SA)	99
t-butylbenzene	Sigma Aldrich (SA)	99
1,2-di-t-butylbenzene	Sigma Aldrich (SA)	98
1,3-di-t-butylbenzene	Sigma Aldrich (SA)	97
1,4-di-t-butylbenzene	Sigma Aldrich (SA)	98
Nonane	Sigma Aldrich (SA)	99
Acetone	Sigma Aldrich (SA)	99.5

3.2   Synthesis of MCM-41 from coal fly ash

The mesoporous silica MCM-41 was synthesised from coal fly ash collected from Arnot
power station (South Africa). The first step involved the fusion of the coal fly ash with
sodium hydroxide at a ratio of 1:1.2 in a muffle furnace at a temperature of 550 °C for
1.5 h. The fused ash was then mixed with distilled water at a ratio of 1:5 mass to volume.
The mixture was stirred at room temperature for 2 h and filtered. Sulphuric acid was
added dropwise to the filtrate until the pH of the caustic solution was reduced to about
10. At this point the silica was precipitated out of solution and then filtered out. The
precipitated silica was then rinsed with deionised water and dried overnight in an oven at
a temperature of 70 ^{0}C. After drying, the silica was treated with a saturated solution of

oxalic acid at a solid to liquid ratio of 1:10. This step was meant to remove Al, Ca, and Na from the silica. The oxalic acid treatment was carried out at 80 ^{0}C under stirring for a period of 6 h. After the treatment the mixture was washed, filtered and the silica was then used in the synthesis of MCM-41.

The mesoporous silica MCM-41 was synthesised as depicted in Figure 3.2 using the silica extracted from the coal fly ash. A mass of 1 g of the extracted silica was reacted with (0.23 -00.31 g) cetyltrimethylammonium bromide (CTABr), (0.13 – 0.25 g) tetramethylammonium hydroxide pentahydrate (TMAOH) and (36 -44 g) H_2O. The TMAOH and CTABr were first added to distilled water and stirred for a period of 20 minutes until a clear solution was formed. The fly ash based silica (1 g) was then added to the solution and the mixture stirred for 2 h at a temperature of 30 ^{0}C. The mixture was then aged for 24 h at a temperature of 20 ^{0}C. This step was followed by static crystallisation for 48 h in an oven at a temperature of 150 ^{0}C. The crystallisation was achieved by placing the mixture in Teflon-lined stainless-steel autoclaves. The aging time, crystallisation time, crystallisation temperature and gel molar ratios were varied as presented in Figure 3.2. Upon crystallisation the product was vacuum filtered over nylon membrane filters papers (0.45 µm) and washed using distilled water. The resultant solid product was dried at 70 °C for 10 h, followed by calcination in air to remove the template at a temperature of 550 °C for a period of 4 h. The synthesis condition optimisation are summarised in Table 3.3 and 3.4.

Table 3. 3: Optimisation of aging, crystallisation time and crystallisation temperature.

Sample code	Aging time/h	Crystallisation time /h	Crystallisation temperature /^{0}C
CM1-a	2	6	80
CM1-b	2	6	90
CM1-c	2	6	100
CM1-d	2	6	120
CM1-e	2	6	150
CM1-f	2	6	180
CM2-a	2	6	150
CM2-b	2	12	150
CM2-c	2	18	150
CM2-d	2	24	150
CM2-e	2	36	150
CM2-f	2	48	150
CM3-a	2	6	150
CM3-b	4	12	150
CM3-c	6	18	150
CM3-d	10	24	150
CM3-e	15	36	150
CM3-f	20	48	150

Table 3. 4: Optimisation of synthesis molar regime.

Sample code	SiO2 molar ratio	TMAOH molar ratio	CTABr molar ratio	H2O molar ratio
SM1-a	1	0.13	0.23	36
SM1-b	1	0.13	0.23	38
SM1-c	1	0.13	0.23	40
SM1-d	1	0.13	0.23	42
SM1-e	1	0.13	0.23	44
SM2-a	1	0.13	0.23	40
SM2-b	1	0.13	0.25	40
SM2-c	1	0.13	0.27	40
SM2-d	1	0.13	0.29	40
SM2-e	1	0.13	0.31	40
SM3-a	1	0.13	0.27	40
SM3-b	1	0.16	0.27	40
SM3-c	1	0.19	0.27	40
SM3-d	1	0.22	0.27	40
SM3-e	1	0.22	0.27	40

The summary for the optimisation of the synthesis conditions as well as the synthesis gel molar regime ratios are depicted in Figure 3.2.
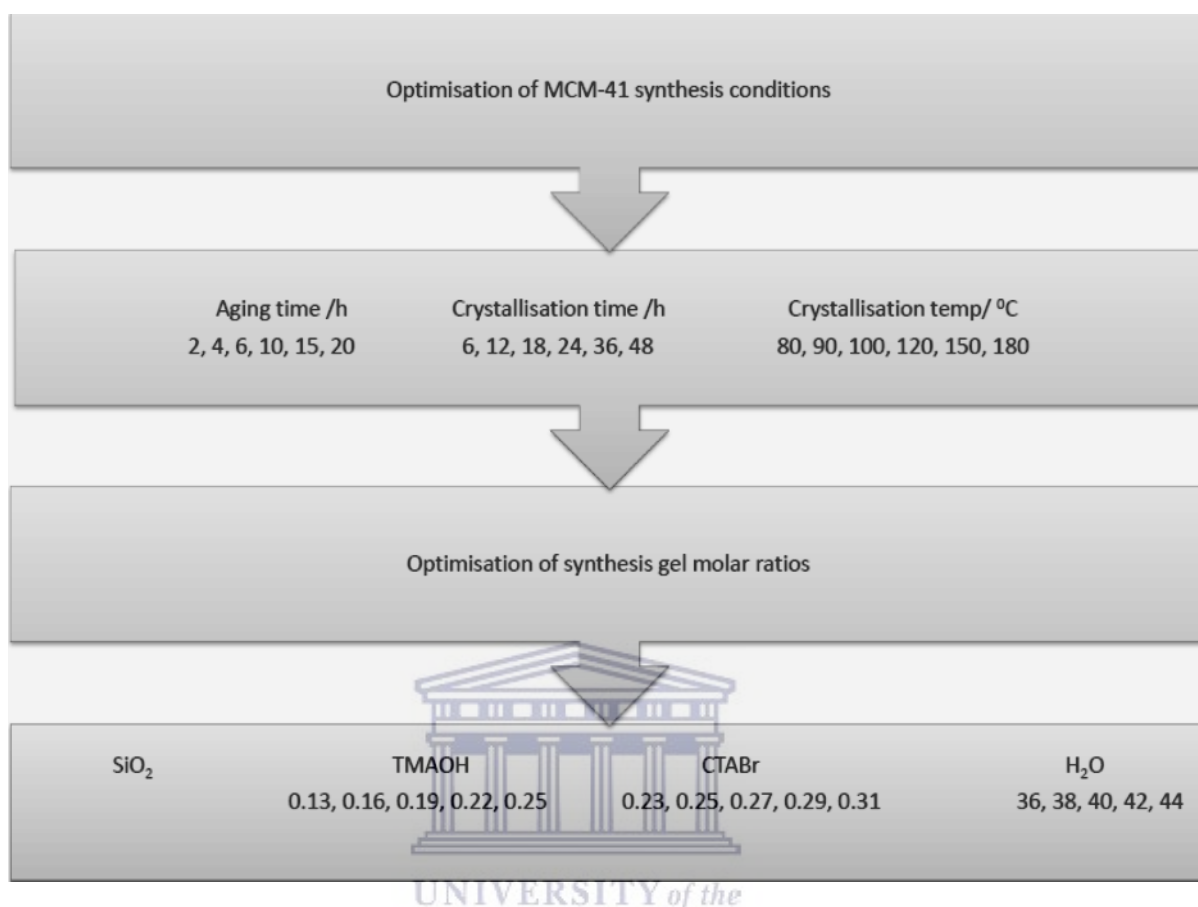
Figure 3. 2: Schematic flow of the MCM-41 synthesis conditions optimisation

3.2.1   Optimum synthesis conditions

The optimum molar ratio of the synthesis gel was SiO_2 : 0.19TMAOH : 0.27CTABr : 40H_2O. The gel was aged for 20 h at room temperature followed by crystallisation for a period of 48 h at a temperature of 150 °C. Upon crystallisation the product was vacuum filtered over nylon membrane filters papers (0.45 μιη) and washed using distilled water. The resultant solid product was dried at 70 °C for 10 h and calcined in air at a temperature of 550 °C for a period of 4 h.

3.3   Synthesis of zeolite BEA from coal fly ash

In the synthesis of zeolite BEA the fusion step and silica extraction were performed in the same manner as described for MCM-41. The resultant silica was then used as a feedstock in the synthesis of zeolite BEA. The extracted silica was mixed with sodium hydroxide, tetraethylammonium hydroxide and deionised water to generate the following

molar composition: 1 Si : 0.017 Al : 0.241 Na : 0.399 TEAOH : 8.980 H_2O (the Si and Al were sourced from the coal fly ash) (Ameh at al, 2019). The mixture was then aged for 30 minutes at room temperature and transferred into a 100 mL Teflon lined stainless steel autoclave. The mixture in the autoclave was subjected to static hydrothermal treatment at a temperature of 140 °C for a period of 72 hours. After synthesis the autoclave was cooled down to room temperature and the recovered solid material was washed several times with deionised water and then filtered. The solid product was dried overnight at a temperature of 70 °C, after which it was calcined in air at 550 °C for 3 hours to remove the template. The resultant solid product was identified as Na-BEA.

3.3.1 Zeolite Na-BEA conversion to protonic form

The synthesised zeolite BEA was obtained in the Na-Zeolite form, and conversion to the H-Zeolite form was performed via ion exchange, using 2.0 M NH_4NO_3 solution with a solid to solution ratio 100:1 (100 mL of solution per 1 g of zeolite sample). The mixture was stirred under reflux at a temperature of 80 °C for a period of 8 hours, upon which it was filtered and washed with deionised water several times until the filtrate pH was between 4.5 – 5. The resultant solid was then dried at 100 °C for 10 hours and calcined at 550 °C in air for 4 hours. The sample was kept in airtight glass bottles prior to metal loading and identified as HBEA.
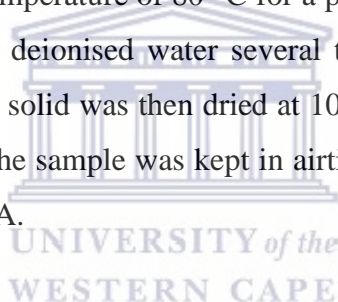
3.4 Metal solution precursors

Two types of metal solution precursors were used, with the first one being Fe extracted from coal fly ash and the second one being AMD. The procedure for Fe extraction from coal fly ash is presented in Section 3.4.1.

3.4.1   Acid leaching of Fe from coal fly ash

A sample of about 10 g of coal fly ash (CFA) was spread on a sheet of paper and a magnetic bar moved underneath the paper. This was to trap the coal fly ash particles rich in Fe. The Fe rich CFA particles were thus magnetically separated and 1 g thereof was placed into a digestion vessel. To the digestion vessel 10 mL of concentrated HCl was added. The digestion vessel was sealed and placed into an oven heated to 150 °C, for 2 h. The digested sample was cooled to room temperature, centrifuged and filtered over a nylon membrane filter (0.45 μm). The orange filtrate was put in a beaker with a magnetic

bar. Concentrated NaOH was added dropwise to the solution until the solution changed from orange to brick red. The solution was taken for ICP-OES analysis to determine the Fe concentration. Upon determination of the Fe concentration the solution was diluted with deionised water to a concentration of 1000 ppm, which was then used as a precursor metal solution in the ion exchange or wet impregnation.

3.4.2   *Sampling and preservation of acid mine drainage*

Raw AMD was collected from Navigation mine, Toeseep shaft (Mpumalanga, South Africa) and sealed in polyethylene bottles. The AMD was allowed to settle and filtered through a nylon membrane filter (0.45 μm) and stored at 4 ^{o}C. The AMD was analysed by ICP-OES to determine the elemental composition and then used as a metal solution precursor.

3.5   **Metal loading on support materials**

The metal loading on the two coal fly ash based support materials (MCM-41 and HBEA) was done via two conventional approaches; liquid phase ion exchange and wet impregnation.

3.5.1   *Liquid phase ion exchange*

Two metal precursor solutions were used in the liquid phase ion exchange approach; Fe extracted from coal fly ash (working concentration of 1000 ppm) and raw filtered acid mine drainage (Fe concentration 1041.65 ppm then diluted with deionised water to a working concentration of 1000 ppm). To prepare catalysts with a range of Fe wt % loading, volumes of 5, 10, 15, 20 and 25 mL of the respective 1000 ppm precursor solutions was made up to 25 mL with deionised water and contacted with the detemplated H-form zeolite HBEA of mass 0.68 g. The mixture was stirred under reflux at 80 ^{o}C for 24 h over a silicon oil bath. The sample was then washed with 500 mL of deionised water and vacuum filtered over a nylon membrane filter paper (0.45 μm). The metal loaded HBEA support was dried in air at 100 ^{o}C for 10 h, and the metals converted to the oxide form by calcination in air at 550 °C at a heating rate of 10 °C /min and held at the temperature for 4 hours. Upon cooling to room temperature the sample was packed in a polypropylene bottle, sealed and labelled. This metal loading approach was only applied to HBEA, and the catalyst coding for the series of catalysts prepared is presented in Table 3.5.

3.5.1.1 Ion exchange prepared catalysts sample coding

only HBEA support was loaded via ion exchange

Table 3.2 presents the catalyst coding used to identify ion exchanged catalysts. The coding is based on the volume of precursor solution used, type of precursor solution and the loading approach applied. A catalyst with code 5AHI refers to a sample prepared using 5 mL of the precursor solution AMD (A), supported on zeolite HBEA (H) and prepared via ion exchange (I). A sample with code 5FHI refers to a catalyst with the same description but Fe extracted from ash (FeAsh) was used as precursor solution (F). Table 3.5 presents the catalyst coding, the theoretical Fe wt % loading as well as the precursor solution used.

Table 3. 5: Sample coding for HBEA supported catalysts prepared via Ion exchange

Sample code	Theoretical Fe wt/ %	Metal precursor	Support material
HBEA	0	-	HBEA
5AHI	0.7	AMD	HBEA
10AHI	1.4	AMD	HBEA
15AHI	2.1	AMD	HBEA
20AHI	2.8	AMD	HBEA
25AHI	3.5	AMD	HBEA
5FHI	0.7	FeAsh	HBEA
10FHI	1.4	FeAsh	HBEA
15FHI	2.1	FeAsh	HBEA
20FHI	2.8	FeAsh	HBEA
25FHI	3.5	FeAsh	HBEA

3.5.2   Wet impregnation

The same liquid to solid ratio and metal solution precursors applied for ion exchange were also used for wet impregnation. The respective metal precursor solution and support were placed into a 150 mL round bottomed flask and mounted on a Rotary Evaporator. The loading was performed under vacuum for 24 h at a temperature of 80 ^{o}C, after which all the water had evaporated leaving behind a dry powdery solid product. The solid material was dried and calcined to convert the metals to the oxide form under the same conditions

as outlined for the catalyst prepared via ion exchange. The catalyst coding for the wet impregnated samples is presented in Table 3.6.

3.5.2.2 Wet impregnation prepared catalysts sample coding
both HBEA and MCM-41 were loaded using this approach

Table 3.3 presents the catalyst coding used to identify wet impregnated catalysts. The coding is based on the volume of precursor solution used, type of precursor solution and the loading approach applied. A catalyst with code 5AHW refers to a sample prepared using 5 mL of the precursor solution AMD (A), supported on zeolite HBEA (H) and prepared via wet impregnation (W). A sample with code 5FHW refers to a catalyst with the same description but Fe extracted from ash was used as precursor solution (F). The corresponding catalysts supported on MCM-41 have M in the code instead of H, for instance 5AMW has the same description as 5AHW, but supported on MCM-41 instead of HBEA. The catalysts codes are presented in Table 3.6.

Table 3.6: Sample coding for HBEA AND MCM-41 supported catalysts prepared via wet impregnation

Sample code	Theoretical Fe wt/%	Metal precursor	Support material
HBEA	0	-	HBEA
5AHW	0.7	AMD	HBEA
10AHW	1.4	AMD	HBEA
15AHW	2.1	AMD	HBEA
20AHW	2.8	AMD	HBEA
25AHW	3.5	AMD	HBEA
5FHW	0.7	FeAsh	HBEA
10FHW	1.4	FeAsh	HBEA
15FHW	2.1	FeAsh	HBEA
20FHW	2.8	FeAsh	HBEA
25FHW	3.5	FeAsh	HBEA
MCM-41	0	-	MCM-41
5AMW	0.7	AMD	MCM-41
10AMW	1.4	AMD	MCM-41
15AMW	2.1	AMD	MCM-41
20AMW	2.8	AMD	MCM-41
25AHW	3.5	AMD	MCM-41
5FMW	0.7	FeAsh	MCM-41
10FMW	1.4	FeAsh	MCM-41
15FMW	2.1	FeAsh	MCM-41
20FMW	2.8	FeAsh	MCM-41
25FMW	3.5	FeAsh	MCM-41

3.6   Catalyst characterisation

The catalyst characterisation was performed via various techniques which are presented in the following sections.

3.6.1   X-ray diffraction

The mineralogical characterisation of the metal loaded supports as well as the pristine materials was carried out on a Philips X-pert pro MPD X-ray diffractometer with Cu-K radiation at 40 kV and 40 mA and a step size of 0.02 º. The analysis was conducted between 4º and 60º 2θ. Identification of the mineral phases was done using Highscore Xpert software, comparing the generated patterns to those in the International Centre for Diffraction Data (ICDD) library.

3.6.1.1 Sample preparation

Using a motor and pestle, the samples were ground to fine powder and placed in a polypropylene holder, and then introduced into the X-ray diffractometer.

3.6.2   Scanning electron microscopy

The morphology and particle size of the synthesised supported metal catalysts was determined by high resolution scanning electron microscopy (HRSEM) on a Hitachi X-650 Scanning Electron Micro-analyser.

3.6.2.1 Sample preparation

A minute amount of fine powdered catalyst sample was placed on top of an aluminium stub coated with carbon tape. In order to make the sample conductive, the stub with the sample was coated with carbon in an Emitech K950X carbon evaporator for 6 sec. prior to introduction into the analyser.

3.6.2.2 Set up conditions

The instrumental set-up conditions during analysis are presented in Table 3.7.

Table 3. 7: Instrument set up conditions for high resolution scanning electron microscopy

Name of the instrument	Hitachi X 650 Scanning electron microscope
Applied voltage	25 kV
Emission current	1 µA
Illumination	0,1 mrad
Magnification	Varied depending on sample
Resolution	0.35x to 1Kx
Exposure time	Varied depending on sample
Working distance	15 nm

3.6.3   High resolution transmission electron microscopy

In order to determine the structure, shape and size of the prepared metal supported catalysts, crystallographic analysis was carried out determined using high resolution transmission electron spectroscopy (HRTEM), in accordance with the following outlined steps.

3.6.3.1 Sample pre-treatment

A minute sample of the powdered catalyst was added to a polypropylene vial, followed by a 5 mL aliquot of methanol. The resultant suspension was vigorously shaken and placed in an ultrasonic vessel (Labcon Ultra-Sonic 5019U) for 15 min. To a carbon coated

copper grid, a drop of the suspension was placed and allowed to air dry at room temperature. The grid was then placed into the HRTEM machine (Technai G2 F 20 X-Twin MAT) and analysed under the conditions presented in Table 3.8.

3.6.3.2 Instrument operation conditions

The instrument set up conditions applied during HRTEM analysis of the catalyst samples are presented in Table 3.8.

Table 3. 8: Instrument set up conditions for high resolution transmission electron microscopy

Name of the instrument	Technai G^2 F 20 X-Twin MAT
Applied voltage	200 kV
Emission current	48 µA
Illumination angle	15 °
Magnification	Varied depending on sample
Resolution	0.24 nm
Exposure time	Varied depending on sample

3.6.4   Selected area electron diffraction

The crystallinity and d-spacing of the crystal planes of the metal loaded supports were determine using selected area electron diffraction (SAED) analysis. The analysis was carried out on the same samples prepared for HRTEM analysis under the same operational conditions as presented in Table 3.8.

3.6.5   Inductively coupled plasma-optical emission spectrometry

The respective metal percentage loading on the loaded supports was determined by inductively coupled plasma-optical emission spectrometry (ICP-OES) on a Varian 710-ES series spectrometer equipped with a CCD detector, axially-viewed plasma, a cooled cone interface, and ICP Expert II software.

3.6.5.1 Sample Digestion

Prior to analysis by ICP-OES, a sample of 0.1 g of catalyst (parent supports HBEA/MCM-41 and metal loaded supports) was added to a Teflon beaker to which a volume of 5 mL aqua regia and 2 mL HF were added. The beaker was covered and heated for 2 h, at a temperature of 100 ºC. The mixture was taken out and cooled to room temperature, after which 1 mL of saturated boric acid solution was added. The mixture was further heated

in an oven for 15 min, again at a temperature of 100 ^{o}C. The resultant solution was cooled to room temperature and diluted to 50 mL with deionised water.

3.6.6   Nitrogen-adsorption

The BET surface area, pore size diameter and pore size distribution was determined by N_2-adsoption on an Austosorb-1C (Quantachrome Instruments). A sample of about 0.36 g of the solid catalyst (HBEA, MCM-41 and the metal loaded supports) sample was weighed and degassed in flowing He at 90 ^{o}C for 1 h, then held at 350 ^{o}C for 16 h in order to desorb the water from the sample surface and pores. The sample was weighed, cooled and N_2-adsoption analysis carried out based on a 39 points analysis. The instrumental set up conditions are summed up in Table 3.9.

3.6.6.1 Instrumental set up conditions

The instrumental set up conditions for the N_2-absorption analysis are presented in Table 3.9.

Table 3. 9: Instrumental set up condition for the N_2-adsorption analysis

Instrument model	Austosorb-1C (Quantachrome Instruments)
Gas	N_2
Pressure table	39 points (20 adsorption and 20 desorption)
Pressure range	0 to 999 mmHg

3.7   Friedel-Crafts alkylation of benzene with *t*-butyl chloride

The pristine fly ash based supports HBEA and MCM-41 and their respective metal loaded catalysts were screened for their activity in the Friedel-Crafts alkylation of benzene with *t*-butylchloride. In the screening, benzene was used as both solvent and reactant. The catalyst activation and reactant proportions are presented in the following sections.

3.7.1   Catalyst activation

Using an analytical balance, 320 mg of the catalyst was weighed and transferred into a round bottomed flask. To activate the catalyst, the flask was placed in an oven and heated to 250 ^{o}C for a period of 2 h. The catalyst was allowed to cool to room temperature before the reactants were added in accordance with the following catalytic evaluation procedure.

3.7.2   Catalytic evaluation

To a 50 mL round bottomed flask containing the activated catalyst, a volume of 10 mL of benzene was added together with 1 mL of *t*-butylchloride and 1 mL of nonane (used as an internal standard). The mixture was stirred under reflux over a silicon oil bath at a temperature of 45 °C. Using a micro pipette, sample aliquots of volume 0.1 mL were taken at 0.5, 1, 2, 3, 4 and 5 h. The samples were diluted with 0.5 mL of acetone, and then filtered using nylon membrane syringe filters (0.45 μm).   Samples were sealed in a glass vial and immediately analysed using a GC equipped with FID and HP-5 (phenylmethylsilicon) capillary column, (Agilent technologies). Pure standards of the reactants and the anticipated products were also injected and analysed in order to identify the respective retention times and response factors. The standards analysed all gave a linear relationship within the analysed concentration ranges.

3.7.3   Activity determination

The data obtained from the gas chromatograph analysis was used to calculate the conversion, selectivity, yield and product distribution in accordance to the following equations:

$$conversion = \frac{[\% \, t-BB]+[\% \, 1,3-di-t-BB]+[\% \, 1,4-di-t-BB]}{[\% \, t-BC]+ [\% \, t-BB]+[\% \, 1,3-di-t-BB]+ [\% \, 1,4-di-t-BB]} \, x \, 100\% \qquad (3.1)$$

$$selectivity = \frac{[\% \, t-BB]}{[\% \, t-BB]+[\% \, 1,3-di-t-BB]+ [\% \, 1,4-di-t-BB]} \, x \, 100\% \qquad (3.2)$$

$$yield = \, conversion \, (\%) \, x \, selectivity \, (\%)/100 \qquad (3.3)$$

{t-butyl benzene (t-BB); t-butyl chloride (t-BC); 1,3-di-t-butyl benzene (1,3-di-t-BB); 1,4-di-t-butyl benzene (1,4-di-t-BB)}

*It should be noted that of the possible products expected, the tri-alkylated (2,3,4-tri-t-butylbenzene) as well as the ortho isomer (1,2-di-t-butylbenzene) were not obtained in all the testing and are omitted in the calculations for conversion, selectivity and yield.

3.7.4   Effect of various metals supported on fly ash based HBEA on the catalytic activity

The evaluation of various metals in AMD on the catalytic activity was investigated over metal loaded HBEA catalysts. The catalysts were prepared via wet impregnation by via

sequential impregnation. The various metals were added to HBEA in accordance with the proportion in the catalyst 10AHW. The metals were added in the order Fe, Mn, Mg, Na, Ca and Ni. The wet impregnation was performed using the same conditions as presented in Section 3.5.2. Another bimetallic catalyst consisting only of Fe and Na was also synthesised on HBEA in the same manner using the proportions in the catalyst 10FHW. The metal solution precursors used in all the synthesis were the sulphate salts. The following table presents the catalyst coding.

Table 3.10: Coding for fly ash based HBEA supported catalysts used in the investigation of various metals on the activity in the FC alkylation reaction.

Catalyst code	Composition - wt % loading
Fe-H	*Fe (1.4)*
FeMnH	*Fe (1.4) Mn (0.08)*
FeMnMg-H	*Fe(1.4) Mn (0.8) Mg 0.24)*
FeMnMgNa-H	*Fe(1.4) Mn (0.8) Mg 0.24) Na (0.38)*
FeMnMgNaCa-H	*Fe(1.4) Mn (0.8) Mg 0.24) Na (0.38) Ca (0.62)*
FeMnMgNaCaNi-H	*Fe(1.4) Mn (0.8) Mg 0.24) Na (0.38) Ca 0.62) Ni (0.86)*
FeNa-H	*Fe (1.4) Na (1.49)*

3.8   Chapter summary

The coal fly ash which was used as a feedstock in the synthesis of zeolite HBEA and MCM-41 was collected in air tight polyethene bags, sealed and labelled. The acid mine drainage which was used as a metal solution precursor was collected from Toeseep mine shaft (Navigation coal mine, Mpumalanga, South Africa) and filtered with 0.45 μm pore size membrane filter paper and placed in polypropylene bottles just prior to analysis and use as metal precursor. The synthesis of both zeolite HBEA and MCM-41 was carried out via a novel approach which involved acid assisted silica extraction from the CFA. Further purification of the silica to remove Al, Ca and Na was achieved by treatment with oxalic acid. The pure silica was then used in the preparation of the two support materials HBEA and MCM-41.

Metal loading onto the respective support materials was done using two metal precursor solutions, namely AMD and FeAsh (Fe extracted from CFA via acid leaching). The

catalysts series supported on zeolite HBEA were prepared via two conventional metal loading approaches namely, liquid phase ion exchange and wet impregnation. Metal loading onto the MCM-41 support was achieved only via wet impregnation using the two respective metal solution precursors. The sample coding for the different series of Fe catalysts prepared was also presented. The resultant metal loaded supports were subjected to various characterisation techniques namely, XRD, SEM, HRTEM, SAED, ICP-OES and nitrogen-adsorption. The respective instruments used as well as the instrument set up conditions were outlined in this chapter.

The chapter went on to outline the procedure and experimental conditions applied in the catalytic activity of the metal loaded catalysts in the Friedel-crafts alkylation of benzene with t-butyl chloride. The reaction was used as a probe and the reaction condition were not optimised but standard conditions available in open literature were applied. The procedure for the determination of the effects of various metals in AMD was also outlined. The following chapter (chapter 5) presents the catalytic evaluation of the Fe catalysts prepared using AMD as metal solution precursor. The outcomes for the catalytic activity of the FeAsh based catalysts is presented in chapter 6.
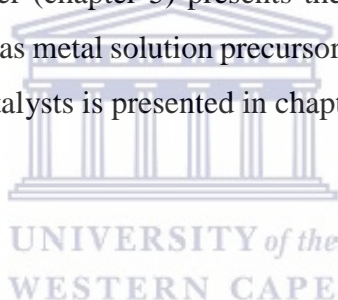
CHAPTER 4

The chapter presents a comprehensive account of the characterisation outcomes obtained on the prepared metal supported catalysts. The nature of the outcomes is discussed in relation to the metal loading approach applied as well as the metal percentage loading achieved on the respective catalysts.

4.0   Characterisation of metal loaded catalysts

During catalyst preparation two conventional metal loading approaches were used, namely liquid phase ion exchange and wet impregnation. Using both metal loading approaches, FeAsh or AMD were used as metal precursors for loading both HBEA and MCM-41. It should be noted that the liquid phase ion exchange approach was only used for catalysts supported on zeolite HBEA. The catalyst preparation and coding are presented in Section 3.5. Upon metal loading both support materials (zeolite HBEA and MCM-41) changed from white to brown with the colour depending upon increasing metal wt % loading. The physicochemical properties of the catalysts were determined using a range of techniques namely; XRD, SAED, SEM, HRTEM, ICP-OES, and N_2 adsorption.

4.1 Crystallographic studies by X-ray diffraction spectroscopy

The crystallographic studies on the metal supported catalysts were done using XRD in accordance with the procedure outlined in Section 3.6.1. The aim of the analysis was to determine and compare the crystallinity of the fly ash based parent support materials with the metal loaded ones and assess if there were any alterations in their crystallinity. The XRD analysis was performed on a Philips X-pert pro MPD X-ray diffractometer with Cu-K radiation at 40 kV and 40 mA. The analysis was conducted between 4º and 60º 2θ.

4.1.1 The XRD profiles of HBEA loaded with Fe from fly ash via ion exchange

The XRD profiles of the HBEA supported metal catalysts prepared via ion exchange using Fe extracted from coal fly ash are presented in Figure 4.1. The profiles are arranged with the catalyst with the highest metal loading at the top.
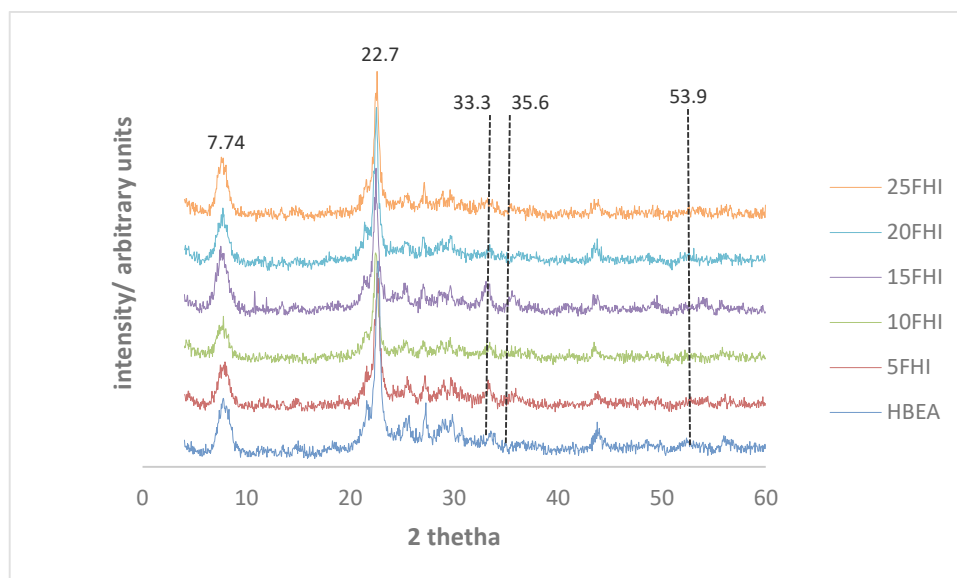
Figure 4. 1: XRD profiles of the HBEA supported metal catalyst prepared via ion exchange using Fe extracted from coal fly ash (refer to coding in Table 3.2).

The XRD patterns presented in Figure 4.1 show the characteristic peaks of polymorph A and B of HBEA at 2 θ values of 7.74 and 22.7. These characteristic peaks were observed on both the pristine zeolite support as well as the metal loaded supports. Upon metal loading the peak intensities remain unaltered indicating that the support was stable and the Fe and Na did not disrupt the framework (the presence of Na was due to the fact that the precursor solution pH was regulated by NaOH). The peak intensities due to iron oxide crystallites were not well pronounced (the characteristic peaks for α-Fe_2O_3 oxide crystallites appear at 33.3, 35.6 and 53.6 2 θ values, as indicated by the drop lines on the figure). The first 2 θ values, 33.3 and 35.6 are also characteristic of the zeolite HBEA itself (Balle et al., 2009) (also refer to Appendix A1 showing zeolite HBEA and α-Fe_2O_3 characteristic peaks). The outcome observed could be due to the fact that Fe was monoatomically dispersed on the support or simply existed as non-crystalline phases. Using $Fe(NO_3)$ as metal solution precursor the same outcomes were observed and reported by Ma et al. (2012) and Boroń et al. (2013)

4.1.2 The XRD profiles of HBEA loaded with metal via ion exchange using acid mine drainage as precursor

The crystalline phase of the HBEA supported catalyst prepared via ion exchange and using acid mine drainage as metal solution precursor are presented in Figure 4.2.
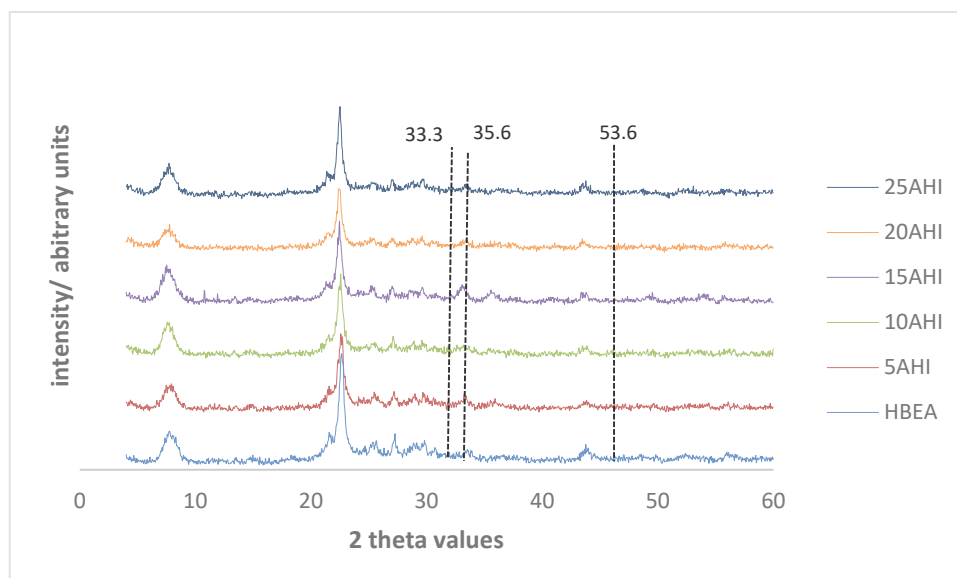
Figure 4. 2: XRD profiles of the HBEA supported metal catalyst prepared via ion exchange using AMD as metal precursor (refer to coding in Table 3.2).

The diffractograms presented in Figure 4.2 show that the characteristic peaks of the HBEA zeolite are present for both the parent material as well as the metal loaded zeolites. The incorporation of the metals in AMD on the zeolite did not alter the positions and intensities of the typical peaks of the zeolite support material. The outcome indicated that the zeolite BEA support was stable and metal heteroatoms from AMD did not get incorporated into the support framework. From the XRD profiles it could be seen that there were no characteristic peaks due to the metal crystallites. This may be attributed to the good metal dispersion associated with the loading approach applied (liquid phase ion exchange). The results obtained using FeAsh and those obtained using AMD are comparable and in both cases the crystallinity of the parent support was retained upon metal loading. Similar outcomes were observed and reported in related studying where commercial sources of Fe were used in the preparation of Fe loaded zeolite HBEA (Høj et al., 2009; Ma et al., 2013; Boroń et al., 2013).

4.1.3 The XRD profiles of HBEA loaded with Fe from fly ash by wet impregnation
The XRD diffractograms obtained over the HBEA supported metal catalysts prepared via wet impregnation using Fe extracted from CFA are presented in Figure 4.3.
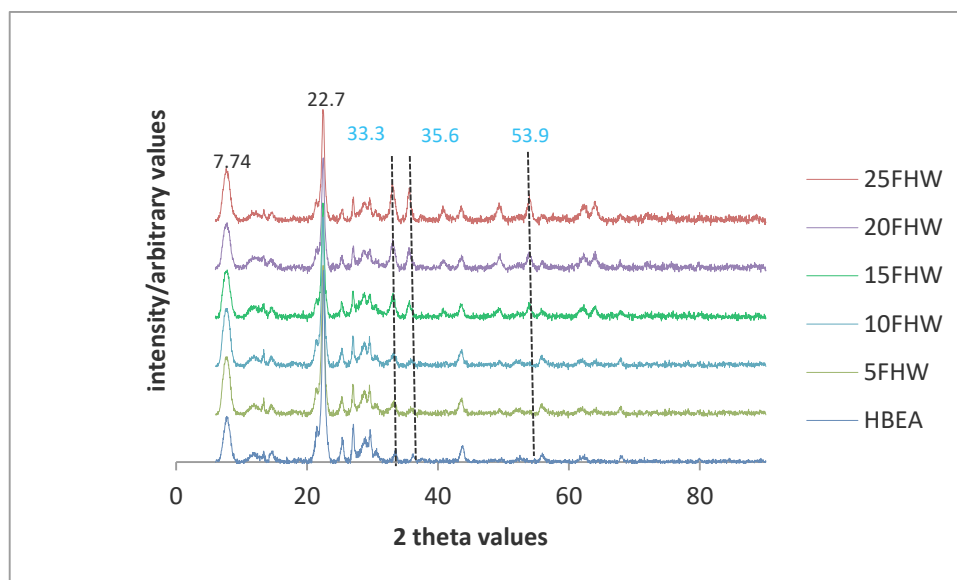
Figure 4. 3: XRD profiles of the HBEA supported metal catalyst prepared via wet impregnation using Fe extracted from coal fly ash. (refer to coding in Table 3.3)

The XRD profiles of the catalysts presented in Figure 4.3 show that the characteristic peaks of the HBEA polymorphs A and B at 2 θ values of 7.74 and 22.7 were present in both the parent zeolite as well as the wet impregnated zeolites. This confirms that the metal introduction did not result in long-range amorphisation of zeolite. Moreover, peaks due to the α-Fe_2O_3 crystallites were observed to increase in intensity as the metal loading by wet impregnation increased. The characteristic α-Fe_2O_3 peaks are labelled in Figure 4.3 at 33.3, 35.6 and 53.9° 2θ. Confirmation that the peaks were due to the α-Fe_2O_3 was obtained from the XRD JCPDS library and presented in appendix Section A1. The presence of the α-Fe_2O_3 can be attributed to the wet impregnation metal loading approach applied. Wet impregnation favours the formation of oligomeric metal clusters while ion exchange favours the formation of monomeric Fe species on the exchange sites (Høj et al., 2009). In their study in which commercial zeolite BEA was loaded via impregnation and ion exchange (Hoj et al., 2009) reported that ion exchange was associated with formation of a higher proportion of Fe monomers relative to impregnation upon analysing the two different catalysts by UV-Vis. The observation is consistent with the outcomes observed in the present study.

4.1.4 The XRD profiles on HBEA loaded via wet impregnation using AMD as metal precursor

The XRD diffractograms obtained over the HBEA supported metal catalysts prepared via wet impregnation using AMD as metal solution precursor are presented in Figure 4.4.
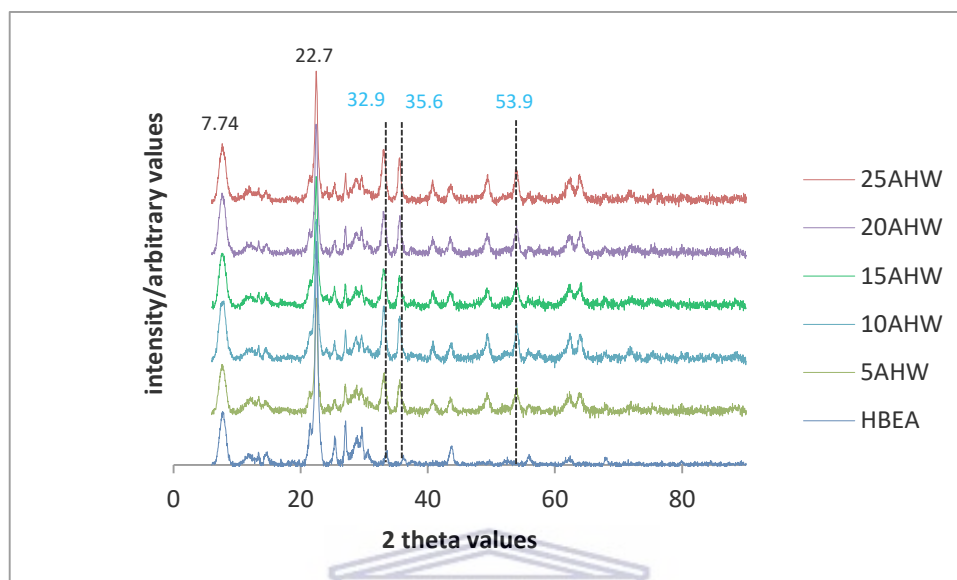
Figure 4. 4: XRD profiles of the HBEA supported metal catalyst prepared via wet impregnation using AMD as metal precursor. (refer to coding in Table 3.3)

The diffractograms in Figure 4.4 also show the characteristic peaks of both the parent zeolite HBEA and the α-Fe$_2$O$_3$. Again, the presence of the metal crystallites can be attributed to the metal loading approach (wet impregnation), which is associated with formation of Fe oligomers on the external surface of the zeolite (Høj et al., 2009). However, the only metal crystallites peaks observed were those due to α-Fe$_2$O$_3$ despite the fact that AMD contains other metals apart from Fe. This outcome was expected since Fe was the major ion in the AMD. A related study by Høj et al., (2009) reported the same observations when commercial HBEA was loaded with commercial Fe via wet impregnation. Although AMD was used in this study the outcomes were comparable to thoese reported by Høj et al. (2009) in which commercial sources were used in catalysts preparation.

4.1.5 The XRD profiles MCM-41 loaded with Fe from fly ash by wet impregnation

The XRD diffractograms generated upon analysis of the MCM-41 supported catalysts prepared via wet impregnation using Fe extracted from CFA are presented in Figure 4.5.
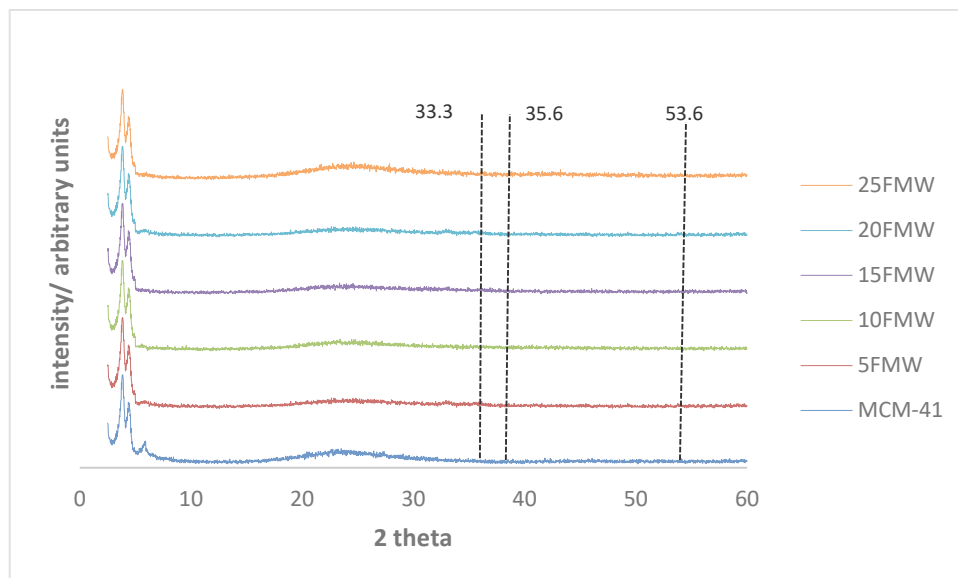
Figure 4. 5: XRD profiles of the MCM-41 supported catalyst prepared via wet impregnation using Fe extracted from coal fly ash. (refer to coding in Table 3.3)

The X-ray diffraction (XRD) profiles of the metal loaded MCM-41 resembled the profile of the pristine MCM-41 support material. The characteristic peaks of MCM-41 were observed at 3.91 and 4.49 º 2 θ values. Unlike the observation made with the HBEA wet impregnated counterparts, there were no peaks observed due to the Fe metal crystallites. This may be attributed to the larger pore structure MCM-41, which allows for easier metal diffusion into the pore system during wet impregnation. Again the larger surface area of MCM-41 would allow for greater metal dispersion. These factors suppress the formation of Fe oligomeric species on the external surface of the support (Mokhonoana, 2005). The dotted drop lines on the figure are positioned where peaks due to the α-Fe_2O_3 crystallites would appear if present in the sample. Using commercial sources to synthesis MCM-41 supported Fe catalysts the same observations were reported (Mokhonoana, 2005; Sirotin et al., 2011). In their respective studies, peaks due to α-Fe_2O_3 were only observed with metal wt % loadings above 5 and 7 % respectively.

4.1.6 The XRD profiles MCM-41 loaded using AMD as metal precursor

The X-ray diffraction spectra for the MCM-41 supported metal catalysts prepared via wet impregnation using AMD as metal solution precursor are presented in Figure 4.6.
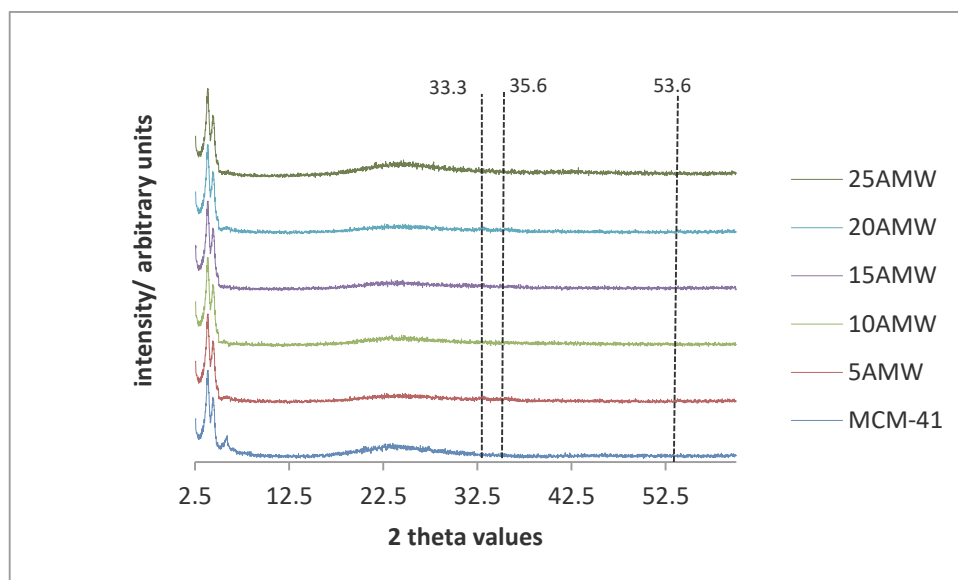
Figure 4. 6: XRD profiles of the MCM-41 supported catalyst prepared via wet impregnation using AMD as metal precursor. (refer to coding in Table 3.3)

The XRD spectra of the AMD impregnated samples presented in Figure 4.6 exhibited characteristic peaks at 3.0 and 3.7 which are attributed to the reflection in the (100) plane. These peaks are characteristic of the MCM-41 hexagonal structure. The metal introduction did not alter the crystallinity of the support material since the characteristic peaks of MCM-41 were still observed after metal loading the support. There however was a slight decrease in peak intensity as the metal wt % loading increased. The profiles obtained also were very much comparable with the profiles generated when using FeAsh as metal solution precursor. Again the peaks due to the metal oxide crystallites were not observed (the position of these peaks are marked by the drop lines in the figure). In a related study by Krishna & Bhattacharyya, (2008) in which Fe, Co and Ni were loaded onto MCM-41 via wet impregnation, it was observed that the metal introduction caused slight to no distortions to the hexagonal structure of MCM-41.

4.2 Surface structure and topology studies

The morphology of the metal loaded supports (HBEA and MCM-41) was determined using high resolution transmission electron microscopy (HRTEM). The intent was to make an evaluation on whether the crystallinity and micropore structure of the supports was retained upon metal loading. The analysis was carried on a Technai G2 F 20 X-Twin MAT, in accordance with the steps outlined in Section 3.6.2.

4.2.1 Morphological studies of HBEA supported catalyst prepared via ion exchange

The crystallinity and morphology of the HBEA metal loaded catalysts prepared via ion exchange was performed using HRTEM. The catalysts were prepared using FeAsh or AMD as metal solution precursors. The micrographs of the ion exchanged HBEA catalysts with the highest metal loading achieved using the respective metal solution precursors are presented in Figure 4.7. The samples were chosen since it is expected that as the metal wt % loading increases there would be a corresponding decrease in crystallinity.

(a)   (b)
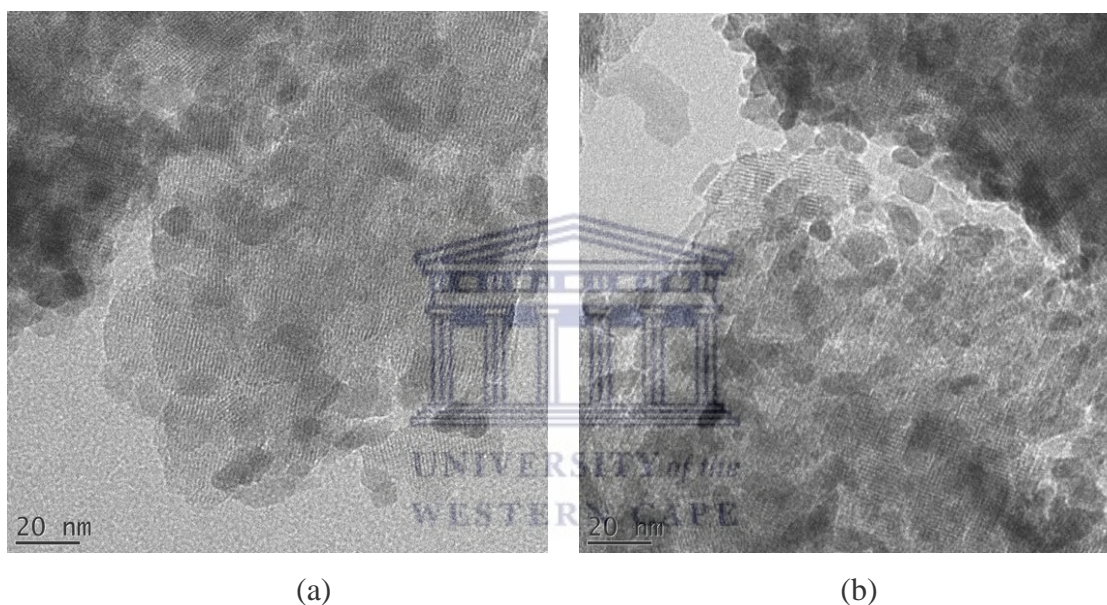
Figure 4. 7: HRTEM micrographs for HBEA supported metal catalysts prepared via conventional liquid phase ion exchange [(a) 25FHI (prepared using FeAsh via ion exchange) and (b) 25AHI (prepared using AMD via ion exchange)]

The HRTEM generated micrographs presented in Figure 4.7 attest to the fact that both the porosity and the porous lattice structure of the parent HBEA material was retained upon metal loading via liquid phase ion exchange. Zhou et al., (2019) prepared Fe loaded zeolite HBEA catalysts from commercial sources via ion exchange and reported similar outcomes.

4.2.2 Morphological studies of HBEA supported catalyst prepared via wet impregnation

The HBEA supported metal catalysts prepared via wet impregnation were subjected to HRTEM analysis. The micrographs of the catalysts with the highest metal loading are presented in Figure 4.8.

(a)   (b)

Figure 4. 8: HRTEM micrographs for HBEA supported metal catalysts prepared via wet impregnation (a) 25FHW (prepared via wet impregnation using FeAsh as precursor) and (b) 25AHW (prepared via wet impregnation using AMD as precursor)

The micrographs of the wet impregnated HBEA presented in Figure 4.8 closely resemble the micrographs observed with the ion exchanged counterparts except that the metal loading appears to be higher. The porous lattice structure and crystalline habit of the HBEA was preserved upon metal loading. The outcome is in line with the results from XRD analysis presented in Section 4.1. It should however be noted that the 25AHW prepared using AMD as metal precursor contained other metals in addition to Fe (the ICP-OES data for the elemental composition of the catalysts are presented in Section 4.5.2.3). Despite the differences in the elemental composition of the FeAsh versus AMD impregnated catalysts presented in Figure 4.8, there were no observable differences on the generated micrographs.

In a related study by Balle et al., (2009) in which commercial HBEA was loaded with Fe, metal oxide crystallites were observed on the micrographs, but only for the catalysts with

high metal loading. The micrographs of the samples with lower metal wt % loading on the support did not confirm the presence of metal oxide species on the zeolite surface. Zhou et al., (2019) reported similar outcomes as observed in the micrographs presented in Figure 4.8.

4.2.3 Morphological studies of MCM-41 supported catalyst prepared via wet impregnation

Morphological studies of the metal loaded fly ash based MCM-41 prepared via wet impregnation was carried out by HRTEM and the generated micrographs are presented in Figure 4.9.

(a)   (b)

Figure 4.9: HRTEM micrographs for MCM-41 supported metal catalysts prepared via wet impregnation (a) 25FMW (prepared via wet impregnation using FeAsh as precursor) and (b) 25AMW (prepared via wet impregnation using AMD as precursor)

The micrographs presented in Figure 4.9, both show the existence of the ordered pore arrangement of MCM-41 characterised by long mesochannels with pore size in the range of 20 - 27 Å. This further confirms that the metal doping did not interfere with the mesoporous silica matrix of the support. The observation is consistent with the XRD data obtained in presented in Sections 4.1.5 and 4.1.6. Dark spots were observed on crystals which are due to the presence of metal oxides on the external surface of the MCM-41. Although different metal solution precursors were used, there was no marked difference in the HRTEM images obtained. The outcomes are in agreement with observations made

in related studies although commercial sources were used in the catalyst preparations (Zhang et al., 2018; Brezoiu et al., 2019; Sánchez-Velandia, & Villa, 2019)

4.3 Crystalline phases study by selected area electron diffraction

Selected area electron diffraction was used to carry out the crystalline phase analysis on both the parent supports (HBEA and MCM-41) and the metal loaded supports. The analysis was done on a Technai G2 F 20 X-Twin MAT following the procedure outlined in Section 3.6.4. In this section the discussion is centred on the catalysts with the highest metal wt % loading using the two metal precursors. It should however be noted that there was not much difference in the SAED patterns obtained with lower metal loadings.

4.3.1 Crystalline phase studies of HBEA catalysts prepared via ion exchange

The crystalline phase studies of the parent fly ash based support HBEA and the metal loaded support prepared via ion exchange are presented in Figure 4.10. In this section only the highest metal wt % loading achieved using the respective metal solution precursors are presented (25FHI and 25AHI).
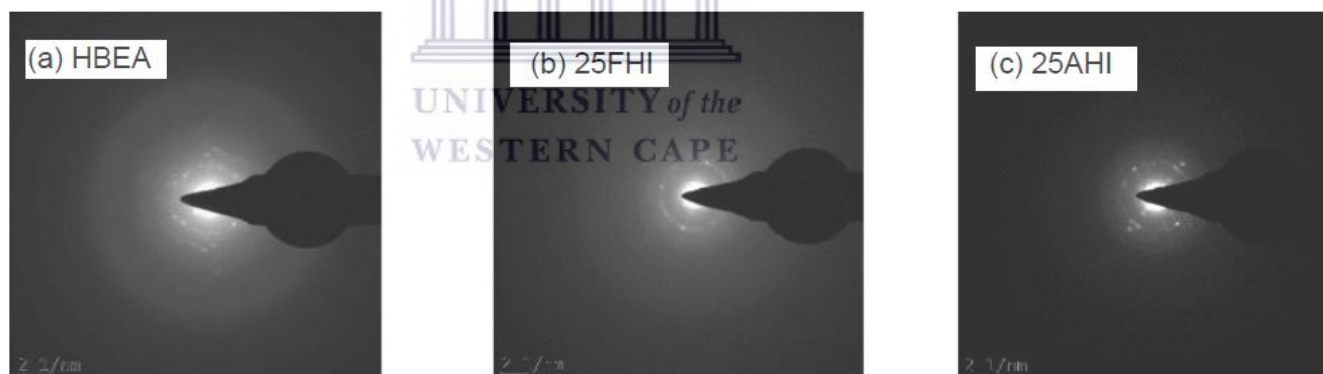
Figure 4. 10: SAED images of the pristine fly ash based HBEA and the metal loaded HBEA loaded ion exchange(HBEA - fly ash based zeolite HBEA; 25FHI- sample prepared via ion exchange using FeAsh as precursor; 25AHI- sample prepared via ion exchange using AMD as precursor)

The SAED pattern for the parent support HBEA exhibited discrete bright diffraction dots rather than the diffraction halos as observed with the pristine MCM-41 presented in Figure 4.12. The diffraction patterns observed for the ion exchanged loaded HBEA confirmed the presence of well dispersed metal oxides in the case of FeAsh. The 25AHI showed more bright dots relative to the 25FHI counterpart. The outcome was expected considering the fact that the AMD loaded support contained metal oxides other than

Fe$_2$O$_3$. Comparable outcomes were observed in related studies involving commercial HBEA loaded with commercial available metal salts and reported in (Hlatywayo, 2013; Ma et al., 2015; Liu et al., 2017)

4.3.2 Crystalline phase studies of HBEA catalysts prepared via wet impregnation

The SAED patterns for the HBEA supported catalysts prepared via wet impregnation are presented in Figure 4.11.
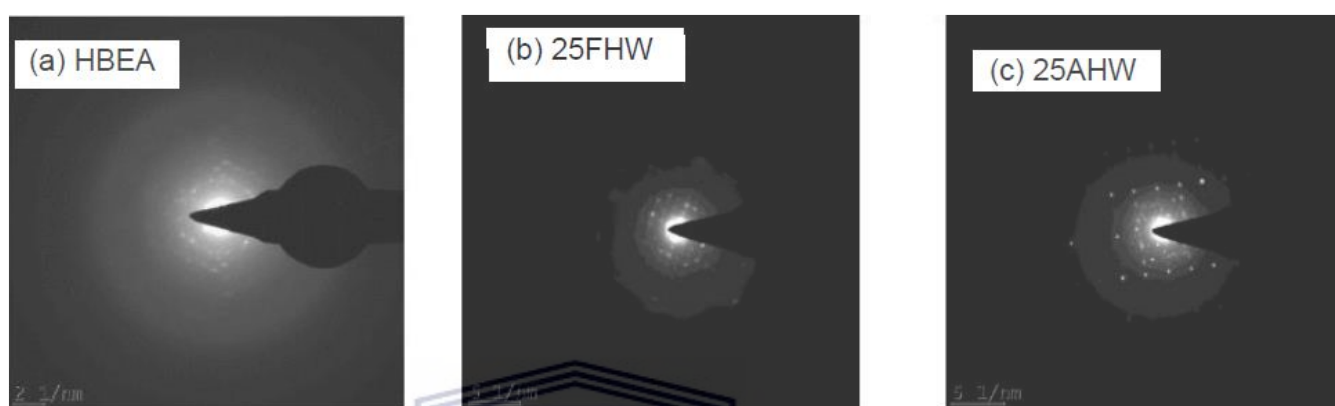
Figure 4. 11: SAED images of the pristine fly ash based HBEA and the metal loaded HBEA loaded via wet impregnation (HBEA - fly ash based zeolite HBEA; 25FHW- sample prepared via wet impregnation using FeAsh as precursor; 25AHW- sample prepared via wet impregnation using AMD as precursor)

The observed SAED patterns obtained on the HBEA supported catalysts prepared via wet impregnation closely resembled their counterparts prepared via ion exchange. There were however more of the bright diffraction dots on the SAED images of wet impregnation prepared catalysts in comparison to their corresponding ion exchanged ones. The outcome can be attributed to the tendency for large metal crystallites to be associated with wet impregnation.

4.3.3 Crystalline phase studies of MCM-41 supported metal catalysts

The selected area electron diffraction SAED images for the pristine fly ash based MCM-41, as well as sample 25AMW (prepared using AMD) and the 25FMW (prepared using FeAsh as metal precursor) are presented in Figure 4.12.
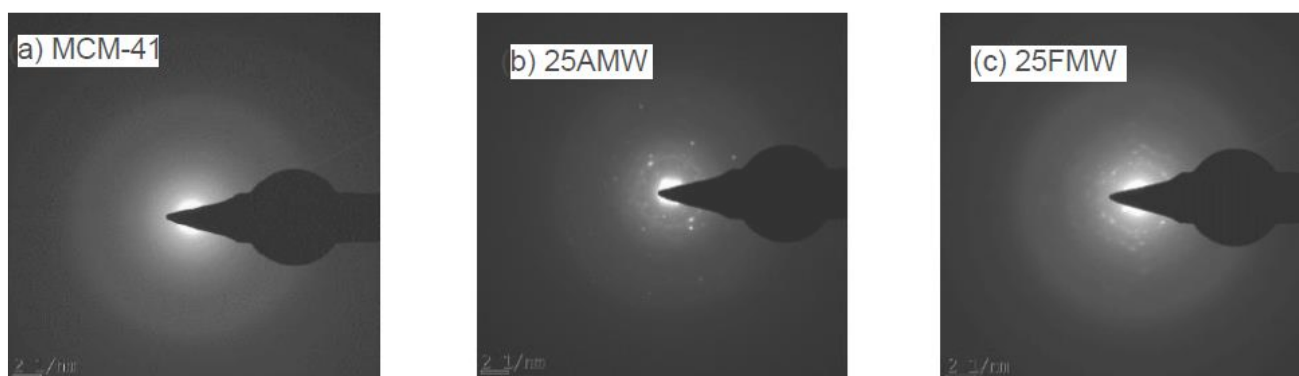
Figure 4. 12: SAED images of the pristine fly ash based MCM-41 and the metal loaded MCM-41(MCM-41 - fly ash based MCM-41; 25AMW- sample prepared via wet impregnation using AMD as precursor; 25FMW- sample prepared via wet impregnation using FeAsh as precursor)

The SAED pattern of the pristine MCM-41 shows diffuse rings and no bright dots, which is characteristic of the amorphous nature of the pore walls in MCM-41. This is in contrast with the pattern observed with the pristine HBEA presented in Figure 4.10, which has some bright dots signifying the crystalline nature of the parent HBEA zeolite. The SAED images of the metal loaded MCM-41 confirms the presence of metal crystallites on the support material. These can be seen as small bright diffraction dots on the images in Figure 4.12. The sample 25FMW only contained Fe, sample 25AMW contained Fe as well as other metals found in the AMD solution precursor. Comparison of the images shows that sample 25FMW has more of the bright diffraction dots than sample 25AMW. This outcome is due to the presence of metals other than Fe in AMD. Using commercial sources for the preparation of Fe loaded MCM-41 catalysts, similar observations were reported (Díaz, 2004: Wa Kasongo, 2011: Hlatywayo, 2013: Pradhan et al., 2016). Thus the use of waste materials in the preparation of the Fe supported catalysts did not compromise the quality of the resultant products.

4.4 Morphological studies of metal loaded HBEA

Morphological studies on the HBEA and MCM-41 supported catalysts were examined using scanning electron microscope (SEM). The studies were carried out using a Hitachi X-650 Scanning Electron Micro-analyser.

4.4.1 Morphological studies HBEA catalysts prepared via ion exchange

The typical scanning electron microscopy (SEM) images generated on the catalysts prepared via liquid phase ion exchange are presented in Figure 4.13. The metal solution precursors used were Fe extracted from CFA and AMD and the catalysts with the highest metal loading are presented for discussion (25FHI and 25AHI respectively).

(a)   (b)
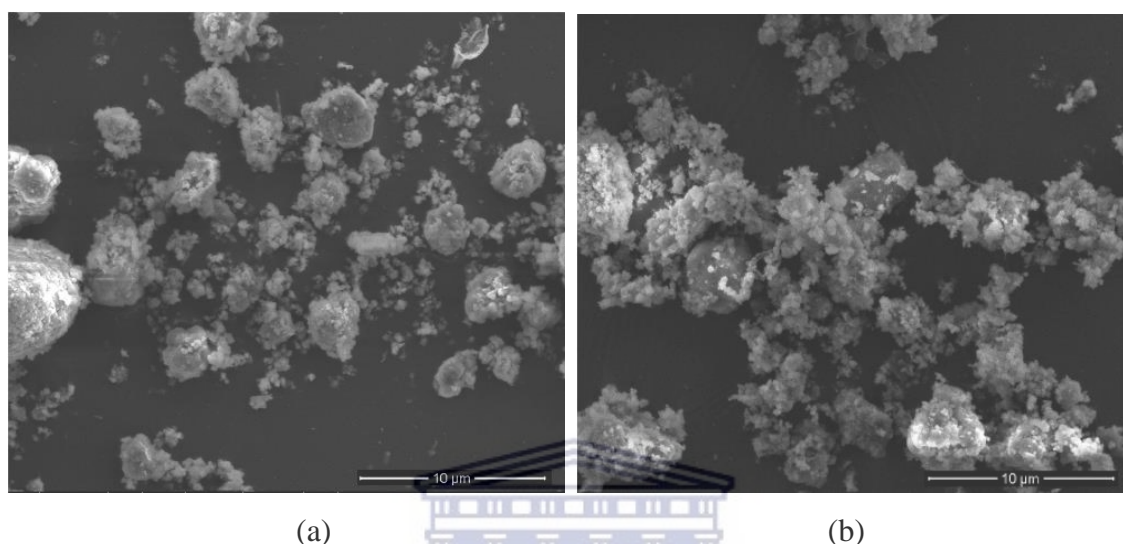
Figure 4. 13: SEM micrographs for HBEA supported metal catalysts prepared via conventional liquid phase ion exchange (a) 25FHI (sample prepared using FeAsh as precursor) and (b) 25AHI (sample prepared using AMD as precursor)

The SEM images presented in Figure 4.13 show an overview of the agglomerated but particulate morphology of metal loaded zeolite HBEA. The general morphologies of metal loaded zeolite crystals observed were irregular in shape implying that the samples are polycrystalline agglomerates rather than single crystals. Despite the fact that the two catalysts were metal loaded using different metal solution precursors, there was no marked difference in their overall morphology. The outcome is consistent with the description presented by Akbar, (2010), that zeolite HBEA does not exhibit a particular crystal habit. Using commercial sources in the synthesis of Fe loaded zeolite HBEA the same observation was reported by (Najjar et al., 2009: Ye et al., 2018).

4.4.2 Morphological studies of HBEA catalysts prepared via wet impregnation

The SEM micrographs of the fly ash based HBEA and the metal supported catalysts 25FHW and 25AHW synthesised via wet impregnation are shown in Figure 4.1.4. The

catalysts were prepared using FeAsh (25FHW) and AMD (25AHW). Again the catalysts with the highest metal wt % loading were chosen for discussion.

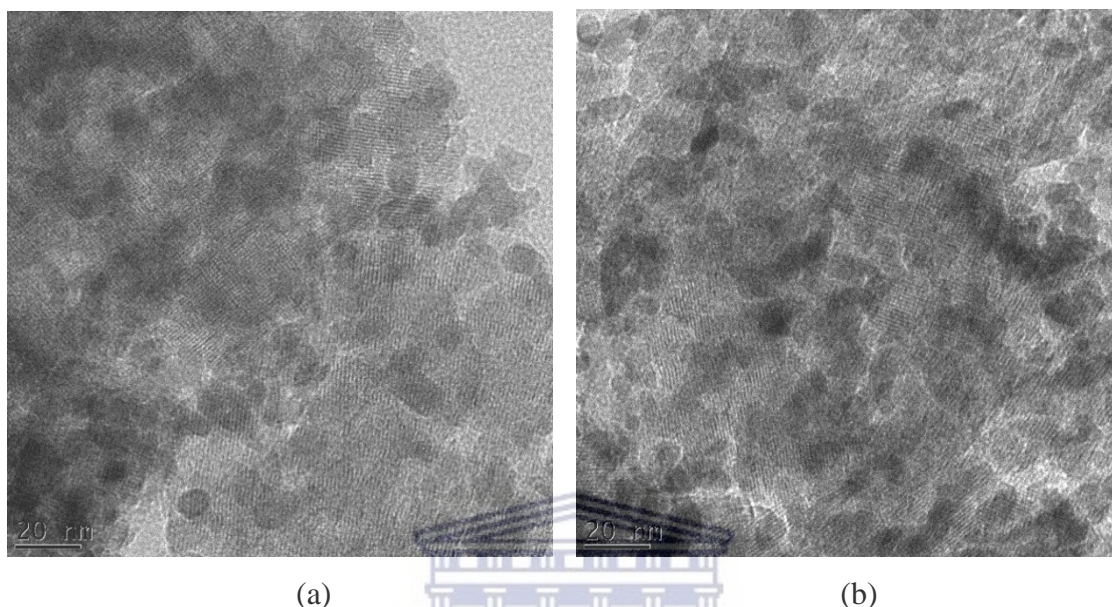(a)   (b)
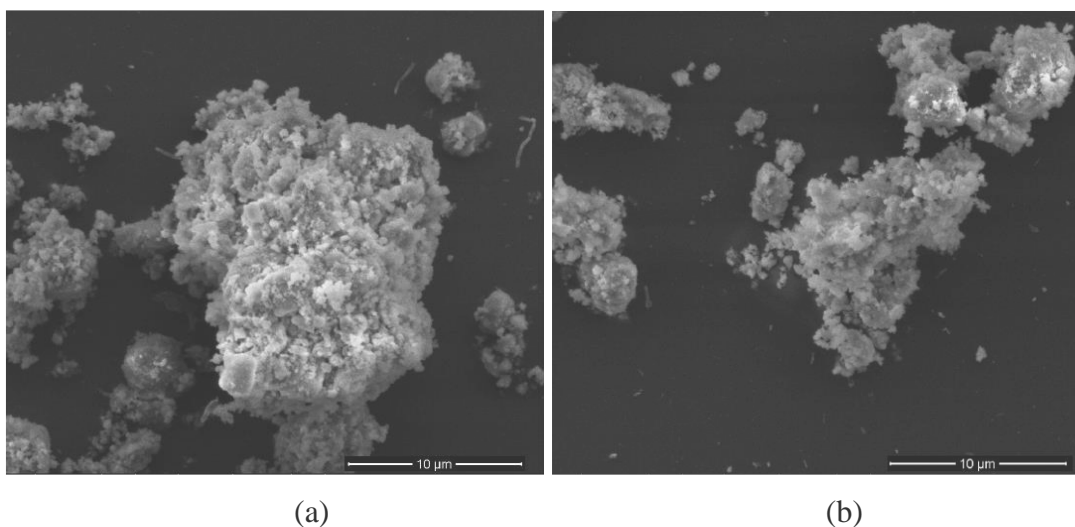
Figure 4. 14: SEM micrographs for HBEA supported metal catalysts prepared via wet impregnation. (a) 25FHW (prepared using FeAsh as precursor) and (b) 25AHW (prepared using AMD as precursor)

As was observed with the catalyst prepared via ion exchange, the wet impregnation prepared catalysts exhibited an irregular morphology consisting of agglomerated small particles. There was no marked difference in the morphology of the two catalysts presented in Figure 4.14 even though different metal precursor solutions were used. Related outcomes were observed and reported in various studies in which wet impregnation was used to introduce metals on HBEA using commercial supports and metal sources (Ausavasukhi et al., 2012; Murcia-López et al., 2017)

4.4.3   Morphological studies of MCM-41 catalysts prepared via wet impregnation

Metal loaded MCM-41 catalysts prepared via wet impregnation were also subjected to SEM analysis. The micrographs presented in Figure 4.15 are for the catalysts with the highest metal loading. The metal precursor solutions used were Fe extracted from CFA and AMD giving the catalysts 25FMW and 25AMW respectively.
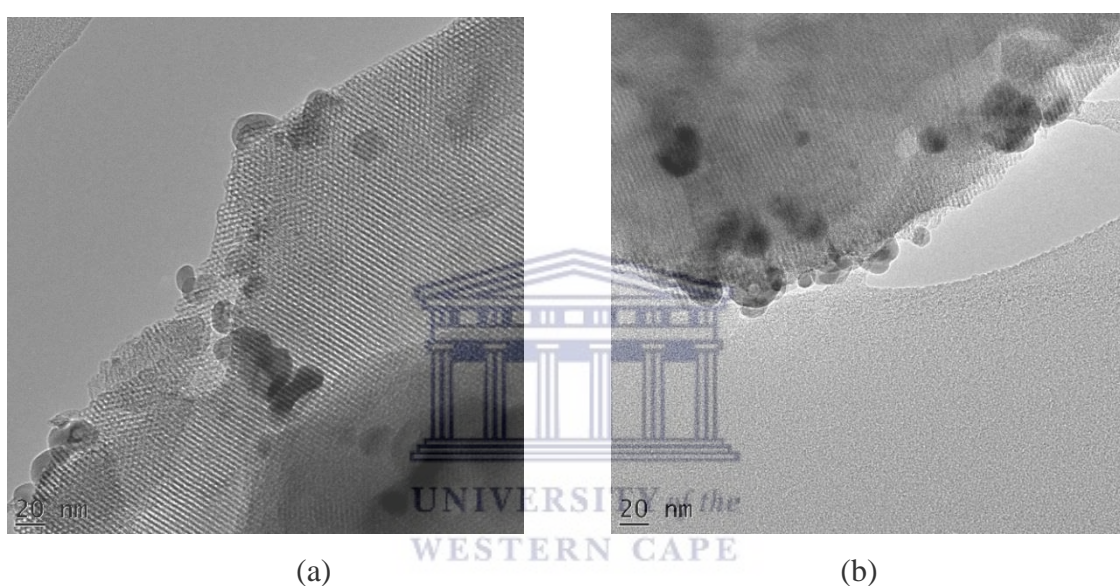
(a)   *(b)*
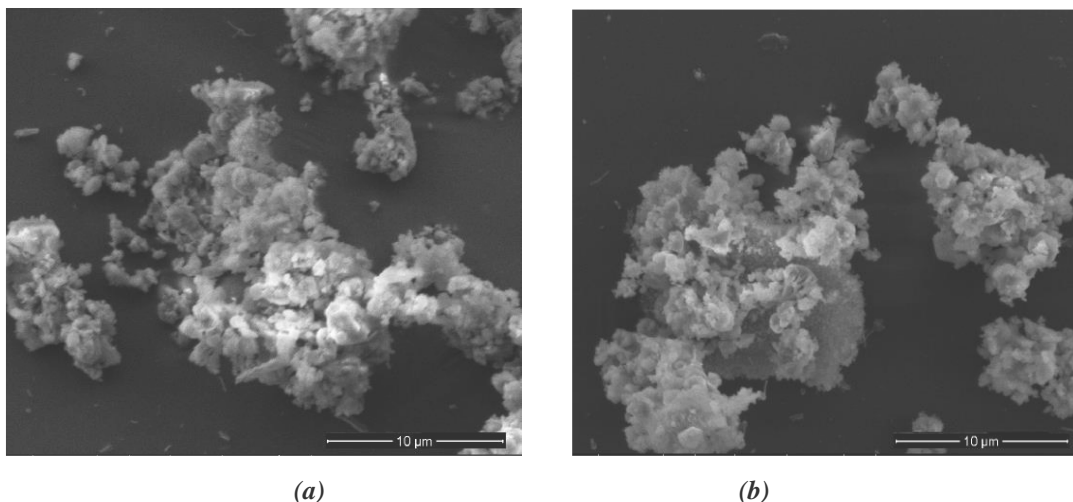
Figure 4. 15: SEM micrographs for MCM-41 supported metal catalysts prepared via wet impregnation (a) 25FMW (prepared using FeAsh as precursor) and (b) 25AMW (prepared using AMD as precursor).

The micrographs in Figure 4.15 show that the metal loaded MCM-41 have a general morphology of agglomerated particles of average size of 2 µm. Again there were no marked differences in the micrographs obtained despite the fact that the catalysts were prepared using different metal precursor solutions. It should be noted that the catalyst prepared using AMD contained additional metals apart from Fe. This condition did not alter the morphology of the metal loaded MCM-41. Generally, the morphology of MCM-41 is reported to be mostly composed of spherical agglomerates, however addition of metals to the support may alter the morphology by forming some hexagonal agglomerates (Hong et al., 2015). This observation is consistent with outcomes reported in related studies (Parvulescu & Su, 2001; Li et al., 2012; Hong et al., 2015)

4.5 Quantitative Elemental Composition

Inductively coupled plasma optical emission spectrometry (ICP-OES) was used to determine the quantitative elemental composition of the prepared catalysts. The sample digestion, dilution and analysis were carried out in accordance with the procedure outlined in Section 3.6.5.

4.5.1 Catalysts loaded via liquid phase ion exchange

Of the two support materials used, zeolite HBEA was the only support to which metals were loaded using liquid phase ion exchange. The metal solution precursors used were

FeAsh and AMD. The metal loading was performed following the procedure outlined in Section 3.5.1. The following sections present the elemental composition of the metal loaded supports starting with those prepared via ion exchange and then wet impregnation.

4.5.1.1 Catalysts loaded using Fe extracted from coal fly ash

The ICP-OES generated data on the quantitative elemental composition of the ion exchanged prepared metal loaded HBEA, synthesised using FeAsh is tabulated in Table 4.1. The same data is graphically presented in Figure 4.16.

Table 4. 1: Elemental composition of the ion exchanged HBEA prepared using Fe extracted from fly ash

Catalyst code	Metal wt % loading	
	Fe	Na
HBEA	0.01	0.03
5FHI	0.69	0.68
10FHI	1.42	1.49
15FHI	2.07	2.13
20FHI	2.83	3.22
25FHI	3.52	2.86
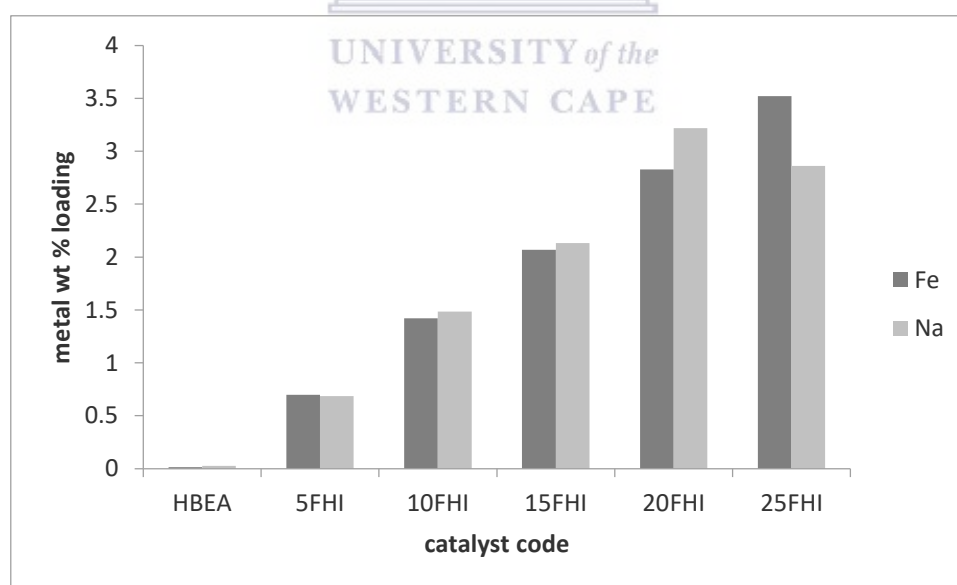
Figure 4. 16: Elemental composition of the ion exchanged HBEA prepared using Fe extracted from fly ash.

The data presented in Figure 4.16, shows that the catalysts were systematically loaded with significant quantities of both Fe and Na. The presence of Na was expected since the pH adjustment of the acid extracted Fe from fly ash was modified using NaOH. The amount of Fe:Na was almost 1:1 for catalysts with lower metal loadings. However, as the metal loading increased further the Na content went higher and then lower than that of Fe. The adsorption of Na onto the zeolite is dependent mostly on the number of exchange sites, pH and the concentration of the competing ion(s). As the loading of Fe increases the selectivity towards Na adsorption falls. In addition, the selectivity of the proton (H^+) is higher than that of Na, and the adsorption of Fe onto the exchange sites increases the H^+ concentration in solution further increasing the cation competition (Kabwadza-Corner et al., 2014). However, the wt % loading of Fe produced a linear relationship (increase in Fe concentration resulted in a corresponding increase in Fe wt % loading). Thus the Fe loading could be carefully controlled.

4.5.1.2 Catalysts loaded via ion exchange using acid mine drainage as metal precursor

The actual Fe wt % loading obtained on the HBEA support loaded via liquid phase ion exchange using AMD as metal solution precursor was also determined by ICP-OES and the data is presented in Table 4.2.

Table 4. 2: Elemental composition of the ion exchanged HBEA prepared using AMD

	catalyst				
Fe	5AHI	10AHI	15AHI	20AHI	25AHI
wt % loading	0.73	1.43	2.10	2.79	3.49

The actual metal wt % loading achieved using AMD as a metal precursor was comparable to that obtained using Fe solution extracted from coal fly ash. However, unlike the case with the latter, no other significant metals or cations were detected on the zeolite despite the fact that AMD contains not only Fe but a host of other metals. This outcome can be ascribed to the high selectivity of HBEA toward Fe relative to other metal ions. In addition, the relatively high concentration of Fe in AMD would further enhance its preferential adsorption and hence, the catalysts were found to be composed mostly of Fe.

Traces of other metals were detected by ICP-OES but the wt % loading of these metals were very low and were discounted.

4.5.2 Catalysts loaded via wet impregnation

The wet impregnation approach was used to load both HBEA and MCM-41 using the two metal solution precursors, Fe extracted from ash and AMD. The loading was carried out in accordance with the procedure outlined in Section 3.5.2.

4.5.2.1 Catalysts loaded on HBEA using Fe extracted from coal fly ash

The catalysts supported on HBEA prepared via wet impregnation were analysed for their elemental composition by ICP-OES and the data obtained tabulated in Table 4.3 and graphically represented in Figure 4.17.

Table 4. 3: Elemental composition of the wet impregnated HBEA prepared using Fe extracted from fly ash.

catalyst code	metal wt % loading	
	Fe	Na
5FHW	0.72	0.75
10FHW	1.38	1.49
15FHW	2.08	2.28
20FHW	2.76	3.04
25FHW	3.48	3.76
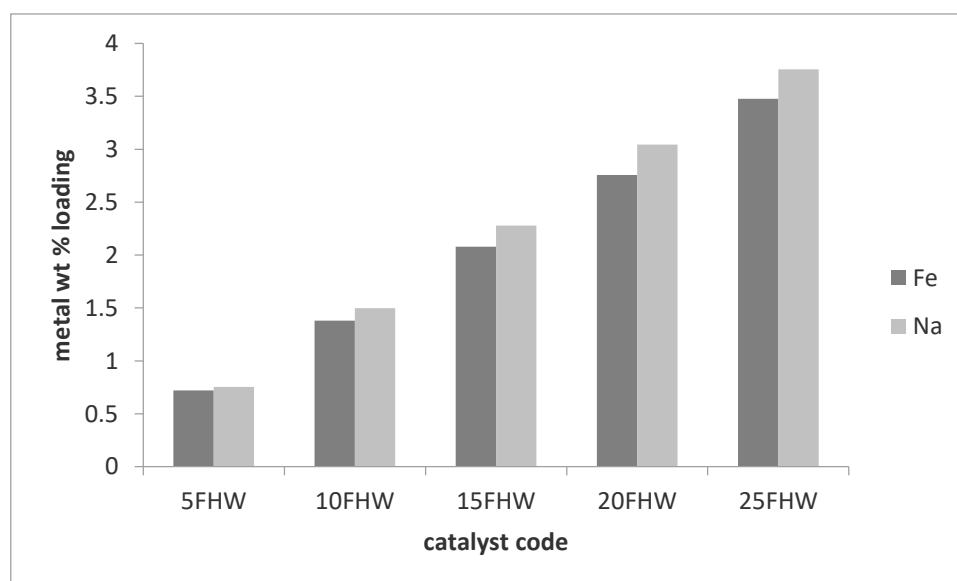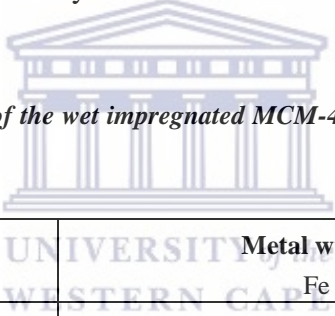
Figure 4. 17: Elemental composition of the wet impregnated HBEA prepared using Fe extracted from fly ash

The data presented in Figure 4.17 shows that the wet impregnated catalysts were composed of Fe and Na. It should be noted that the presence of Na was due to the fact that NaOH was used to regulate the pH after acid extraction of Fe from coal fly ash. The ratio of Fe:Na was constant in all the prepared catalysts. This outcome was expected, since with wet impregnation, all the metals present in the precursor solution are loaded onto the support, and competitive adsorption does not play a role in loading. The metals could either be present on the exchange sites or on the external surface of the zeolite. The exact location of the metals could not be established using ICP-OES. Again, as the metal solution concentration was increased there was a corresponding increase in wt % loading on the support.

4.5.2.2 Catalysts loaded on MCM-41 using Fe extracted from coal fly ash

The elemental composition the catalysts supported on MCM-41 prepared via wet impregnation was also determined by ICP-OES. The data is presented in Table 4.4 and Figure 4.18 respectively.

Table 4. 4: Elemental composition of the wet impregnated MCM-41 prepared using Fe extracted from fly ash.

Catalyst code	Metal wt % loading	
	Fe	Na
5FMW	0.69	0.72
10FMW	1.38	1.44
15FMW	2.07	2.31
20FMW	2.69	2.86
25FMW	3.50	3.62
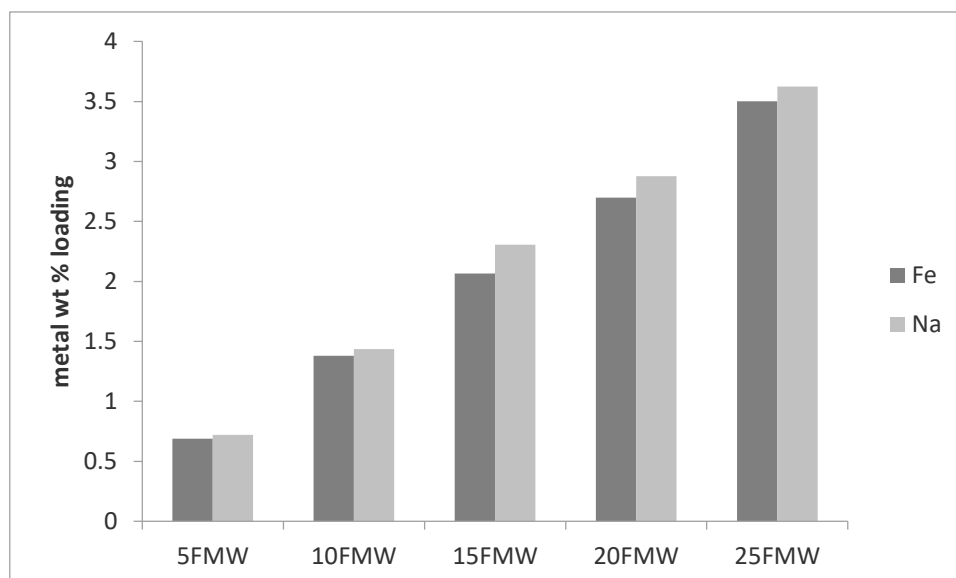
Figure 4. 18: Elemental composition of the wet impregnated MCM-41 prepared using Fe extracted from fly ash.

The data for MCM-41 supported Fe catalysts presented in Figure 4.18 is closely related to the data obtained for the HBEA supported counterparts. This outcome was expected since the approach allows all the metals in the precursor solution to be loaded onto the support. Hence if the same metal solution concentration is used and the solid liquid ratio maintained it is expected to get comparable outcomes. The actual metal wt % loading obtained with the catalyst with the highest metal loading was 3.501 % and the theoretical metal wt % loading was 3.5 %. The actual wt % and the theoretical wt % loading are very much comparable. The same was observed with the HBEA supported metal catalysts prepared via wet impregnation, hence it can be concluded that the approach is effective and can easily be tailored to give intended wt % loadings. In a study by Ereña et al. (2013) in which Cu and Zn were loaded onto zeolite ZSM5, the reproducibility of the wet impregnation approach was also observed.

4.5.2.3 Catalysts loaded on HBEA using AMD as metal precursor

The ICP-OES generated elemental composition data for the HBEA supported catalyst prepared via wet impregnation and using AMD as metal solution precursor are presented in Table 4.5 and Figure 4.19.

https://etd.uwc.ac.za

Table 4. 5: Elemental composition of the wet impregnated HBEA prepared using AMD as precursor.

Catalyst code	Metal wt % loading on HBEA					
	Fe	Ni	Ca	Na	Mg	Mn
5AHW	0.84	0.38	0.31	0.29	0.14	0.04
10AHW	1.46	0.85	0.61	0.39	0.24	0.08
15AHW	2.28	1.36	1.01	0.63	0.35	0.13
20AHW	2.62	1.42	1.22	0.80	0.41	0.16
25AHW	3.19	1.79	1.25	0.91	0.42	0.18
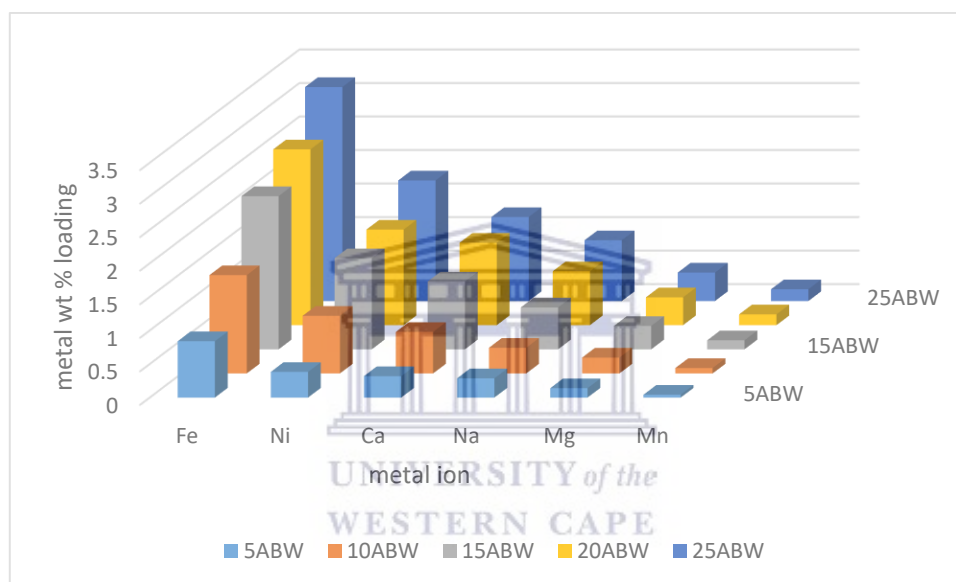
Figure 4.19: Elemental composition of the wet impregnated HBEA prepared using AMD as precursor.

The data presented in Figure 4.19 shows that not only Fe was loaded onto the support, but other metals found in AMD were also loaded onto the support. The outcome is ascribed to the fact that with wet impregnation all the metals in the precursor solution are deposited onto the support in the same proportions they are in the precursor solution (refer to AMD ICP-OES data presented in Appendix Section A1). Metals such as Ca, Na and Mg are exchangeable cations and would block Brønsted acid sites. This is in agreement with the expectation when wet impregnation is used as a loading approach. It should however be noted that the data presented only shows the metals that had significant quantities. Other metals present in the AMD were also loaded but their wt % loading in the final catalyst were minimal and hence discounted in the data presented.

4.5.2.4 Catalysts loaded on MCM-41 using AMD as metal precursor

The elemental composition data obtained from the MCM-41 supported catalyst prepared via wet impregnation are presented in Table 4.6 and Figure 4.20.

Table 4. 6*: Elemental composition of the wet impregnated MCM-41 prepared using AMD as precursor.*

Catalyst code	Metal wt % loading on MCM-41					
	Fe	Ni	Ca	Na	Mg	Mn
5AMW	0.8124	0.3698	0.2986	0.2523	0.1458	0.0399
10AMW	1.3986	0.8397	0.5987	0.3645	0.0986	0.0789
15AMW	2.0125	1.3068	0.98758	0.5978	0.3056	0.1281
20AMW	2.458	1.3998	1.1875	0.7856	0.3899	0.1576
25AMW	3.0879	1.8014	1.3001	0.8678	0.40458	0.1628
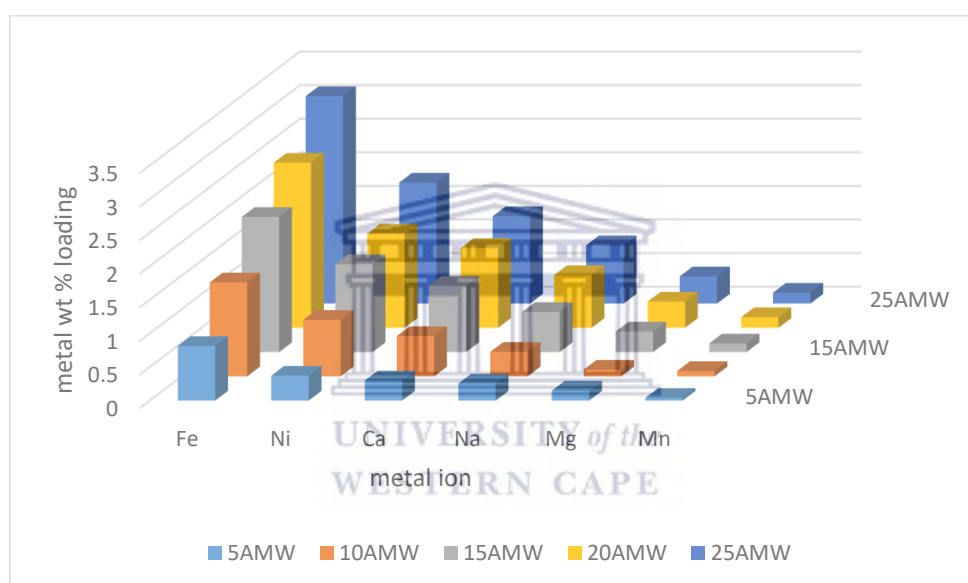
Figure 4.20: Elemental composition of the wet impregnated MCM-41 prepared using AMD as precursor.

The data presented in Figure 4.20 on wet impregnated MCM-41 is closely comparable to the data obtained with the corresponding HBEA catalysts. The outcome is expected since with wet impregnation all the available metals in the precursor solution are loaded onto the support in accordance with their respective proportions in the metal solution precursor. The increase in metal concentration resulted in an increase in the Fe wt % loading achieved. Again the theoretical Fe wt % loading was comparable to the actual metal wt % loading achieved. The presence of metals such as Na, Mg and Ca would not influence the acidity of the catalysts since there are no exchange sites in MCM-41 unlike in HBEA.

4.6 Surface area and pore area

The surface area studies for the synthesised catalysts were carried out by nitrogen adsorption-desorption studies. Surface area determination was performed using the Brunauer-Emmett-Teller (BET) equation and the pore size distribution determined using the Barrett, Joyner, Halenda (BJH) equation. The analyses were both carried out on an Autosorb-1C (Quantachrome Instruments) machine in accordance to the procedure outlined in Section 3.6.6. For the respective support materials only the catalyst with the highest metal loading for each loading approach employed was analysed, alongside the respective parent support materials. The outcomes are presented in the following sections.

4.6.1 Surface area studies over HBEA supported metal catalysts

The surface area, micropre area and micropore volume of metal catalysts supported on HBEA are presented in Table 4.7. The catalysts were prepared using Fe extracted from coal fly ash or AMD as metal precursors. Figure 4.21 presents the correlation between the BET surface area and Fe wt % loading.

Table 4. 7: Nitrogen adsorption surface area and pore size of the HBEA supported metal catalysts

Catalyst	BET surface area (m²/g)	Micropore area (m²/g)	Micropore volume (cm²/g)
HBEA	492	341	0.1602
25AHI	483	312	0.1465
25FHI	408	283	0.1398
25FHW	397	249	0.1265
25AHW	361	237	0.1185
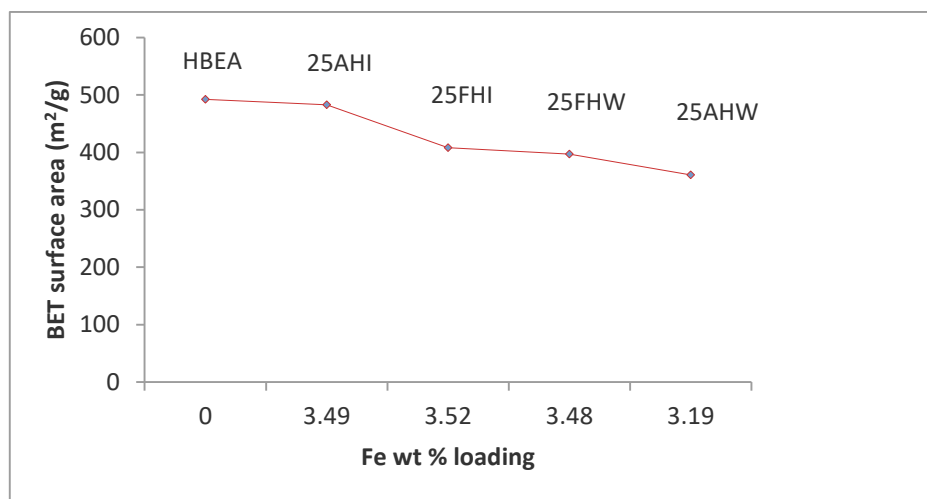
Figure 4.21: Relationship between BET surface area and Fe wt % loading of HBEA supported catalysts.

The data presented in Table 4.7 and Figure 4.21, shows that there was a near linear decrease in the BET surface area and micropore area with increasing metal loading. The parent material had a surface area of 492 m^2/g while the lowest surface area obtained with the analysed samples was 361 m^2/g on the 25AHW. There was also a corresponding decrease in both the micropore volume and the micropore area as the metal wt % loading increased showing that metals were hosted in the micropores. It is well known that surface area decreases with increasing metal loading especially with catalysts of metal loading below 5 % metal loading (Miskolczi et al., 2019). Similar outcomes were observed by (Miskolczi et al., 2019; Ahmed et al., 2017). The pore size distribution curves for the catalysts are graphically depicted in Figure 4.22.
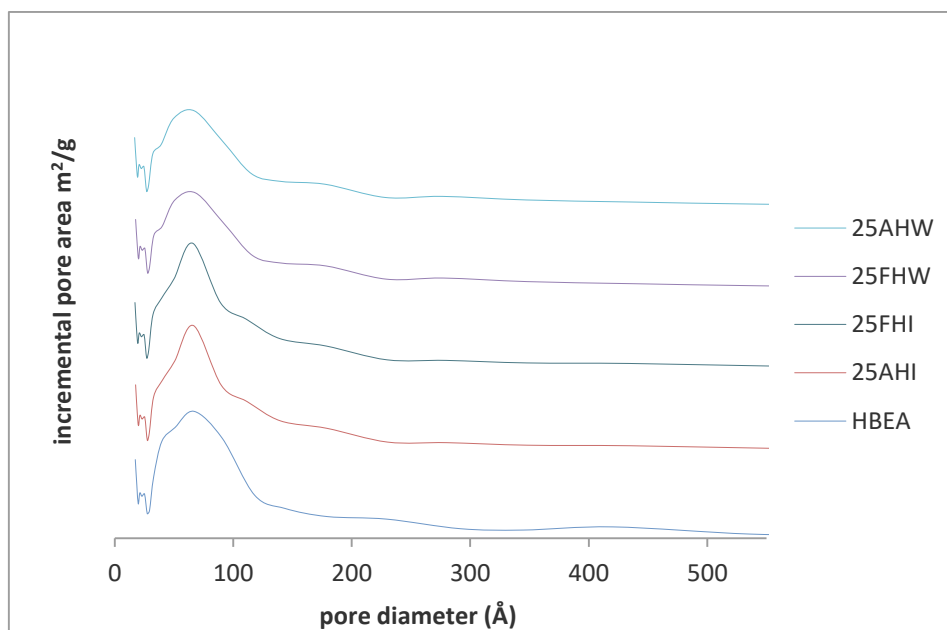
Figure 4.22: Pore size distribution of the metal catalysts supported on zeolite HBEA.

The parent zeolite HBEA mesopore diameter was not altered much upon metal loading, indicating that the metal did not disrupt the mesopore structure and the mesopore size range was from 28.1 – 118.1 Å. This outcome is indicative of the fact that the metals were in the micropores and well dispersed monoatomically. This can be further confirmed by the XRD profiles of the respective catalysts presented in Section 4.1. The data obtained is in agreement with the outcomes reported by (Carvalho et al., 2017; Zhou et al., 2019).

4.6.1.2 The nitrogen sorption isotherms for the metal loaded HBEA

The nitrogen adsorption-desorption isotherms of the metal loaded HBEA catalysts are shown in Figure 4.22.
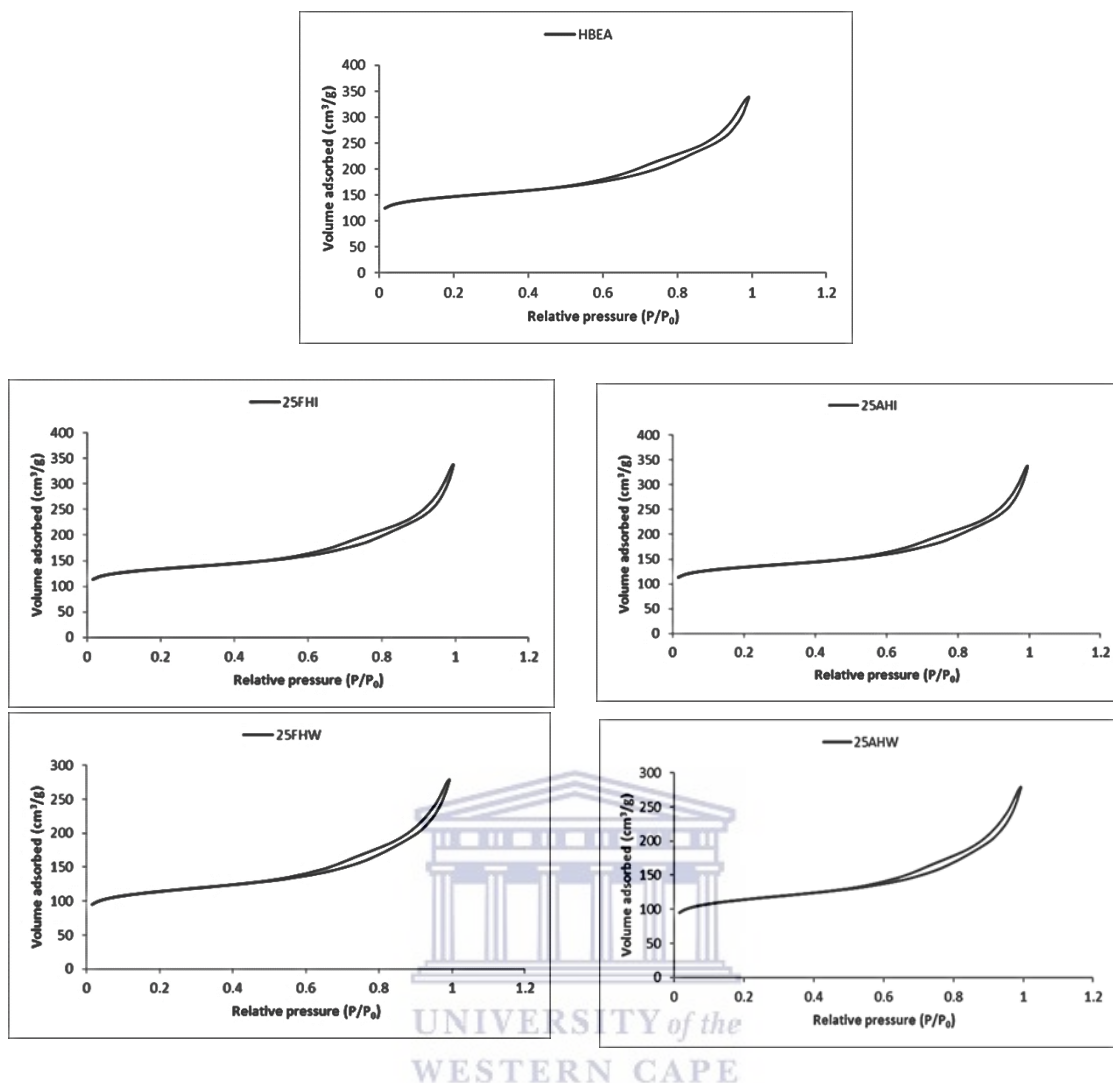
Figure 4. 23: Nitrogen adsorption–desorption isotherms of HBEA and the metal loaded HBEA.

The nitrogen adsorption-desorption isotherms for the HBEA supported metals presented in Figure 4.23 corresponded to type I and IV isotherms according to IUPAC empirical classification of hysteresis loops. The isotherm of the parent zeolite HBEA material displayed a sharp uptake at low P/P_0) values followed by a plateau without a hysteresis. There was a hysteresis at P/P_0) values above 0.6, which was due to filling of the intercrystalline pores of the zeolite. The metal loaded zeolites had similar isotherms, indicating that the pore structure was not greatly affected by the introduction of the metals. This further confirms the observations made with the XRD profiles in which no significant changes in the parent zeolite crystallinity were made. Similar observations were made by Miskolczi et al. (2019).

4.6.2 Surface area studies over MCM-41 supported metal catalysts

The surface area and the pore diameter of metal catalysts supported on MCM-41 are presented in Table 4.8. The catalysts were prepared using Fe extracted from coal fly ash or AMD as metal precursors in accordance with the procedure presented in Section 3.5.2.

Table 4. 8: Nitrogen adsorption surface area and pore size of the MCM-41 supported metal catalysts

catalyst	BET surface area (m²/g)	external surface area (m²/g)
MCM-41	867	911
25FMW	815	1244
25AMW	801	1241

The data presented in Table 4.8 shows that the BET surface area decreased upon metal loading. This suggests that metals are located in the mesopores of the MCM-41 support but are well dispersed and hence cause a slight reduction in pore diameter. The pore distribution curves are presented in Figure 4.24.
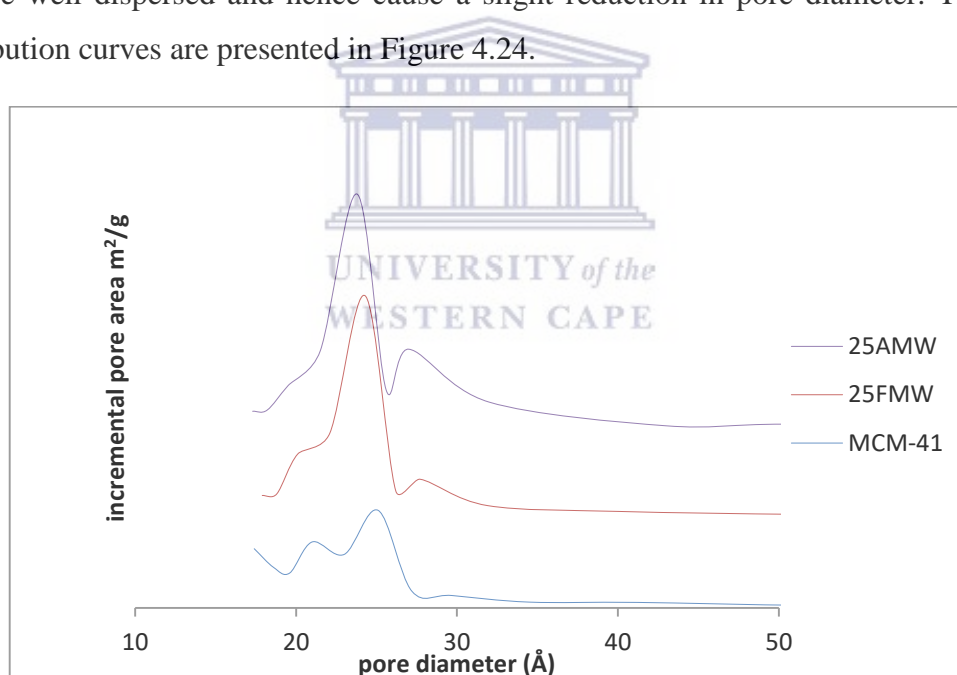
Figure 4. 24: Pore size distribution of the metal catalysts supported on zeolite MCM-41.

The mesopore diameter of the parent MCM-41 material was not altered much upon metal loading using either FeAsh or AMD. The pore diameter ranged from 20 - 27 Å and the pore diameter range became narrower as more of the metal was loaded. This outcome is in agreement with the observed shift of the XRD peaks towards higher 2 θ values (refer to Sections 4.1.5 and 4.1.6). The closeness of the pore sizes attests to the fact that the

integrity of the support was preserved upon metal loading. However, the metal loaded supports had a bimodal distribution curve and a smaller peak appeared around 27.4 and 27.7 for the 25AMW and 25FMW respectively. The peak shift proves that the metal was dispersed into the mesopores and not just on the surface. Related studies reported similar outcomes (Jiang et al., 2012; Jeirani, & Soltan, 2017).

4.6.2.1 The nitrogen sorption isotherms for the metal loaded MCM-41

The nitrogen sorption isotherms for the MCM-41 supported Fe catalysts prepared via wet impregnation are presented in Figure 4.25.
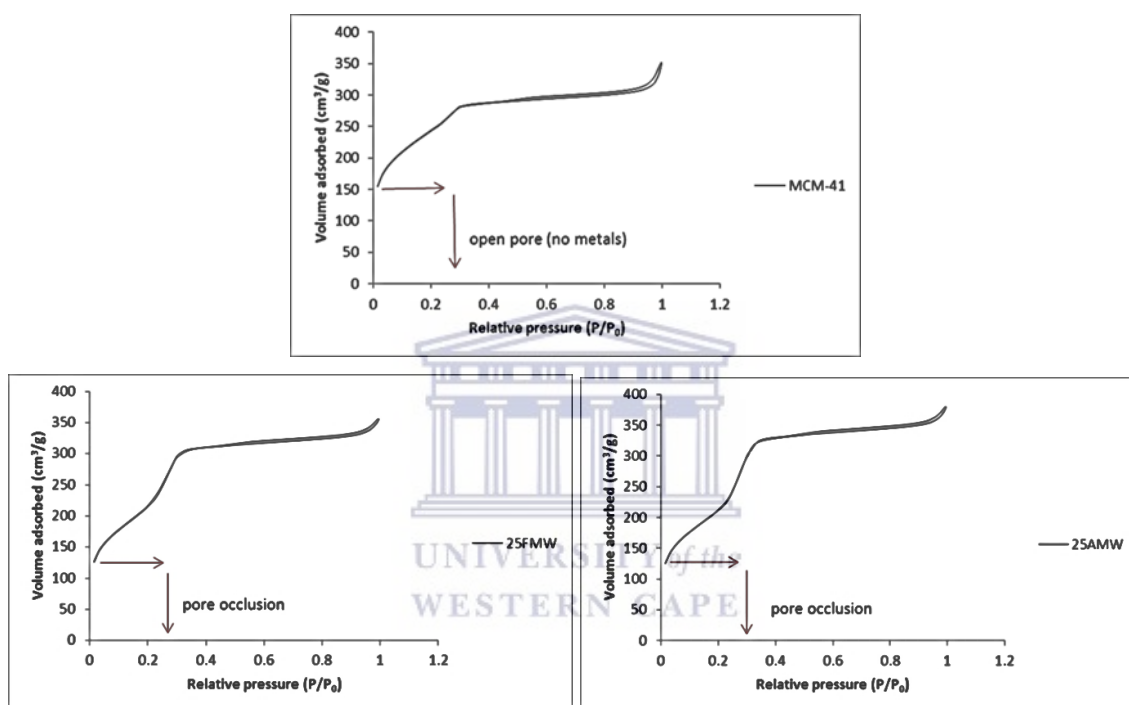
Figure 4. 25: Nitrogen adsorption–desorption isotherms of MCM-41 and the metal loaded MCM-41

The nitrogen isotherms presented in Figure 4.25 are completely reversible, indicating size uniformity of the tubular unidirectional mesopores typical of MCM-41 and showing that Si from waste CFA was suitable to prepare the MCM-41 structure. According to the IUPAC classification the isotherms exhibited belong to type IV and are characterised by a visible step in the (P/P_0) range of 0.25 to 0.35 arising from condensation of nitrogen inside the primary mesopores. The isotherms also showed a hysteresis loop above P/P_0 of 0.9, which are indicative of the presence of large mesopores or macropores. The outcomes are similar to those reported by (Jiang et al., 2012; Xu et al., 2018). Increase in metal loading resulted in pore occlusion and reduction in surface area. The observed pore occlusion apart from being influenced by the increase in metal wt % loading, it can also

be further enhanced by the calcination step undertaken on the catalyst to convert the loaded metals to the oside form (Tomatis et al., 2018).

4.7 Chapter summary

The fly ash based HBEA and MCM-41 alongside their respective metal loaded catalysts were subjected to a range of characterisation techniques namely XRD, HRTEM, SAED, ICP-OES and N_2-adsorption. The characterisation showed that high silica zeolite HBEA and MCM-41 were successfully made from waste CFA. The metal loading on the HBEA support was done via convention liquid phase ion exchange and wet impregnation while metal loading on MCM-41 was done only via wet impregnation. Two metal precursor solutions were used namely FeAsh and AMD. With the Fe supported on HBEA prepared via ion exchange using either FeAsh or AMD it was found that the crystallinity of the parent material was retained upon Fe loading. This confirms that the approach as well as the source of metal precursors did not alter the crystallinity of the pristine support. With ion exchange there was no evidence of the presence of metal oxide clusters on the support. However, when wet impregnation was used to load metals onto zeolite HBEA, peaks due to the αFe_2O_3 clusters were observed on the XRD profiles. This attests to the fact that wet impregnation has a tendency to form metal clusters on the support. The observation was made when wet impregnation was used to introduce the metals using either FeAsh or AMD as metal precursors. On the other hand, no metal oxide peaks were observed on the XRD profiles of the MCM-41 supported catalysts prepared via wet impregnation. The outcome can be attributed to the larger surface area of the mesoporous support allowing for greater metal dispersion. Further confirmation of the preservation of the support crystallinity was done using HRTEM. The HRTEM micrographs generated on all the catalysts analysed confirmed that the crystallinity of the respective parent materials was retained upon metal loading using the two metal precursors.

The morphology studies on the catalysts was done by SEM analysis and again the outcomes confirm that the particle size and morphology of the respective support materials was preserved when loading was done using either metal solution precursors as well as the two different metal loading approaches in the case of HBEA. The ICP-OES

data generated showed that the two approaches are effective in the preparation of Fe loaded supports. The theoretical and actual metal wt % loadings achieved were comparable indicating that both approaches can be easily tailored to achieve desired Fe wt % loadings. However, ion exchange proved to be associated with better metal dispersion compared to wet impregnation. In the case of the HBEA supported catalysts prepared using AMD as metal precursor the elemental composition analyses showed that when ion exchange was used there was selectivity towards Fe rather than to other metals and cations in the AMD. The catalysts supported on HBEA prepared via ion exchange using AMD as metal precursor only contained Fe but when wet impregnation was used all the metals in the AMD were introduced onto the zeolite in the respective ratios as they were in the original AMD solution. From the N_2-adsorption studies carried out over the pristine materials as well as the metal loaded supports it was generally found that an increase in metal loading resulted in a decrease in the BET surface area on both supports. There was also an observable reduction in the micropore area and volume in the case of HBEA with increasing metal wt % loading showing good dispersion of metals in the pores.

The characterisation on the metal supported catalysts carried out shows that both MCM-41 and HBEA can be synthesised via a novel approach that involves acid assisted silica extraction followed by hydrothermal synthesis. It further goes on to prove that both FeAsh and AMD are suitable metal precursors in the preparation of metal supported catalysts as shown by the close similarities in the characterisation outcomes obtained in the present study against other observations made in related studies that involved the use of commercial sources in both the synthesis of the support as well as the metal precursor. The characterisation proved that Fe supported on high silica zeolite HBEA and MCM-41 can be synthesised using CFA as a feedstock and FeAsh and AMD as metal precursors. This is the first time these waste materials were used in the preparation of supported Fe catalysts.

CHAPTER 5

5.0 Activity of supported metals prepared using acid mine drainage as metal precursor

The chapter presents the activity of metal catalysts loaded on HBEA and MCM-41 using acid mine drainage as metal solution precursor. The Friedel-Crafts alkylation of benzene with t-butyl chloride was used as the probe reaction. The catalyst testing was carried out as outlined in Chapter 3, focusing on the conversion, selectivity, yield and product distribution. The chapter further explores the effects of different reaction parameters namely, reaction time, metal loading, nature of support and the effect of metals on the support other than iron. The chapter closes with a brief summary of the overall catalytic activity of the tested materials.

5.1 Catalytic activity studies over ion exchanged HBEA metal catalysts

The conversion, selectivity, product distribution studies and yield over the HBEA supported metal catalysts were carried out at a temperature of 45 °C over a reaction time of 5 h. The screening was carried out in accordance to the procedure outlined in Section 3.7. In the reaction mixture benzene was in excess as it served as both solvent and reactant, thus the conversion studies were carried out based on the levels of t-butyl chloride against reaction time. The Friedel-Crafts alkylation of benzene with t-butyl chloride proceeds as follows:
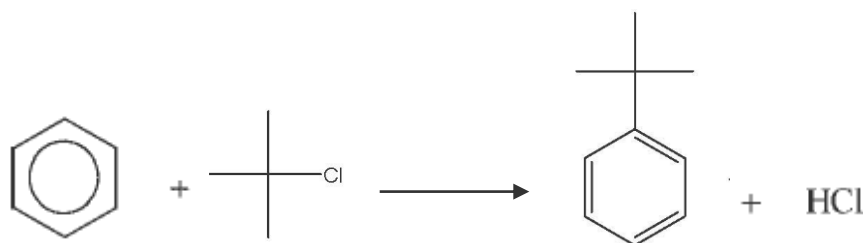
The reaction however results in other by products alongside the *t*-butyl benzene and HCl. Alkylation reactions are generally associated with transalkylation polymerization and polyalkylation. The outcomes generated over the range of catalysts tested are presented in the following sections**.**

5.1.1 Conversion studies over ion exchanged HBEA

The percentage conversion of *t*-butyl chloride over the metal loaded HBEA prepared using AMD as metal solution precursor is plotted against reaction time and depicted in Figure 5.1.

Figure 5. 1: Conversion of t-butyl chloride over the series of HBEA supported metals prepared using AMD as metal precursor at reaction temperature of 45 °C (benzene : tBC ratio of 10mL : 1 mL and 320 g of catalyst)

The profiles presented in Figure 5.1 depict the conversion of *t*-butyl chloride as a function of time. Generally, all the profiles for the catalysts tested apart from that of the pristine HBEA support, are characterised by a rapid increase in conversion in the first 0.5 h, then leading to a steady state after about 0.5 h time on stream. The observed trend is typical of an autocatalytic reaction (Choudhary et al., 1999). The conversion over the parent HBEA support rises gradually in the first 2 h, reaching a steady state thereafter. The highest conversion achieved over the parent zeolite HBEA was 30.7 % after 4 h on stream. Although there are no Lewis acid sites on the parent material, the Brønsted acid sites are active in the alkylation of benzene with *t*-butyl chloride hence the activity. It however, is evident that the introduction of Fe on the zeolite significantly increased the activity as can be seen from the profiles, showing that as the Fe wt % loading was increased the percentage conversion of the *t*-butyl chloride increased as well. The high activity of the Fe loaded HBEA can be attributed to the presence of both Brønsted and Lewis acid sites, which have a synergic effect on the activity. The Brønsted sites effect the carbonium ion

formation while the deprotonation to form the alkylated product occurs on the Lewis acid sites (Nur et al., 2011). The activation of the benzene nucleus on the Fe oxide species, having redox function, present in close proximity with the zeolite protons is attributed to the high activity (Choudhary et al., 1999). Furthermore, the metal dispersion on the support has a significant influence on the catalytic activity. It has been revealed that nanoparticle phased iron oxide activates the benzene, forming $C_6H_5–H$ ($C_6H_5{}^{\delta-}\cdots\cdots H^{\delta+}$) species which are more reactive than benzene (Lin et al., 2011). Considering the XRD profiles and the TEM micrographs presented in Section 4.1.2 and 4.2.1 respectively, it could be deduced that the metal was well dispersed and no large metal crystallites were formed, thus the pores were accessible.

It should also be noted that although AMD has numerous metal ions present in it, the major metal that was loaded onto the zeolite by ion exchange was Fe (refer to ICP-OES data in Section 4.5.1.2). The selective ion exchange of Fe in relation to the other metals is due to its higher concentration in solution, smaller hydration shell as well as higher charge density. The theoretical metal wt % loading for the catalysts whose profiles are presented were (0.7; 1.4; 2.1; 2.8 and 3.5) with the lowest Fe loading on sample 5AHI and the highest loading on sample 25AHI. The actual Fe wt % loading for the respective catalysts were (0.73, 1.43, 2.10, 2.79, 3.49). Sample 5AHI had a relatively high conversion of 84.53 % after 2 h on stream while the highest Fe loaded catalyst (25AHI) had a conversion of 100 % at the same time on stream.

The high activity of the catalyst series presented in Figure 5.1 can further be attributed to the high dispersion of the metal in the pores of the support. The loading approach applied (liquid phase ion exchange) is associated with high metal dispersion. This minimises diffusional constraints within the zeolite pores. It is well know that increase in metal loading results in decrease in pore diameter and the BET surface area. The BET surface area for the parent HBEA zeolite and the 25AHI were 492 and 482 m^2/g respectively (refer to Table 4.7). The FC alkylation of benzene with tBC is accompanied by the liberation of HCl (refer to reaction scheme in Section 5.1). In a related study by Choudhary et al., (1999) in which the alkylation of benzene by benzyl chloride over H-ZSM-5 modified by Fe and Ga was conducted, it was found that the presence of chlorine

activated the reaction in the initial reaction stages resulting in high conversions. The effect of chlorination on the activity was however not studied in this present study, but the effect may also be the cause of the high activity observed. In a related study by Bidart et al. (2006) the alkylation of benzene was studied over Fe loaded zeolite Y, and base addition was carried out to neutralise the produced HCl. The base addition step was found to reduce the catalytic activity which might further indicate that the produced HCl, via chlorination of the Lewis acid sites improves the catalytic activity instead. Work by Arata and Hino (1980) in which the alkylation of benzene with various alkylating agents was conducted concluded that the iron chloride formed on the surface of the iron oxide surface by the reaction with HCl is a catalytically active species for alkylation. The trends presented in Figure 5.1 are similar to those that have been observed in earlier studies involving the alkylation of benzene and reported by (Vinu et al., 2005; Choudhary et al., 1999). The outcomes presented in Figure 5.1 show that fly ash based HBEA loaded with AMD can be used as an alternative in the preparation of metal loaded catalysts for the FC-alkylation reaction.

5.1.2 Selectivity studies over ion exchanged HBEA

The alkylation of benzene by t-butyl chloride gives rise to numerous by-products alongside the monoalkylated product. The other by products are the dialkylated ones (1.2-di-t-butyl benzene, 1.3-di-t-butyl benzene and 1,4-di-t-butyl benzene), and the trialkylated product (1,3,5-tri-tert-butylbenzene). In the present study the desired product was the monoalkylated product and hence the selectivity studies were carried out based on the formation of t-butyl benzene. The profiles are presented in Figure 5.2.
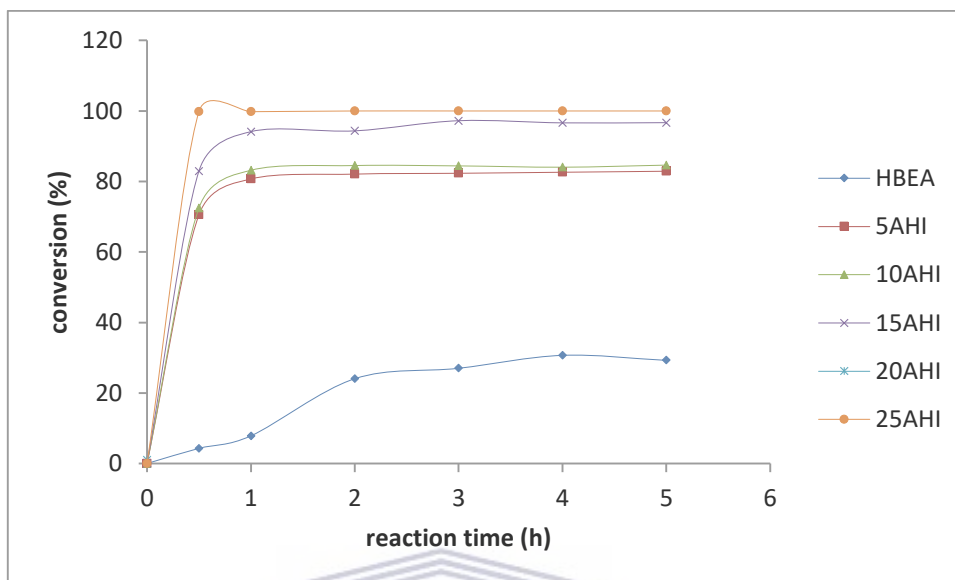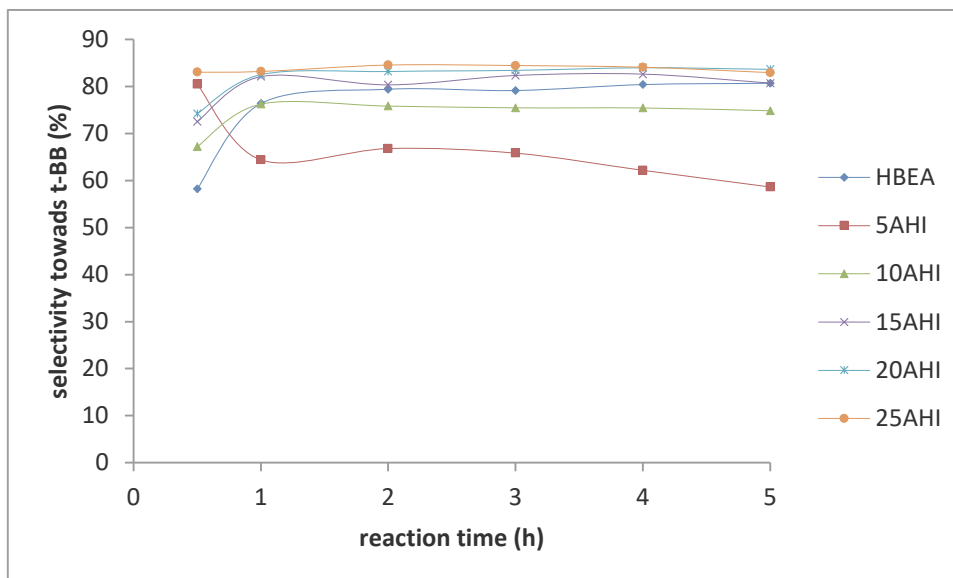
Figure 5. 2: Selectivity of t-butyl benzene over the series of HBEA supported metals prepared using AMD as metal precursor at reaction temperature of 45 °C (benzene : tBC ratio of 10mL : 1 mL and 320 g of catalyst)

The highest selectivity towards the formation of the monoalkylated product over the pristine zeolite HBEA was 80.6 % after a reaction time of 5 h. The selectivity was 58.2 % after 0.5 h on stream rising to a steady state after 1 h. Generally, the selectivity obtained over the series of HBEA supported metal catalysts presented in Figure 5.2 are comparable to that of the pristine material. The high selectivity over HBEA is due to the fact that the pore openings are slightly larger than the size of benzene molecule and do not allow the formation of molecules whose critical diameters are significantly larger (Perego & Ingallina 2002). However, the selectivity obtained over the 5AHI (Fe wt % loading of 0.73) had a slightly different profile The catalyst was characterised with an initial high selectivity in the first 0.5 h (80.5 %) followed by a reduction after 1 h (64.4 %) reaching a steady state. The selectivity over sample 10AHI (Fe wt % loading of 1.43) was also lower than that of the parent material. The lower selectivity on these two catalysts may be ascribed to the low metal loading. The conversion reaches a steady state after the first hour. This may then lead to polyalkylation after steady state is reached since the monoalkylated product has a higher reactivity relative to that of benzene. Furthermore, the specific adsorption of benzene on the H-zeolite is higher on the parent material than on zeolites with lower Fe wt % loading of about 5 %. An increase in the metal loading to higher wt % loadings further increased the specific adsorption (D´ıaz et al., 2005). This

phenomenon may be responsible for the observed lower selectivity on the 5AHI and 10AHI relative to that of the parent material.

The catalysts with relatively higher metal loadings gave a higher selectivity towards t-butyl benzene formation. The 25AHI (Fe wt % loading of 3.49) had the highest selectivity of 84.5 % after 2 h on stream. The higher selectivity observed with higher wt % loadings may be attributed to the larger amount of reactive sites giving high conversions. It should however be noted that the increase in reactive sites does not always result in an increase in selectivity. Selectivity over porous materials is at times governed by the pore system of the support rather than metal loading. In the present study, the zeolite pore system was not altered much by metal introduction and could not have had a profound effect on selectivity (refer to Figure 4.20). Another factor that may influence product selectivity is the molar ratio of the reactants. In the present study, an excess of benzene was used and this suppresses the tendency of forming polyalkylated products. In a related study by D´ıaz et al., (2005), in which the alkylation of benzene with benzyl chloride over Fe loaded ZSM-5 was conducted, it was observed that as the metal loading increased there was a decrease in the selectivity towards formation of the monoalkylated product (diphenyl methane). Their outcome is not in exact agreement with the observations made in this study since a general increase in selectivity with an increase in metal loading was observed. The differences ought to be due to the differences in reaction conditions, nature of support (ZSM-5 pores are smaller than than those of HBEA, and high metal loading may block the pores) and catalyst preparation. Contrary to the observations reported by D´ıaz et al., (2005), Kostrab (2010) carried out a study on the effect of zeolite shape selectivity on the alkylation of toluene with t-butanol over Ce-modified zeolite HMOR. In their study, it was observed that an increase in the metal loading resulted in an increase in selectivity towards the formation of the monoalkylated product. The parent HMOR gave the lowest selectivity, and selectivity increased with an increase in metal loading. The similarities in the trends observed over HMOR supported Ce and those observed in the present study can be attributed to the fact that the pore system of MOR and BEA are comparable in size.

5.1.3 Product distribution over HBEA supported catalysts prepared via ion exchange using AMD as metal precursor.

The alkylation of benzene with t-butyl chloride is characterised by the formation of various dialkylated products (1,2-di-teritiary butyl benzene, 1,3 di-teritiary butyl benzene & 1.4-di-teritiary butyl benzene) and the tri alkylated product (1,3,5-tri-tertiary butyl benzene). Isomer distribution can be either kinetically or thermodynamically controlled. Furthermore, the molar ratio of the benzene to the alkylating agent influences the isomer distribution. In cases where porous supports are used the support channels have a marked influence on the product distribution. The factors affecting product distribution are outlined in Section 2.8. For discussion purposes the catalyst with the lowest and highest metal loading for the different catalyst series prepared using AMD as metal precursor are considered. This is done against the product distribution studies over the parent HBEA zeolite as a baseline.

5.1.3.1 Product distribution over the pristine HBEA support

The product distribution obtained over the parent zeolite HBEA is presented in Figure 5.3
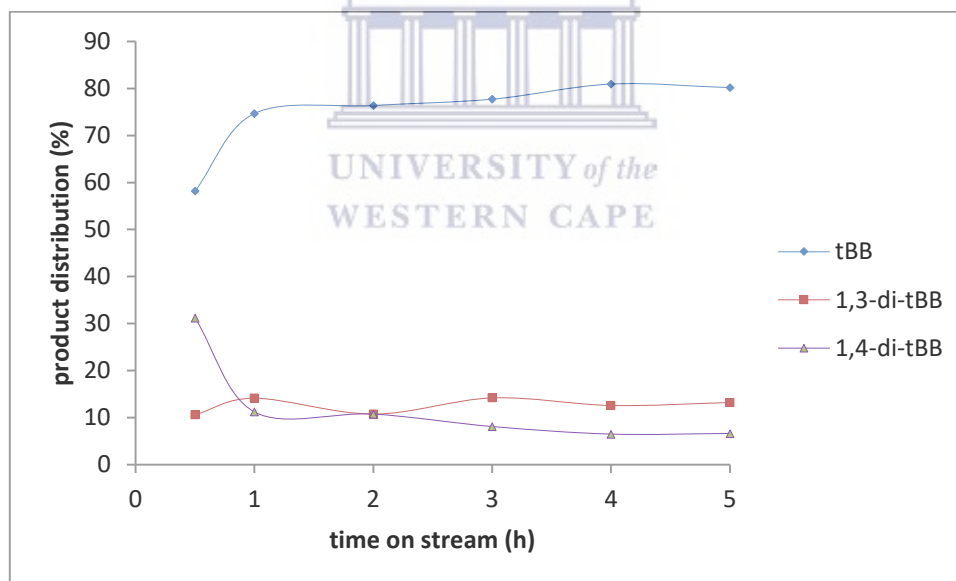
Figure 5. 3: Product distribution for benzene alkylation with t-butyl chloride over the parent HBEA at 45 °C (benzene : tBC ratio of 10mL : 1 mL and 320 g of catalyst)

*{t-butyl benzene (t-BB); 1,3-di-t-butyl benzene (1,3-di-t-BB); 1,4-di-t-butyl benzene (1,4-di-t-BB) }

The primary product obtained over the pristine fly ash based zeolite HBEA was the monoalkylated product (tertiary butyl benzene). The percentage of the monoalkylated product increased in the reaction mixture with time. There was a rapid increase in the

amount of tBB from the first 0.5 h to 1 h which then increased slowly at steady state conversion. The rapid rise in the initial stages of the reaction may be ascribed to the availability of the HCl which is also a by-product of the reaction, but it has been found to catalyse the alkylation reaction as well. In the initial stages the only active centres for alkylation are the Brønsted acid sites of the zeolite. The highest amount of tBB obtained over the parent HBEA was 80.9 % after 4 h on stream.

The only dialkylated products obtained over the parent material were the meta and *para* isomers. The ortho isomer was not detected in the product mixture and neither was the tri alkylated product detected. The ortho isomer is subjected to steric hindrances between the substituent and the entering group. It is well established that the reaction between benzene and t-butyl chloride does not give the ortho isomer despite the effects of reactant molar ratios (Roberts & Caserio, 1977). The first alkylation activates the *para* position and hence there is significant amount of the *para* isomer in the initial stages of the reaction. The percentage of the *para* isomer decreases with prolonged reaction time while the percentage of the *meta* isomer starts to increase. The *meta* isomer is more thermodynamically stable and the outcome is expected with longer reaction times. In addition to the thermodynamic stability of the *meta* isomer, the HCl produced by the alkylation reaction (refer to reaction scheme in Section 5.1) also affects the isomer distribution. In a study by Bidart et al., (2006) in which a base was added to remove the produced HCl, it was found that the base addition resulted in the reduction of the *meta* isomer and it was concluded that at least part of the isomerisation is catalysed by the HCl formed, and occurs outside the zeolite pore system. The formation of the trialkylated product would be expected in the case that the benzene to alkylating agent ratio is small, however in this study an excess of benzene was used which could have suppressed polyalkylation.

5.1.3.2 Product distribution over 5AHI

The product distribution over the catalyst with the lowest metal loading (5AHI prepared via ion exchange using AMD as metal precursor) is presented in Figure 5.4.
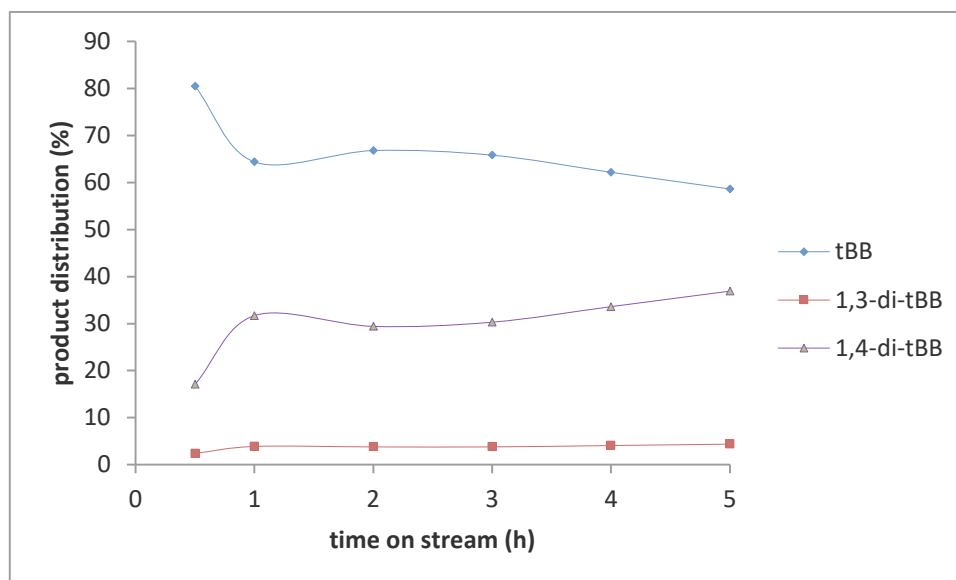
Figure 5. 4: Product distribution for benzene alkylation with t-butyl chloride over the 5AHI at 45 °C (benzene : tBC ratio of 10mL : 1 mL and 320 g of catalyst)

The product distribution curve, over 5AHI (actual Fe wt % loading of 0.73) presented in Figure 5.4 shows that the primary product was the monoalkylated product. The percentage of the monoalkylated product was high in the initial stages of the reaction with 80.5 % after 0.5 h on stream. The percentage decreased with prolonged reaction time at steady state conversion while the amounts of the dialkylated products were increasing with time. The profile of the *para* isomer is characterised with a sharp increase in the first 0.5 h on stream reaching a steady state and a highest percentage of 36.9 after 5 h on stream. Although the *meta* isomer is more thermodynamically stable relative to the *para* isomer it was the *para* isomer that was dominating throughout the entire reaction period studied. The outcome may be ascribed to the relatively lower conversion obtained over the catalyst (highest conversion of 84.5 % after 2 h on stream), which consequently limited the amount of HCl evolved. Furthermore, HCl chlorinates the Fe sites leaving limited amounts of HCl in the reaction mixture. The effect of HCl on isomer distribution has been covered in the previous section. Again, the ortho and the trialkylated products were not detected for the reasons mentioned previously. The outcomes are in agreement with those reported by Bidart et al., (2001) in a study in which the alkylation of benzene with t-butyl chloride was carried out over Fe loaded zeolite Y.

5.1.3.3 Product distribution over 25AHI

The product distribution over the catalyst with the highest metal loading the 25AHI prepared via ion exchange using AMD as metal precursor is presented in Figure 5.5.
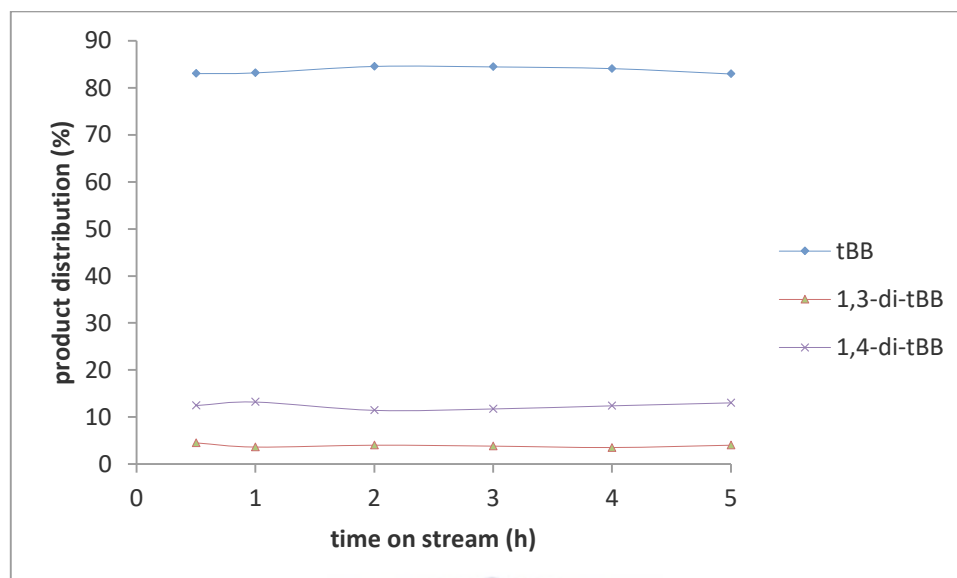
Figure 5. 5: Product distribution for benzene alkylation with t-butyl chloride over the 25AHI at 45 °C (benzene : tBC ratio of 10mL : 1 mL and 320 g of catalyst)

The profiles in Figure 5.5 depict the product distribution obtained over the 25AHI (Fe wt % loading of 3.49). Again the primary product was found to be the monoalkylated product with a highest percentage of 84.5 after 3 h on stream. The profiles in Figure 5.5 are different from the other profiles which were characterised with significant variations of the products with time. Since the catalyst had a high metal wt % loading recording a conversion of 99.8 % after 0.5 h, it can be said that the reaction reached a steady state within that period and no variations of product distribution occurred over time nor did the catalyst deactivate in the time tested. In a related study by Lin et al., (2011) the alkylation of benzene with benzyl chloride was carried out over Fe modified zeolite ZSM5 and 100 % selectivity towards the formation of the monoalkylated product was achieved (reaction condition applied - 30 mL benzene, 2.7 mL benzyl chloride, 0.2 g catalyst at 80 °C).

5.1.3.4 Product Yield over ion exchanged HBEA

One of the fundamental parameters used in expressing catalyst activity is the yield of the desired product, and the percentage yields of the *t*-butyl benzene produced over the HBEA supported metal catalysts are presented in Figure 5. 6.

Figure 5. 6: Product yield of t-butyl benzene over the series of HBEA supported metals prepared using AMD as metal precursor at reaction temperature of 45 °C (benzene : tBC ratio of 10mL : 1 mL and 320 g of catalyst)

The profiles presented in Figure 5.6 depict the percentage yield for the fly ash based HBEA supported catalysts prepared using AMD as metal precursor. From the trends presented it can be seen that the yield generally increased with an increase in the metal loading. The parent HBEA material had the lowest yield in comparison to the metal loaded support. The yield obtained over the parent material was only 24.7 % after 4 h on stream. The highest yield obtained was 84.6 % over the 25AHI (Fe wt % loading of 3.49) after 2 h on stream. The high Fe content and porous structure provided many active sites with accessible Lewis acidity. From the pore size distribution and surface area studies presented in Section 4.6 it was shown that there was not much difference induced in pore size by metal incorporation onto the support, hence catalytic activity was mainly dependent on the amount of metal loading. Furthermore, the yield is calculated based on the conversion and selectivity according to the equation presented in Section 3.7.3. Hence the factors affecting these two parameters consequently affect the percentage yield.

5.2 Catalytic activity studies over wet impregnated HBEA metal catalysts

The catalytic activity of the HBEA supported metal catalysts prepared via wet impregnation using AMD as metal solution precursor were studied based on the conversion of t-butyl chloride, selectivity towards formation of t-butyl benzene, product distribution and percentage yield of t-butyl benzene.

https://etd.uwc.ac.za

5.2.1 Conversion studies over wet impregnated HBEA

The conversion studies for the HBEA supported catalysts prepared via wet impregnation and using AMD as metal solution precursor were carried out on 5 different catalysts with different metal loadings alongside the parent HBEA material. The benzene alkylation with t-butyl chloride was carried out at a temperature of 45 °C according to the procedure outlined in Section 3. 7. 2. The catalyst coding is presented in Table 3.2. The profiles for the conversion of t-butyl chloride against time on stream are presented in Figure 5.7 for the catalysts series.
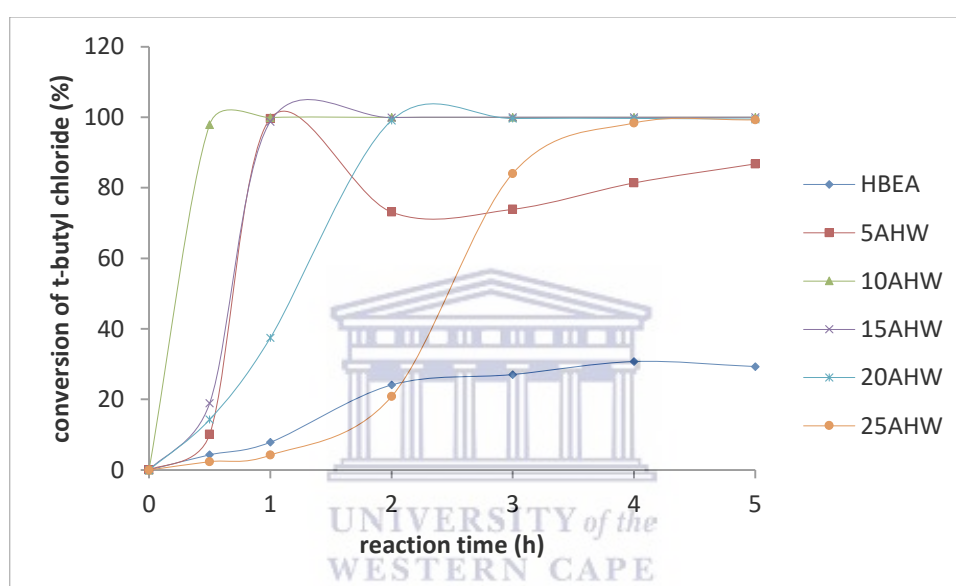
Figure 5. 7: Conversion of t-butyl chloride over the series of HBEA supported metals prepared using AMD as metal precursor at reaction temperature of 45 °C (benzene : tBC ratio of 10mL : 1 mL and 320 g of catalyst)

The profiles presented in Figure 5.7 show that there was a rapid rise in the conversion of the t-butyl chloride with time on stream in several cases. The lowest conversion was observed on the parent HBEA material which was discussed in Section 5.1.1. It should be noted that the catalysts prepared via wet impregnation contained all the metals found in AMD and the elemental composition of the major metals loaded onto the zeolite are presented in Table 4.5. These catalysts had comparable amounts of Fe but also additional metals which increased their Lewis acidity. Unlike the ion exchanged counterparts the catalyst with the highest metal loading, sample 25AHW (Fe wt % loading of 3.19), did not give the best conversion. The reduction in activity can be ascribed to the decreased

surface area (refer to Table 4.7). This consequently reduced the available number of active sites. It can be seen that moderate metal loading gave the best overall outcome (consider the 10AHW with 100 % conversion after 0.5 h on stream). All the metal impregnated catalysts managed to give a conversion of 100 % although at different times on stream.

It is also clear that the profile obtained for the 5AHW was different from the rest since it was characterised by a rapid increase in conversion reaching 100 % within 0.5 h and then decreased significantly with a gradual rise in the end. This outcome may be ascribed to the limited Fe sites on the catalyst which may get chlorinated by the produced HCl. The chlorination of the Fe sites may allow Mn and Mg which have dealkylating effects to convert the produced alkylated products back to reactants. Hlatywayo, (2013) in a study on the alkylation of benzene with t-butyl chloride reported that Mn reduced the benzene conversion but however increased the selectivity towards formation of the monoalkylated product. In addition, Mg has been found to reduce benzene conversion in alkylation reactions. In the alkylation of benzene with ethanol Yuan & Gevert (2004) found that Mg reduced the benzene conversion and improved the selectivity towards formation of the monoalkylated product.

Comparing the profiles in Figure 5.7 against their corresponding counterparts prepared via ion exchange it can be deduced that overal, the wet impregnated HBEA gave a higher conversion. This can be ascribed to the synergic effect that other metals have on the conversion. For instance, Ni is active in the alkylation of benzene. Ali et al., (2014) reported on the activity of Ni supported on zirconia in the alkylation of benzene using benzyl chloride. On the other hand, the presence of numerous metals in close proximity results in cooperative action of the active sites leading to an increase in the HOMO (highest occupied molecular orbital) energy level of one reactant while there is a decrease in the LUMO (lowest unoccupied molecular orbital) energy level of the other reactant (Huang et al., 2017). Due to this combination polymetallic catalysts are more efficient relative to monometallic ones. The activity of the Fe-containing catalysts for alkylation of benzene is not directly related to their acidity but controlled mainly by their redox properties (Choudhary et al., 2002). Similar profiles to those presented in Figure 5.7 were reported in other related studies (Bachari et al., 2004; Ali et al., 2014). Thus the outcomes generated in this study are consistent with other observation reported in related studies

despite the fact that waste CFA and AMD were used to prepare the catalysts tested in this study.

5.2.2 Selectivity studies over wet impregnated HBEA

The selectivity studies over the wet impregnated HBEA catalysts prepared using AMD as metal precursor are depicted in Figure 5.8.

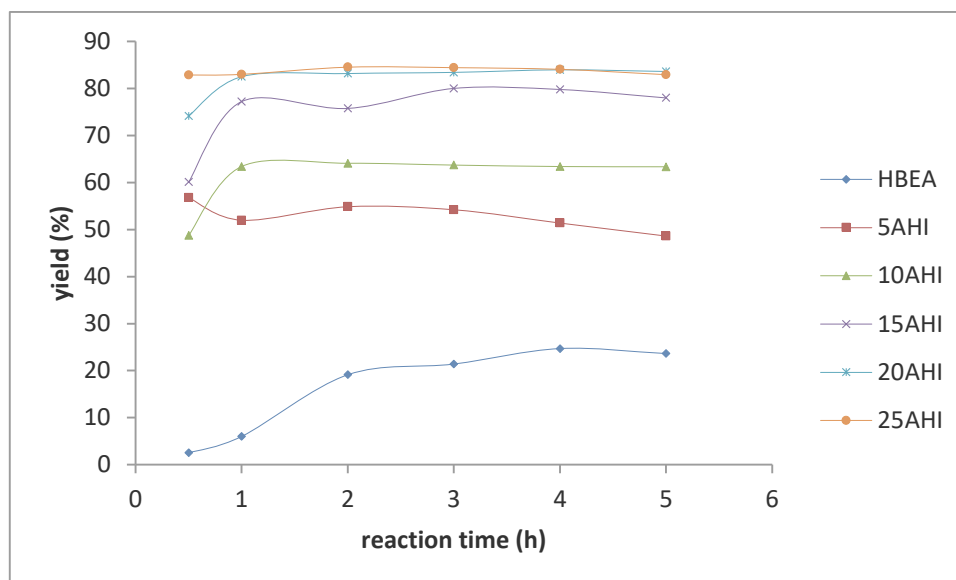*Figure 5. 8: Selectivity of t-butyl benzene over the series of HBEA supported metals prepared using AMD as metal precursor at reaction temperature of 45 °C (benzene : tBC ratio of 10mL : 1 mL and 320 g of catalyst)*

The highest selectivity obtained over the series of HBEA supported metal catalysts prepared via wet impregnation was observed over the 25AHW (actual Fe wt % loading of 3.19). A selectivity of 100 % was observed after 0.5 and 1 h time on stream. Although this may seem interesting, the conversion at those periods were very low (check Figure 5.7). Since the amount of t-butyl benzene in the product mixture was so low, the selectivity was high. Higher conversions allow for a variety of products to be formed. As the time elapsed the conversion rose and the selectivity started to reduce reaching a low value of 74.3 % after 4 h on stream. The selectivity of the parent HBEA zeolite was comparable to that of the 20AHW and the 5AHW.

The selectivity of the ion exchanged counterparts presented in Figure 5.2 showed a correlationship between selectivity and metal loading. The higher the metal loading

achieved the higher the observed selectivity. This however cannot be said about the wet impregnated HBEA catalysts. There was no systematic correlation that was observed. The fact that different AMD related metals that were simultaneously loaded onto the catalysts have different effects on the overall reaction can be the cause behind the observed profiles. Metals such as Mn and Mg, when tested in bimetallic catalytic system in alkylation reactions, were found to enhance selectivity towards the monoalkylated product (Hlatywayo, 2013; Emana & Chand, 2015). Formation of the monoalkylated product mainly occurs within the pore system of the zeolite. The external surface of the zeolite is usually responsible for the formation of bulky moieties. However, Mg reduces the number of acid sites on the external surface by coating it, and consequently reducing further oligomerisation reactions (Emana & Chand, 2015). On the other hand, Mn suffers a partial reduction (redox) of the Mn_2O_3/MnO_4, which may result in the decrease in acid strength, which consequently might affect product selectivity (Wang et al., 2012).

Selectivity studies on porous materials are also governed by the pore system and BET surface area of the support. The data presented in Table 4.7 showed that there was not a very significant change in the pore diameter of the HBEA upon metal loading. However, there was a significant reduction in the BET surface area [HBEA (492 m^2/g) and 25AHW (361 m^2/g)]. There was no linear relationship observed between the selectivity vs surface area. The trends presented in Figure 5.8 cannot be compared with any available trends from related studies since most of the reported studies usually used either monometallic or bimetallic catalyst systems. The effect of various metals on selectivity is further discussed in Section 5.6.

5.2.3 Product distribution over HBEA supported catalysts prepared via wet Impregnation

The product distribution over the HBEA supported metal catalysts prepared via wet impregnation using AMD as metal precursor are presented in the following sections. The catalyst with the lowest metal wt % loading and the one with the highest are presented for discussion. The product distribution over the parent material is presented in Section 5.1.3.1.

5.2.3.1 Product distribution over 5AHW

The product distribution obtained over the 5AHW (Fe wt % loading 0.84) obtained over the HBEA catalyst loaded via wet impregnation using AMD as metal solution precursor is presented in Figure 5.9.
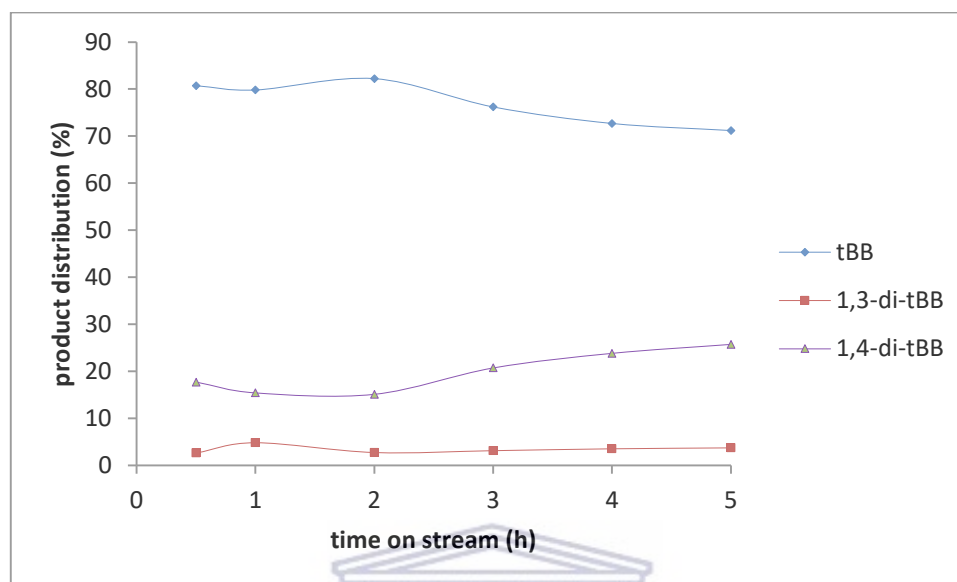
Figure 5. 9: Product distribution for benzene alkylation with t-butyl chloride over the 5AHW at 45 °C (benzene : tBC ratio of 10mL : 1 mL and 320 g of catalyst)

The product distribution curves obtained over the 5AHW shows that the primary product for the entire 5 h period under study was the t-butyl benzene. The dialkylated products observed were the *meta* and *para* isomers. The ortho isomer and the trialkylated product were again not detected in the reaction mixture for reasons already outlined in Sections 5.1.3.1 and 5.1.3.2. Although the *meta* isomer is more thermodynamically stable, the percentage of the isomer in the reaction mixture was relatively low in comparison to the *para* isomer. The relative abundance of the *para* isomer can be attributed to the ease with which it can diffuse through the zeolite pore channels. As previously mentioned, zeolite HBEA pore channels are slightly larger than the benzene molecule and so suppresses the formation of large moieties within its pore channels. In addition, the HCl formed by the alkylation reaction is said to favour formation of the *meta* isomer on the external surface of the support, this would increase the meta percentage with prolonged reaction times. However, this was not the observation and the outcome can be attributed to the antagonistic effect that Mg (refer to ICP-OES data in Table 4.5) has of reducing surface

acidity hence supressing the effect of HCl on isomer distribution (Yuan & Gevert, 2004; Bidart et al., 2001). Similar outcomes were obtained in various related studies (Wang et al., 2012; Bidart et al., 2001), despite the fact that waste CFA and AMD were used in catalyst preparation.

5.2.3.2 Product distribution over 25AHW

The product distribution over the highest loaded catalyst (25AHW with 3.19 % Fe) supported on HBEA prepared via wet impregnation using AMD as metal solution precursor is presented in Figure 5.10.
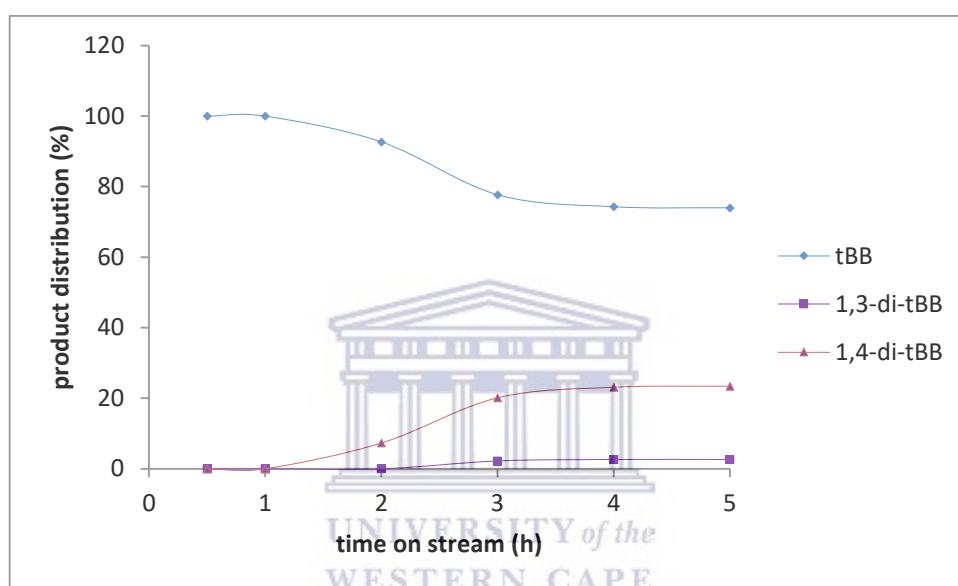
Figure 5. 10: Product distribution for benzene alkylation with t-butyl chloride over the 25AHW at 45 °C (benzene : tBC ratio of 10mL : 1 mL and 320 g of catalyst)

The product distribution obtained over the 25AHW exhibited similar trends as seen in the profiles obtained over the 5AHW. The only difference was in the relative proportions of the respective products. The differences in proportion were expected considering the differences in the metal wt % loading. However, the same submissions made on the 5AHW also hold for 25 AHW.

5.2.3.3 Product Yield over wet impregnated HBEA

The product yield over the series of HBEA supported metal catalysts prepared via wet impregnation using AMD as metal precursor are presented in Figure 5.11.
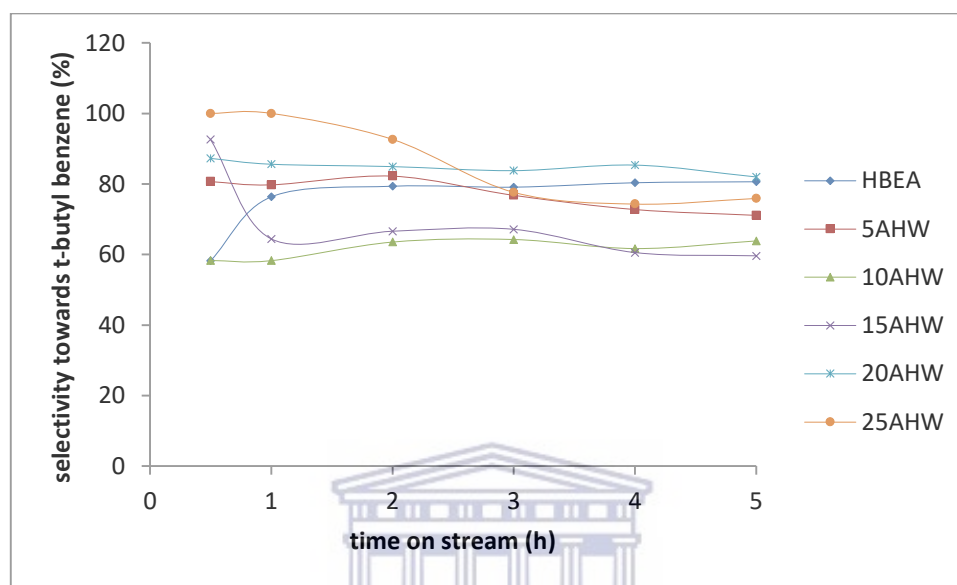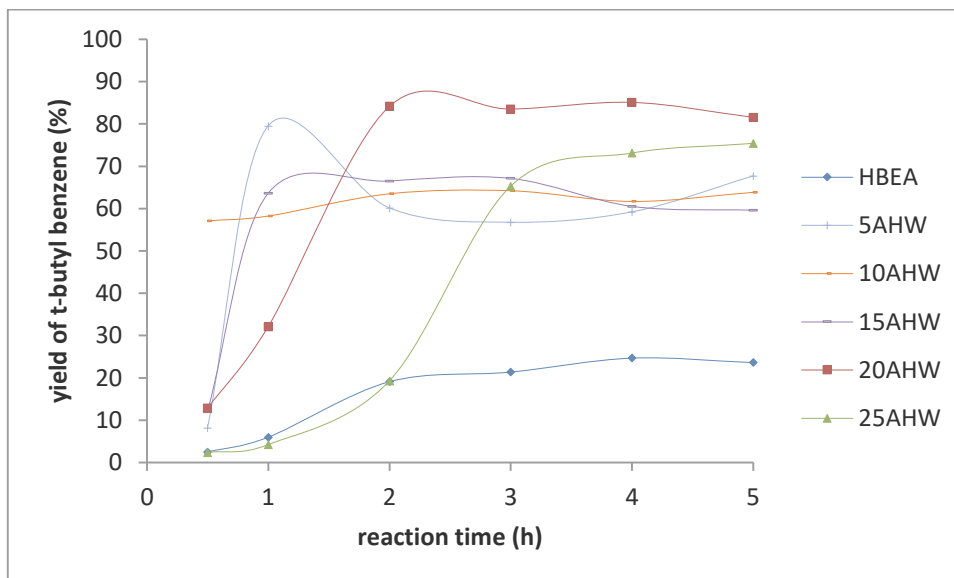
Figure 5. 11: Product yield of t-butyl benzene over the series of HBEA supported metals prepared using AMD as metal precursor at reaction temperature of 45 °C (benzene : tBC ratio of 10mL : 1 mL and 320 g of catalyst)

Again, the lowest performing catalyst in the series was the parent HBEA support. The parent HBEA exhibited good selectivity but low conversion percentages over the 5 h reaction period which is ascribed to the Brønsted acid sites. Although sample 25AHW gave good selectivity as well, it too was characterised by low conversion and hence the yield obtained over the catalyst was not the best despite the fact that it had the highest metal loading of the series of catalysts under study. The highest yield of 85.08 % was obtained over the 20AHW (Fe wt % loading of 2.62) after 4 h on stream. From the outcomes it can be concluded that there is a threshold wt % loading that gives maximum performance and going below or beyond the threshold results in reduced activity. Since yield is calculated from conversion and selectivity, the factors governing the two parameters consequently affect the overall yield of the catalyst.

5.3 Catalytic activity studies over the MCM-41 supported metal catalysts

The alkylation of benzene over the MCM-41 supported metal catalysts prepared using AMD as a metal solution precursor were studied based on the conversion of t-butyl chloride, selectivity towards formation of t-butyl benzene, product distribution as well as the percentage yield of t-butyl benzene. The reaction was carried at a moderate temperature of 45 °C in accordance with the procedure outlined in Section 3.7. It was found that the parent MCM-41 was inactive in the reaction and thus is omitted in this discussion. The inactivity of the parent MCM-41 attests to the fact that Brønsted acidity takes part in the FC alkylation reaction since the parent HBEA was found to be active.

5.3.1 Conversion studies over wet impregnated MCM-41

The conversion of t-butyl chloride was studied as a function of reaction time in the alkylation of benzene with t-butyl chloride over metal loaded MCM-41 prepared via wet impregnation using AMD as metal precursor. The outcomes are presented in Figure 5.12.
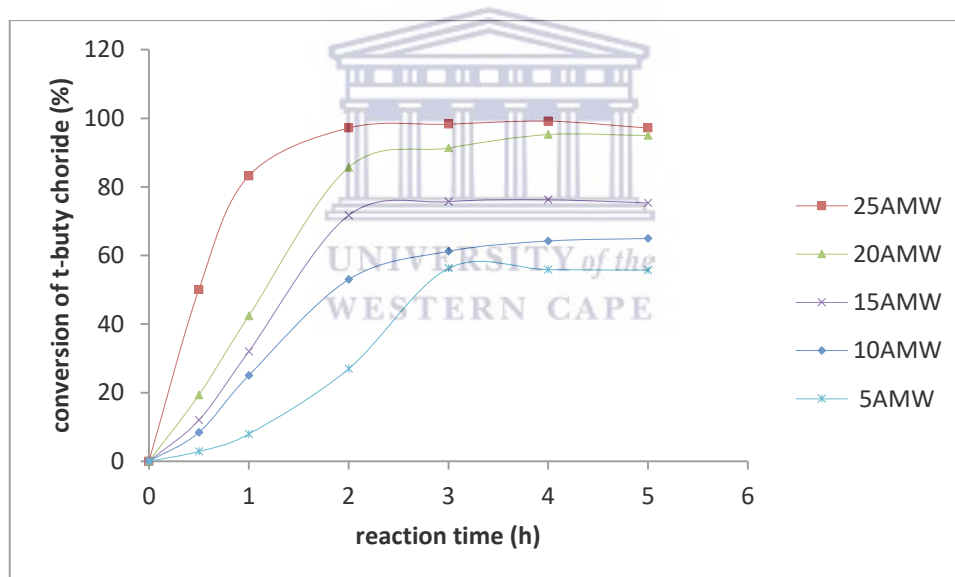
Figure 5. 12: Conversion of t-butyl chloride over the series of MCM-41 supported metals prepared using AMD as metal precursor at reaction temperature of 45 °C (benzene : tBC ratio of 10mL : 1 mL and 320 g of catalyst)

The profiles presented in Figure 5.12 are characterised by a fairly rapid initial increase in conversion reaching a steady state after 2 – 3 h on stream. The pristine MCM-41 was found not to be active in the alkylation of benzene with t-butyl chloride and the profile is omitted from the profiles presented. The reaction is facilitated by either Brønsted acidity

or Lewis acidity of the support, and the pristine siliceous MCM-41 does not have either of these acid sites. The dependence of the alkylation reaction on both the Brønsted and Lewis acidity can be seen by the activity of the parent zeolite HBEA and the metal loaded HBEA. Both the parent and the metal loaded zeolites were active as shown in Figure 5.1 and metal addition was seen to increase the activity. Although there are no Brønsted acid sites in the MCM-41 support the metal introduction by itself (Lewis acidity) was responsible for the observed activity.

The highest conversion of 99.1 % was obtained over the 25AMW (actual Fe wt % loading of 3.09) after 4 h on stream. Unlike the corresponding catalyst supported on HBEA which had a low conversion in the first 3 h on stream, and only gave a high conversion after 4 h, sample 25AMW reached steady state after 2 h on stream. The better activity can be attributed to the larger surface area of the MCM-41 supported catalyst and thus better metal dispersion. The delay of the 25AHW to reach maximum activity was ascribed to the reduction in pore size as well as reduced surface area upon highest metal loading. In addition, the MCM-41 supported catalyst had a better monoatomic metal dispersion as could be seen from the absence of metal related peaks on the XRD profiles presented in Figure 4.6. On the other hand, metal crystallite peaks were observed on the corresponding HBEA supported catalysts, indicating longer range order and larger metal clusters.

The catalyst that gave the lowest performance of the MCM-41 series was sample 5AMW (actual Fe wt % loading of 0.81). The highest conversion obtained over the catalyst was 56.3 % after 3 h on stream. The profiles in Figure 5.12 attest to the fact that as the metal loading increases there was a corresponding increase in the conversion of t-butyl chloride. Generally, the conversion obtained over the MCM-41 catalyst series was lower than that obtained over the HBEA counterparts. This can be attributed to the synergistic effects of both Brønsted and Lewis acid sites in the HBEA, and hence better catalytic activity. Similar trends were reported in related studies in which the alkylation of benzene was undertaken over Fe loaded MCM-41 (He et al., 1998; Bachari et al., 2004; Preethi et al., 2010; Shuvaeva et al., 2014) although different reaction conditions were applied.

5.3.2 Selectivity studies over wet impregnated HBEA

The profiles of the selectivity towards the formation of the monoalkylated product (t-butyl benzene) over the MCM-41 supported metals catalysts are depicted in Figure 5.13.
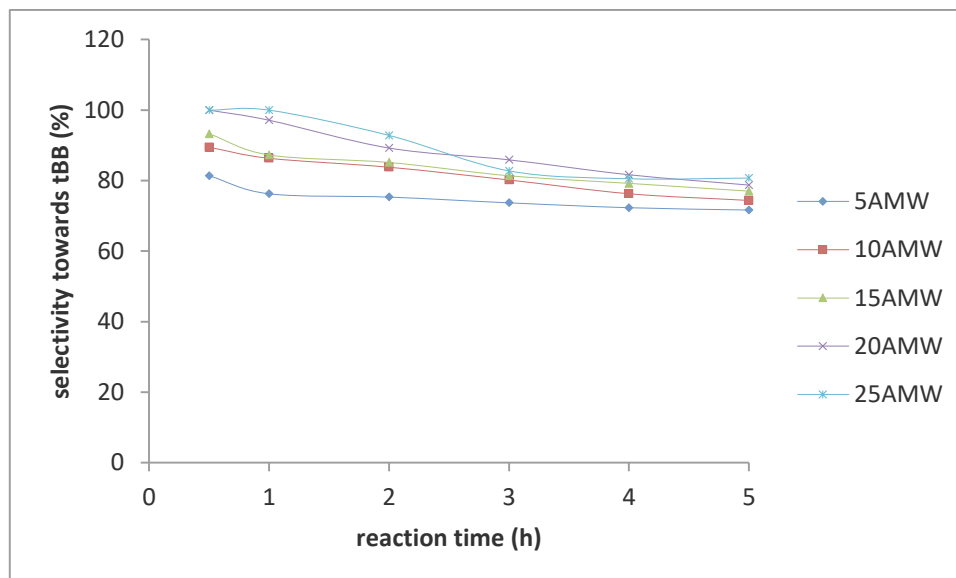
Figure 5. 13: Selectivity of t-butyl benzene over the series of MCM-41 supported metals prepared using AMD as metal precursor at reaction temperature of 45 °C (benzene : tBC ratio of 10mL : 1 mL and 320 g of catalyst)

The trends for the selectivity towards the formation of t-butyl benzene presented in Figure 5.13 are characterised by a general decrease with time on stream. As has been highlighted previously, the monoalkylated product is more active than benzene itself, and once the first alkylation occurs the monoalkylated product is prone to further alkylation to form polyalkylated products. From Figure 5.12, it could be seen that the conversion generally increased with reaction time, hence as more of the monoalkylated product is formed, the more the chances of poly alkylation, and hence reduced selectivity towards the monoalkylated product with time. The highest selectivity obtained was 100 % after 2 h on stream over the 25AMW (actual Fe wt % loading of 3.09). The lowest selectivity recorded was 71.6 % over sample 5AMW (actual Fe wt % loading of 0.81) after 5 h on stream. It is evident on the presented profiles that the selectivity increased with an increase in the metal loading. It should be noted that in the present study, benzene was used in excess (used as both reactant and solvent) hence it suppressed polyalkylation even in cases where the metal loading was relatively higher (high metal loading increases the number of active sites and susceptibility to polyalkylation). Furthermore, the pore channels of MCM-41 are relatively larger allowing easy movement of the monoalkylated product out of the pores once it is formed.

The selectivity towards t-butyl benzene might have also been enhanced by the polar nature of the channel surface owing to the presence of activated metal oxides. The t-butyl benzene due to its lower polarity should be quickly expelled out of the pore channels of MCM-41 (Preethi et al., 2010). It should be noted that although the discussion is centred on the Fe loading, the catalysts included other metals as AMD contains various metals. Despite the fact, the selectivity profiles presented in Figure 5.13 follow the general trend observed in most reported alkylation reactions. Comparable outcomes have been obtained in similar studies on commercial catalysts and reported in various publications (Preethi et al., 2010; Shuvaeva et al., 2014). Thus the waste based catalyst in this study are highly active under moderate conditions.

5.3.3 Product distribution over MCM-41 supported catalysts prepared via wet impregnation

The product distribution over the MCM-41 supported metal catalyst prepared via wet impregnation using AMD as metal solution was studied and the catalysts with the lowest and highest metal wt % loading are discussed in the following sections.

5.3.3.1 Product distribution over 5AMW

The product distribution over the 5AMW (Fe wt % loading of 0.81) is presented in Figure 5.14.
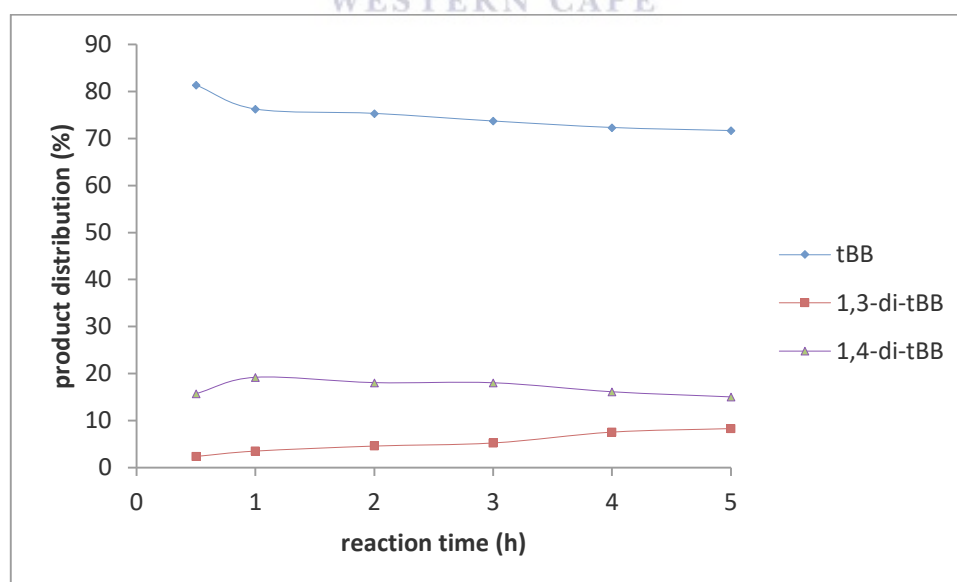
Figure 5. 14: Product distribution for benzene alkylation with t-butyl chloride over the 5AMW at 45 °C (benzene : tBC ratio of 10mL : 1 mL and 320 g of catalyst)

The product distribution obtained over sample 5AMW consisted of t-butyl benzene as the primary product alongside the 1,3-ditertiary butyl benzene and the 1,4-di-tertiary butyl benzene. Again, the ortho isomer and the trialkylated products were not detected in the product mixture due to the same reasons as mentioned in Sections 5.1.3.1 and 5.1.3.2. The amount of the *para* isomer was almost constant throughout the entire reaction period studied. The levels of the *meta* isomer increased gradually with reaction time. Again, as has been previously mentioned, the *meta* isomer is more thermodynamically stable relative to the *para* isomer hence the increase with reaction time. It would be expected to have more of the *meta* isomer at prolonged reaction times. However, this was not the case as the amount of the *para* isomer was more than that of the *meta* isomer at all times. The formation of the *para* isomer at the expense of the *meta* isomer can be attributed to the product shape selectivity of the support. The pores of MCM-41 can accommodate all the isomers that can be formed by the reaction. However, the orientation of the *para* isomer allows the isomer to easily move out of the pore channels of the support because its diffusivity is much greater than that of the *meta* isomer. Even if the primary product of the alkylation reaction might not be the *para* isomer, the rapid exit of the isomer from the pore system of the support allows for further isomerisation of the *meta* isomer resulting in elevated levels of the *para* isomer in the product mixture (Fechete et al., 2012).

5.3.3.2 Product distribution over 25AMW

The product distribution obtained over the MCM-41 catalyst with the highest metal loading (sample 25AMW) is depicted in Figure 5.15.
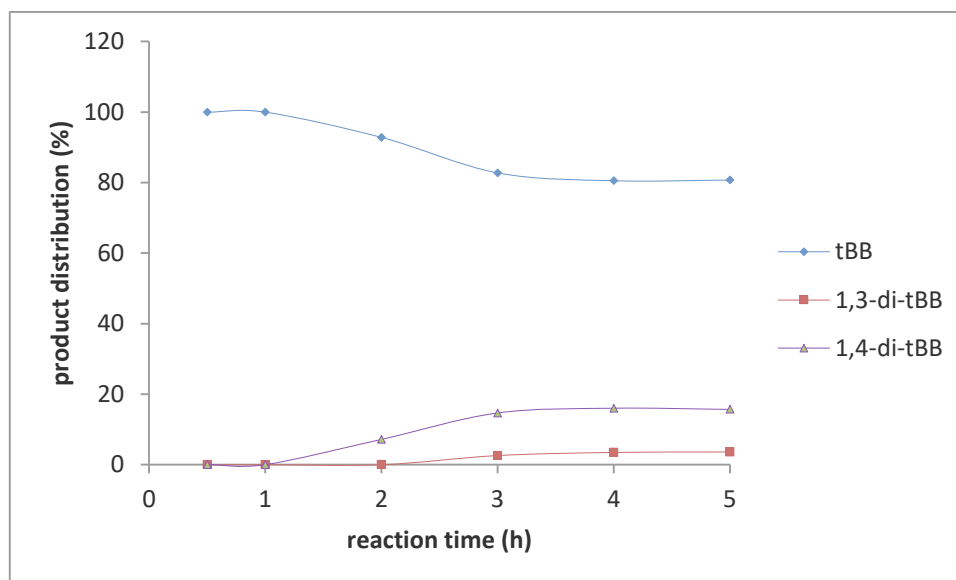
Figure 5. 15: Product distribution for benzene alkylation with t-butyl chloride over the 25AMW at 45 °C (benzene : tBC ratio of 10mL : 1 mL and 320 g of catalyst)

The product distribution over sample 25AMW prepared via wet impregnation using AMD as metal solution precursor is presented in Figure 5.15. Again it can be seen that the primary product was the monoalkylated product. In the intial stages of the reaction the primary product was high but reduced with reaction time. The reduction is attributed to the formation of more thermodynamically stable *meta* isomer as well as the tendency towards polyalkylation due to the relatively higher activity of the monoalkylated product which increases its chances of being further alkylated. The *para* isomer is again relatively abundant in comparison to the *meta* isomer. This is due to the product selectivity associated with the size of the pore channels of the support as discussed in the previous section. The profiles presented in Figure 5.15 are similar to the profiles obtained over the corresponding HBEA supported catalyst (25AHW) presented in Figure 5.10. There is only a slight difference in the product ratios. It can be seen that the selectivity towards the formation of the primary product (the tertiary butyl benzene) is relatively higher on the MCM-41 supported catalysts. This may be attributed to the larger pore system of the MCM-41 which allows for easy migration of the product from the active sites inside the MCM-41 channels to the product solution. Numerous studies based on commercial MCM-41 and commercial Fe salts have reported similar outcomes (Preethi et al., 2010; Shuvaeva et al., 2014). This leads to the conclusion that coal fly ash based MCM-41 and

AMD can be used to produce an effective green catalyst for the alkylation of benzene with tertiary butyl chloride.

5.3.3.3 Product Yield over wet impregnated MCM-41

The percentage yield of t-butyl benzene produced over the MCM-41 supported metal catalysts prepared via wet impregnation using AMD as a metal solution precursor are presented in Figure 5.16
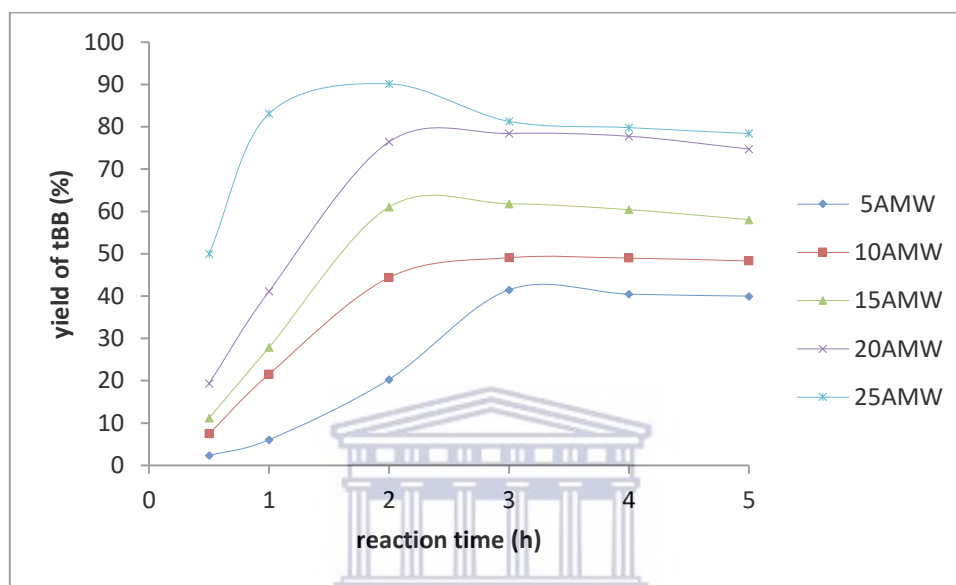
Figure 5. 16: Product yield of t-butyl benzene over the series of MCM-41 supported metals prepared using AMD as metal precursor at reaction temperature of 45 •C (benzene : tBC ratio of 10mL : 1 mL and 320 g of catalyst)

It can be seen from the profiles presented in Figure 5.16 that after 2 h time on stream most of the catalysts tested reached steady state. The highest yield obtained was 90.2 % over the 25AMW (actual Fe wt % loading of 3.09) after 2 h time on stream. The lowest performing catalyst was sample 5AMW (actual Fe wt % loading of 0.81). The lower activity of this catalyst can be attributed to the lower metal loading on the catalyst. An increase in metal loading resulted in an increase in product yield as can be seen from the profiles. The phenomenon of increasing yield with increase in metal loading was also reported by Okumura et al., (2001) in a study on the alkylation of benzene with benzyl chloride over different Ga wt loadings supported on MCM-41. Since the percentage product yield is calculated from conversion and selectivity in accordance with the

equation presented in Section 3.7.3, it follows that the factors affecting conversion and selectivity consequently affect the percentage yield.

The yield of t-butyl benzene obtained over the HBEA supported Fe catalyst was relatively higher compared to that obtained over the corresponding MCM-41 catalysts. The HBEA supported catalysts gave higher conversions but lower selectivity. The absence of Brønsted acid sites on the MCM-41 may have contributed to the observed higher selectivity. Bronsted acid sites are largely responsible for the formation of the arenium ions (rate determining step), and rapid arenium ion formation may lead to high rates of alkylation which consequently may lead to increased chances of polyalkylation. The profiles presented in Figure 5.16 are in agreement with profiles presented in literature on studies related to the present one although different alkylating agents and experimental conditions were applied (Okumura et al., 2001; Mantri et al., 2005).

5.4 Effect of support on the catalytic activity

The effect of the support material on the catalytic activity of the supported metals in the Friedel-Crafts alkylation of benzene with tertiary butyl chloride was assessed by evaluating the activity of comparable metal wt % loadings on HBEA and MCM-41. The assessment was based on the conversion of tertiary butyl chloride, selectivity towards formation of tertiary butyl benzene and the yield of tertiary butyl benzene.

5.4.1 Effect of support on conversion

Since most of the profiles for the conversion of tertiary butyl chloride showed that after 2 h time on stream the reaction would have reached steady state, the percentage conversion after 2 h on stream for the highest metal loading (25AHI, 25AHW & 25AMW), intermediate (15AHI, 15AHW & 15AMW) and the lowest metal loading (5AHI, 5AHW & 5AMW) were considered for discussion. In addition, the highest conversions achieved within the 5 h reaction period studied on the respective catalysts are presented. The conversion percentages of the respective catalysts are presented in Table 5.1. The "**X**" on the catalyst code in the table represents the support, either HBEA or MCM-41. It should also be noted that only the catalysts prepared via wet impregnation are considered in the discussion, as ion exchange did not work in the case of MCM-41.

Table 5. 1: Effect of support material on the percentage conversion of t-butyl chloride

	catalyst support			
	HBEA		**MCM-41**	
	highest con. %	*con. at 2 h %*	*highest con. %*	*con. at 2 h/ %*
parent material	30.7	24.1	0	0
5A**X**W	99.7	73.1	56.3	26.9
15A**X**W	99.9	99.9	76.2	71.7
25A**X**W	99.3	20.8	99.1	97.1

Catalytic activity over metals supported on porous materials is generally governed by a four main factors namely; pore diameter, surface area, Brønsted acidity and the metal wt % loading. In the case where catalysts have comparable metal wt % loadings then the differences in activity would be mainly due to their differences in surface area as well as acidity. The outcomes presented in Table 5.1 show that the parent HBEA was active while the parent MCM-41 was inactive. This outcome can be ascribed to the presence of Brønsted acid sites on the HBEA which are absent on MCM-41. It can be seen from the data presented in Table 5.1 that the highest conversion achieved on the HBEA supported catalyst was always higher relative to the corresponding MCM-41 supported catalyst. The high activity on the HBEA supported catalyst can be ascribed to the synergic effect of the Lewis acidity and the Brønsted acidity on the HBEA as previously discussed in Sections 5.3.1, 5.2.1 and 5.3.1.

However, the 25AHW (supported on HBEA) gave a lower conversion in comparison to the corresponding 25AMW (supported on MCM-41) after 2 h time on stream. The lower activity on the HBEA supported catalyst can be attributed to reduced surface area since the pore diameter was not greatly altered as can be seen in the data presented in Figure 4.20. However, the data shows that an increase in metal loading significantly altered the BET surface area, the parent HBEA had a BET surface area of 492 m^2/g compared to that of the 25AHW of 361 m^2/g. The outcomes presented in Table 5.1 lead to the conclusion that Brønsted acidity of the support enhances the catalytic activity and that the support ought to have reasonable surface area to achieve high conversion percentages of the

tertiary butyl chloride. HBEA supported metal catalysts gave higher conversions relative to the corresponding MCM-41 supported metal catalysts.

5.4.2 Effect of support on selectivity

The product selectivity over porous catalysts are said to be influenced mainly by the nature of the support, pore size, number and strength of the acid centres and the reactant molar ratios. In the case of the catalysts under investigation, the reactant molar ratios were kept constant and the catalysts evaluated had comparable metal wt % loadings. The selectivity towards formation of the monoalkylated product over the same catalysts presented in the previous section are presented in Table 5.2.

Table 5. 2: Effect of support material on the percentage selectivity of t-butyl benzene

	catalyst support			
	HBEA		MCM-41	
	highest sel. %	*sel. at 2 h %*	*highest sel. %*	*sel. at 2 h/ %*
parent material	80.7	79.4	0	0
5AXW	82.2	82.2	81.4	75.3
15AXW	92.6	66.6	93.2	85.1
25AXW	100	92.7	100	92.8

The outcomes presented in Table 5.2 show that the selectivity obtained over the HBEA and MCM-41 supported metal catalysts were comparable despite the differences these supports have in terms of surface area, pore size as well as acidity. Generally, catalysts with strong acid sites have been found to have less selectivity, and in this case the HBEA has more acid sites since there is a combination of both Lewis and Brønsted acid sites (Fechete et al., 2012). This would lead to the expectation that the HBEA would give a lower selectivity, however the pore size of HBEA is relatively smaller than that of MCM-41 and slightly larger than the size of the benzene molecule and hence HBEA would have more controlled product shape selectivity based on its pore size (Perego & Ingallina 2002). This compensated for the acidity of the HBEA and hence gave higher selectivity towards the monoalkylated product. Hence based on the outcomes presented in Table 5.2, the effect of the support could not be well defined since the two supports gave comparable product selectivity percentages. The selectivity percentages obtained on either support

were very high and both supports can be effectively applied in the alkylation of benzene with tertiary butyl chloride.

5.4.3 Effect of support on yield of t-butyl benzene

The percentage yield of *t*-butyl benzene, obtained over the selected catalysts is presented in Table 5.3.

Table 5. 3: Effect of support material on the percentage yield of t-butyl benzene

	catalyst support			
	HBEA		**MCM-41**	
	highest yield %	*yield at 2 h %*	*highest yield %*	*yield at 2 h/ %*
parent material	23.6	21.4	0	0
5AXW	79.5	60.1	41.5	20.3
15AXW	67.1	66.5	61.8	61
25AXW	75.4	19.2	90.1	90.1

The percentage yield data presented in Table 5.3 shows that the HBEA supported catalysts gave higher yield percentages relative to the corresponding MCM-41 counterparts; apart from the 25AXW case where the MCM-41 supported catalysts had a much better yield percentage. Sample 25AMW had a higher yield of 90.1 compared to 75.4 % over sample 25AHW after 2 h time on stream. The reduction of surface area on the HBEA catalyst with high metal loading can be the cause of its lower yield. The factors governing conversion and selectivity are responsible for the observed outcomes since selectivity is calculated from these two parameters. Both conversion and selectivity issues were discussed in the previous sections.

5.5 Effect of metal loading on catalytic activity

The effect of Fe wt % loading on the catalytic activity can be followed by considering the conversion of t-butyl chloride, selectivity and yield of the t-butyl benzene at 2 h time on stream (most catalysts achieved steady state after 2 h time on stream). The different series of catalysts were considered, the HBEA prepared via ion exchange or wet impregnation, as well as the MCM-41 supported catalysts prepared via wet impregnation. The effect of

https://etd.uwc.ac.za

the loading approach will be discussed in the following sections, making comparison of the activity based on the Fe wt % loading.

5.5.1 Effect of Fe loading on conversion of t-butyl chloride after 2 h on stream

The effect of Fe wt % loading on the conversion of t-butyl chloride is depicted in Figure 5.17. The conversion percentages of each series of catalysts prepared using AMD as a metal precursor are plotted against the theoretical metal wt % loading (0.7; 1.4; 2.1; 2.8; 3.5 %).

Figure 5. 17: Conversion of t-butyl chloride after 2 h on stream against theoretical Fe wt % loading at 45 °C (benzene : tBC ratio of 10mL : 1 mL and 320 g of catalyst)

The catalysts supported on HBEA were prepared via two conventional approaches, ion exchange or wet impregnation while those supported on MCM-41 were prepared using only wet impregnation. From the profiles presented in Figure 5.17, it can be seen that the MCM-41 based catalysts gave a linear relationship between conversion percentages of *t*-butyl chloride and the Fe wt % loading. It follows that as the metal increases the conversion also increases. The profile for the HBEA supported catalysts prepared via ion exchange [HBEA(IE)] also shows that as the Fe wt % loading increased there was an increase in the conversion of the t-butyl chloride. However, the increase did not follow a perfectly linear relationship but rather the curve obtained can be best described as a bounded exponential growth curve. The HBEA supported catalyst prepared via wet

impregnation [HBEA(WI)] had a similar bounded exponential curve but after a Fe wt % loading of 2.8 the conversion dropped off. The decrease can be ascribed to the significant reduction in the surface area of the HBEA with higher metal wt % loadings as discussed in previous sections.

The outcomes in Figure 5.17 lead one to the conclusion that the conversion increased as the Fe wt % loading increases but higher loadings that impacted significantly on the support surface area may lead to reduction in the conversion. Again the catalytic activity in the alkylation of benzene over acid zeolites is based on the the Lewis acid/ Brønsted acid ratio, and there is an optimum ratio that gives best activity (Ding et al., 2014). The changes in this ratio with metal loading could have also impacted the reaction and hence the observed reduction in conversion at higher metal wt % loading. The work by He et al., (1998) focused on the alkylation of benzene with benzyl chloride over Fe loaded MCM-41 with wt % loadings of up to 7.7 %. In their study, an increase in Fe wt % loading was found to increase the conversion. This observation is in agreement with the outcomes obtained in the present study up to a point. The ion exchange approach gives better conversion with higher metal loadings compared to the wet impregnation. This can be attributed to the good metal dispersion associated with ion exchange. Again ion exchange did not alter the surface area to a great extent [BET surface area: HBEA ~ 492 m^2/g; 25AHI ~483 m^2/g; 25AHW~ 361 m^2/g]. Furthermore, the XRD profiles presented in Section 4.1 show that the HBEA supported catalysts prepared via wet impregnation exhibited peaks due to Fe_2O_3 oxide species which were not present in the ion exchanged HBEA supported metal catalysts. Well dispersed and smaller Fe particles allow for higher conversion, high initial reaction rate and shorter induction periods relative to larger metal particles. The smaller particles accelerate the diffusion rate of reactants in the pore channels of the support (Jiang et al., 2012).

5.5.2 Effect of Fe loading on selectivity of t-butyl benzene after 2 h on stream

The effect of the Fe wt % loading on the selectivity towards formation of the t-butyl benzene is presented in Figure 5.18.

Figure 5. 18: Selectivity towards t-butyl benzene after 2 h on stream against theoretical Fe wt % loadingat 45 °C (benzene : tBC ratio of 10mL : 1 mL and 320 g of catalyst)

The profile for the MCM-41 supported catalysts series show that the selectivity towards the formation of the monoalkylated product increased with an increase in Fe wt % loading. Again the increase is linear (note the parent MCM-41 was inactive for the reaction hence zero selectivity point on the profile). An increase in the metal loading would be expected to give rise to a decrease in selectivity considering that fact that the monoalkylated product is more activated than the benzene itself. However, this holds if the stoichiometric ratio of the benzene to the alkylating agent is 1:1(Fechete et al., 2012). The use of an excess of benzene has an influence over the selectivity and it favours formation of the monoalkylated product (Bidart et al., 2001). In the present study an excess of benzene was used and hence it suppressed the tendency of polyalkylation with increased metal wt % loading.

The profiles for the HBEA supported Fe catalysts in Figure 5.18 show that with lower metal wt % loading the catalysts prepared via ion exchange gave relatively higher selectivity. The ion exchanged HBEA contained only Fe while the wet impregnated HBEA contained Fe and other metals from AMD. The effect of these other metals on selectivity will be discussed in detail in Section 5.6. However, some of the metals such as Mn and Mg have been found to enhance the selectivity of the monoalkylated product (Hlatywayo, 2013; Emana & Chand 2015). However, the wet impregnated HBEA gave

relatively higher selectivity when the Fe metal loading was 3.5 %. This increase in selectivity can be ascribed to the presence of Fe_2O_3 species on the zeolite. The presence of these oxide species in close proximity to isolated Fe^{3+} species have been found to have a synergistic activity in the alkylation of benzene. Lin et al., (2011) studied this synergistic effect of isolated Fe^{3+} species with Fe_2O_3 supported on HZSM5 and concluded that it was responsible for the high activity obtained over the catalysts. In their study a selectivity of 100 % towards the formation of the monoalkylated product was observed in the alkylation of benzene with benzyl chloride. The increase in selectivity increased with Fe wt % loading. It can then be concluded that the loading approach and the type of support affect the selectivity. Generally, catalysts supported on MCM-41 gave higher selectivity percentages relative to the corresponding HBEA supported counterparts and in the case of HBEA supported Fe catalysts those prepared via wet impregnation gave higher selectivity percentages.

5.5.3 Effect of Fe loading on yield of t-butyl benzene after 2 h on stream

The effect of the Fe wt % loading on the yield of t-butyl benzene is presented in Figure 5.19.

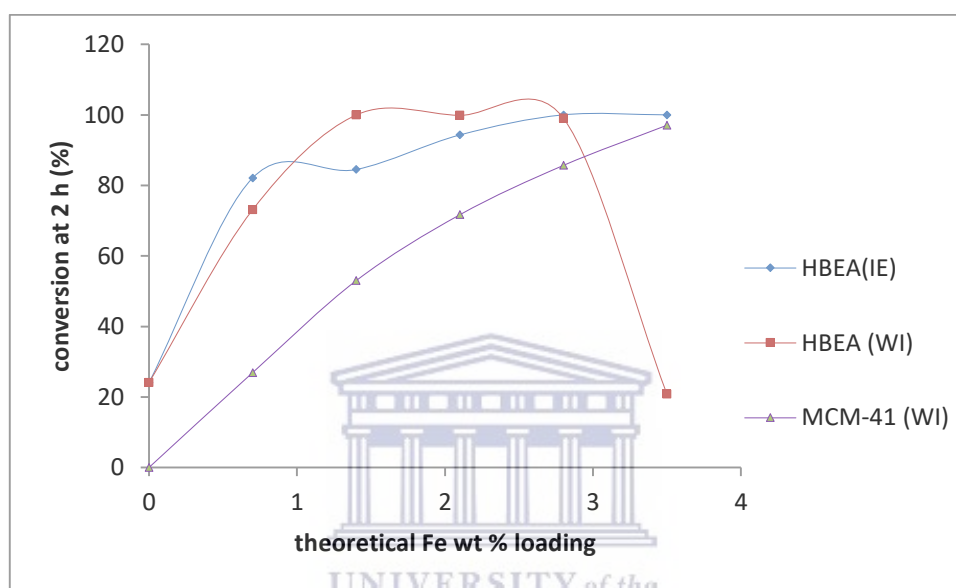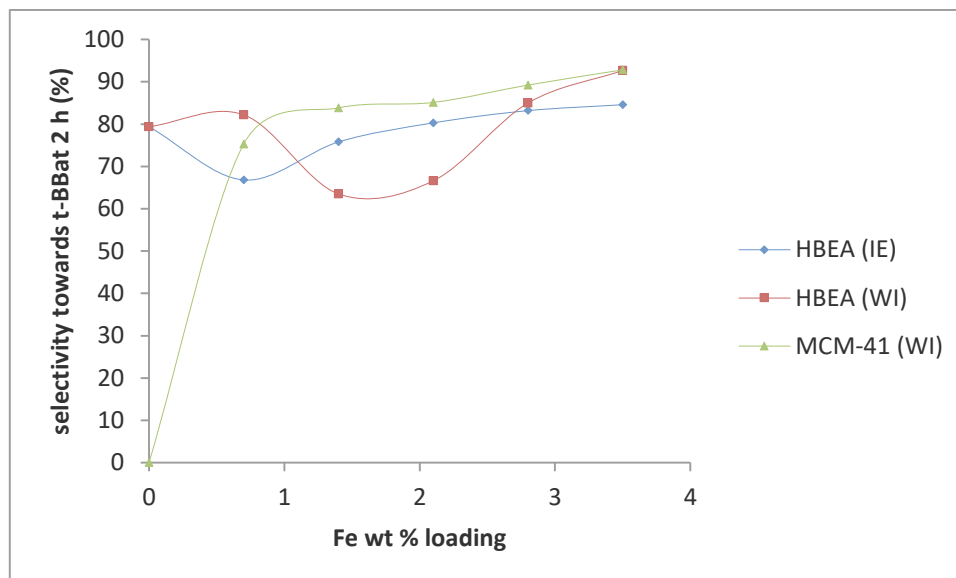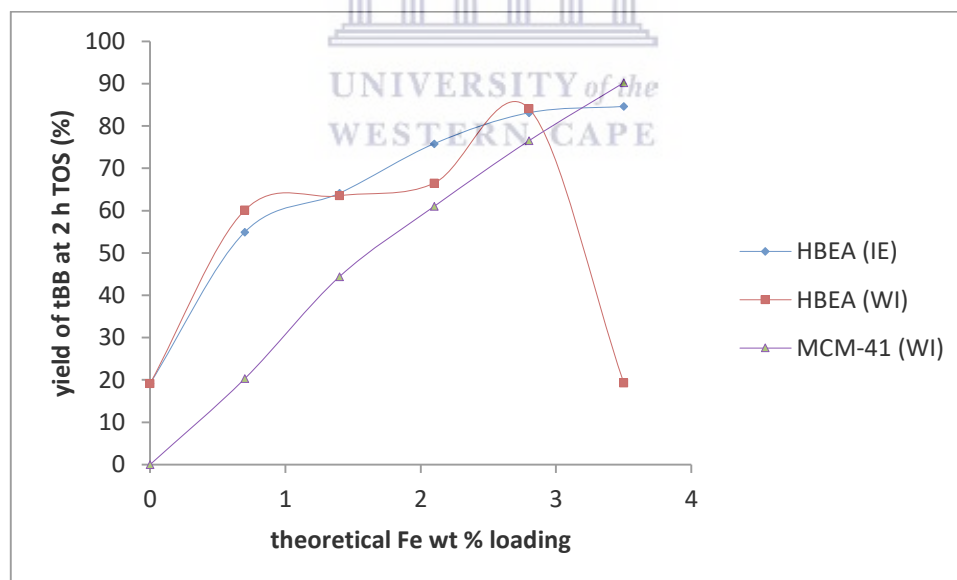**Figure 5. 19: Yield of t-butyl benzene after 2 h on stream against theoretical Fe wt % loading at 45 °C (benzene : tBC ratio of 10mL : 1 mL and 320 g of catalyst).**

The profiles for the yield against Fe wt % loading for the catalysts under evaluation presented in Figure 5.19 had the same trends as the trends obtained for the conversion against Fe wt % loading. The yield is a parameter calculated from the conversion as well as the selectivity in accordance to the equation presented in Section 3.7.3. It follows that the parameters affecting conversion and selectivity are the same parameters influencing the trends. The correlation between metal loading and yield was direct in the case of MCM-41 whereas the support role can be seen at lower Fe loadings for HBEA.

5.6 Effect of other metals in AMD

Acid mine drainage consists of numerous metal ions and the major metal ion is Fe. The complete ICP-OES data for the AMD used as metal solution precursor is presented in the appendix Section A2. The other metal ions that were present in AMD in significant quantities are Ni, Ca, Na, Mg and Mn. The effect of these metals on the Friedel-Crafts alkylation of benzene was evaluated by preparing HBEA supported metals, with the same elemental composition as sample 10AHW, using commercial sulphate salts, adding one metal at a time and assessing the conversion, selectivity and yield over the metal loaded support. The composition of the metal loaded HBEA is presented in Table 5.4. The effect of the other metals that existed in low quantities was not assessed but it should be noted that although their concentration was lower on the support they definitely had an influence on the overall catalytic activity observed over the series of catalysts prepared via wet impregnation using AMD as metal solution precursor. The preparation of the catalysts was done in accordance with the procedure outlined in Section 3.7.4.

Table 5. 4: Elemental composition of the metal loaded HBEA catalysts prepared via wet impregnation with selected metal salts. (data obtained from ICP-OES)

metal species	Fe	Ni	Ca	Na	Mg	Mn
wt % loading	1.4647	0.8586	0.6185	0.3825	0.236	0.0804

5.6.1 Effect of different metals on conversion of t-butyl chloride

The effect of the metals presented in Table 5.4 on the conversion of t-butyl chloride was assessed by first testing the catalyst with Fe alone and adding the respective metals starting with the one with the lowest wt % loading, and in this case, it was Mn. The

conversion profiles of t-butyl chloride over the series of catalysts prepared is presented in Figure 5.20.

Figure 5. 20: Effect of various metals on the conversion of t-butyl chloride at 45 °C over metal loaded HBEA support (benzene : tBC ratio of 10mL : 1 mL and 320 g of catalyst)

The profiles presented in Figure 5.20 show that the catalysts were very active giving almost 100% conversion after 4 h time on stream. The catalyst containing all the metals with the same proportion as they were in 10AHW was found to be the most active giving a conversion of 95.3 % after 0.5 h time on stream. To fully understand the effect of these metals on the conversion, it would be rational to start by considering the monometallic Fe catalyst. The catalyst had a conversion of 91.9 % after 0.5 h time on stream. This conversion was second highest of all the catalysts containing the metals under investigation. It could be seen from the profiles that addition of Mn, Mg, Na and Ca only served to decrease the activity, as the conversion percentages were reducing in their presence. However, addition of Ni significantly improved the conversion to 95.3 %. It follows that the presence of Ni promotes the catalytic activity of Fe.

Addition of Mn: The addition of Mn to the Fe-HBEA resulted in a decrease in the conversion of t-butyl chloride from 91.9 % to 89.5 % after 0.5 h time on stream. The outcome is in agreement with the observation made by Hlatywayo (2013). In the study monometallic and bimetallic Mn and Fe catalysts supported on HBEA were tested in the

alkylation of benzene with t-butyl chloride, and it was found that addition of Mn decreased the conversion. The conversion obtained over the Mn modified zeolite HBEA was even lower than that obtained over the pristine HBEA support material. In the same prior study, Mn modified MCM-41 showed no activity on the alkylation of benzene with t-butyl chloride. The outcomes in this present study are in agreement with the reported observations.

Addition of Mg, Na and Ca: Alkali and alkali earth metals are known to reduce the acidity of a zeolite when loaded onto a zeolite (Emana & Chand 2015). The alkylation of benzene over acid catalysts belong to a carbenium ion type mechanism, and both Brønsted acid site and Lewis acid site are the active sites. The introduction of these exchangeable cations onto a zeolite resulted in a decrease in acidity and consequently reduced the activity in terms of conversion. From the profiles in Figure 5.20, the addition of Mg slightly decreased the conversion from 89.5 % to 88.3 % after 0.5 h time on stream. This implies that the Mg is not an active catalyst for the alkylation of benzene with t-butyl chloride. It also masks the Brønsted sites, preventing their contribution to the reaction. The addition of Na decreased the conversion from 88.3 % to 85.3 % after 0.5 h time on stream. The addition of Ca also was found to slightly reduce the conversion from 85.5 % to 85.1 % after 0.5 h time on stream.

In a related study by Emana & Chand (2015) in which the alkylation of benzene with ethanol was studied over Mg modified ZSM-5 it was found that the addition of Mg did not improve or enhance the conversion. The conversion obtained over the pristine ZSM-5 was 71.3 compared to 71.7 % obtained over the modified support. In the alkylation of benzene with benzyl chloride over Fe-Na modified MCM-41, He at al, (1998) found that the presence of Na decreases the conversion of the benzyl chloride significantly. Furthermore, the Na^+ reduction potential is very low and a mechanism involving ion radicals is not expected over Na catalyst (Bidart et al., 2006). In another related study by Dong et al. (2018) the alkylation of benzene with methanol over zeolite Y was carried out and it was found that zeolite Na-Y was inactive while the H-Y showed some activity. The conclusion was that Na was not an active metal for the alkylation reaction. Thus the observation made in the present study is consistent with previously reported outcomes.

Addition of Ni: From the profiles presented in Figure 5.20, it can be seen that the addition of Ni significantly increased the conversion from 85.1 % to 95.3 % after 0.5 h time on stream. This outcome is indicative of the promoting effect of Ni towards the conversion of t-butyl chloride. Further confirmation of the promoting effect of Ni on the conversion of t-butyl chloride is presented in Apendix A5. Several studies are available in open literature that attest to the catalytic activity of Ni in the Friedel-Crafts alkylation reaction. Sebti et al. (2001) reported on the use of Ni supported on hydroxyapatite in the alkylation of benzene with benzyl chloride. In a related study Ali et al. (2014) report on the use of Ni supported on zirconia in the alkylation of benzene with benzyl chloride. However, these mentioned studies focused only on monometallic systems whereas the present study is based on polymetallic systems. The higher conversion observed over the FeNi system in the present study may be attributed not only to the fact that these metals are active for the reaction under study but also the fact that when they are mobilised together on the support there is metal-to-metal charge transfer which further enhances the activity (Shen et al., 2014).

5.6.2 Effect of different metals on selectivity towards t-butyl benzene formation

The profiles of the effect of the different metals on the selectivity towards formation of t-butyl chloride are presented in Figure 5.21.
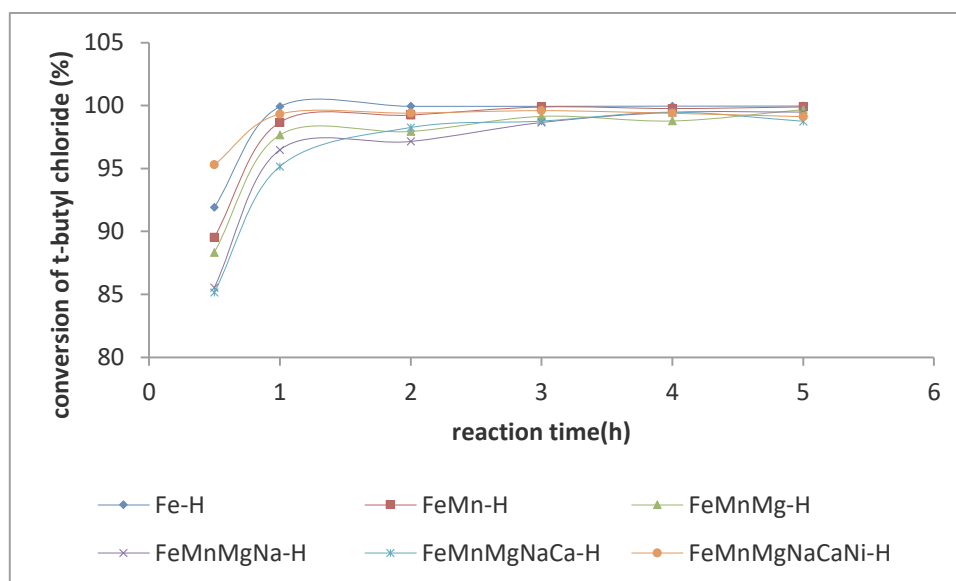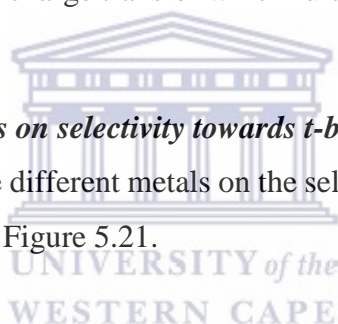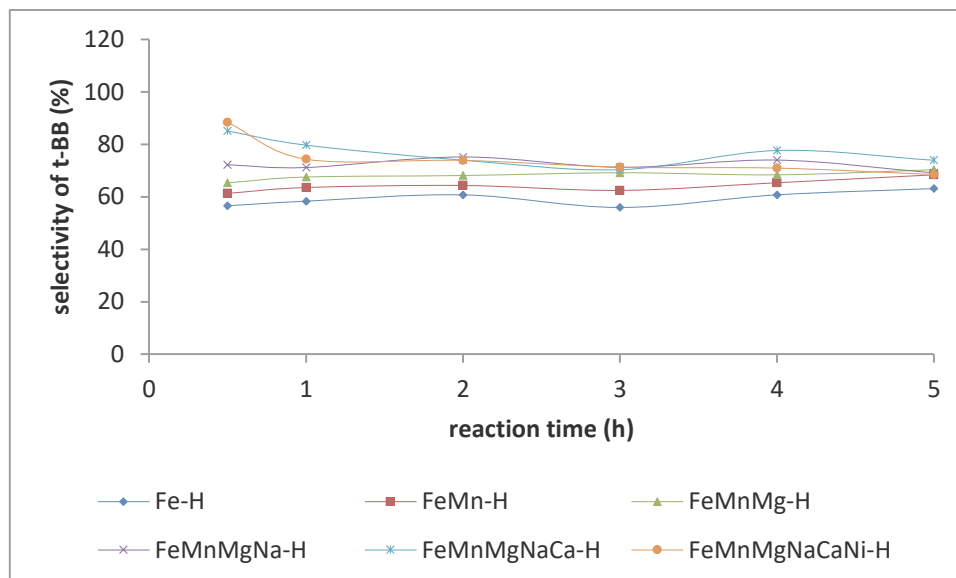
Figure 5. 21: Effect of various metals on the selectivity of t-butyl benzene at 45 °C over metal loaded HBEA support (benzene : tBC ratio of 10mL : 1 mL and 320 g of catalyst)

The lowest selectivity after 0.5 h time on stream was obtained over the monometallic Fe catalyst. Although the catalyst showed very high conversion, the same could not be said about the selectivity. As the metals were added to the Fe catalyst, starting with Mn, it was found that the selectivity increased from 56.6 % to 61.3 %. This confirms that Mn enhances the selectivity towards the monoalkylated product although the metal is inactive in the conversion of the t-butyl chloride. The same observation was made by Hlatywayo (2013) in which bimetallic and monometallic Fe/Mn catalysts were tested for the alkylation of benzene with t-butyl chloride. The improved selectivity on addition of Mn can be attributed to the fact that Mn suffers partial reduction of the Mn_2O_3/MnO_4, which may result in the decrease in acid strength, which consequently might affect product selectivity (Wang et al., 2012)

Addition of Mg, Na and Ca: The addition of Mg, Na and Ca resulted in improvement in the selectivity from 56.6 to 85.1 % after 0.5 h time on stream. These metals also reduce the acid strength and rather impose basicity (Marakatti et al., 2014). Alkali metals and alkaline earth metals reduce the number of acid sites on the external surface by masking them, and consequently reducing further oligomerisation (Emana & Chand, 2015). A study by Ko & Huang (1993) in which the alkylation of ethylbenzene with methanol was performed over modified HZSM-5 showed that Ca and Mg reduced the conversion while

concomitantly increasing selectivity. These outcomes were attributed to the diminution of both the strong acid sites and the pore size of zeolites.

Addition of Ni: The addition of Ni was found to further enhance the selectivity towards formation of the monoalkylated product in the initial stages of the reaction. The selectivity after 0.5 h time on stream increased from 85.1 to 88.4 %. However, with prolonged reaction times the selectivity of the catalyst loaded with Ni decreases. This may be attributed to the high alkylating activity of the Ni which may result in further alkylation forming dialkylated products.

5.6.3 Effect of different metals on yield of t-butyl benzene formation

The profiles of the effect of the different metals loaded on HBEA on the yield of t-butyl benzene are presented in Figure 5.22.
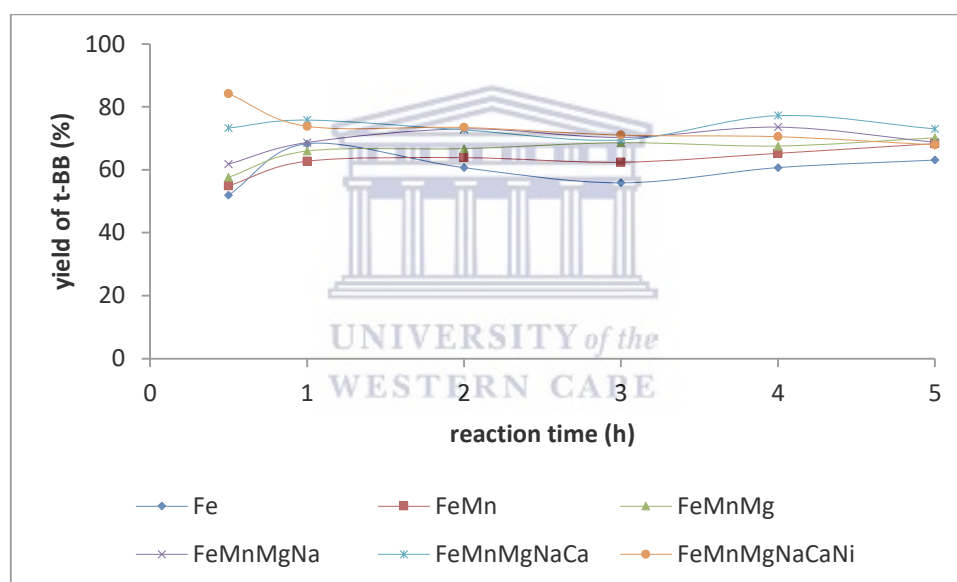
Figure 5. 22: Effect of various metals on the yield of t-butyl benzene at 45 °C over metal loaded HBEA support (benzene : tBC ratio of 10mL : 1 mL and 320 g of catalyst)

The highest yield obtained over the series of metal loaded catalysts presented in Figure 5.22 was 84.2 % obtained over the FeMnMgNaCaNi catalyst after 0.5 h time on stream. It can be seen from the profile of the catalyst that with prolonged time on stream the yield decreased slightly. The best yield is obtained in the first 0.5 h. Longer reaction periods showed that the FeMnMgNaCa had better yields. After a reaction time of 4 h, the catalyst gave a t-butyl benzene yield of 77.2 %. The yield is calculated from percentage

conversion and selectivity, hence it is influenced by the factors controlling those parameters and these have been discussed in previous sections.

5.6.4 Other important reaction parameters

Other important reaction parameters in the alkylation of benzene with t-butyl chloride are; reactant molar ratios, temperature and catalyst dose. In the present study the effect of reactant molar ratios was not investigated, an excess of benzene was used instead. The use of excess benzene is well known to enhance product selectivity and when a 1:1 molar ratio of benzene to t-butyl chloride is used the selectivity towards the monoalkylated product is greatly compromised since the monoalkylated product is more active relative to benzene (Fechete et al., 2012). The reaction temperature and catalyst dose also impact on the conversion, selectivity and yield percentages. Again, the effect of these parameters was not investigated in the study. However, a study by Bidart et al., (2001) investigated the effect of these parameters in the alkylation of benzene with tertiary halides and observed that temperature changes only produced slight increases in the yield and selectivity towards the monoalkylated product. In the same study it was also found that low catalyst dosages did not affect the yield but there was some slight increase in the selectivity.
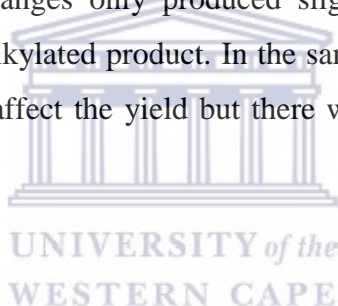
5.7 Chapter summary

The highest conversion of t-butyl chloride achieved over the fly ash based HBEA and MCM-41 prepared using AMD as metal solution precursor was 100 % over the 10AHI (prepared via ion exchange) after 2 h time on stream. The catalyst had a conversion of 99.8 % after 0.5 h on stream. The HBEA series prepared via wet impregnation also had very high conversion percentages with all the catalyst reaching conversion percentages of above 98 % after 4 h time on stream. Of the wet impregnated HBEA catalyst the best performing in terms of conversion was the 10AHW which had a conversion of 97.9 % after 0.5 h time on stream. The pristine HBEA was also found to be relatively active in the alkylation of benzene with t-butyl chloride giving a conversion of 30.7 % after 4 h time on stream showing the role of Brønsted acidity. The wet impregnated MCM-41 supported catalysts were also very active for the alkylation of benzene, giving a high conversion of 99.1 % after 4 h on stream over sample 25AMW (Fe wt % loading of 3.09). The pristine MCM-41 showed no activity. From the outcomes it can be said that the

HBEA supported catalysts gave higher conversion percentages in comparison to the MCM-41 counter parts. Of the HBEA supported catalysts higher conversions were obtained over the wet impregnated samples than on the ion exchanged samples showing the impact of additional trace metals from AMD. The ion exchanged samples were composed of only Fe as the active metal while the wet impregnated samples additionally contained Ni which was found to enhance the conversion.

The highest selectivity towards the formation of *t*-butyl benzene obtained over the HBEA supported Fe catalysts prepared via ion exchange was 84.5 % after 2 h on stream over the 25AHI. The highest selectivity over the parent HBEA support was 80.6 % after a reaction time of 5 h. The highest selectivity over the HBEA series prepared via wet impregnation was   100 % over sample 25AHW after 0.5 and 1 h time on stream. The selectivity was found to increase with an increase in metal wt % loading. The MCM-41 supported catalyst gave highest selectivity of 100 % after 2 h on stream. Again the selectivity was found to positively correlate with an increase in metal wt % loading. Comparing the two different supports it was found that the MCM-41 series gave better selectivity percentages but lower conversions relative to the corresponding HBEA supported catalysts.

The highest yield of *t*-butyl benzene obtained over the HBEA catalysts prepared via ion exchange was 84.6 % over sample 25AHI. The parent HBEA had a yield of 24.7 % after 4 h time on stream. The highest yield over the wet impregnated HBEA series was 85.08 % over sample 20AHW after 4 h on stream. The highest yield over the MCM-41 series prepared via wet impregnation was 90.2 % over sample 25AMW after 2 h time on stream. The effect of other metals that could be incorporated onto the supports when the wet impregnation approach was used was also investigated for their respective effects on catalytic activity. It was found that Mn, Mg, Na and Ca reduced the conversion but improved the selectivity. The Ni was found to improve both the conversion and selectivity. It can generally be concluded that an increase in metal loading resulted in an increase in both conversion and selectivity apart from the case of the HBEA wet impregnated sample 25AHW, which showed reduced activity due to reduced surface area as the metal wt % was increased to 3.5 % (in terms of Fe). Furthermore, the outcomes in this chapter clearly show that AMD can be used as a metal solution precursor for wet impregnation or ion exchange of Fe in the preparation of solid acid catalysts for use in

the Friedel-Crafts alkylation of benzene with t-butyl chloride. The catalytic activity obtained over the AMD based catalysts was higher relative to activity obtained over monometallic Fe catalysts based on commercial salts.

CHAPTER 6

6.0 Activity of supported metals prepared using Fe extracted from fly ash as metal precursor

The chapter presents the activity of metal catalysts loaded on HBEA and MCM-41 using iron extracted from coal fly ash as metal solution precursor. The catalytic activity was assessed based on the Friedel-Crafts alkylation of benzene with t-butyl chloride. A comparison of the conversion of t-butyl chloride, selectivity towards formation of t-butyl benzene, yield of t-butyl benzene and product distribution over the FeAsh catalysts was made against the corresponding Fe catalysts prepared using acid mine drainage as metal solution precursor. The chapter closes with a brief summary of the overall catalytic activity of the tested materials.

6.1 Introduction

The catalytic activity of the prepared supported metal catalysts was tested for the Friedel-Crafts alkylation of benzene with t-butyl chloride. The catalysts were prepared using Fe extracted from coal fly ash (FeAsh) as metal solution precursor. The Fe extraction from coal fly ash was carried out via an acid assisted extraction as outlined in Section 3.4.1. The pH of the extracted Fe solution was moderated by addition of NaOH, and this resulted in the presence of Na in the precursor solution and consequently on the support. Thus, the catalysts prepared either via ion exchange or wet impregnation using FeAsh contained significant amounts of Na. the elemental composition of the catalysts is presented in Section 4.5.

The probe reaction (alkylation of benzene with t-butyl chloride) was carried out in a batch reactor at a temperature of 45 °C, under reflux and stirring using a magnetic bar as detailed in Section 3.7. Sample aliquots were taken at time intervals over 5 h and analysed by gas chromatography as set out in Section 3.7.2. Again, the Fe catalysts supported on HBEA were prepared via two approaches namely; liquid phase ion exchange and wet

impregnation as outlined in Section 3.5.1 and 3.5.2 respectively. The catalysts supported on MCM-41 were prepared only via wet impregnation.

6.2 Catalytic activity studies over ion exchanged HBEA metal catalysts

The conversion, selectivity, product distribution studies and yield over the HBEA supported metal catalysts were carried out at a temperature of 45 °C over a reaction time of 5 h. The outcomes are presented in the following sections.

6.2.1 Conversion studies over ion exchanged HBEA

The results for the conversion over the ion exchanged series of HBEA supported catalysts prepared via ion exchange using FeAsh as metal solution precursor are presented in Figure 6.1. The percentage conversion of *t*-butyl chloride is plotted as a function of reaction time.
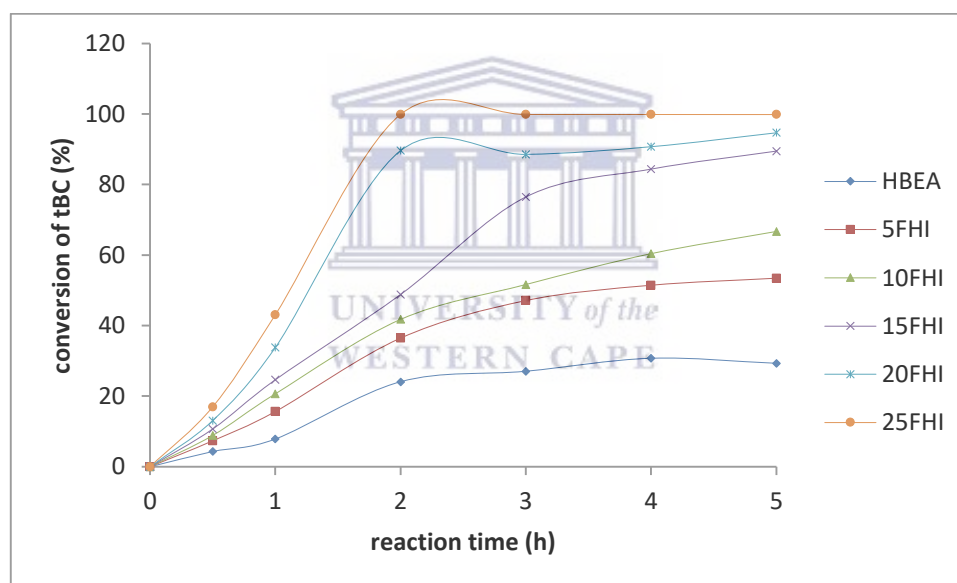
Figure 6. 1: Conversion of t-butyl chloride (tBC) over the series of HBEA supported metals prepared using FeAsh as metal precursor at reaction temperature of 45 °C (10:1 benzene to t-BC ratio and 320 mg of catalyst).

The general trend exhibited by the profiles in Figure 6.1 show a rapid increase in the conversion of t-butyl chloride in the first 2 h for sample 25FHI and 20FHI, followed by a levelling off of the profiles after the reaction reached steady state. It can be seen from the profiles that an increase in metal wt % loading resulted in an increase in the conversion of the t-butyl chloride. The lowest conversion was obtained over the parent HBEA

showing the role of Brønsted acid sites. The conversion over the parent HBEA material was discussed in Section 5.1.1. The best performing catalyst in terms of conversion was the 25FHI (actual Fe wt % of 3.52). The catalyst had a conversion of 99.9 % after a reaction time of 2 h on stream. Although the conversion was high, it should be noted that the corresponding catalyst prepared using AMD as metal precursor gave a conversion of 99.8 % after only 0.5 h on stream. The lower activity over the FeAsh prepared catalyst can be attributed to the presence of Na (the catalyst had an actual Na wt % of 2.86 %, refer to Table 4.1). The presence of Na reduces the total acidity of the catalyst by neutralising the Brønsted acidic centres and enhancing the basic properties of lattice oxygen (Corma, 2003). In addition, the 25FHI had a reduced BET surface area in comparison to the 25AHI (25FHI = 408 m^2/g whilst 25AHI = 482 m^2/g). The reduction in surface area could also have contributed to the reduced activity.

Furthermore, the FeAsh based 25FHI did not show the characteristic peaks due to Fe_2O_3 crystallites on the XRD profiles (refer to Figure 4.1). This outcome signified good metal dispersion. However, the presence of the Fe_2O_3 crystallites in close proximity to isolated Fe^{3+} species (Fe at ion-exchanged sites) has a synergic effect on the catalytic activity. On the other hand, the AMD based 25AHI showed characteristic peaks of the Fe_2O_3 on the XRD profile. This could have further increased the activity relative to that of the 25FHI. In a related study by Lin et al. (2011) in which the Friedel-Crafts alkylation of benzene was studied over Fe loaded commercial zeolite ZSM-5, enhanced activity was observed due to the occurrence of synergistic catalysis between isolated Fe^{3+} species and Fe_2O_3. The profiles presented in Figure 6.1 are typical of alkylation conversion profiles reported in related studies using commercial catalysts (Ali et al., 2014; Lin et al., 2011).

6.2.2 Selectivity studies over ion exchanged HBEA

As has been mentioned in Section 5.1.2, the alkylation of benzene with t-butyl chloride gives rise to polyalkylated products alongside the monoalkylated product. The selectivity towards the formation of the monoalkylated product as a function of time is presented in Figure 6.2.
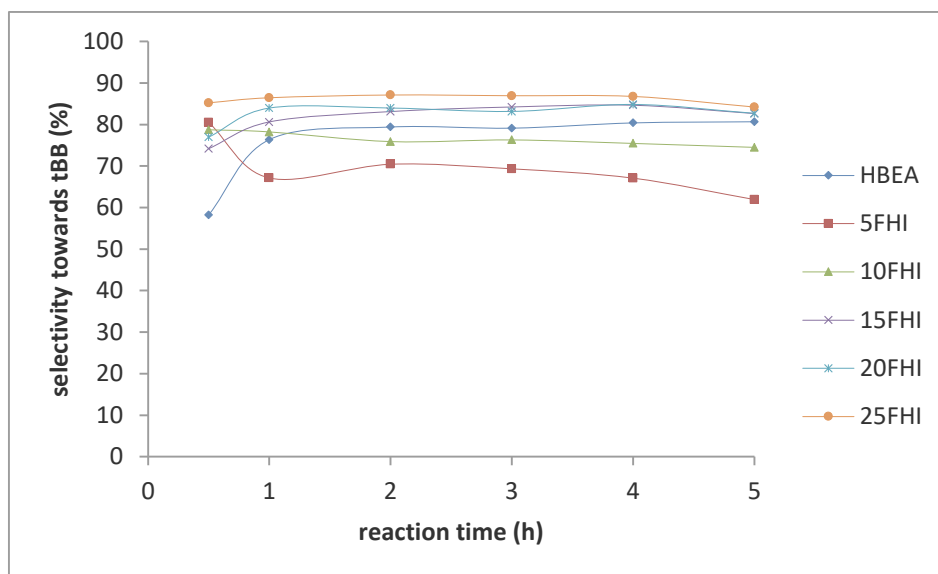
Figure 6. 2: Selectivity of t-butyl benzene over the series of HBEA supported metals prepared using FeAsh as metal precursor at reaction temperature of 45 °C.

The selectivity towards formation of the monoalkylated product presented in Figure 6.2 shows that after 1 h, the respective catalysts generally maintained the same selectivity over the entire 5 h duration which was studied. Product selectivity over porous materials can be influenced by the pore channels of the support. However, based upon the outcomes obtained over the HBEA series in Figure 6.2 it cannot be concluded that the pore system of the zeolite influenced the selectivity since some catalysts had a selectivity lower than the parent material while other catalysts had selectivity percentages higher than that of the parent material. In addition, the pore size was not greatly affected by the metal loading as was shown in Figure 4.20. The highest selectivity obtained was 87.1 % over the 25FHI after 2 h time on stream. The lowest selectivity obtained was 58.2 % over the 5FHI after 0.5 h time on stream.

The outcomes obtained are indicative of the fact that the higher selectivity was based mostly on the higher metal loading of the catalysts. StrongBrønsted acidity leads to poor selectivity and formation of polyalkylated products (Wang et al., 2008). The addition of metals onto the zeolite reduced the Brønsted acidity. It should be noted that the catalysts prepared using FeAsh had varying Fe:Na ratios, this resulted in a variation in the manner in which the zeolite acidity was affected (refer to ICP-OES data in Section 4.5.1.1). Generally, an increase in Fe wt % loading should result in a decrease in selectivity,

however the presence of Na on the support can be said to have suppressed this tendency. From the data presented in Section 5.6.2, it could be seen that although it suppressed the conversion, the addition of Na increased the selectivity by modifying the surface acidity by coating the Brønsted acid sites on the surface of the zeolite. Several studies have concluded that there is an optimum number of acid sites that are required for optimum selectivity in the alkylation of aromatics (Kamalakar et al., 1999; Wang et al., 2008).

In comparison to the AMD loaded counterparts, the FeAsh catalysts in Figure 6.2 showed higher selectivity percentages. The higher selectivity can be ascribed to the reduction in acid strength that is induced by the presence of Na. (It should be noted that the AMD based catalyst prepared via ion exchange were composed mostly of Fe as the metal centre and no other metal existed in reasonable quantities).

6.2.3 Product distribution over HBEA supported catalysts prepared via ion exchange

The product distribution over the HBEA supported metal catalysts prepared via ion exchange using FeAsh as metal precursor are presented in the following sections. The catalyst with the lowest metal wt % loading and the one with the highest are presented for discussion. The product distribution over the parent material is presented in Section 5.1.3.1.

6.2.3.1 Product distribution over 5FHI

The product distribution obtained over the 5FHI (Fe wt % loading = 0.69; Na wt % loading = 0.68) obtained over the HBEA catalyst loaded via ion exchange using FeAsh as metal solution precursor is presented in Figure 6.3.
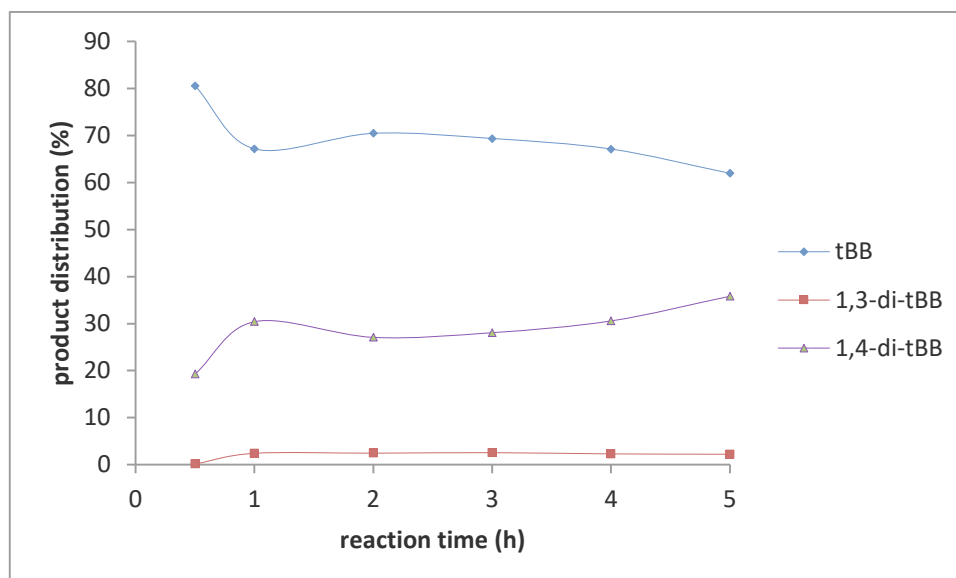
Figure 6. 3: Product distribution for benzene alkylation with t-butyl chloride over the 5FHI at 45 °C.

The profiles for the product distribution obtained over the 5FHI catalyst show that the primary product was the monoalkylated product (t-butyl benzene), the *meta* isomer (1,3-di-tertiary butyl benzene) and the *para* isomer (1,4-di-tertiary butyl benzene. Again the ortho isomer (1,2-di-tertiary butyl benzene and the tri alkylated product (1,3,5-tri-tertiary butyl benzene) were not detected in the product mixture. The alkylation of benzene with t-butyl chloride does not give the ortho isomer as has been mentioned previously. The absence of the trialkylated product may be attributed to the use of excess benzene which supresses polyalkylation. From the profile, it can be seen that the *para* isomer is relatively more abundant than the *meta* isomer despite the fact that the *meta* isomer is thermodynamically more stable than the *para* isomer. The relatively higher selectivity of the *para* isomer can be ascribed to the product shape selectivity of the pores of the zeolite support. The shape of the *para* isomer offers less diffusional constraints in the zeolite channels and hence promoted higher selectivity. Furthermore, the presence of Na induces basicity on the zeolite surface and suppresses the effect of HCl, which is known to favour the *meta* isomer (Yuan & Gevert, 2004; Bidart et al., 2001). Comparison of the 5FHI catalyst prepared using FeAsh as metal precursor shows that the percentage of the *para* isomer in the product distribution was relatively higher than the amount of the *para* isomer obtained over the corresponding 5AHI prepared using AMD as metal precursor. This outcome can be attributed to the presence of Na in the FeAsh prepared catalyst. The highest percentage of the *para* isomer over the FeAsh prepared catalyst was 35.8 % after 5 h while that obtained over the AMD prepared counterpart was 31.2 % after 0.5 h time

on stream. Comparable outcomes were reported in related studies (Wang et al., 2012; Bidart et al., 2001).

6.2.3.2 Product distribution over 25FHI

The product distribution profiles obtained over the 25 FHI (Fe wt % =3 .52 and Na wt % = 2.86) are presented in Figure 6.4.
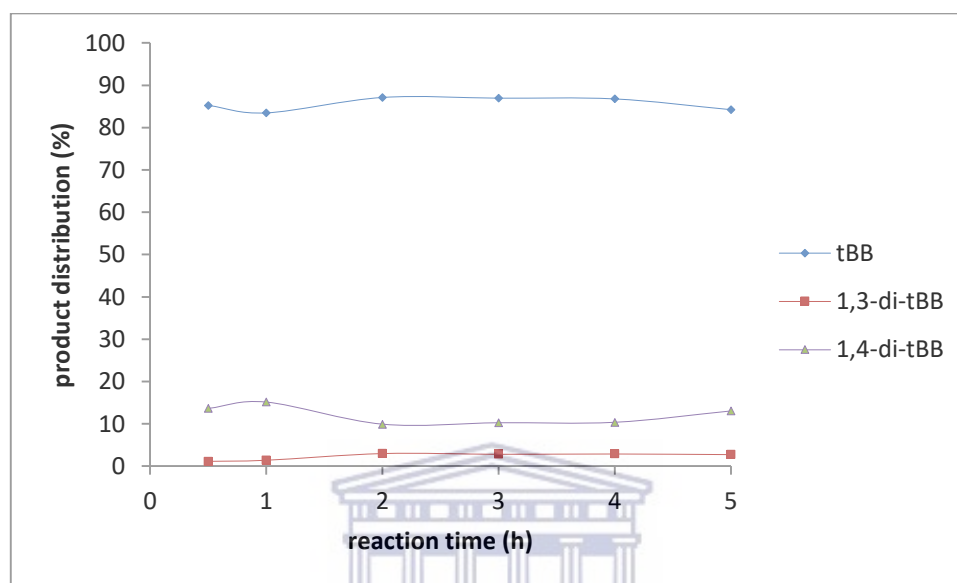
Figure 6. 4: Product distribution for benzene alkylation with t-butyl chloride over the 25FHI at 45 °C.

The profiles presented in Figure 6.4 show that the primary product obtained over the 25FHI was the monoalkylated product. Again the absence of the ortho isomer as well as the trialkylated product was observed over the catalyst. The same reasons previously discussed are responsible for the absence of these two from the product mixture. Of the dialkylated products it was again found that the *para* isomer was relatively abundant in comparison to the *meta* isomer. The trends are comparable to those obtained over the 5FHI and the corresponding AMD prepared catalyst (the 25AHI). The only difference is on the exact proportions of the products. The 25FHI was more selective compared to the corresponding catalyst prepared using AMD. The higher selectivity again can be attributed to the presence of Na as has been previously discussed. The highest selectivity towards formation of the monoalkylate achieved was 87.1 % after 2 h time on stream while the highest selectivity achieved over the corresponding AMD based catalyst was 84.5 after 3 h time on stream.

6.2.3.3 Product Yield over ion exchanged HBEA

The percentage yield of t-butyl benzene obtained over the HBEA supported catalysts prepared via ion exchange using FeAsh as metal solution precursor are presented in Figure 6.5.
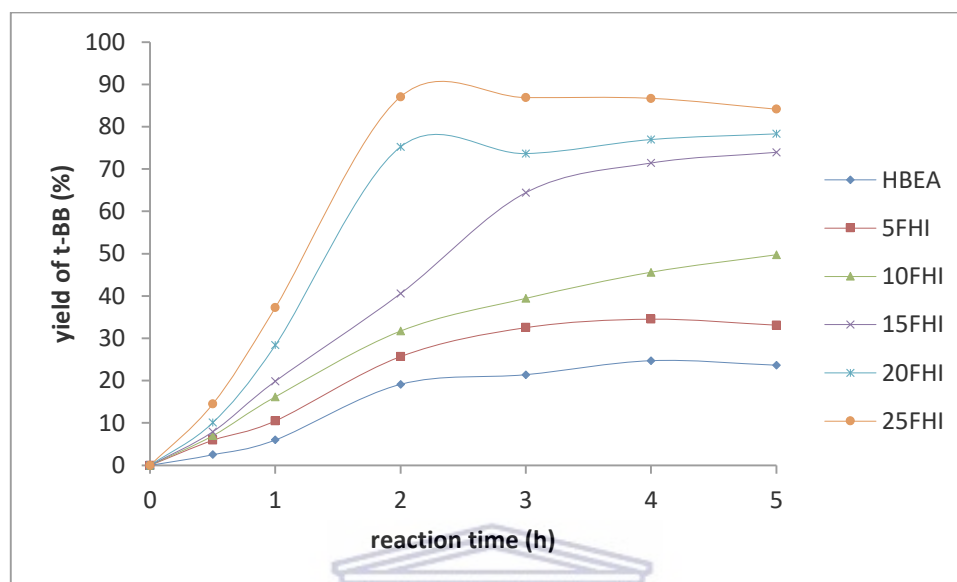
Figure 6. 5: Product yield of t-butyl benzene over the series of HBEA supported metals prepared using FeAsh as metal precursor at reaction temperature of 45 °C and 10:1 benzene to t-BC ratio.

The highest yield of t-butyl benzene of 87.0 % was obtained over the 25FHI (Fe wt % =3 .52 and Na wt % = 2.86). Of the catalysts prepared via ion exchange using FeAsh as metal precursor, sample 25FHI had the highest conversion as well as selectivity. From the profiles presented in Figure 6.5, it can be seen that as the metal wt % increased there was a corresponding increase in the percentage yield of *t*-butyl benzene. The percentage yield is calculated from conversion and selectivity, hence the factors governing these two parameters consequently affect the percentage yield. Relative to the corresponding catalyst prepared using AMD as metal precursor it can be said that the catalysts prepared using FeAsh gave a higher yield of t-butyl benzene. This is due the improved product selectivity obtained over the FeAsh based catalysts. Although the conversion over the FeAsh catalyst was relatively lower the selectivity was much improved which consequently resulted in improved yields. The yields are however comparable, since the highest yield percentage obtained over the FeAsh based series was 87.5 % over the 25FHI after 2 h time on stream, while the 25AHI gave a high yield of 84.6 % after 2 h time on stream. The highest percentage yield obtained over the catalyst with the lowest metal wt

% loading, the 5FHI (Fe wt % loading 0.69; Na wt % loading 0.68) was 34.5 % while the corresponding AMD based catalyst the 5AHI (Fe wt % loading of 0.73) gave a much higher yield of 56.8 after 0.5 h time on stream. The lower yield on the FeAsh based catalyst can be ascribed to the lower amount of Fe coupled with the fact that there was an almost 1:1 ratio of Fe to Na which further neutralised the already low Lewis acidity. The selectivity was even lower than that of the pristine HBEA support.

6.3 Catalytic activity studies over wet impregnated HBEA metal catalysts

The catalytic activity of the HBEA supported catalysts prepared via wet impregnation using FeAsh as metal solution precursor was evaluated based on the conversion of t-butyl chloride, selectivity towards formation of t-butyl benzene, product distribution as well as percentage yield of t-butyl benzene.

6.3.1 Conversion studies over wet impregnated HBEA

The conversion studies of t-butyl chloride over the HBEA series prepared via wet impregnation using FeAsh as metal solution precursor are presented in Figure 6.6.

Figure 6. 6: Conversion of t-butyl chloride over the series of HBEA supported metals prepared using FeAsh as metal precursor at reaction temperature of 45 °C and a 10:1 benzene to t-BC ratio.

The profiles presented in Figure 6.6 were again characterised by a rapid initial increase reaching steady state between 2 – 3 h on stream. The highest conversion of 100 % was achieved over the 25FHW (Fe wt % loading = 3.48; Na wt % loading = 3.76) after 3 h

time on stream. The catalyst with the lowest metal loading, the 5FHW (Fe wt % loading = 0.72; Na wt % loading = 0.75) had a conversion of 45.99 % after 4 h time on stream. Again, from the profiles it can be seen that the inclusion of Fe had a positive effect on the activity of the catalysts. As the metal wt % loading was increased there was a corresponding increase in the conversion of the t-butyl chloride. The conversion obtained over the wet impregnated HBEA catalyst prepared using FeAsh as metal precursor was slightly lower in relation to the conversion percentages obtained over the ion exchanged counterparts. This observation can be attributed to the increased amount of Na in the wet impregnated samples. It was found that the inclusion of Na reduced the conversion and the outcomes obtained with the series presented in Figure 6.6 were anticipated.

Comparing the wet impregnated catalysts supported on HBEA prepared using FeAsh against the corresponding counterparts prepared using AMD (refer to Figure 5.7) as metal precursor it can be see that with lower metal loadings the AMD based catalysts were more active. The high activity of the AMD based catalyst can be attributed to the presence of Ni which gives synergistic catalysis to the reaction. In addition, the different metals (transition and alkali and earth alkaline metals) modify the redox properties of Fe and resulted in improved activity (Vivier & Duprez, 2010). Although the AMD based catalyst also contained metals such as Ca, Na, Mg and Mn that have been seen to reduce the conversion, these metals were present in much smaller quantities and their effect was not as pronounced compared to the activity suppression effect that the Na in the FeAsh catalyst had on the conversion, since the Na was present in significant quantities (the Fe : Na ratio was almost 1 : 1) With the highest metal loaded catalysts, sample 25AHW was less active compared to the 25FHW, this can be attributed to the reduction in surface area that the AMD based catalyst suffered on metal incorporation (BET surface area, 25AHW = 361 m^2/g; 25FHW = 397 m^2/g). Furthermore, catalytic activity is based on the Lewis acid/ Brønsted acid ratio, and there is an optimum ratio that gives best activity (Ding et al., 2014). In the case of the 25AHW, it can be said that the lower activity was due to the reduced Brønsted acid sites as more metals from the AMD were loaded onto the support. The alkylation performance is reduced with reduction in the Brønsted acid site strength, since they are responsible for the formation of the aryl cation intermediates via the attack of the electronegative chlorine atom in the alkylating agent t-butyl chloride (Wang et al., 2017). The trends presented in Figure 6.6 are similar in pattern to profiles obtained in

related studies on the Friedel-Crafts alkylation of benzene over bimetallic and monometallic catalyst available in open literature (Bachari et al., 2004; Ali et al., 2014). The present work established that FeAsh can be used as an alternative metal precursor to commercial salts and furthermore, the fly ash based zeolite HBEA can be used as a suitable support in the preparation of green catalysts for the FC alkylation reaction.

6.3.2 Selectivity studies over wet impregnated HBEA

The selectivity profiles towards the formation of t-butyl benzene over the wet impregnated HBEA catalysts prepared using FeAsh as metal solution precursor are presented in Figure 6.7.
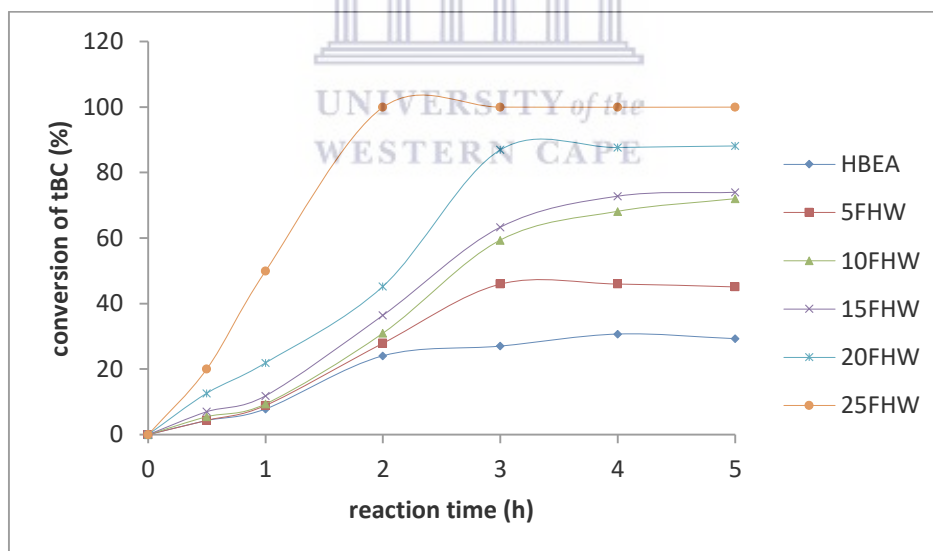

Figure 6. 7: Selectivity of t-butyl benzene over the series of HBEA supported metals prepared using FeAsh as metal precursor at reaction temperature of 45 °C and a benzene to t-BC ratio of 10:1.

The selectivity profiles obtained over the HBEA supported catalyst series presented in Figure 6.7 show that after a reaction time of 1 h, the respective catalysts maintained an almost constant ($> 80 \%$) selectivity except for samples 5FHW and 10FHW. As has been outlined in Section 6.2.2, the selectivity was mainly influenced by the metal composition rather than the pore channels of the zeolite, since there were minimal alterations to the pore size of the zeolite upon metal loading. The highest selectivity achieved over the series in Figure 6.7 was 88.1 %, obtained over the 25FHW after 1 h on stream. This value was slightly higher than the value obtained over the corresponding catalyst prepared via ion exchange of 87.1 %. The slight increase in the selectivity can be ascribed to the

increased amount of Na in the wet impregnated sample. As has been previously presented, the presence of Na, was found to increase the selectivity, although it had a negative effect on the conversion. The profiles obtained over the wet impregnated samples closely resemble those obtained over the corresponding ion exchanged samples due to the reasons already discussed under Section 6.2.2.

6.3.3 Product distribution over HBEA supported FeAsh catalysts prepared via wet impregnation

The product distribution over the HBEA supported FeAsh metal catalysts prepared via wet impregnation using FeAsh as metal precursor is presented in the following sections. The catalyst with the lowest metal wt % loading and the one with the highest are presented for discussion. The product distribution over the parent HBEA material is presented in Section 5.1.3.1.

6.3.3.1 Product distribution over 5FHW

The product distribution obtained over the 5FHW (Fe wt % loading = 0.72; Na wt % loading = 0.75) obtained over the HBEA catalyst loaded via wet impregnation using FeAsh as metal solution precursor is presented in Figure 6.8.
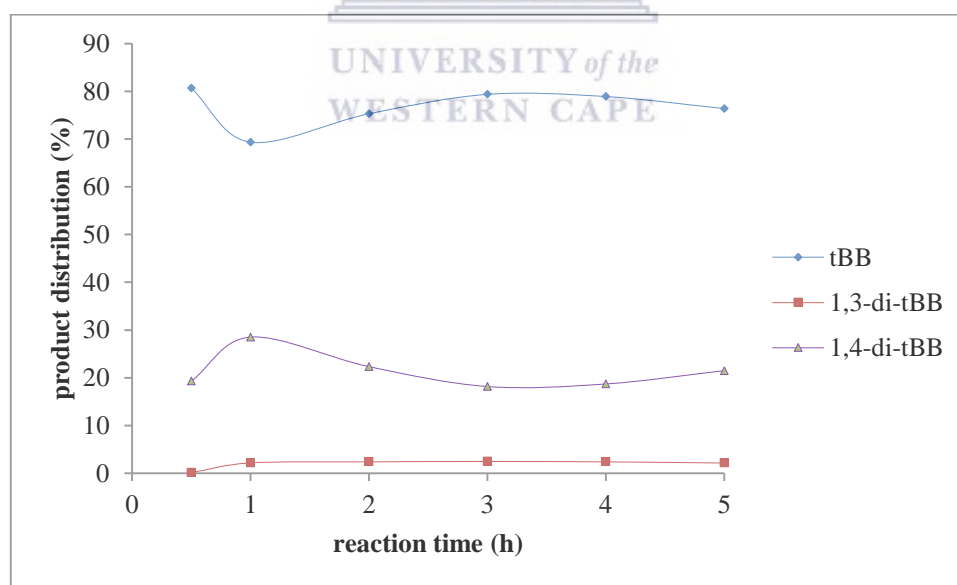
Figure 6. 8: Product distribution for benzene alkylation with t-butyl chloride over the 5FHW at 45 °C and benzene to t-BC ratio of 10:1.

The product distribution over the 5FHW showed that the primary product was the monoalkylated product (t-butyl benzene). Again the product mixture was composed of

two dialkylated isomers, the 1,3-di-tertiary butyl benzene and the 1,4-di-tertiary butyl benzene. The amount of the primary product (*t*-butyl benzene) was high in the initial stages of the reaction, followed by a decrease and a gradual rise after steady state was achieved maintaining an almost constant level in the product mixture. The amount of the *meta* isomer was almost constant after 1 h on stream and was the lowest in terms of concentration despite the fact that it is the more thermodynamically stable isomer. The lower concentration of the *meta* isomer can be ascribed to product selectivity of the zeolite pore system. The profiles in Figure 6.8 closely resemble the profiles obtained over the 5FHI apart from the fact that the primary product over the 5FHW is slightly higher due to the increased amount of Na. The effect of Na on the selectivity has been discussed in previous sections.

6.3.3.2 Product distribution over 25FHW

The product distribution obtained over the 25FHW (Fe wt % loading = 3.48; Na wt % loading = 3.76) obtained over the HBEA catalyst loaded via ion exchange using FeAsh as metal solution precursor is presented in Figure 6.9.
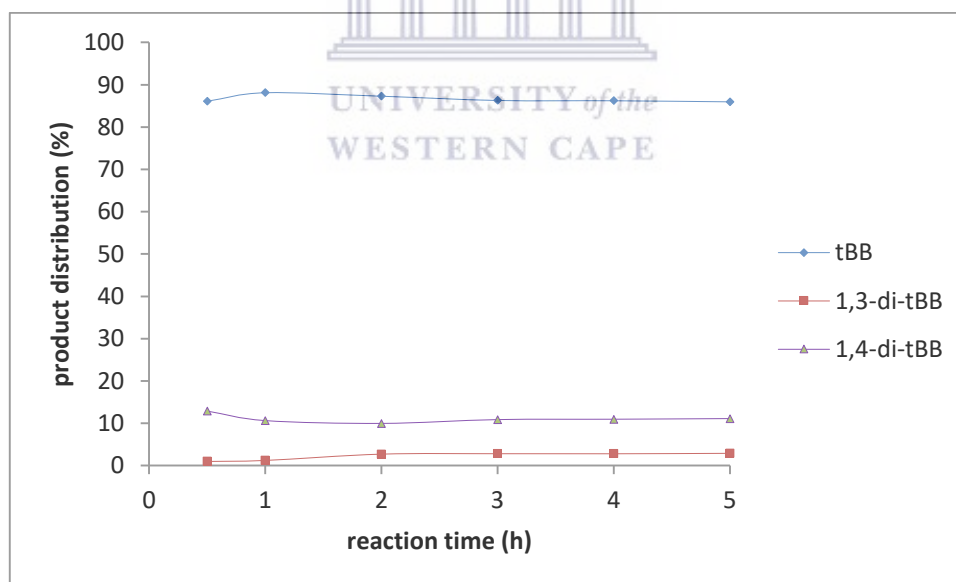
Figure 6. 9: Product distribution for benzene alkylation with t-butyl chloride over the 25FHW at 45 °C and benzene to t-BC ratio of 10:1.

Again, the primary product obtained over the 25FHW was the monoalkylated product. The para and *meta* isomers were also detected in the product mixture. The composition

of the product mixture was almost constant for the entire period studied. Comparison of the isomer distribution over sample 25FHW and 5FHW (presented in the previous section) show that the amount of the *para* isomer was relatively higher over sample 5FHW. This outcome can be attributed to the availability of more Brønsted acid sites on the 5FHI. Brønsted acidity tends to favour formation of the *para* isomer (Sunajadevi & Sugunan, 2006). The product distribution profiles of sample 25FHW are similar to those obtained over the 25FHI although the wet impregnated samples gave slightly higher selectivity towards the monoalkylated product relative to the ion exchanged counterparts. This outcome is again attributed to the presence of increased amounts of Na on the zeolite support. It however should be noted that the AMD based catalysts prepared via wet impregnation gave different profiles. The concentration of the primary product over the AMD based catalysts decreased with prolonged reaction times. The variation can be attributed to the effect of the different metals in AMD that got loaded onto the zeolite. The effect of these metals on selectivity is presented in Section 5.6.2. Furthermore, the AMD based catalysts had a reduced surface area in comparison to the FeAsh based catalyst.

6.3.3.3 Product Yield over wet impregnated FeAsh HBEA

The percentage yield of t-butyl benzene obtained over the HBEA supported catalysts prepared via wet impregnation using FeAsh as metal solution precursor are presented in Figure 6.10.
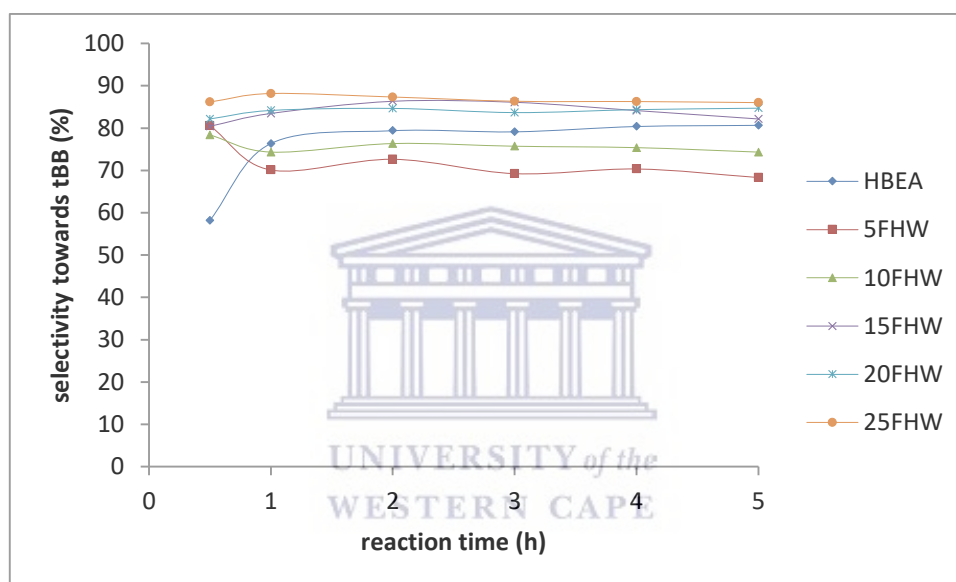
Figure 6. 10: Product yield of t-butyl benzene over the series of HBEA supported metals prepared using FeAsh as metal precursor at reaction temperature of 45 °C and benzene to t-BC ratio of 10:1.

The highest yield on the FeAsh based catalysts prepared via wet impregnation and supported on HBEA was 87.2 % that was obtained over the 25FHW (Fe wt % loading = 3.48; Na wt % loading = 3.76) after 2 h time on stream. The highest yield over the ion exchanged catalysts was 87 % over the 25FHI after 2 h time on stream. It can be seen from the profiles presented in Figure 6.10 that an increase in metal wt % loading resulted in an increase in the percentage yield of t-butyl benzene. The yield obtained over the ion exchanged samples and the wet impregnated samples were comparable despite the fact that the conversions and selectivity were slightly different. The ion exchanged catalysts had higher conversions but lower selectivity. Since the percentage yield is calculated from conversion and selectivity, it follows that the factors influencing these two parameters consequently influence the yield. The AMD based catalyst also gave comparable yield percentages. The highest yield over the AMD based catalysts prepared via wet impregnation was 85.1 % obtained over the 20AHW whereas sample 25FHW gave 87.2 %.

6.4 Catalytic activity studies over wet impregnated MCM-41 metal catalysts

The conversion studies for the MCM-41 supported metal catalysts were carried out over 5 catalysts with different metal loadings. The catalysts were prepared via wet impregnation, using FeAsh as metal solution precursor. The Friedel-Crafts alkylation of benzene with *t*-butyl chloride was carried out at a temperature of 45 °C as presented in

Section 3.7.2. The parent MCM-41 without metal was found to be inactive and is not presented for discussion in this section, but its inactivity compared to HBEA parent highlights the beneficial role of Brønsted acidity.

6.4.1 Conversion studies over wet impregnated MCM-41

The conversion studies of t-butyl chloride over the MCM-41 series prepared via wet impregnation using FeAsh as metal solution precursor are presented in Figure 6.11.

Figure 6. 11: Conversion of t-butyl chloride over the series of MCM-41 supported metals prepared using FeAsh as metal precursor at reaction temperature of 45 °C and benzene to t-BC ratio of 10:1.

The general trend observed over the MCM-41 supported catalyst series was characterised by a rapid initial increase reaching a steady state between 2 – 3 h on stream. From the profiles presented in Figure 6.11, it can be seen that an increase in metal loading resulted in a corresponding increase in the conversion. This outcome was anticipated, since in the absence of mass transfer resistance, the rate of reaction is directly proportional to metal catalyst loading based on the entire volume of the liquid phase (Lande et al., 2013). The highest conversion of 77.9 % was obtained over the 25FMW (Fe wt % = 3.50; Na wt % = 3.62) after 4 h time on stream. The highest conversion over the catalyst with the lowest metal wt % loading, the 5FMW (Fe wt % = 0.69; Na wt % = 0.72) was only 8.2 % after 5 h on stream. In comparison to the corresponding HBEA supported metal catalysts prepared via wet impregnation using FeAsh as metal precursor it can be seen that the

HBEA based catalysts were much more active. The highest conversion obtained over the 25FHW was 100 % after 3 h on stream. The higher activity over the HBEA supported catalysts can be attributed to the presence of Brønsted acid sites on the HBEA. The Brønsted acid sites are active in the Friedel-Crafts alkylation of benzene with t-butyl chloride as evinced by the fact that the pristine HBEA was active, giving a conversion of 30.7 %. The MCM-41 supported metal catalyst prepared via wet impregnation using AMD as metal precursor were more active relative to the corresponding counterparts prepared using FeAsh. The highest conversion obtained over the AMD based catalyst supported on MCM-41 was 99.1 % obtained over the 25AHW (Fe wt % loading of 3.09) after 4 h on stream. The higher activity over the AMD based catalyst can be ascribed to the presence of Ni, which was found to enhance conversion (refer to the discussion on the effect of Ni presented in Section 5.6.1). It also should be noted that there were other metals in AMD that could compromise the conversion (Ca, Na, Mg and Mn), however these metals were relatively lower in quantity relative to the Fe and did not compromise the conversion to any great extent.

In a related study by He et al., (1998) in which monometallic Fe and bimetallic Fe/Na catalysts supported on commercial MCM-41 were tested on the Friedel-Crafts alkylation of benzene with benzyl chloride, it was found that the addition of Na greatly compromised the conversion. The highest conversion obtained over the monometallic (Fe wt % = 4.1) catalyst was ~ 95 % and addition of Na of comparable amount to the Fe resulted in a reduction in the conversion to ~ 70%. The outcomes in the present study are in line with the reported outcomes by He et al., (1998). In another related study in which different Fe wt % loadings were supported on MCM-41 and tested for their activity in the alkylation of benzene with benzyl chloride, Jiang et al., (2012) also reported that an increase in Fe loading resulted in an increase in conversion. The outcomes reported in their study are consistent with the findings in this present study.

6.4.2 Selectivity studies over wet impregnated MCM-41

The trends of the selectivity towards the formation of the monoalkylated product (t-butyl benzene) over the MCM-41 supported metal catalysts are presented in Figure 6.12.

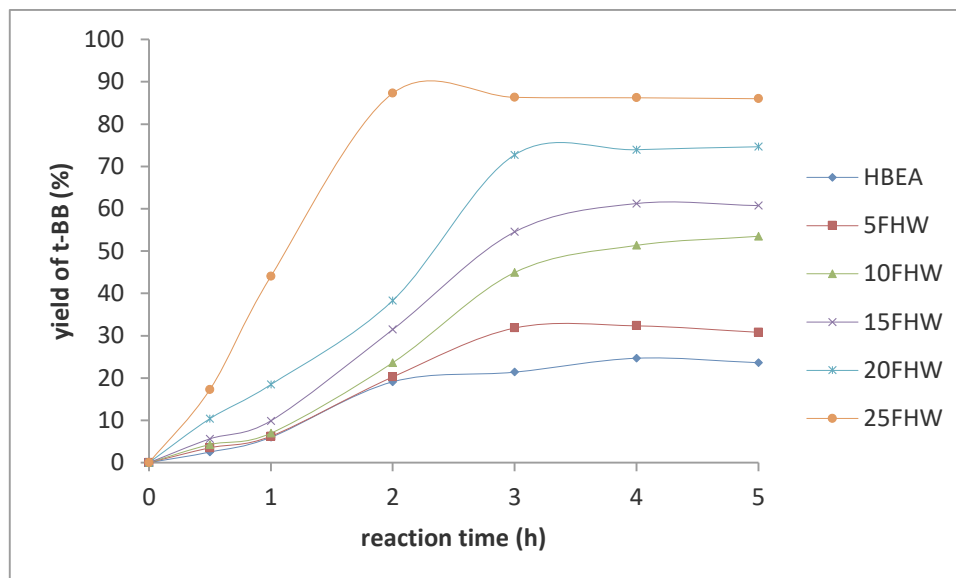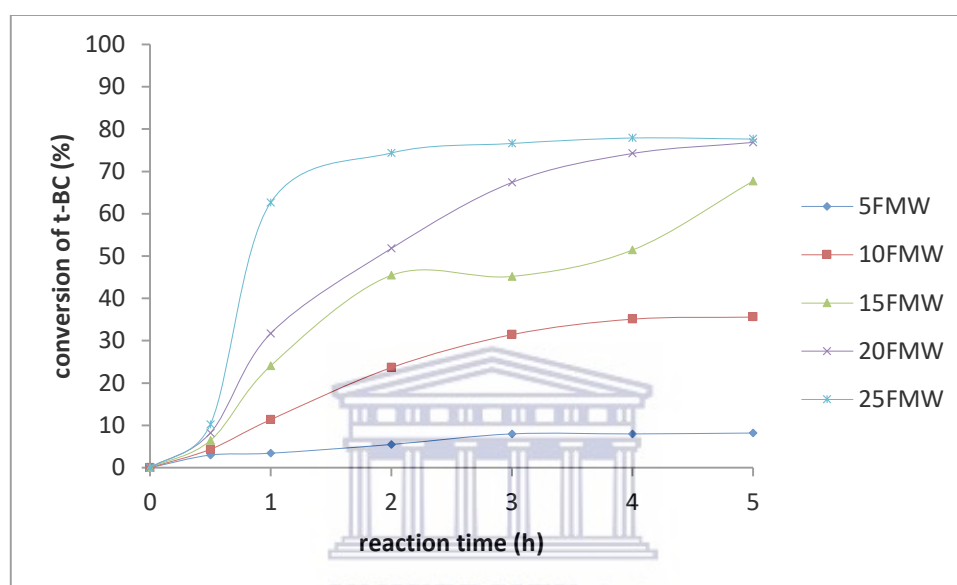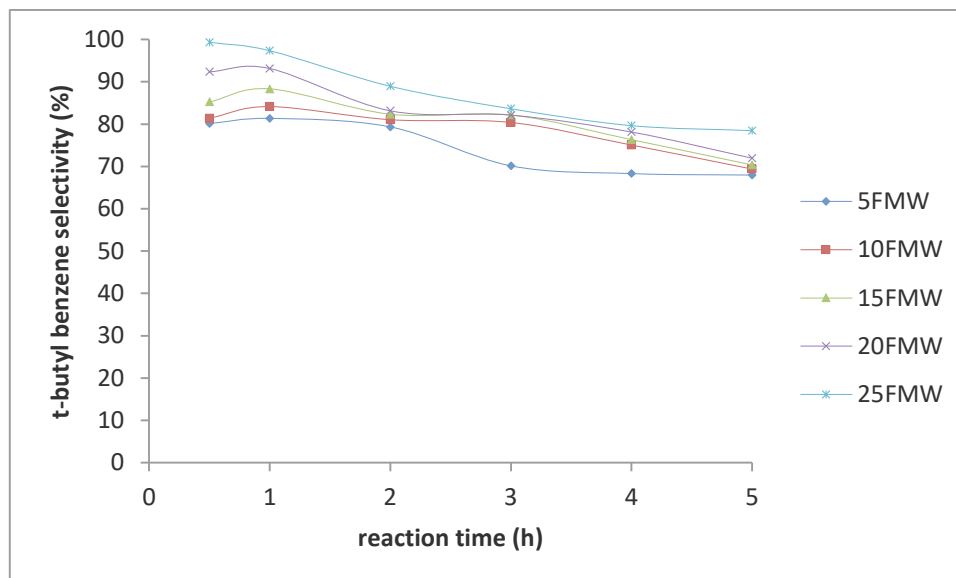*Figure 6. 12: Selectivity of t-butyl benzene over the series of MCM-41 supported metals prepared using FeAsh as metal precursor at reaction temperature of 45 °C and benzene to t-BC ratio of 10:1.*

The selectivity profiles presented in Figure 6.12 shows that as the metal wt % increased there was a corresponding increase in selectivity towards formation of the monoalkylated product (t-butyl benzene). Furthermore, it can be seen that the selectivity on all the profiles decreased with prolonged reaction time. The highest selectivity over the series was 99.4 %, obtained over the 25FMW (Fe wt % = 3.50; Na wt % = 3.62) after 0.5 h on stream. The sample had the highest metal wt % loading. The sample with the lowest metal wt % loading was sample 5FHW (Fe wt % = 0.69; Na wt % = 0.72), and on the sample (5FHW) the highest selectivity achieved was 81.3 % again after 2 h on stream. The decrease in selectivity with time can be attributed to the fact that the monoalylated product is more active than the benzene itself and increased contact time with the catalyst may lead to further alkylation producing dialkylated products. This depreciates the amount of t-butyl benzene in the product mixture. Generally, the selectivity percentages obtained over the series presented in Figure 6.12 are high. The high selectivity over the series can be attributed to the shorter diffusion path associated with mesoporous materials which supress further alkylation in the pores (Christensen et al., 2003).

Despite the different metal composition, the catalyst prepared using AMD as metal precursor had comparable selectivity to the catalysts prepared using FeAsh. Studies on the effect of different metals in AMD showed that the presence of Ca, Na, Mn, Mg and

Ni improved the selectivity towards formation of the monoalkylate (refer to Section 5.6.2). However, these metals were in lower quantities relative to Fe, and with the FeAsh based catalyst the only metal other than Fe that was present was Na, and it was present in significant quantities, almost a 1 : 1 Fe/Na ratio. Again, as was observed with the AMD based catalysts, the selectivity over the HBEA based catalysts was comparable to that observed over the MCM-41 based catalysts despite the differences of these support materials in terms of pore size and surface area. While MCM-41 has shorter diffusional path lengths that enhance selectivity towards the monoalkylate, HBEA is highly selective based on the shape selectivity induced by the zeolite channel system. This catalytic performance is in line with the nucleophilicity and proton affinity of benzene, and shape selectivity has been found to dominate the reaction when carried out over HBEA based catalysts (Wang et al., 2017). The selectivity profiles presented in Figure 6.12, follow the general trend observed in most alkylation reactions and similar profiles have been obtained in related studies on commercial catalysts and reported (Rac et al., 2007; Zhang et al., 2012, Lande et al., 2013). Again, the outcomes obtained in the present study point out that the fly ash based MCM-41 can be used as a support in the preparation of green catalysts for the FC alkylation reaction. Furthermore, FeAsh proved to be a suitable metal solution precursor giving high activity comparable to those obtained when pure commercial sources were used.

6.4.3 Product distribution over MCM-41 supported catalysts prepared via wet impregnation

The product distribution over the MCM-41 supported metal catalysts prepared via wet impregnation using FeAsh as metal precursor is presented in the following sections. The catalyst with the lowest metal wt % loading and the one with the highest are presented for discussion.

6.4.3.1 Product distribution over 5FMW

The product distribution obtained over the 5FMW (Fe wt % = 0.69; Na wt % = 0.72) obtained over the MCM-41 catalyst loaded via wet impregnation using FeAsh as metal solution precursor is presented in Figure 6.13.
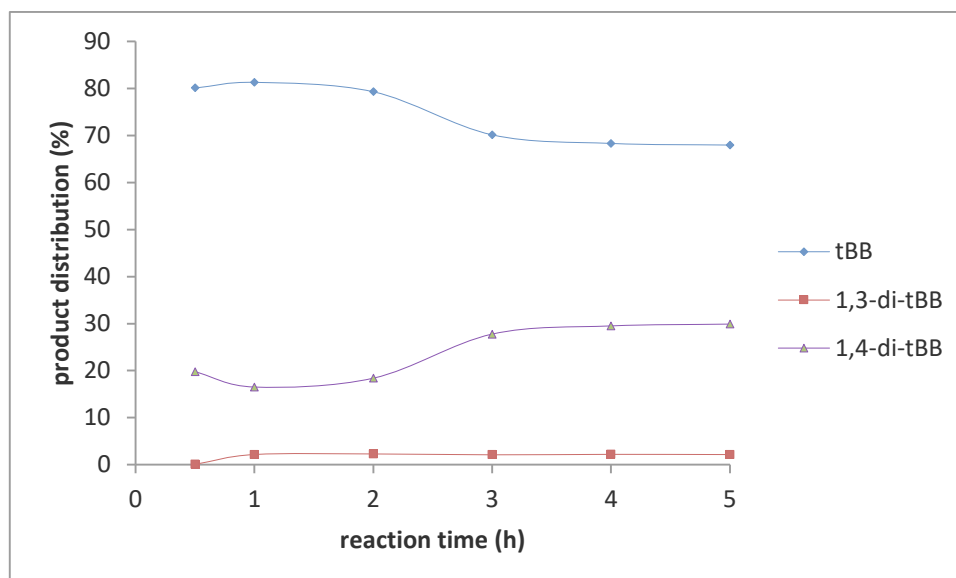
Figure 6. 13: Product distribution for benzene alkylation with t-butyl chloride over the 5FMW at 45 °C and benzene to t-BC ratio of 10:1.

The primary product obtained over sample 5FMW was the monoalkylated product and the secondary product being the *para* isomer. The selectivity of the primary product was high in the initial stages of the reaction and decreased with prolonged reaction time. The outcome was anticipated since prolonged contact with the catalyst may lead to further alkylation forming polyalkylated products. Again, the percentage of the *meta* isomer was the least in the product mixture despite the fact that the isomer is more thermodynamically stable than the *para* isomer. This can be ascribed to the shape selectivity phenomenon in the pore channels of the MCM-41 support as previously discussed. The profiles in Figure 6.13 are similar to those obtained over HBEA supported catalysts of comparable Fe wt % loading despite the differences in support and metal loading approach.

6.4.3.2 Product distribution over 25FMW

The product distribution obtained over the 25FMW (Fe wt % = 3.50; Na wt % = 3.62) obtained over the MCM-41 catalyst loaded via wet impregnation using FeAsh as metal solution precursor is presented in Figure 6.14.
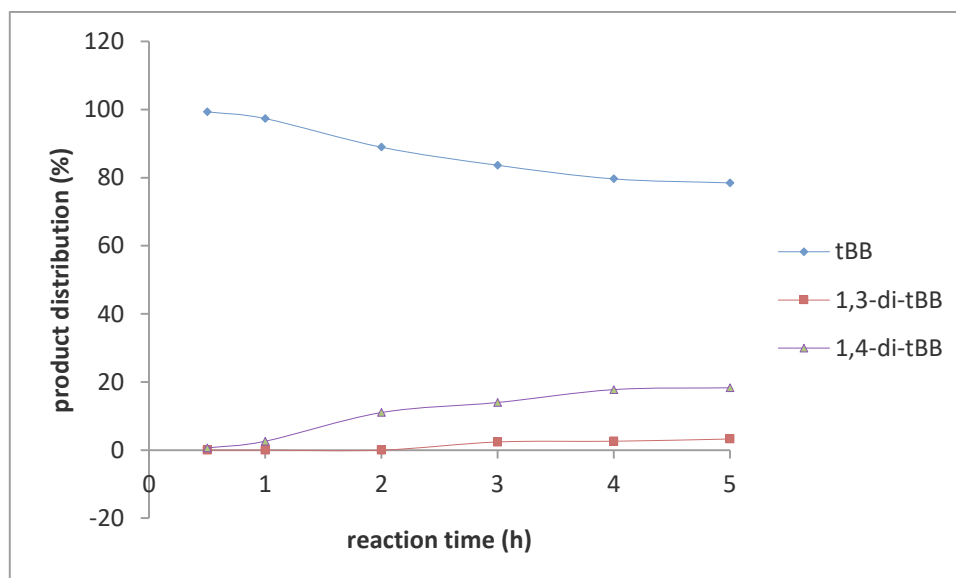
Figure 6. 14: Product distribution for benzene alkylation with t-butyl chloride over the 25FMW at 45 °C and benzene to t-BC ratio of 10:1.

The product distribution over the sample 25FMW again shows that the primary product was the monoalkylated product (t-butyl benzene) while the secondary product was the *para* isomer (1,4-t-butyl benzene). The amount of the primary product decreased with prolonged reaction time due to the tendency of polyalkylation as contact time is increased with the monoalkylated product due to its higher activity relative to the benzene itself. As has been previously discussed in Section 5.3.3.1, the *para* isomer is favoured due to shape selectivity since its diffusivity is much greater than that of the *meta* isomer. This occurs despite the fact that the *meta* isomer should theoretically be the secondary product (Fechete et al., 2012). The outcomes presented in Figure 6.14 are consistent with the findings reported in related studies (Preethi et al., 2010; Shuvaeva et al., 2014). However, in these studies commercial sources were used as the starting material in the synthesis of the support and as metal solution precursors.

6.4.3.3 Product Yield over wet impregnated MCM-41

The percentage yield of t-butyl benzene obtained over the MCM-41 supported catalysts prepared via wet impregnation using FeAsh as metal solution precursor are presented in Figure 6.15.
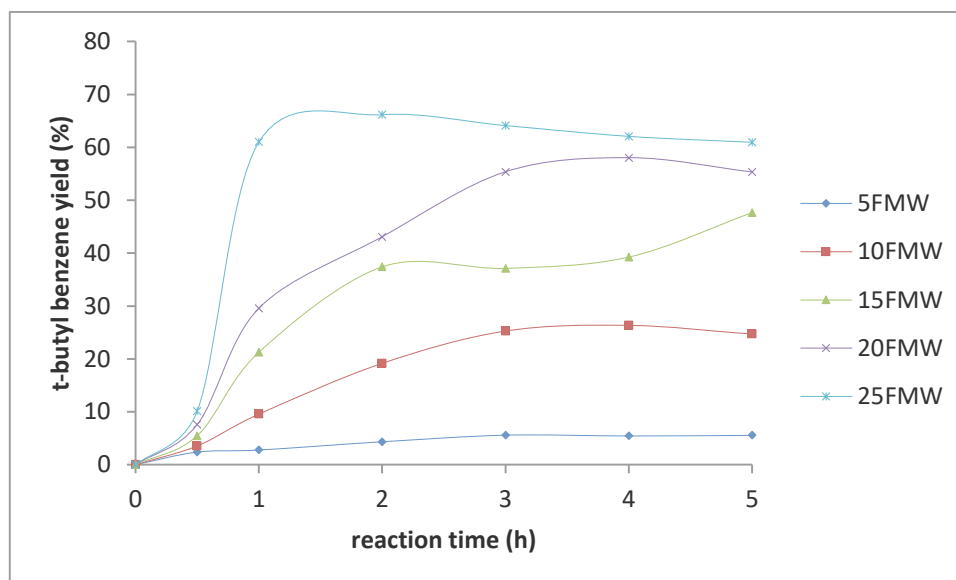
Figure 6. 15: Product yield of t-butyl benzene over the series of MCM-41 supported metals prepared using FeAsh as metal precursor at reaction temperature of 45 °C and benzene to t-BC ratio of 10:1.

The highest yield t-butyl benzene obtained over the MCM-41 supported metal catalysts prepared via wet impregnation using FeAsh as metal precursor was 66.2 % obtained over sample 25FMW (Fe wt % = 3.50; Na wt % = 3.62) after 2 h time on stream. The sample 5FMW (Fe wt % = 0.69; Na wt % = 0.72) with the lowest metal wt % loading had a highest yield of 5.60 % after 3 h on stream. The highest yield obtained over the corresponding HBEA catalysts prepared via wet impregnation using FeAsh as metal precursor followed a similar trend but the yields were generally higher. The better yield obtained over the HBEA series can be ascribed to the presence of Brønsted acid sites in the HBEA zeolite, which happen to be absent in MCM-41. Comparing the percentage yields obtained over the corresponding MCM-41 supported catalysts prepared using AMD as solution precursor (refer to Section 5.3.3.3) it can be seen that the FeAsh based catalysts gave lower yields. The highest yield obtained over sample 25AHW was 90.2 % after 2 h on stream. The lower yields are due to the compromised conversion obtained over the FeAsh based catalysts. The presence of significant amounts of Na on the FeAsh based MCM-41 supported catalysts resulted in the reduced yields. Since percentage yield is calculated from conversion and selectivity, it implies that the factors affecting these two parameters consequently affect the overall yield obtained over the catalyst. The different factors have been discussed in previous sections.

6.5 Effect of Na on the catalytic activity

The FeAsh was prepared from CFA via an acid leaching approach in accordance to the procedure outlined in Section 3.4.1. The resultant Fe solution was highly acidic and the pH was regulated using a concentrated solution of NaOH. The use of NaOH introduced Na ions in the solution and the Na consequently got loaded onto the support alongside the Fe. The following sections discuss the effect of the Na on the catalytic activity, based on the conversion of t-butyl chloride, selectivity towards formation of t-butyl benzene and the percentage yield of the t-butyl benzene. Comparison is based on the catalyst prepared using commercial $Fe_2(SO_4)_3$ supported on the fly ash based HBEA and having an Fe wt % loading of 1.4 %. The catalyst code is Fe-H and was prepared via wet impregnation as presented in section 3.7.4.

6.5.1 Effect of Na on conversion

The effect of Na on the conversion of t-butyl chloride in the Friedel-Crafts alkylation of benzene is depicted in Figure 6.16.
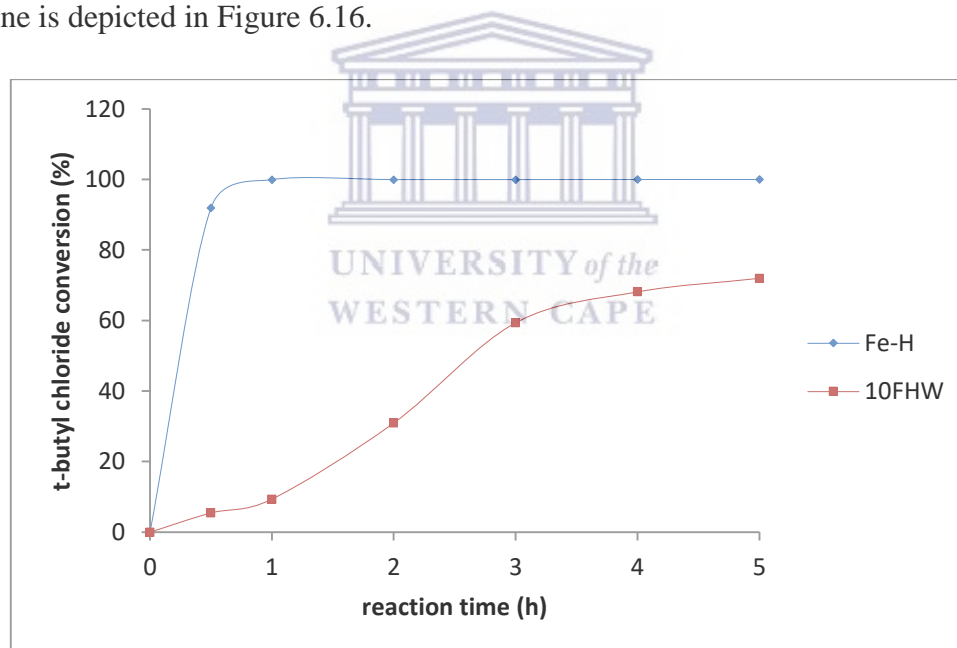
Figure 6. 16: Effect of Na in FeAsh on the conversion of t-butyl chloride at 45 °C and benzene to t-BC ratio of 10:1.

The profiles in Figure 6.16 show that the presence of Na on sample 10FHW negatively impacted the conversion significantly. The monometallic catalyst sample Fe-H (Fe wt % = 1.4) had a highest conversion of almost 100 % after 1 h on stream. On the other hand,

sample 10FHW (Fe wt % = 1.42; Na wt % = 1.49) had a highest conversion of 71.8 % after 5 h on stream. The reduction in conversion on the bimetallic 10FHW catalyst can be ascribed to the reduction in acidity since the Na induces basicity and neutralises the acid sites on the catalyst (Emana & Chand 2015). The outcomes obtained in this study are consistent with the findings reported by He et al. (1998). In the study the alkylation of benzene with benzyl chloride was carried out over Fe-Na supported on MCM-41 and it was found that Na significantly reduced the conversion from about 95 % to 70 %. Again, the outcomes in the present study are consistent with the findings reported by Cao et al. (1999) where FAU, EMT and BEA were tested in the Friedel-Crafts alkylation of benzene with dodecene. In their study it was found that as the residual Na increased there was a corresponding decrease in the initial activity. In their study the introduction of Na was to evaluate its effect on the activity and in the present study Na was present in the support since NaOH was used to regulate the low pH of the prepared Fe (the low pH was as a result of the use of concentrated HCl acid for leaching the Fe from CFA).

6.5.2 Effect of Na on selectivity

The effect of Na on the selectivity towards formation of t-butyl benzene was evaluated against reaction time, and the outcomes are depicted in Figure 6.17.
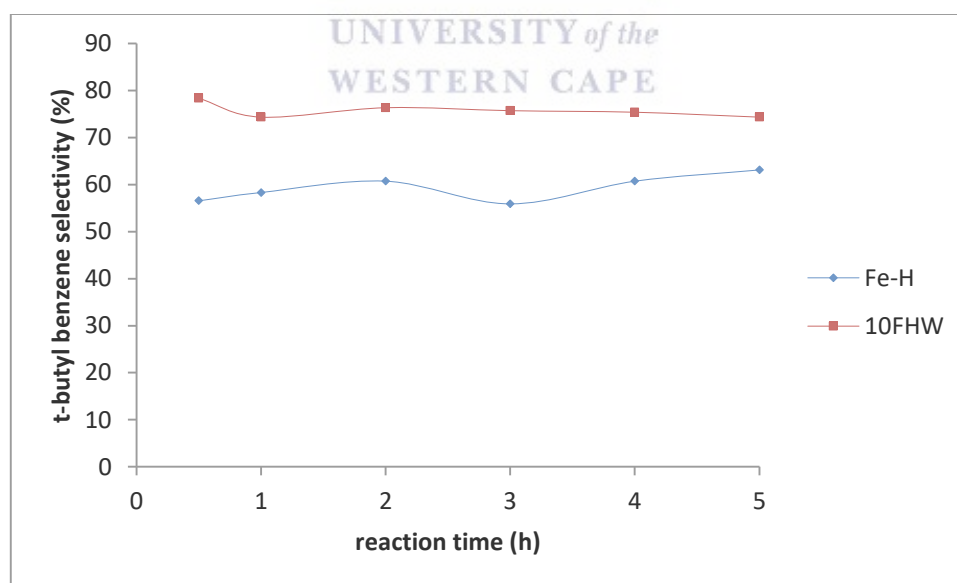
Figure 6. 17: Effect of Na in FeAsh on the selectivity of t-butyl benzene at 45 °C and benzene to t-BC ratio of 10:1.

Although the presence of Na was found to decrease the conversion, it had a positive effect on the selectivity towards formation of the monoalkylate t-butyl benzene. The highest selectivity over the bimetallic 10FHW catalyst was 78.3 % after 0.5 h on stream while the highest selectivity over the monometallic Fe-H catalyst was 63.1 % after 5 h on stream. The low selectivity over the monometallic catalyst can be attributed to strong Brønsted acid sites that favour polyalkylation. On the other hand, Na loaded onto the 10FHW during wet impregnation with FeAsh reduces the number of acid sites on the external and internal surface of the catalyst and consequently suppressed further oligomerisation reaction (Emana & Chand, 2015). The outcomes in the present study are in agreement with the findings reported by Ko & Huang (1993), in which it was found that alkaline earth metals (which like alkali metals) reduced conversion with concomitantly increased selectivity.

6.5.3 Effect of Na on yield

The effect of Na on the percentage yield of t-butyl benzene as a function of time is presented in Figure 6.18.
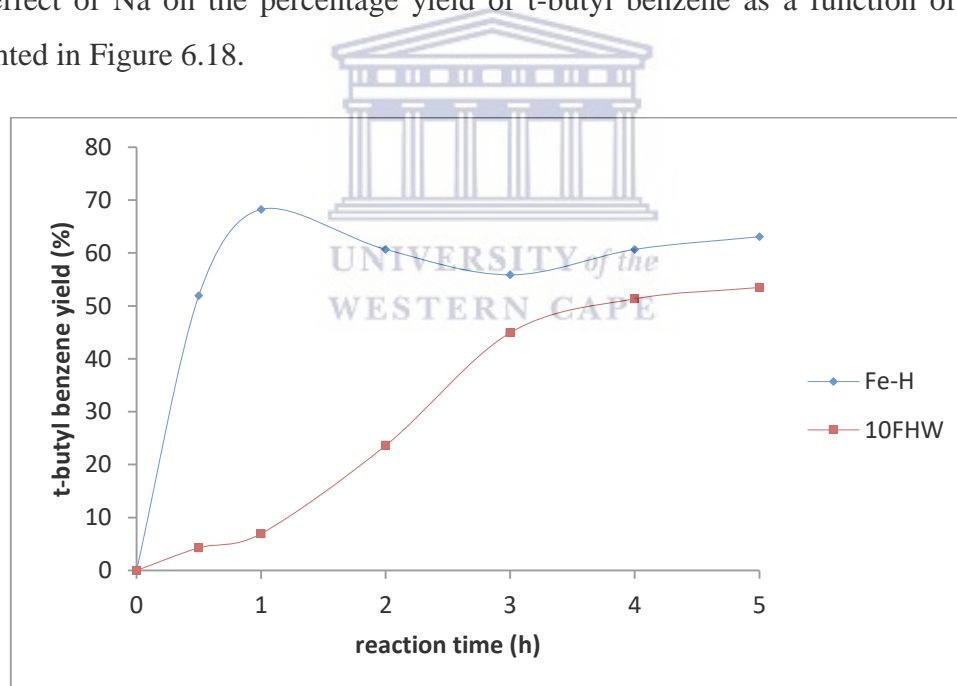
Figure 6. 18: Effect of Na in FeAsh on the yield of t-butyl benzene at 45 °C and benzene to t-BC ratio of 10:1.

The profiles in Figure 6.18 show that the monometallic FeH catalyst (supported on HBEA) gave higher yields relative to the bimetallic Fe-Na catalyst. The highest yield of

the *t*-butyl benzene achieved on the monometallic catalyst was 68.2 % after 1 h on stream while the highest yield was achieved over the bimetallic system was 53.5 % after 5 h on stream. The outcome is in agreement with the conclusion presented by Ding et al. (2014) that in the alkylation of benzene over metal loaded zeolites, there is an optimum ratio of Lewis/Bronsted acid sites that give maximum activity. Since Na was found to decrease conversion but enhance selectivity, there definitely is an optimum ratio of the two metals that should give better activity. However, the effect of different Fe/Na ratios was not investigated further in the present study.

6.6 Chapter summary

The highest conversion of t-butyl chloride achieved over the series of catalysts prepared using FeAsh as metal solution precursor was 100 % over sample 25FHW (Fe wt % loading = 3.48; Na wt % loading = 3.76) after 3 h time on stream. The corresponding catalyst prepared via ion exchange sample 25FHI (Fe wt % of 3.52) had a highest conversion of 99.9 % after 2 h on stream. The fly ash based HBEA supported Fe catalysts had very good conversions when metal loadings were high. The highest conversion over the MCM-41 supported catalysts made via wet impregnation was 77.9 % achieved over sample 25FMW (Fe wt % = 3.50; Na wt % = 3.62) after 4 h on stream. Generally, the conversion over the HBEA catalysts was higher relative to the conversions achieved over the MCM-41 supported catalysts. This was due to the presence of both Brønsted and Lewis acidity in HBEA whereas only Lewis acidity was responsible for the activity observed over the MCM-41 supported catalyst series. The pristine MCM-41 was found to be inactive in the Friedel-Crafts alkylation of benzene with t-butyl chloride showing the positive role of Brønsted acidity of the HBEA support.

The highest selectivity obtained over the series of MCM-41 supported Fe catalysts prepared using FeAsh as metal solution precursor was 99.4 % obtained over sample 25FMW (Fe wt % = 3.50; Na wt % = 3.62) after 0.5 h on stream. The sample was prepared via wet impregnation and supported on MCM-41. Of the HBEA supported catalysts the highest conversion of 88.1 % was achieved over sample 25FHW (Fe wt % loading = 3.48; Na wt % loading = 3.76) after 1 h on stream. The sample was prepared via wet impregnation. The selectivity was comparable to the selectivity obtained over the

corresponding sample supported on HBEA and prepared via ion exchange, sample 25FHI (Fe wt % of 3.52) which was 87.1 % after 1 h on stream. As was the case with the AMD based catalysts, higher selectivity percentages were observed over the MCM-41 series than the HBEA series.

The highest yield over the series of catalysts prepared using FeAsh as metal solution precursor was 87.2 % over sample 25FHW (Fe wt % loading = 3.48; Na wt % loading = 3.76) after 2 h time on stream. The sample was prepared via wet impregnation. The corresponding catalyst prepared via ion exchange sample 25FHI (Fe wt % = 3.52 and Na wt % = 2.86) and supported on HBEA gave a comparable yield of 87.0 % after 2 h on stream. The highest yield obtained over the MCM-41 supported metal catalyst series was 66.2 % obtained over sample 25FMW (Fe wt % = 3.50; Na wt % = 3.62) after 2 h time on stream. The HBEA supported catalyst generally had higher yield percentages relative to the corresponding MCM-41 supported catalysts. The same outcomes were observed with the AMD based catalyst series. The effect of Na on the activity was also evaluated and it was found that Na decreases the conversion but enhances the selectivity towards formation of the monoalkylate. It can be concluded that FeAsh can be used as a metal precursor solution in the preparation of active Friedel-Crafts alkylation catalysts. It should however be noted that the presence of Na, compromises the activity since comparison of samples with theoretical loading of 1.4 % showed that the FeAsh based catalyst was less active relative to the counterpart prepare using commercial $Fe_2SO_4{}^3$ (the comparison is based on yield percentages of t-butyl benzene).

The present study proved that high quality HBEA and MCM-41 can be synthesised from CFA via a novel approach that involved acid assisted silica extraction followed by conventional hydrothermal synthesis. The prepared materials were successfully used as supports in the preparation of heterogeneous Fe catalysts using FeAsh as metal solution precursors. For the first time the use of FeAsh as a precursor was attempted and the outcomes were comparavble or better than those obtained over commercial catalysts.

CHAPTER 7

7.0 Conclusion and recommendations

This chapter presents the overall conclusion of the outcomes generated in the present work. The chapter further presents the significance of the study, novelty and some recommendations for further research as inspired by the very outcomes accrued in the present work.

7.1 Conclusion

The present study has shown that both high silica zeolite HBEA and MCM-41 can be synthesised from coal fly ash via a novel approach which involves a fusion step, acid assisted silica extraction and removal of residual Al, Ca and Na from the silica by treatment with oxalic acid. The final step in the synthesis of the porous supports involved subjecting the generated silica to conventional hydrothermal treatment. The study further showed that acid mine drainage and Fe extracted from coal fly ash (FeAsh) via acid leaching can both be used as metal solution precursors in the preparation of heterogeneous Fe loaded catalysts for application in the Friedel-Crafts alkylation of benzene with t-butyl chloride. The metal incorporation onto zeolite HBEA was carried out via two conventional approaches namely, liquid phase ion exchange and wet impregnation. Metal loading on the MCM-41 was carried out via wet impregnation since the support does not have exchange sites.

The prepared catalysts were subjected to a range of characterisation techniques namely, XRD, SEM, HRTEM, SAED, ICP-OES and N_2 adsorption analysis. The integrity of the respective support materials was retained upon metal loading. The XRD profiles of the metal loaded catalysts closely resembled the respective pristine supports. The catalysts supported on HBEA prepared via wet impregnation showed some peaks due to the presence of Fe_2O_3 metal crystallites. Analysis by SEM and HRTEM also confirmed that the crystallinity and morphology of the respective parent materials were retained upon metal loading. Furthermore, the data obtained from the elementary composition via ICP-OES showed that the theoretical and actual metal loading achieved showing control of

loading and were comparable over the two different metal loading approaches applied in the study.

Unlike the case where commercial salts are used as metal solution precursors, when AMD is used, especially via wet impregnation, it leads to polymetallic catalyst systems. The major ion in the AMD used was Fe, however there were other metals in significant quantities and these include; Ca, Na. Mg, Mn and Ni. The activity of the prepared catalysts was tested on the Friedel-Crafts alkylation of benzene with t-butyl chloride as a probe reaction. The benzene was used as both reactant and solvent. The reaction was carried out in a batch reactor under reflux conditions and stirring at a temperature of 45 °C. In total 38 catalysts were tested and the general trend obtained with the majority of the catalysts was characterised with a rapid initial increase and then steady state was achieved. Generally, after a reaction time of 2 h almost all the catalysts had reached steady state in terms of the percentage conversion obtained.

The presence of other AMD derived metals in addition to Fe had a significant effect on the overall catalytic activity of the resultant materials. It was found that Ca, Na, Mg and Mn had a negative effect on the conversion of tertiary butyl chloride but a positive effect on the selectivity towards the formation of the desired monoalkylated product (tertiary butyl benzene). On the other hand, Ni was found to both enhance the conversion and the selectivity. On the catalyst series prepared using (FeAsh), the metals that eventually got loaded onto the respective supports were Fe and Na. The Na was present since NaOH was used in regulating the pH of the precursor solution. The Na had a negative effect on the conversion but a positive effect on the selectivity towards formation of the monoalkylate. In comparison to the Fe catalyst based on commercial salt ($Fe_2SO_4)_3$ as metal precursor, both the AMD and FeAsh based catalysts showed higher yield percentages of the monoalkylated product. This was due to the enhanced selectivity induced by the Ca, Na, Mg, Mn and Ni in the case of AMD based catalysts, and Na in the case of the FeAsh based catalysts. This leads to the conclusion that both AMD and FeAsh are appropriate metal precursors in the preparation of metal loaded porous supports for use in the Friedel-Crafts alkylation reaction. In the case of the FeAsh based catalysts both the support and the metal solution precursor are prepared from CFA, thus the approach maximises the CFA utilisation.

The highest conversion of t-butyl chloride achieved over the fly ash based HBEA and MCM-41 prepared using AMD as metal solution precursor was 100 % over the 10AHI (prepared via ion exchange) after 2 h time on stream. The catalyst had a conversion of 99.8 % after 0.5 h on stream. The HBEA series prepared via wet impregnation also had very high conversion percentages with all the catalyst reaching conversion percentages of above 98 % after 4 h time on stream. Of the wet impregnated HBEA catalyst the best performing in terms of conversion was the 10AHW which had a conversion of 97.9 % after 0.5 h time on stream. The pristine HBEA was also found to be active in the alkylation of benzene with t-butyl chloride giving a conversion of 30.7 % after 4 h time on stream. The highest conversion of t-butyl chloride achieved over the HBEA supported catalysts prepared using FeAsh as metal solution precursor was 100 % over sample 25FHW (Fe wt % loading = 3.48; Na wt % loading = 3.76) after 3 h time on stream. The catalyst was prepared via wet impregnation, and the corresponding catalyst prepared via ion exchange sample 25FHI (Fe wt % of 3.52) had a highest conversion of 99.9 % after 2 h on stream. The MCM-41 supported catalysts prepared using AMD as metal precursor also showed very good activity. The highest conversion achieved was 100 % over sample 25AMW (Fe wt % loading of 3.09) after 4 h on stream. Of the catalyst prepared using FeAsh as metal precursor the highest conversion over the MCM-41 supported catalysts was 77.9 % achieved over sample 25FMW (Fe wt % = 3.50; Na wt % = 3.62) after 4 h on stream. Generally, the conversion over the HBEA catalysts was higher relative to the conversions achieved over the MCM-41 supported catalysts. This was due to the presence of both Brønsted and Lewis acidity in HBEA whereas only Lewis acidity was responsible for the activity observed over the MCM-41 supported catalyst series. The pristine MCM-41 was found to be inactive in the Friedel-Crafts alkylation of benzene with t-butyl chloride. From the outcomes it can be said that the HBEA supported catalysts gave higher conversion percentages in comparison to the MCM-41 counter parts. Of the HBEA supported catalysts higher conversions were obtained over the wet impregnated samples than over the ion exchanged samples. The ion exchanged samples were composed of only Fe as the active metal while the wet impregnated samples contained Ni which was found to enhance the conversion. The AMD based catalysts were more active relative to the FeAsh based catalysts.

The highest selectivity towards the formation of t-butyl benzene obtained over the HBEA supported catalysts prepared via ion exchange using AMD as metal precursor was 84.5 % after 2 h on stream over sample 25AHI. The highest selectivity over the parent HBEA support was 80.6 % after a reaction time of 5 h. The highest selectivity over the HBEA series prepared via wet impregnation was   100 % over the 25AHW after 0.5 and 1 h time on stream. The MCM-41 supported catalysts prepared using AMD as metal precursor achieved a highest selectivity of 100 % after 2 h on stream over sample 25AMW. Again, the selectivity was found to increase with an increase in metal wt % loading. Of the catalysts prepared using FeAsh as metal precursor the highest selectivity obtained was 99.4 % obtained over sample 25FMW (Fe wt % = 3.50; Na wt % = 3.62) after 0.5 h on stream. The sample was prepared via wet impregnation and supported on MCM-41. Comparing the two different supports it was found that the MCM-41 series gave better selectivity percentages relative to the corresponding HBEA supported catalysts and the FeAsh based catalysts had better selectivity percentages relative to the corresponding AMD based catalysts.

Generally, the catalysts studied proved to be viable alternatives to the traditionally applied non-porous Lewis acids or strong mineral acids. The use of the tested catalysts would ease separation challenges and the environmental hazards associated with traditional catalytic systems.
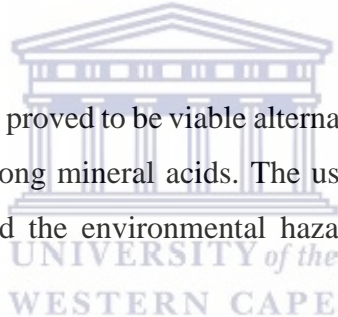
7.2 Significance of study

The findings of this research redound to the benefit of scientists, government, mining and water treatment industry. Considering the fact that the economic feasibility of Fe based catalysts keeps on increasing relative to that of other noble transition metals, it is apparent it will keep on growing in the near future. It is perceptible that Fe cannot be employed in every catalytic transformation, but it has proved to be applicable in numerous reactions. The successful application of waste materials based Fe heterogeneous catalysts in the Friedel-Crafts alkylation of benzene opens a new avenue in the exploration of these catalysts in various reactions that are based on Fe catalysts systems. Often the approaches reported in open literature involve the use of commercial Fe sources as metal precursors in catalysts preparation. The study successfully proved that Fe extracted from coal fly ash and acid mine drainage can be used as Fe precursor solutions resulting in catalysts of

comparable activity to those based on commercial sources. The fact that the catalysts employed in this study are based on waste materials presents a cheap and sustainable metal source for catalyst preparation. In addition, waste utilisation and beneficiation is achieved.

The two waste materials CFA and AMD used in this study are problematic waste materials since they have negative environmental effects and conversion of these waste materials into usable commodities has significant economic advantages. In the case of AMD in South Africa, the government through the Department of Water and Sanitation (DWS) in the National Water Resource Strategy 2 (NWRS2), (2014) acknowledges that that there is not enough done in addressing both groundwater and surface water pollution resulting from the release of AMD. However, the report goes on to point out that AMD when treated can serve as an additional water source to supplement traditional existing ones. The treatment or use of AMD was suggested as the way forward. On the other hand, coal fly ash in South Africa is currently classified as a hazardous waste due to the high toxic metal levels it contains. However, in 2017 Eskom, the country's power utility, submitted regulation 9 and a section 74 request to the Department of Environmental Affairs (DEA). The DEA went on to convene a forum aimed at finding solutions to improve the waste economy, including coal fly ash beneficiation (Reynolds-Clausen & Singh, 2017). This implies that both coal fly ash and AMD are key issues that the government requires solutions to, and this study leads the way in beneficiating waste.

7.3 Novelty of study

The research managed to show that high quality, high silica zeolite HBEA and MCM-41 can be synthesised from CFA via a novel approach involving an acid assisted silica extraction step prior to hydrothermal synthesis. These materials were prepared for the first time using the approach. The approach has the advantage of producing silica of high purity from coal fly ash. Furthermore, the use of Fe extracted from coal fly ash in catalysts preparation was attempted for the first time and the results obtained in this study prove that the metal solution can be used as a metal precursor in preparation of heterogeneous Fe catalysts. Zeolites have been used for the removal of metals from AMD as numerous studies have been reported. However, the catalytic application of the metal pregnant zeolite has not previously been attempted. This study managed to show for the first time

that AMD can be used as a metal precursor in catalyst synthesis and the resultant catalysts have very high activities, comparable to those based on commercial sources. Preparation of Fe catalysts via wet impregnation using AMD as a metal precursor showed that all the metals in the AMD were incorporated onto the support and the effect of these metals all present at once has not been explored in the past. The present study reports for the first time the effect of the major metal ions (Ca, Na, Mg, Mn and Ni) that got incorporated on to the supports when wet impregnation was used. It was noteworthy that ion exchange offered a route to selectively load only Fe onto the catalyst, which was a unique finding, given the polymetallic nature of AMD.

7.2 Recommendations and future outlook

The outcomes generated in this research are encouraging and serve as a good background in the full exploitation of CFA and AMD in the preparation of solid acid catalysts for use in the Friedel-Crafts alkylation of benzene. Based on the successful outcomes generated in this study it is recommended to test the AMD and CFA based Fe catalysts for various applications in both organic and inorganic synthesis. Apart from the Friedel-Crafts alkylation reaction, Fe based catalysts have been successfully applied in numerous reactions including; C-H activation, hydrometallation, oxidative coupling, transfer hydrogenation, dehyroxylation, epoxidation, hydrosilylation, reduction, metathesis, oxidation, cycloaddition, polymerisation, hydrogenation, cycloaddition, cascade, cyclisation, reductive amination, domino and amination. Based on the successful application of the Fe based catalysts on the Friedel-Crafts alkylation reaction, it will be commendable to test these catalysts for the aforementioned reactions and evaluate their activity.

Furthermore, the industrial application of powdered zeolite catalysts is limited and therefore pelletising using appropriate binders may be an attractive intervention. Investigation on the effect of commonly used microporous and mesoporous binders such as alumina, zirconia, silica and kaoline may be an interesting exploration. Furthermore, there is need to investigate the reusability of these cataysts, the present study did not investigate that. Generally, metal loading on porous materials via wet impregnation and ion exchange is influenced by a number of mixing parameters, for instance the type of

metal salt, temperature, duration of mixing and pH. These parameters have a significant effect on the type of bond that will be formed between the metals and the support. Investigation of these parameters ought to be carried out in order to come up with conditions that result in catalysts with optimum activity. The effect of the metal particle size on the conversion and selectivity also needs to be further investigated. For the case of catalysts prepared using FeAsh as metal precursor it was shown that the inclusion of Na on the catalysts reduced the conversion of t-butyl chloride while enhancing the selectivity towards formation of the monoalkylated product (t-butyl benzene). Considering that there is an optimum Fe:Na ratio that gives optimum activity, it follows that there is a need to investigate the optimum ratio and use an appropriate amount of NaOH during pH regulation and further regulation could be done using a base such as NH_4OH to avoid the effects of Na.

The removal of metals from AMD by zeolites leaves behind a solution that is rich in SO_4^{2-} and H^+ ions. It would be beneficial if the solution could be used as a feed stock in the preparation of H_2SO_4 for various industrial applications. Furthermore, the SO_4^{2-} can be precipitated as gypsum which has numerous industrial and agricultural applications. This would see a complete utilisation of the AMD.
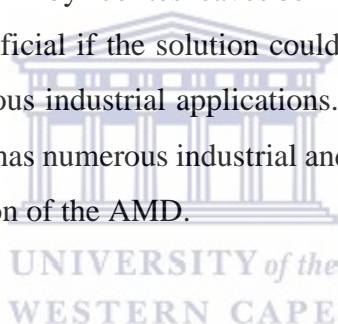
REFERENCES

Abdullahi, T., Harun, Z. & Othman, M.H.D. (2017) A review on sustainable synthesis of zeolite from kaolinite resources via hydrothermal process. Advanced Powder Technology, 28: 1827–1840.

Adamczyk, Z. & Białecka, B. (2005) Hydrothermal synthesis of zeolites from Polish coal fly ash. Polish Journal of Environmental Studies, 14(6):713–719.

Adami, I. (2009) Production of linear alkylbenzene sulfonate and α-olefinic sulfonates, *in* Handbook of Detergents, Part F: Production, Surfactant Science Serie**s**, Vol,142, CRC Press, New York, p.83.

Adams R. (1946) Organic reactions, Vol. 3, John Wiley and Sons Inc. New York, p. 2.

Adelodun, A.A., Vellingiri, K., Jeon, B.H., Oh, J.M. Kumar, S. & Kim, K.H. (2017) A test of relative removal properties of various offensive odors by zeolite. Asian Journal of Atmospheric Environment, 11(1):15-28.

Ahmad, N.N.R., Leo, C.P., Mohammad, A.W. & Ahmad, A.L. (2017) Modification of gas selective SAPO zeolites using imidazolium ionic liquid to develop polysulfone mixed matrix membrane for CO_2 gas separation. Microporous and Mesoporous Materials, 244:21-30.

Ahmed, M.H.M., Muraza, O., Jamil, A.K., Shafei, E.N., Yamani, Z.H. & Choi, K.H., (2017) Steam catalytic cracking of n-dodecane over Ni and Ni/Co bimetallic catalyst supported on hierarchical BEA zeolite. Energy 31(5): 5482-5490.

Alam, A.M.D., Shahruzzaman, M.D., ALAM, M.S. & Saha, M. (2015) Effect of temperature, molar ratio of reactants and amount of catalyst on the yield of alkylation of phenol with benzyl alcohol in the presence of p-toluenesulphonic acid. International Journal of Earth Science and Engineering, 8: 909-912.

Ali, T.T., Narasimharao, K., Ahmed, N.S., Basahel, S., Al-Thabaiti, S. & Mokhtar, M. (2014) Nanosized iron and nickel oxide zirconia supported catalysts for benzylation of benzene: Role of metal oxide support interaction. Applied Catalysis A: General 486: 19–31.

Alotaibi, A., Hodgkiss, S., Kozhevnikova, E.F. & Kozhevnikov, I.V. (2017) Selective alkylation of benzene by propane over bifunctional Pd-acid catalysts. Catalysts, 7(8): 233 – 243.

Aman, S., Utama, P.S. & Saputra, E. (2017) High purity silica from palm oil mill fly ash for catalyst ZSM-5 zeolite synthesis. Applied Science and Technology, 1(1): 267-272.

Amorim, R., Vilac ́, N., Martinho, O., Reis, R.M Sardo, M., Rocha,̃ J., Fonseca, ́A.M., Baltazar, ́F. & Neves, I.C. (2012) Zeolite structures loading with an anticancer compound as drug delivery systems. The Journal of Physical Chemistry C 116: 25642−25650.

Arata, K. & Hino, M. (1980) High catalytic activity of iron oxide for benzylation, t-butylation, and acetylation of toluene with benzyl, t-butyl, and acetyl chlorides. Chemistry Letters, 9(12): 1479-1480.

Ausavasukhi, A., Huang, Y., Ahn, T., Sooknoi, T., & Resasco, D.E. (2012). Hydrodeoxygenation of m-cresol over gallium-modified beta zeolite catalysts. Journal of Catalysis, 290: 90–100.

Ayele, L., Pérez-Pariente, J., Chebude, Y. & Díaz, I. (2016 (a)) Conventional versus alkali fusion synthesis of zeolite A from low grade kaolin. Applied Clay Science, 132–133: 485-490.

Ayele, L., Pérez-Pariente, J., Chebude, Y. & Diaz, I. (2016(b)) Synthesis of Zeolite A using kaolin from Ethiopia and its application for detergents. New Journal of Chemistry, 40: 3440-3446.

Ayoola A. A., Hymore F. K., Modupe, O.E. & Osayomwanbo, U.J. (2018) Effects of sodium hydroxide concentration on zeolite Y synthesized from Elefun kaolinite clay in Nigeria. International Journal of Applied Engineering Research, 13(3): 1536-1542.

Ayoola, A. A., Hymore, F. K., Omodara, O. J., Oyeniyi, Adenike, E., Fayomi, O. S. I. & Chisom, U.C. (2017) Effect of crystallisation time on the synthesis of zeolite Y from Elefun kaolinite clay. International Journal of Applied Engineering Research, 12 (21): 10981-10988.

https://etd.uwc.ac.za

Bachari, K., Millet, J.M.M., Benaïchouba, B., Cherifi, O & Figueras, F. (2004) Benzylation of benzene by benzyl chloride over iron mesoporous molecular sieves materials. Journal of Catalysis 221: 55–61.

Balle, P., Geiger, B. & Kureti, S. (2009) Selective catalytic reduction of NOx by NH_3 on Fe/HBEA zeolite catalysts in oxygen-rich exhaust. Applied Catalysis. B: Environmental, 85:109–119.

Bandini M., & Umani-Ronchi, A. (2009) Catalytic asymmetric Friedel-Crafts alkylations, Wiley-VCH. Weinheim, p. 3 – 10.

Bandini, M. & Tragni, M. (2009) π-Activated alcohols: an emerging class of alkylating agents for catalytic Friedel–Crafts reactions. Organic & Biomolecular Chemistry (7): 1501–1507.

Bárcia, P. S., Silva, J. A. C., Rodrigues, A. E. (2005) Adsorption equilibrium and kinetics of branched hexane isomers in pellets of Beta zeolite. Microporous and Mesoporous Materials, 79: 145-163.

Bare, S.R., Kelly, S.D., Sinkler, W., Low, J.J., Modica, F.S., Valencia, S., Corma, A., & Nemeth, L.T. (2005) Uniform catalytic site in Sn-A-zeolite determined using X-ray absorption fine structure. Journal of the American Chemical Society, 127: 12924-12932.

Belluck, D.A. & Benjamin, S.L. (2001) Environmental sampling and analysis of coal fly ash intended for use in roads in radionuclides and heavy metals in environment. Frontasyeva, M.V., Perelygin, V.P. and Vater, P. (eds). Kluwer Academic Publishers, Dordrecht, Netherlands, p. 227 – 236.

Belviso, C, Giannossa, L.C., Huertas, J.F., Lettino, A., Mangone, A. & Fiore, S. (2015) Synthesis of zeolites at low temperatures in fly ash-kaolinite mixtures. Microporous and Mesoporous Materials 212: 35-47.

Bereciartua, P.J., Cantín, A., Corma, A., Jordá, J.L., Palomino, M., Rey, F., Valencia, S., Corcoran, E.W., Kortunov, P., Ravikovitch, P.I., Burton, A., Yoon, C., Wang, Y., Paur, C., r Guzman, J., Bishop, A.R., Casty, G.L. (2017) Control of zeolite framework flexibility and pore topology for separation of ethane and ethylene. Science 358: 1068–1071

Bhattacharya, A., Shukla, P.M. & Maji, B. (2017) Fe(OTf)3-catalysed Friedel–Crafts reaction of benzenoid arenes with α,β-unsaturated carbonyl compounds: easy access to 1,1-diarylalkanes.Royal Society. open sci. 4: 170748

Bhavornthanayod, C. & Rungrojchaipon, P. (2009) Synthesis of zeolite A membrane from rice husk ash. Journal of Metals, Materials and Minerals, 19 (2): 79-83.

Bidart A.M.F., Borges A.P.S, Chagas H.C., Nogueira L., Lachter E.R., & Mota C.J.A. (2006) Mechanistic aspects of Friedel-Crafts alkylation over FeY zeolite. Journal of the Brazilian Chemical Society, 17(4): 758-762.

Borm, P.J.A. (1997) Toxicity and occupational health hazards of coal fly ash (CFA). A review of data and comparison to coal mine dust. The Annals of Occupational Hygiene, 41(6): 659-676.

Boroń, P., Chmielarz, L. Gurgul, J. Łątka, K., Shishido, T., Krafft, J-M., Dzwiga, S (2013) BEA zeolite modified with iron as effective catalyst for N_2O decomposition and selective reduction of NO with ammonia. Applied Catalysis B: Environmental, 138: 434-445.

Brezoiu, A.M. Deaconu, M., Nicu, I., Vasile, E., Mitran, R.A., Matei, C. & Berge, D. (2019) Heteroatom modified MCM-41-silica carriers for Lomefloxacin delivery systems. Microporous and Mesoporous Materials, 275: 214-222.

Bukhari, S.S., Behina, J., Kazemiana, H. & Rohani, S. (2015) Conversion of coal fly ash to zeolite utilizing microwave and ultrasound energies: A review. Fuel, 140: 250-266.

Burrows, A., Holman, J., Parsons, A, Pilling, G. & Price, G. (2013) Chemistry[3]: Introducing inorganic, organic and physical chemistry. Oxford University Press, Oxford, p. 1013.

Burton, A. (2018) Recent trends in the synthesis of high-silica zeolites. Catalysis Reviews 60 (1): 132–175.

Byrappa, K. & Yoshimura, M. (2001) Handbook of hydrothermal technology: A technology for crystal growth and materials processing. Noyes Publications, New Jersey.

Caeiro, G., Carvalho, R. H., Wang, X., Lemos, M. A. N. D. A., Lemos, F., Guisnet, M. & Ramoa Ribeiro, F. (2006) Activation of C2-C4 Alkanes over Acid and bifunctional zeolite catalysts. Journal of Molecular Catalysis A, Chemical, 255, 131−158.

Cai, M. & Wang, X. (2015) Activity investigation of imidazolium-based ionic liquid as catalyst for friedel-crafts alkylation of aromatic compounds. Asian Journal of Chemistry; 27(2): 649-653.

Cai, X., Cui, S., Qu, L., Yuan, D., Lu, B. & Cai, Q. (2008) Alkylation of benzene and dichloromethane to diphenylmethane with acidic ionic liquids. Catalysis Communications 9: 1173–1177

Camblor, M. A., Mifsud, A. & Perez-Pariente J. (1991) Influence of the synthesis conditions on the crystallization of zeolite beta. Zeolites, 11 (8): 792-797

Canfield, G.M., Bizimis, M. & Latturner, S.E. (2010) Transition-metal ion exchange using poly(ethylene glycol) oligomers as solvents. Chemistry of Materials 22: 330-337.

Cao, Y., Kessas, R., Naccache, C., Taarit, B.Y. (1999) Alkylation of benzene with dodecene. The activity and selectivity of zeolite type catalysts as a function of the porous structure. Applied Catalysis A: General 184: 231-238.

Carvalho, A., Marinova, M., Batalha, N., Marcilio, N.R., Khodakov, A.Y. & Ordomsky, V.V. (2017) Design of nanocomposites with cobalt encapsulated in the zeolite micropores for selective synthesis of isoparaffins in Fischer–Tropsch reaction. Catalysis Science & Technology, 7: 5019–5027.

Cejka, J.C. & Zone, A.S. (2010). Zeolite and catalysis: Reactions and application. John Willey & Sons inc., 6(3), 212-234.

Chen, L., Jansson, J., Skoglundh, M. & Grönbeck, H. (2016) Mechanism for Solid-State Ion Exchange of Cu^+ into Zeolites. The Journal of Physical Chemistry C, 120: 29182−29189

Choudhary, V.R., Jana, S.K. & Kiran, B.P. (1999) Alkylation of benzene by benzyl chloride over H-ZSM-5 zeolite with its framework Al completely or partially substituted by Fe or Ga. Catalysis Letters 59: 217–219.

Choudhary, V.R., Jana, S.K. & Mamman, A.S. (2002) Benzylation of benzene by benzyl chloride over Fe-modified ZSM-5 and H-β zeolites and Fe_2O_3 or $FeCl_3$ deposited on micro-, meso- and macro-porous supports. Microporous and Mesoporous Materials 56: 65–71.

Christensen, C.H., Johannsen, K., Schmidt, I. &, Christensen, C.H. (2003) Catalytic benzene alkylation over mesoporous zeolite single crystals: Improving activity and selectivity with a new family of porous materials. Journal of the American Chemical Society, 125: 13370-13371.

Cooper, E.R., Andrews, C.D., Wheatley, P.S., Webb, P.B., Wormald, P. & Morris, R.E. (2004) Ionic liquids and eutectic mixtures as solvent and template in synthesis of zeolite analogues. Nature, 430: 1012–1016.

Corma, A. (2003) State of the art and future challenges of zeolites as catalysts. Journal of Catalysis, 216(1-2): 298-312.

Corma, A., Moliner, M., Cantín, A., Díaz-Cabañas M.J., José L. Jordá, J.L., Zhang, D., Sun, J., Jansson, K., Hovmöller, S., & Zou, X. (2008) Synthesis and structure of polymorph B of Zeolite Beta. Chemistry of Materials, 20: 3218–3223.

Corma, A., Rey, F., Rius, J., Sabater, M.J. & Valencia, S. (2004) Supramolecular self-assembled molecules as organic directing agent for synthesis of zeolites. Letters to Nature, 431: 287-290.

Csicsery, S.M. (1984) Shape-selective catalysis in zeolites. Zeolites 4, p.202.

Dai, W-L., Chen, H., Cao, Y., Li, H., Xie, S. & Fan, K. (2003) Novel economic and green approach to the synthesis of highly active W-MCM41 catalyst in oxidative cleavage of cyclopentene. Chemical Communications, 7: 892–893.

Davis, M.E. & Lobo, R.F. (1992) Zeolite and molecular sieve synthesis. Chemistry of Materials, 4: 756-768.

Dayal, U. & Sinha, R. (2005) Geo environmental design practice in fly ash disposal & utilization. Allied Publishers, New Delhi, p.7.

Degnan, T., Smith, C.M. &Venkat, C.R. (2001) Alkylation of aromatics with ethylene and propylene: recent developments in commercial processes. Applied Catalysis A General (221)1-2: 283-294

Derewinski, M. & Machowska, M. (2004) Effect of stirring on the selective synthesis of MEL or TON zeolites in the presence of 1,8-diaminooctane. Studies in Surface Science and Catalysis, 154: 349-354.

Devaki, H. & Priya, G.P. (2016) Corrosion studies using zeolite synthesized from fly ash. Indian Journal of Science and Technology, 9(20): 1-10.

Devassy, B.M., Lefebvre, F. & Halligudi, S.B. (2005) Zirconia-supported 12-tungstophosphoric acid as a solid catalyst for the synthesis of linear alkyl benzenes. Journal of Catalysis, 231(1): 1-10.

Dı´az, E., Ordo´n˜ez, S., Vega, A., Auroux, A. & Coca, J. (2005) Benzylation of benzene over Fe-modified ZSM-5 zeolites: Correlation between activity and adsorption properties. Applied Catalysis A: General 295: 106–115.

Díaz, I., Pérez-Pariente, J. & Terasak, O. (2004) Structural study by transmission and scanning electron microscopy of the time-dependent structural change in M41S mesoporous silica (MCM-41 to MCM-48, and MCM-50). Journal of Materials Chemistry, 14: 48-53.

Dimian, A.C. & Bildea, C.S. (2008) Chemical process design: Computer-aided case studies. Wiley-VCH Verlag, Weinheim, Germany.

Ding, W., Cui, Y., Li, J., Yang, Y. & Fang, W. (2014) Promoting effect of dual modification of H-ZSM-5 catalyst by alkali treating and Mg doping on catalytic performances for alkylation of benzene with ethanol to ethylbenzene. Royal Society of Chemistry, Advances, 4: 50123-50129.

Dong, P., Li, Z., Wang, X., Yun, H., & Li, G. (2018) The alkylation reaction of benzene with methanol to produce toluene: Y-C and Y-CCs catalyst. Green Chemistry Letters and Reviews, 11(2): 158–164.

Dorwald, F.Z. (2014) Side Reactions in organic synthesis II: Aromatic substitutions, 1st ed. Wiley-VCH, Verlag.

Dutilh, C. (1998) The environmental improvement process at Uniliver, *in* Product Innovation and Eco-Efficiency: Twenty-two industry efforts to reach the factor 4 (eds) Judith E.M. Klostermann, J.E.M. & Tukke, A. Springer Science& Business Media, Berlin, p. 133.

DWS, (2014) National Water Resource Strategy 2: Water for an equitable and sustainable future, Pretoria.

Emana, A.N. & Chand, S. (2015) Alkylation of benzene with ethanol over modified HZSM-5 zeolite catalysts. Applied Petrochemical Research, 5:121–134.

Ereña, J., Vicente, J., Aguayo, A.T., Gayubo, A.G., Olazar, M. & Bilbao, J. (2013) Effect of combining metallic and acid functions in CZA/HZSM-5 desilicated zeolite catalysts on the DME steam reforming in a fluidized bed. International Journal of Hydrogen Energy, 38: 10019-10028.

Eroglu, N., Emekciban, M. & Athanassiou, C.G. (2017) Applications of natural zeolites on agriculture and food production. Journal of the Science of Food and Agriculture, 97: 3487–3499.

Eskandari, A., Anbia, M., Jahangiri, M. & Nejati, F.M. (2017) Investigation of the use of various silica source on NaX zeolite properties. Journal of Chemical and Petroleum Engineering, 50 (2):1-7.

Eskom Holdings Limited (2017) available at http://www.eskom.co.za; [accessed on 25th September 2017.

Eskom Holdings Limited, 2012, available at http://www.eskom.co.za; [accessed on 11th June 2018.

Fechete, I., Wang, Y. & Védrine, J.C. (2012) The past, present and future of heterogeneous catalysis. Catalysis Today 189: 2–27.

Fox M.A. & Whitesell J.K. (2004) Organic Chemistry, 3rd edition, Jones and Barlett Publishers, p. 530.

Franus, W. (2012) Characterization of X-type zeolite prepared from coal fly ash, Polish Journal of Environmental Studies, 21 (2): 337 – 343.

Gallego, E.M., Paris, C., M. D´ıaz-Rey, R.M, Mart´ınez, M.E., Mart´ınez-Triguero, A.M., Mart´ınez, C., Moliner, M. & Corma, A. (2017) Simple organic structure directing agents for synthesizing nanocrystalline zeolites. Chemical Science 8:8138-8149.

Gargiulo, N., Shibata, K., Peluso, A., Aprea, P., Valente, T., Pezzotti, G., Shiono, T. & Caputo, D. (2018) Reinventing rice husk ash: derived NaX zeolite as a high-performing CO2 adsorbent. International Journal of Environmental Science and Technology, 15(7): 1543–1550.

Georgiev, D., Bogdanov, B., Angelova, K., Markovska, I. & Hristov, Y. (2009) Synthetic zeolites and their industrial and environmental applications review, International Science conference 4th - 5th June, Stara Zagora, Bulgaria.

Grand, J., Awala, H. & Mintova, S. (2016) Mechanism of zeolites crystal growth: New findings and open questions. CrystEngComm, 18(5): 650-664.

Grecco, S.T.F., Urquieta-González, E.A, Reyes, P., Oportus, M. & Rangel, M.C. (2014) Influence of temperature and time of seed aging on the properties of Beta zeolite/MCM-41 materials. Journal of the Brazilian Chemical Society. 25(12): 2444-2454.

Grüna, M., Unger, K.K., Matsumoto, A. & Tsutsumi, K. (1999) Novel pathways for the preparation of mesoporous MCM-41 materials: control of porosity and morphology. Microporous and Mesoporous Materials, 27(2-3): 207-216.

Guo, H., Tang, L., Yan, B., Wan, K. & Li, P. (2017) NaA zeolite derived from blast furnace slag: its application for ammonium removal. Water Science and Technology (2017) 76 (5): 1140-1149.

Habeeb, G.A. & Mahmud, H.B. (2010) Study on properties of rice husk ash and its use as cement replacement material. Materials Research, 13(2): 185-190.

Halimehjani, A.Z., Aryanasab, F. & Saidi, M.R. (2009) Catalyst-free Friedel–Crafts alkylation of naphthols with nitrostyrenes in the presence of water. Tetrahedron Letters 50: 1441–1443

Hamed, H.H. (2015) Oxygen and nitrogen separation from air using zeolite type 5A. Al-Qadisiyah Journal for Engineering Sciences, 8(2):1-12.

Hammond, O.S., Edler, K.J., Bowron, D.T. & Torrente-Murciano. L. (2017) Deep eutectic-solvothermal synthesis of nanostructured ceria. Nature Communications, 8:14150.

Harmer M.A. & Sun Q. (2001) Solid acid catalysis using ion-exchange resins, Applied Catalysis A: General 221: 45–62.

He, N., Bao, S. & Xu, Q. (1998) Fe-containing mesoporous molecular sieves materials: very active Friedel-Crafts alkylation catalysts. Applied Catalysis A: General 169: 29-36.

Herndon, M.J. & Whiteside, M. (2017) Further evidence of coal fly ash utilization in tropospheric geoengineering: Implications on human and environmental health. Journal of Geography, Environment and Earth Science International, 9(1): 1-8.

Hlatywayo, T. MSc Thesis (2014) Supported metal catalysts for Friedel-Crafts alkylation. Chemistry Department, University of the Western Cape.

Høj, M., Beier, M.J., Grunwaldt, J-D. & Søren Dahl, S. (2009) The role of monomeric iron during the selective catalytic reduction of NOx by NH_3 over Fe-BEA zeolite catalysts. Applied Catalysis B: Environmental, 93(1–2): 166-176.

Höller, H. & Wirsching, U. (1985) Zeolite formation from fly ash. Fortschritte der Mineralogie, 63(1): 21-43.

Hollman, G.G., Steenbruggen, G., & Janssen-Jurkovičová M. (1999) A two-step process for the synthesis of zeolites from coal fly ash. Fuel 78: 1225-1230.

Hong, G-B., Wu, W-S., Chang, C-T. & Ma, C-M. (2015) Dichloromethane treatment by mesoporous metal catalysts. Journal of the Chinese Institute of Engineers, 38(7): 908–917.

https://chemicalstructure.net/portfolio/linde-type-a (visited 09-11-2017)

Huang, Y-B., Liang, J., Wang, X-S. & Cao, R. (2017) Multifunctional metal–organic framework catalysts: synergistic catalysis and tandem reactions. Chemical Society Reviews, (46): 126-157.

Hui, K.S. & Chao, C.Y.H. (2006) Synthesis of MCM-41 from coal fly ash by a green approach: Influence of synthesis pH. Journal of Hazardous Materials B137: 1135–1148

Iijima, A., (1980). Geology of natural zeolites and zeolitic rocks, Pure and Applied Chemistry, 52: 2115 - 2130.

Iliuta, I., Bozga, G. & Lupascu, M. (2001) Liquid-phase alkylation of benzene with propylene catalysed by HY zeolites. Chemical Engineering & Technology, 24: 933-944.

Inglezakis, V.J. & Poulopoulos, S.G. (2006) Adsorption, ion exchange & catalysis: Design of operations & environmental applications. Elsevier, Amsterdam, p. 248 – 254.

Ingole, A.K., Dixit, D. & Dingare S.V. (2017) A review on Selective Catalytic Reduction technique for diesel engine exhaust after treatment, International Journal of Current Engineering and Technology, 7: 206-210.

Jeirani, Z. & Soltan, J. (2017) Improved formulation of Fe-MCM-41 for catalytic ozonation of aqueous oxalic acid. Chemical Engineering Journal 307: 756–765.

Jha, B. & Singh, D.N. (2011) A review on synthesis, characterization and industrial applications of fly ash zeolites. Journal of Materials Education, 33 (1-2): 65 – 132.

Jiang, Y., Lin, K., Zhang, Y., Liu, J., Li, G., Sun, J. & Xu, X. (2012) Fe-MCM-41 nanoparticles as versatile catalysts for phenol hydroxylation and for Friedel–Crafts alkylation, Applied Catalysis A: General 445– 446: 172– 179.

Johannes, K., Kuznik, F., Hubert, J-L., Durier, F. & Obrecht, C. (2015) Design and characterisation of a high powered energy dense zeolite thermal energy storage system for buildings. Applied Energy 159: 80–86

Johnson, E.B.G. & Arshad, S.E. (2014) Hydrothermally synthesized zeolites based on kaolinite: A review. Applied Clay Science, 97–98: 215-221.

Joni, J., Haumann, M. & Wasserscheid, P. (2009) Development of a supported ionic liquid phase (SILP) catalyst for slurry-phase Friedel–Crafts alkylations of cumene. Advanced Synthesis & Catalysis 351:423–431

Jun, S. & Ryoo, R. (2000) Aluminum impregnation into mesoporous silica molecular sieves for catalytic application to Friedel–Crafts alkylation. Journal of Catalysis 195, 237–243.

Kabwadza-Corner, P., Johan, E., Matsue, N. (2014) pH dependence of lead adsorption on zeolites. Journal of Environmental Protection 06(01):45-53.

Kamalakar, G., Kulkarni, S. J., Raghavan, K. V., Unnikrishnan, S. & Halgeri, A. B. (1999) Isopropylation of naphthalene over modified HMCM-41, HY and SAPO-5 catalysts. Journal of Molecular Catalysis A: Chemical, 149(1-2): 283-288.

Kasture, M.W., Bokade, V.V. & Joshi, P.N. (2005) Conversion of fly ash- an environmentally detrimental waste to zeolite beta (BEA) for commercial catalytic applications. Journal of the American Ceramic Society 88 (11): 3260 – 3263.

Kessler, H. (2001) Synthesis of high-silica zeolites and phosphate-based materials in the presence of fluoride, *in* Verified synthesis of zeolitic materials, 2nd Revised Edition. Robson, H. (ed). Elsiever Science, Netherlands, p. 25.

Khan, M.N., Auerbach, S.M, & Monson, P.A. (2015) Lattice Monte Carlo simulations in search of zeolite analogues: Effects of structure directing agents. The Journal of Physical Chemistry C, 119: 28046−28054.

Khanday, W.A., Kabir, G. & Hameed, B.H. (2016) Catalytic pyrolysis of oil palm mesocarp fibre on a zeolite derived from low-cost oil palm ash. Energy Conversion and Management, 127: 265-272.

Klumpp, D.A. (2016) Electrophilic aromatic substitution: Mechanism, in Arene chemistry: Reaction mechanisms and methods for aromatic compounds, (ed) Mortier, J. John Wiley & Sons Inc. New Jersey.

Ko, A-N, & Huang, C.S. (1993) Alkylation of ethylbenzene with methanol on HY, HM and HZSM-5 zeolite. Journal of the Chinese Chemical Society, 40(4): 345-350.

Kosinov, N., Liu, C., Hensen, E.J.M.& Pidko, E.A. (2018) Engineering of transition metal catalysts confirned in zeolites. Chemistry of Materials, 30: 3177-3198.

Kostrab, G. PhD Thesis (2010) Study of shape-selectivity of zeolite catalysts, Faculty of Chemical and Food Technology, Slovak University of Technology in Bratislava.

Kovo, A. & Holmes, S. (2010) Effect of aging on the synthesis of kaolin-based zeolite Y from Ahoko Nigeria using a novel metakaolinization technique, Journal of Dispersion Science and Technology 31:442–448.

Krishna, S.C. & Bhattacharyya, G. (2008) Wet oxidative method for removal of 2,4,6-trichlorophenol in water using Fe(III), Co(II), Ni(II) supported MCM41 catalysts. Journal of Hazardous Materials, 150(3): 728-736.

Krznaric, I., Antonic, T., Bronic, J., Subotic, B., & Thompson, R.W. (2003) Influence of silica sources on the chemical composition of aluminosilicate hydrogels and the results of their hydrothermal treatment. Croatica Chemica Acta 76 (1): 7-17

Kuhl, G.H., (1999). Modification of zeolites, in Catalysis and Zeolites: Fundamentals and Applications. Weitkamp, J., and Puppe, L., (eds). Springer, Heidelberg, p. 82-83.

Kuwahara, Y., Ohmichi, T., Mori, K., Katayama, I. & Yamashita, H. (2008) Synthesis of zeolite from steel slag and its application as a support of nano-sized TiO_2 photocatalyst. Journal of Materials Science, 43(7): 2407–2410.

Lande, S.V., Sakthivel, A., Katravulapalli, M., Sreedharan, U., Das, J. & Raksh Vir Jasra, R.V. (2013) Zinc-modified MCM-22 as potential solid acid catalyst for Friedel–Crafts alkylation reaction. International Journal of Chemical Reactor Engineering, 11(1): 1–9.

Lechert, H. (2001) The pH-value and its importance for the crystallisation of zeolites, *in* Verified synthesis of zeolitic materials, 2nd Revised Edition. Robson, H. (ed). Elsiever Science, Netherlands.

Lehman, S.E. & Larsen, S.C. (2014) Zeolite and mesoporous silica nanomaterials: greener syntheses, environmental applications and biological toxicity. Environmental Science Nano, 1: 200–213.

Lewis, D.W., Catlow, C.R.A., & Thomas, J.M. (1997) Application of computer modelling to the mechanisms of synthesis of microporous catalytic materials. Faraday Discuss, 106: 451-471.

Li, B., Xu, J., Li, X., Liu, J., Zuo, S. Pan, Z. & Wu, Z. (2012) Bimetallic iron and cobalt incorporated MFI/MCM-41 composite and its catalytic properties. Materials Research Bulletin 47: 1142–1148.

Li, R., Xu, W. & Wang, J. (1992) Nonaqueous synthesis: Iron aluminosilicates with the ZSM-48 structure. Zeolites, 12 (6): 716-719.

Lin, T., Zhang, X., Li, R., Bai, T. & Yang, Y.S. (2011) Synergistic catalysis of isolated Fe^{3+} and Fe_2O_3 on FeOx/HZSM-5 catalysts for Friedel–Crafts benzylation of benzene. Chinese Chemical Letters, 22(6): 639-642.

Liu, J. Du, Y., Liu, J., Zhao, Z., Cheng, K., Chen, Y., Wei, Y., Song, W. & Zhang, X. (2017) Design of MoFe/Beta@CeO2 catalysts with a core−shell structure and their catalytic performances for the selective catalytic reduction of NO with NH3. Applied Catalysis B: Environmental, 203: 704-714.

Livage, J. (1994) Sol-gel chemistry and molecular sieve synthesis, *in* Advanced zeolite science and applications, Studies in Surface Science and Catalysis, Vol. 85, Jansen, J.C., Stticker, M., Karge, H.G. & Weitkamp, J. (eds.) Elsevier Science B.V, Netherlands.

Lobo, A.J.W. PhD Thesis (2012) Modelling structure direction and morphology control in zeolite synthesis, Department of Chemistry, University College London.

Ma, B., Hu, J., Wang, Y. & Zhao, C. (2015) Ni nanoparticles encapsulated into mesoporous single-crystalline HBEA: application for drainage oil hydrodeoxygenation to diesel. Green Chemistry, 17: 4610–4617.

Ma, L., Chang, H., Yang, S., Chen, L., Fu, L., Li, J. (2013) Relations between iron sites and performance of Fe/HBEA catalysts prepared by two different methods for NH_3-SCR. Chemical Engineering Journal, 209: 652-660.

Maghsoodloorad, H., Mirfendereski, S.M., Mohammadi, T. & Pak, A. (2011) Effects of gel parameters on the synthesis and characteristics of W-type zeolite nanoparticles. Clays and Clay Minerals, 59(3): 328–335.

Mandres P., Godfrey L. & Hobbs P. (2009) Briefing note: Acid mine drainage in South Africa. Pretoria: CSIR. http://www.csir.co.za

Mantri, K., Komura, K., Kubota, Y. & Sugi, Y. (2005) Friedel–Crafts alkylation of aromatics with benzyl alcohols catalyzed by rare earth metal triflates supported on MCM-41 mesoporous silica. Journal of Molecular Catalysis A: Chemical, 236: 168–175.

Margeta, K., Farkas, A., Šiljeg, M. & Logar, N.Z. (2013) Natural zeolites in water treatment - how effective is their use. INTECH Open Access Publisher, p. 81 – 84.

Martens, J.A. & Jacobs, P.A. (1988) Synthesis of high silica zeolites. Studies in Surface Science and Catalysis, 33:1-44.

Mayoral, A., Sakamoto, Y. & Diaz, I. (2015) Zeolites and mesoporous crystals under the electron microscope in Advanced transmission electron microscopy: Applications to nanomaterials, Deepak, F.L., Mayoral, A. & Arenal, R. (eds). Springer, Heideberg, p. 94-99.

McCarthy, T.S. (2011) The impact of acid mine drainage in South Africa. South African Journal of Science. 107(5/6): 1-7.

McElfish J.M. & Beier A.E., (1990) Environmental regulation of coal mining: SMCRA's Second decade, Environmental Law Institute, Washington DC, p. 133.

McGinness, S. (1999) Treatment of acid mine drainage.UK House of Commons Library,99/10, London, UK.

McMurry J.E. (2012) Organic Chemistry, 8th Edition, Brooks/Cole, p. 575 – 576.

McNaught, A.D. & Wilkinson, A. (1997) Compendium of chemical terminology, 2nd Edition. (the "Gold Book" IUPAC). Blackwell Scientific Publications, Oxford.

Meng, L., Zhu, X. & Hensen, E.J.M. (2017) Stable Fe/ZSM-5 nanosheet zeolite catalysts for the oxidation of benzene to phenol, American Chemical Society Catalysis. 7(4): 2709–2719

Merkel, B. and Schipek, M. (2011) The new uranium mining boom: challenge and lessons learned. Springer-Verlag, Berlin, p. 390-391

Michels, H.H. & Sienel, T.H. (2003) Refrigeration lubricants- Properties and applications, *in* Fuels and Lubricants Handbook: Technology, properties, performance

and testing (eds) Totten, G.E., Westbrook, S.R. & Shah, R.J. ASTM International, Conshohocken, p. 415.

Mignoni, M.L., de Souza, M.O., Pergher, S.B.C., de Souza, R.F. & Bernardo-Gusmão, K. (2010) Nickel oligomerization catalysts heterogenized on zeolites obtained using ionic liquids as templates. Applied Catalysis A: General, 374: 26–30.

Ameh, A.E., Eze, C.P., Antunes, E., Cornelius, M-L. U., Musyoka, N.M., Petrik, L.F. (2019) Stability of fly ash-based BEA-zeolite in hot liquid phase. Catalysis Today, DO - 10.1016/j.cattod.2019.08.006.

Millini, R. & Bellussi, G. (2017) Zeolite science and perspectives, *in* Zeolites in catalysis: properties and applications, Čejka, J. & Morris R.E. (eds). RCS, London.

Miskolczi, N., Juzsakova, T. & Sója, J. (2019) Preparation and application of metal loaded ZSM-5 and y-zeolite catalysts for thermo-catalytic pyrolysis of real end of life vehicle plastics waste. Journal of the Energy Institute, 92(1): 118-127.

Missengue, R.M., Losch, P., Sedres, G., Musyoka, N.M., Fatoba, O.O. Louis, B., Pale, P. Petrik, L.F. (2017) Transformation of South African coal fly ash into ZSM-5 zeolite and its application as an MTO catalyst. Comptes Rendus Chimie, 20(1): 78-86

Mjimbo, V., Mujuru, M. & Mutanga, S.S. (2017) The legacy of acid mine drainage in South Africa, *in* Management and mitigation of acid mine drainage in South Africa: Input for mineral beneficiation in Africa, Mujuru, M. & Mutanga, S.S. (eds), Africa Institute of South Africa, Pretoria, p.17.

Mohamed, R.M., Mkhalid, A. & Barakat, M.A. (2015) Rice husk ash as a renewable source for the production of zeolite NaY and its characterization. Arabian Journal of Chemistry, 8(1): 48-53.

Mokhonoana, M.P. (2005) PhD Thesis. The synthesis and study of some metal catalysts supported on modified MCM-41. University of the Witwatersrand, Johannesburg, p.168-177.

Moliner, M., Rey, F. & Corma, A. (2013) Towards the rational design of efficient organic structure-directing agents for zeolite synthesis. Angewandte Chemie International Edition, 52: 13880 – 13889.

Morris, R.E. & Weigel. S.J. (1997) The synthesis of molecular sieves from non-aqueous solvents. Chemical Society Reviews, 26: 309-317.

Moshoeshoe, M., Nadiye-Tabbiruka, M.S. & Obuseng, V. (2017) A Review of the chemistry, structure, properties and applications of zeolites. American Journal of Materials Science, 7(5): 196-221.

Motsi, T., Rowson, N.A. and Simmons, M.J.H. (2009) Adsorption of heavy metals from acid mine drainage by natural zeolites. International Journal of Mineral Process, 92, 42-48.

Motsi, T., Rowson, N.A. and Simmons, M.J.H. (2011) Kinetic studies of the removal of heavy metals from acid mine drainage by natural zeolite. International Journal of Mineral Processing 101, 42-49.

Muñiz, R.J.G., Ramírez, M.A., Robles, A.J.M., Melo, G.P., Bocardo, E.J.C. & Martínez, M.A.M. (2010) Synthesis and characterization of high silica zeolites from coal fly ash (CFA): Two cases of zeolite syntheses from the same waste material. Latin American Applied Research, 40:323-328.

Munnik, P., de Jongh, P.E. & de Jong, K.P. (2015) Recent developments in the synthesis of supported catalysts. Chemical Reviews, 115: 6687–6718.

Murayama, N., Yamamoto, H. & Shibata, J. (2002) Mechanism of zeolite synthesis from coal fly ash by alkali hydrothermal reaction. International Journal of Mineral Processing, 64: 1–17.

Murcia-López, S., Bacariza, M.C., Villa, K., Lopes J.M., Henriques, C., Morante, J.R. & Andreu, T. (2017) Controlled photocatalytic oxidation of methane to methanol through surface modification of beta zeolites. American Chemical Society, 7(4): 2878-2885.

Murcott, S, (2012) Arsenic contamination in the world: An International Sourcebook, IWA Publishing, UK.

Nagy, J.B., Bodart, P., Hannus, I. & Kiricsi, I. (1998) Synthesis, characterization and use of zeolitic microporous materials. Deca General Ltd, Szeged, Hungary.

Newsam, J. M.; Treacy, M. M. J.; Koetsier, W. T.; Gruyter, C. B. D., Structural characterization of zeolite beta. Proceedings of the Royal Society of London. Series A, Mathematical and Physical Sciences, 420 (1859): 375-405.

Nikinmaa, M. (2014) An Introduction to Aquatic Toxicology, Academic Press, Oxford, UK. p. 1-17.

Nur, H., Ramli, Z., Efendi, J., Rahman, A.N.A., Chandren, S. & Yuan, L.S. (2011) Synergistic role of Lewis and Brönsted acidities in Friedel–Crafts alkylation of resorcinol over gallium-zeolite beta. Catalysis Communications, 12: 822 – 825.

O'shea H, Msc Thesis, (2005) Backward modelling to prioritize sources of acid mine drainage for remediation: Application to Warden Gulch, Summit County, Colorado, Department of Civil, Environmental and Architectural Engineering, University of Vermont.

Okumura, K., Nishigaki, K. & Niwa, M. (2001) Prominent catalytic activity of Ga-containing MCM-41 in the Friedel-Crafts alkylation. Microporous and Mesoporous Materials. 44-45: 509-516.

Olah, G.A. & Molnar, A. (2003) Hydrocarbon chemistry, 2nd Edition. John Wiley and Sons Inc, New Jersey, p. 230 - 232.

Ooi, Z.X., Ismail, H., Bakar, A.A. and Teoh, Y.P. (2014) A review on recycling ash derived from elaeis guineensis by-product. BioResources 9(4): 8923-7940.

Otterstedt, J.E. & Brandreth, D.A. (1998) Small particles technology, Plenum Press, New York.

Ozdemir, O.D. & Piskin, S. (2017) A novel synthesis method of zeolite X from coal fly ash: alkaline fusion followed by ultrasonic-assisted synthesis method. Waste Biomass Valor, DOI 10.1007/s12649-017-0050-7.

Pa, F.C., Chik, A. & Bari M.D.F. (2015) Zeolite synthesis from oil palm ash using hydrothermal treatment. Applied Mechanics and Materials, 754-755: 1035-1039.

Panek, R., Wdowin, M., Franus, W., Czarna, D., Stevens L.A., Deng, H., Liu, J., Sun, C., Liu, H. & Snape, C.E. (2017) Fly ash-derived MCM-41 as a low-cost silica support for

polyethyleneimine in post-combustion CO_2 capture. Journal of CO_2 Utilization 22: 81–90.

Park, M., Choi, C.L., Lim, W.T., Kim, M.C., Choi, J. & Heo, N.H. (2000) Molten-salt method for the synthesis of zeolitic materials I. Zeolite formation in alkaline molten-salt system. Microporous and Mesoporous Materials 37: 81–89.

Parnham, E.R. & Morris, R.E. (2007) Ionothermal synthesis of zeolites, Metal–Organic Frameworks, and Inorganic–Organic hybrids. Accounts of Chemical Research, 40: 1005–1013.

Parvulescu, V. & Su, B.L. (2001) Iron, cobalt or nickel substituted MCM-41 molecular sieves for oxidation of hydrocarbons. Catalysis Today, 69(1–4): 315-322.

Patet, R.E., Koehle, M., Lobo, R.F., Caratzoulas, S. & Vlachos, D.G. (2017) General acid-type catalysis in the dehydrative aromatization of furans to aromatics in H‑[Al]-BEA, H‑[Fe]-BEA, H‑[Ga]-BEA, and H‑[B]- BEA Zeolites, The Journal of Physical Chemistry C, 121, 13666−13679.

Perego, C. & Ingallina, P. (2002) Recent advances in the industrial alkylation of aromatics: new catalysts and new processes. Catalysis Today, 73(1–2): 3-22.

Perego, C., Amarillia, S., Millinia, R., Bellussia, G., Girottib, G. & Terzonib, G. (1996). Experimental and computational study of Beta, ZSM - 12, Y, Mordenite and ERB - 1 in cumene synthesis. Microporous and Mesoporous Materials, 6: 395 – 404.

Pinna, F. (1998) Supported metal catalysts preparation. Catalysis Today 41: 129-137.

Pradhan, A.C., Sahoo, M.K., Bellamkonda, S., Parida, K.M. & (2016) Rao, G.R. Enhanced photodegradation of dyes and mixed dyes by heterogeneous mesoporous Co–Fe/Al2O3–MCM-41 nanocomposites: nanoparticles formation, semiconductor behavior and mesoporosity. The Royal Society of Chemistry, Advances, 6:94263–94277.

Prafulla, K.S., Kangjoo, K., Powell, M.A. & Equeenuddin, S.M. (2016) Recovery of metals and other beneficial products from coal fly ash: a sustainable approach for fly ash management. International Journal of Coal Science & Technology, 3(3):267-283.

Preethi, M.E.L., Sivakumar, T. & Palanichami, M. (2010) Room temperature efficacious synthesis of diphenylmethane over Fe/Al-MCM-41 catalysts. Catalysis Communications, 11(10): 876-879.

Querol, X., Alastuey, A., Lo´pez-Soler, A., Plana, F., Andre´s, J.M., Juan, R., Ferrer, P. & Ruiz, C.R. (1997). A fast method for recycling fly ash: microwave-assisted zeolite synthesis. Environmental Science & Technology 31 (9): 2527–2533.

Qureshi, Z.S., Deshmukh, K.M. & Bhanage, B.M. (2013) Applications of ionic liquids in organic synthesis and catalysis. Clean Technologies and Environmental Policy, DOI 10.1007/s10098-013-0660-0.

Rac, B., Nagy, M., Palinko, I. & Molnar, A. (2007). Application of sulfonic acid functionalized MCM-41 materials-selectivity changes in various probe reactions. Applied Catalysis A: General 316: 152–159.

Rahmani, E. & Rahmani, M. (2018) Al-Based MIL-53 metal organic framework (MOF) as the new catalyst for Friedel−Crafts alkylation of benzene. Industrial & Engineering Chemistry Research. 57: 169−178

Ramontja, T., Eberle, D., Coetzee, H., Schwarz, R. & Juch, A. (2011) Critical challenges of acid mine drainage in South Africa's Witwatersrand gold mines and Mpumalanga coal fields and possible research areas for collaboration between South African and German researchers and expert teams, *in* The new uranium mining boom: Challenge and lessons learned, Merkel, B.& Schipek M.(eds), Springer-Verlag, Berlin Heidelberg.

Rao, P.R.H.P., Ueyamaa, K. & Matsukata, M., (1998). Crystallization of high silica BEA by dry gel conversion. Applied Catalysis A: General 166: 97-103.

Reynolds-Clausen, K. & Singh, N. (2017) South Africa's power producer's revised coal ash strategy and implementation progress. World of Coal Ash (WOCA) Conference, Lexington, Kentucky.

Riegel, R.E. & Kent, J.A., (2003). Riegel's handbook of industrial chemistry, 10th Edition, Kluwer Academic, New York, p. 1131.

Roberts, J.D. & Caserio, M.C. (1977) Basic principles of organic chemistry, 2nd ed. W. A. Benjamin, Inc., Menlo Park, California.

Rojas, A., Arteaga, O., Kahr, B. & Camblor, M.A. (2013) Synthesis, structure, and optical activity of HPM-1, a pure silica chiral zeolite. Journal of the American Chemical Society, 135: 11975–11984.

Rueping, M. & Nachtsheim, B.J. (2010) A review of the new developments in the Friedel-Craftts alkylation- from green chemistry to asymmetric catalysis. Beilstein Journal of Organic Chemistry (6) 6.

Run, M., Wu, S. & Gang Wu, G. (2004) Synthesis of mesoporous molecular sieve under ultrasonic. Microporous and Mesoporous Materials 74(1):37-47

Rycrof, M. (2017) Exploring the many uses of fly ash. EE Publishers, Muldersdrift, South Africa.

Saer, L.K.A. (2001) Properties and use of coal fly ash: A valuable industrial by-product. Thomas Telford Publishing, London, p. 1-4.

Sánchez-Velandia, J.E. & Villa, A.L. (2019) Isomerization of α- and β- pinene epoxides over Fe or Cu supported MCM-41 and SBA-15 materials. Applied Catalysis A: General, 580: 17-27.

Sangeetha, C. & Baskar, P. (2016) Zeolite and its potential uses in agriculture: A critical review. Agricultural Reviews, 37 (2): 101-108

Schwarz, J.A., Contescu, C. & Contescu, A. (1995) Methods for preparation of catalytic materials. Chemical Reviews, 95: 477-510.

Sebastian, V., Casado, C. & Coronas, J. (2009) Special applications of zeolites, *in* Zeolites and Catalysis: Synthesis, Reactions and Application. Cejka, J., Corma, A. and Zones, S., (eds). Wiley-VCH, Weinheim, p. 389.

Shah, B.A., Patel, A.V., Bagia, M.I. & Shah, A.V. (2017) Green approach towards the synthesis of MCM-41 from siliceous sugar industry waste. International Journal of Applied Chemistry, 13(3): 497-514.

Shaheen, S.M., Derbalah, A.S. & Moghanm, F.S. (2012) Removal of heavy metals from aqueous solution by zeolite in competitive sorption system. International Journal of Environmental Science and Development, 3(4) : 362-367.

Shen, S., Chen, J., Koodali, R.T., Hu, Y., Xiao, Q., Zhou, J., Wang, X. & Guo, L. (2014) Activation of MCM-41 mesoporous silica by transition-metal incorporation for photocatalytic hydrogen production. Applied Catalysis B: Environmental 150– 151: 138– 146.

Shigemoto, N., Hayashi, H. & Miyaura, K. (1993) Selective formation of Na-X zeolite from coal fly ash by fusion with sodium hydroxide prior to hydrothermal reaction. Journal of Materials Science, 28: 4781–4786.

Shinde, S.H. & Rode, C.V. (2018) Friedel−Crafts alkylation over Zr-Mont catalyst for the production of diesel fuel precursors. American Chemical Society, 3, 5491−5501.

Shoppert, A., Loginova, I. V., Chaikin, L. I. & Rogozhnikov, D. A. (2017) Alkali fusion-leaching method for comprehensive processing of fly ash. International Conference with Elements of School for Young Scientists on Recycling and Utilization of Technogenic Formations. KnE Materials Science, 89–96.

Shuvaeva, M.A., Nuzhdin, A.L., Martyanova, O.N. & Bukhtiyarova, G.A. (2014) Benzylation of benzene by benzyl chloride over silica-supported iron sulfate catalysts. Mendeleev Communications, 24: 231–232.

Singh, V.P. (2005) Toxic metals and environmental issues, Sarup & Sons, (New Delhi), India.

Sirotin, S.V., Moskovskaya, I.F. & Romanovsky, B.V. (2011). Synthetic strategy for Fe-MCM-41 catalyst: a key factor for homogeneous or heterogeneous phenol oxidation. Catalysis Science & Technology, 1: 971–980.

Smart, L.E. & Moore, E.A. (2012) Solid state chemistry: An introduction, 4th Ed. CRC Press, Boca Raton.

Smith, M.B. & March, J., (2007). March's advanced organic chemistry: Reactions, mechanisms and structure, 6th edition, John Wiley & Sons, Inc, New Jersey, p. 712.

Smith, M.B., (1946) Organic synthesis. Academic Press, United States of America.

Snyder, R. (1981) The alkyl benzenes, Committee on Alkyl Benzene derivatives, Assembly of Life Sciences (US), National Academy Press, p. 1.

Sparling, D.W., & Lowe, T.P. (1996) Environmental hazards of aluminum to plants, invertebrates, fish, and wildlife. Reviews of Environmental Contamination and Toxicology ,145:1-127.

Speight, J.G. (2013) The chemistry and technology of coal, 3rd edition. CRC Press, Taylor and Francis group, Florida.

Strohmaier, K.G. (2010). Synthesis approaches, in Zeolites and catalysis: Synthesis, reactions and applications. Čejka, J., Corma, A. & Zones, S (eds). Wiley-VCH, Weinheim, p. 50 -86.

Strydom, H.A. & King, N.D. (2009) Environmental management in South Africa, 2nd Edition, Juta Law (RSA) p. 535.

Subbulekshmi, N.L. & Subramanian, E. (2016) New synthesis process of crystalline phase - pure faujasite zeolite material from sialic type coal fly ash. J. Adv. Chem. Sci. 2(2), 284–288.

Sun, X. & Zhao, S. (2006). [bmim]CV[FeC13] ionic liquid as catalyst for alkylation of benzene with 1-octadecene. Chinese Journal of Chemical Engineering, 14(3): 289–293.

Sunajadevi, K.R. & Sugunan, S. (2006) Alkylation of phenol with tert-butyl alcohol catalysed by some sulphated titania systems. Indian Journal of Chemistry, 45A: 1131-1138.

Tatsidjodoung, P., Le Pierrès. N., Heintz, J., Lagre, D., Luo, L. & Durier, F. (2016) Experimental and numerical investigations of a zeolite 13X/water reactor for solar heat storage in buildings. Energy Conversion and Management 108: 488–500.

Taylor J. (2008) Acid Mine Drainage - Is this the end of life in Gauteng?, Cobbing, 2008: 452. http://www.earthlife.org.za.

Taylor, P.G. & Gagan, J.M.F. (2007) Alkenes and aromatics, Royal Society of Chemistry, Cambridge, p. 52.

Thomas, B. PhD Thesis (2004) Alkylation of benzene with higher olefins over zeolites: a green route for lab Synthesis. Department of Applied Chemistry, Cochin University of Science and Technology.

Thompson, R.W. (2001) Nucleation, growth and seeding in zeolite synthesis, in Verified Synthesis of Zeolitic Materials, 2nd Revised Edition. Robson, H. (ed). Elsiever Science, Netherlands.

Tian, D., Liu, Z., Li, D., Shi, H., Pan, W. & Cheng, Y. (2013) Bimetallic Ni–Fe total-methanation catalyst for the production of substitute natural gas under high pressure, Fuel 104: 224–229.

Tomatis, M., Xu, H., Wei, C., Bishop, M.T., He, J., Wang, C., Zhao, M., Xiao, H., Yu, H., Behera, S.N. & Tang, B. (2018) A comparative study of Mn/Co binary metal catalysts supported on two commercial diatomaceous earths for oxidation of benzene. Catalysts 2018, 8(3): 1-22.

Tomljenovic, L. (2011) Aluminum and Alzheimer's Disease: After a century of controversy, is there a plausible link? Journal of Alzheimer's Disease, 23 (4): 567-598.

Tong, M., Zhang, D., Fan, W., Xu, J., Zhu, L., Guo, W., Yan, W., Yu, J., Qiu, S., Wang, J., Deng, F. & Xu, R. (2015) Synthesis of chiral polymorph A-enriched zeolite Beta with an extremely concentrated fluoride route. Scientific Reports | 5:11521 | DOI: 10.1038/srep11521.

Townsend, R.P. & Coker, E.N. (2001) Ion exchange in zeolites in Studies in Surface Science and Catalysis 137, (eds) van Bekkum, H., Flanigen, E.M., Jacobs, P.A. & Jansen, J.C. Elsevier Science B.V., Amsterdam, Netherlands, p. 416-512.

Van Wyk, J.J., Rademeyer, J.I. & van Rooyen, J.A. (2010) Position statement on the Vaal river system and acid mine drainage. DWA, Pretoria.

Velichkova, F., Delmas, H., Julcour, C. & Koumanova, B. (2016) Heterogeneous fenton and photo-fenton oxidation for paracetamol removal using iron containing ZSM-5 zeolite as catalyst, AIChE Journal 63(2): 669-679.

Vermeulen, D &Usher, B (2009) Quantification of the impact of irrigating with coalmine waters on the underlying aquifers, *in* Appropriate technologies for environmental protection in the developing world, Yanful, E.K. & Ernest, K. (eds), Springer Science, Netherlands, p. 235-245.

Vinua, A., Sawant, D.P., Ariga, K., Hartmann, M. & Halligudi S.B. (2005) Benzylation of benzene and other aromatics by benzyl chloride over mesoporous AlSBA-15 catalysts Microporous and Mesoporous Materials 80: 195–203.

Vivier, L. & Duprez, D. (2010) Ceria-based solid catalysts for organic chemistry. ChemSusChem, 3: 654 – 678.

Vuori, K. (1995) Direct and indirect effects of iron on river ecosystems. Annales Zoologici Fennici, 32: 317 – 329.

Wa Kasongo, J.B. MSc Thesis (2011) Synthesis and characterization of micro- and mesoporous materials for low temperature selective catalytic reduction of nitrogen oxides. Department of Chemistry, University of the Western Cape.

Wagner, P. & Davis, M.E. (2000) Introduction to zeolite science, *in* Photofunctional zeolite: Synthesis, characterization, photocatalytic reactions, light harvesting. Anpo, M., (ed). NOVA Science Publishers Inc, New York, p. 33.

Wahiba Najjar, W., Azabou, S., Sayadi, S. & Ghorbel, A. (2009) Screening of Fe–BEA catalysts for wet hydrogen peroxide oxidation of crude olive mill wastewater under mild conditions. Applied Catalysis B: Environmental 88: 299–304.

Wajima, T. (2014) Synthesis of zeolite from blast furnace slag using alkali fusion with addition of EDTA. Advanced Materials Research, 1044-1045: 124-127.

Wang, C., Daimon, H. & Sun, S. (2009) Dumbbell-like Pt-Fe_3O_4 nanoparticles and their enhanced catalysis for oxygen reduction reaction. Nano Letters, 9(4): 1493 – 1496.

Wang, Y., Song, Y., Huo, W., Jia, M., Jing, X., Yang, P., Yang, Z., Liub, G. & Zhang, W. (2012) Vapor phase ortho-selective alkylation of phenol with methanol over silica–manganese mixed oxide catalysts. Chemical Engineering Journal, 181–182: 630-635.

Wang, Y., Xu, L., Yu, Z., Zhang, X. & Liu, Z. (2008) Selective alkylation of naphthalene with tertbutyl alcohol over HY zeolites modified with acid and alkali. Catalysis Communications, 9(10): 1982-1986.

Wang, Z., Wang, L., Zhou, Z., Zhang, Y., Li, H., Stampfl, C., Liang, C. & Huang, J. (2017) Benzylation of arenes with benzyl chloride over H-Beta zeolite: Effects from acidity and shape-selectivity. Journal of Physical Chemistry C, 121(28): 15248-15255.

Warhurst A. (1994) Environmental degradation from mining and mineral processing in developing countries: Corporate Responses and National Policies, OECD (Paris).

Wasserscheid, P. & Joni, J. (2010) Green organic synthesis in ionic liquids *in* Handbook of green chemistry, volume 6: Ionic liquids, (eds) Wasserscheid, P & Stark, A. Wiley-VCH, Weinheim, Germany.

Watanabe, M., Uchida, H., Ohkubo, K. & Igarashi, H. (2003) Hydrogen purification for fuel cells: selective oxidation of carbon monoxide on Pt–Fe/zeolite catalysts, Applied Catalysis B: Environmental 46:595–600.

Wdowin, M., Franus, M., Panek, R., Badura, L. and Franus, W. (2014) The conversion technology of fly ash into zeolites. Clean Technologies and Environmental Policy 16(6): 1217–1223.

Weckhuysen, B.M. & Yu, J. (2015) Recent advances in zeolite chemistry and catalysis. Chemical Society Reviews, 44: 7022-7024.

Weitkamp, J. & Puppe, L. (1999). Catalysis and zeolites: Fundamentals and applications. Springer, German.

Wheatley, P.S., Allan, P.K., Teat, S.J., Ashbrook, S.E. & Morris, R.E. (2010) Task specific ionic liquids for the ionothermal synthesis of siliceous zeolites. Chemical Science, 1: 483 – 487.

Wilson, S.T. (2001). Templating in molecular sieve synthesis, *in* Verified synthesis of zeolitic materials, 2nd Revised Edition. Robson, H. (ed). Elsiever Science, Netherlands p. 28-29.

Wu, Q., Liu, X., Zhu, L., Meng, X., Deng, F., Fan, F., Feng, Z., Li, C., Maurer, S., Feyen, M., Müller, U & Xiao, F-S. (2017) Solvent-free synthesis of ITQ-12, ITQ-13, and ITQ-17 zeolites. Chinese Journal of Chemistry, 35: 572-576.

Wu, Q., Meng, X., Gao, X. & Xiao, F-S. (2018) Solvent-free synthesis of zeolites: mechanism and utility. American Chemical Society, 51: 1396−1403.

Xiang-Hong Fang, X.H., Fang, F., Lu, C.H. & Zheng, L. (2016) Organics and suspended solids aqueous solutions by zeolites. Nuclear Engineering and Technology, 43(3): 555-561.

Xu, R., Pang, W., Yu, J., Huo, Q. & Chen, J., (2007) Chemistry of zeolites and related porous materials: Synthesis and structure. John Wiley and Sons, Singapore, p. 632-635.

Xu, W., Ollevier, T. & Kleitz, F. (2018) Iron-modified mesoporous silica as an efficient solid lewis acid catalyst for the Mukaiyama Aldol reaction. Catalysis 8: 1932−1944.

Xu, Y. & Usher, B. (2006) Groundwater pollution in Africa, Taylor and Francis, Balkema, p. 304.

Yan X, & Xu, Y., (2010) Chemical vapour deposition: An integrated engineering design for advanced materials, Springer, London.

Yanful, E.K. (2009) Appropriate technologies for environmental protection in the developing world. Springer Science, p. 236-240.

Yang, H., Zhang, C., Gao, P., Wang, H., Li, X., Zhong, L., Wei, W. & Sun, Y. (2017) A review of the catalytic hydrogenation of carbon dioxide into value-added hydrocarbons, Catalysis Science & Technology, 7: 4580-4598.

Yashima, T., Sato, K., Hayasaka, T. & Hara, N. (1972) Alkylation on synthetic zeolites: III. Alkylation of toluene with methanol and formaldehyde on alkali cation exchanged zeolites. Journal of Catalysis, (26) 3: 303-312.

Ye, G., Sun, Y., Guo, Z., Zhu, K., Liu, H., Zhou, X. & Coppens, M-O. (2018) Effects of zeolite particle size and internal grain boundaries on Pt/Beta catalyzed isomerization of n-pentane. Journal of Catalysis, 360: 152-159.

Yilmaz, B. & Müller, U. (2009) Catalytic applications of zeolites in chemical industry. Topics in Catalysis, 52(6–7): 888–895.

Yılmaz, M.S., Özdemir, O.D. & Pişkin, S. (2015) Synthesis and characterization of MCM-41 with different methods and adsorption of Sr2+ on MCM-41. Research on Chemical Intermediates. 41(1): 199 -211.

Yuan, J-J. & Gevert, B.S (2004) Alkylation of benzene with ethanol over ZSM-5 catalyst with different SiO_2/Al_2O_3 ratios. Indian Journal of Chemical Technology, 11: 337-345.

Zaarour, M., Dong, B., Naydenova, I., Retoux, R. & Mintova, S. (2014) Progress in zeolite synthesis promotes advanced applications. Microporous and Mesoporous Materials, 189: 11-21.

Zahmakiran, M & Ozbar, S. (2013) Preparation of metal nanoparticles stabilized by the framework of porous materials in Sustainable preparation of metal nanoparticles method and applications, (eds) Luque, R. & Varma, R.S. The Royal Society of Chemistry, Cambridge, UK.

Zhang, B., Ji, Y., Wang, Z., Liua, Y., Sun, H., Yang, W. & Wu, P. (2012) Liquid-phase alkylation of benzene with ethylene over postsynthesized MCM-56 analogues. Applied Catalysis A: General 443– 444: 103– 110.

Zhang, X., Dong, J., Hao, Z., Cai, W., & Wang, F. (2018) Fe–Mn/MCM-41: Preparation, characterization, and catalytic activity for methyl orange in the process of heterogeneous Fenton reaction. Transactions of Tianjin University, 24:361–369.

Zhou, H., Ge, M., Zhao, H., Wu, S., Li, M. & Su, Y. (2019) Selective catalytic reduction of nitric oxide with propylene over Fe/Beta catalysts under lean-burn conditions. Catalysts, 9(205): 1-17.

Zhu, W., Wang, J., Wu, D., Li, X. Luo, Y., Han, C., Ma, W., & He, S. (2017b) Investigating the Heavy Metal Adsorption of Mesoporous Silica Materials Prepared by

Microwave Synthesis. Nanoscale Research Letters 12: 323, DOI 10.1186/s11671-017-2070-4.

Zhu, W., Wu, D., Li, X., Yu, J., Zhou, Y., Luo, Y., & Ma, W. (2017a) Synthesis of mesoporous silica materials (MCM-41) using silica fume as the silica source in a binary surfactant system assisted by post-hydrothermal treatment and its Pb^{2+} removal properties. The Canadian Journal of Chemical Engineering, 95: 46-54.

Zhu, Y., Lin, K., Ye, D. & Zhou, W. (2015) A novel Friedel–Crafts alkylation of naphthols without Lewis acid. Tetrahedron Letters 56: 5039–5042.
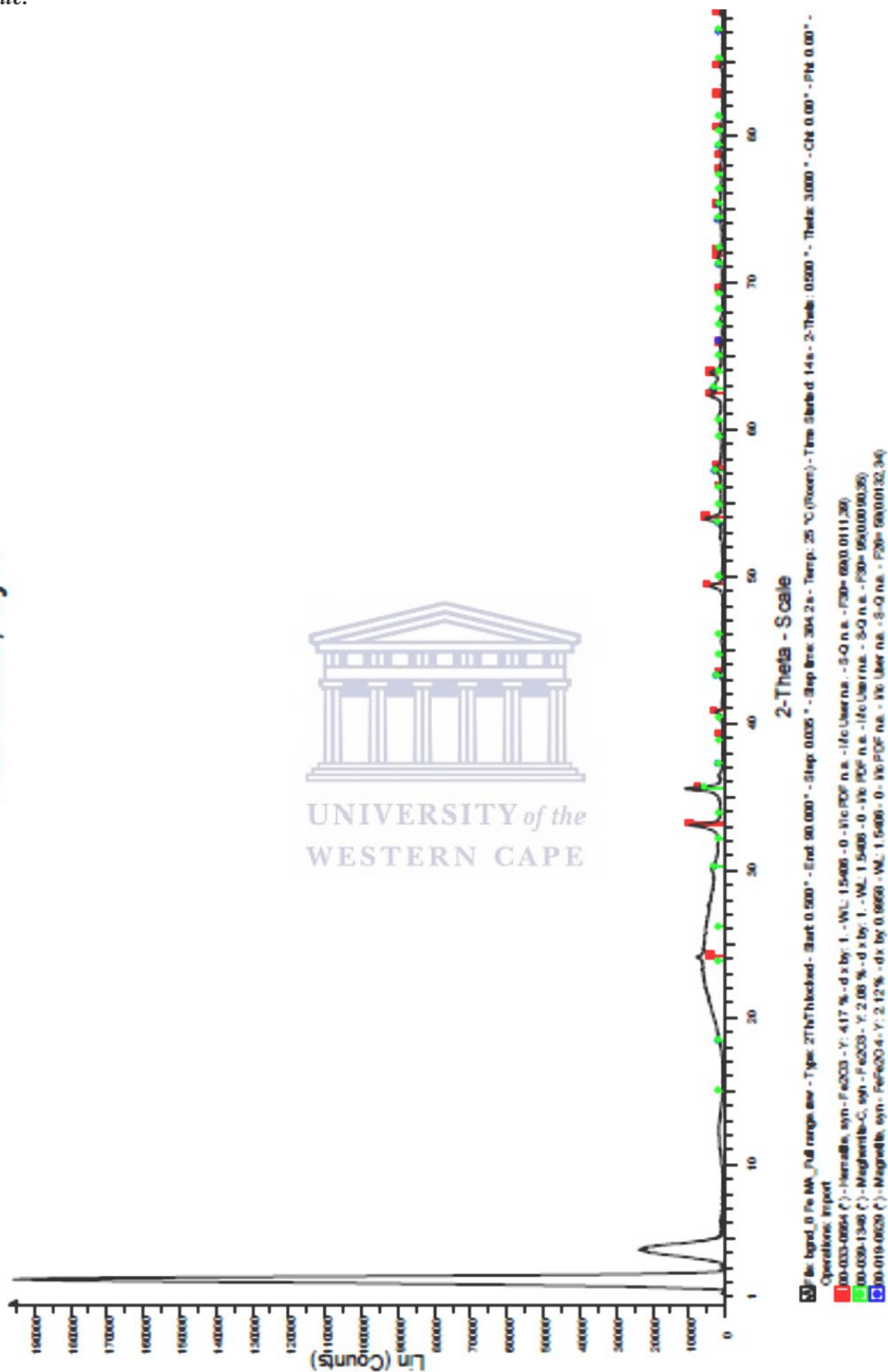
https://etd.uwc.ac.za

APPENDIX A1

https://etd.uwc.ac.za
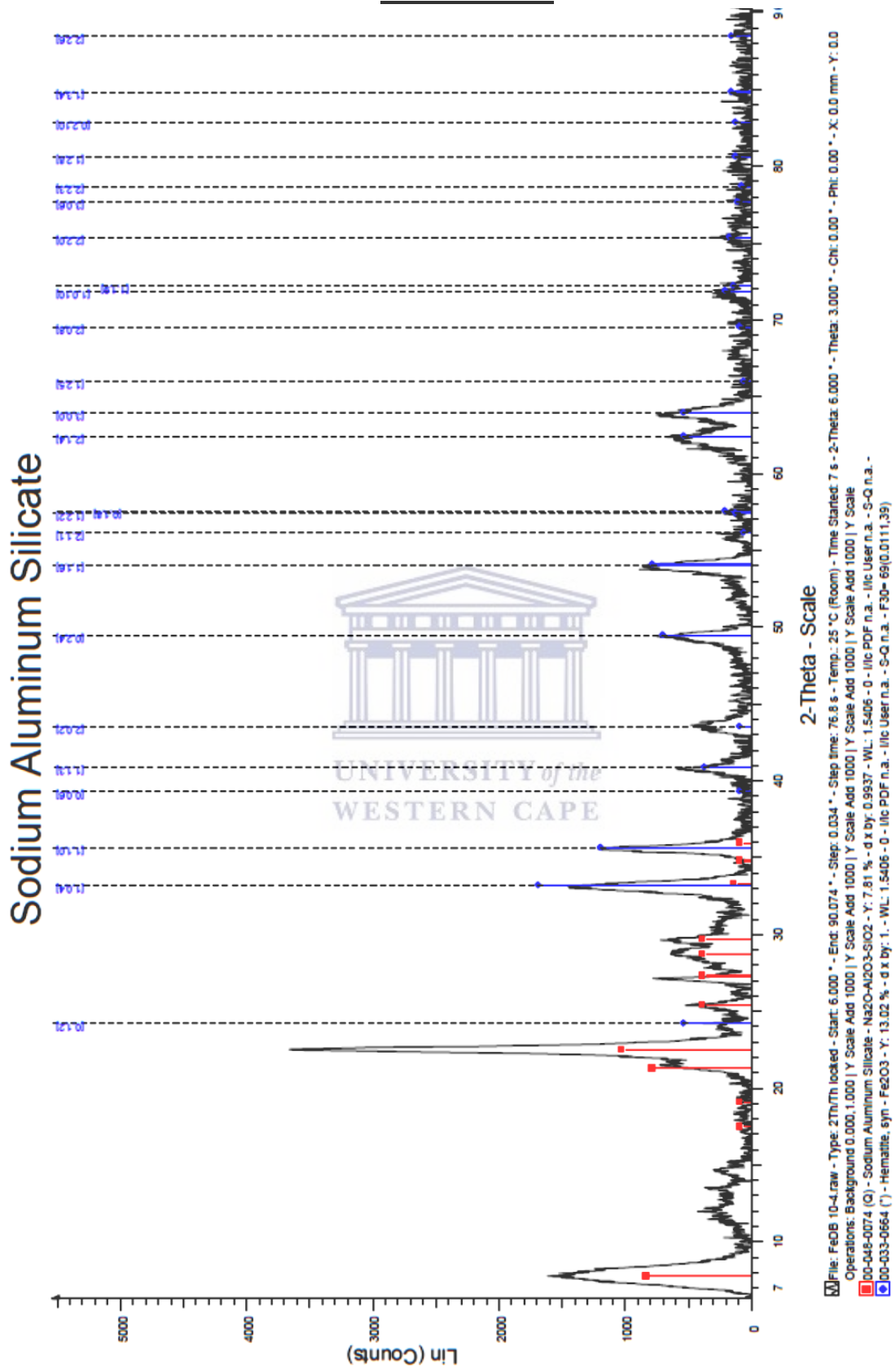
Appendix A1.1: XRD profile of sample 25AHW showing the peaks due to the Fe crystallites on the zeolite.

Appendix A1.2: XRD profile of sample 8% Fe-MCM-41 showing the peaks due to the metal crystallites.

CFA &AMD based, heterogeneous Fe catalysts for the FC alkylation reaction

223

note the catalysts was not tested in this study, only catalysts with Fe wt % loading less than 3.5 % were tested and catalysts with lower metal loading did not show peaks due to the metal crystallites.


CFA &AMD based, heterogeneous Fe catalysts for the FC alkylation reaction   224
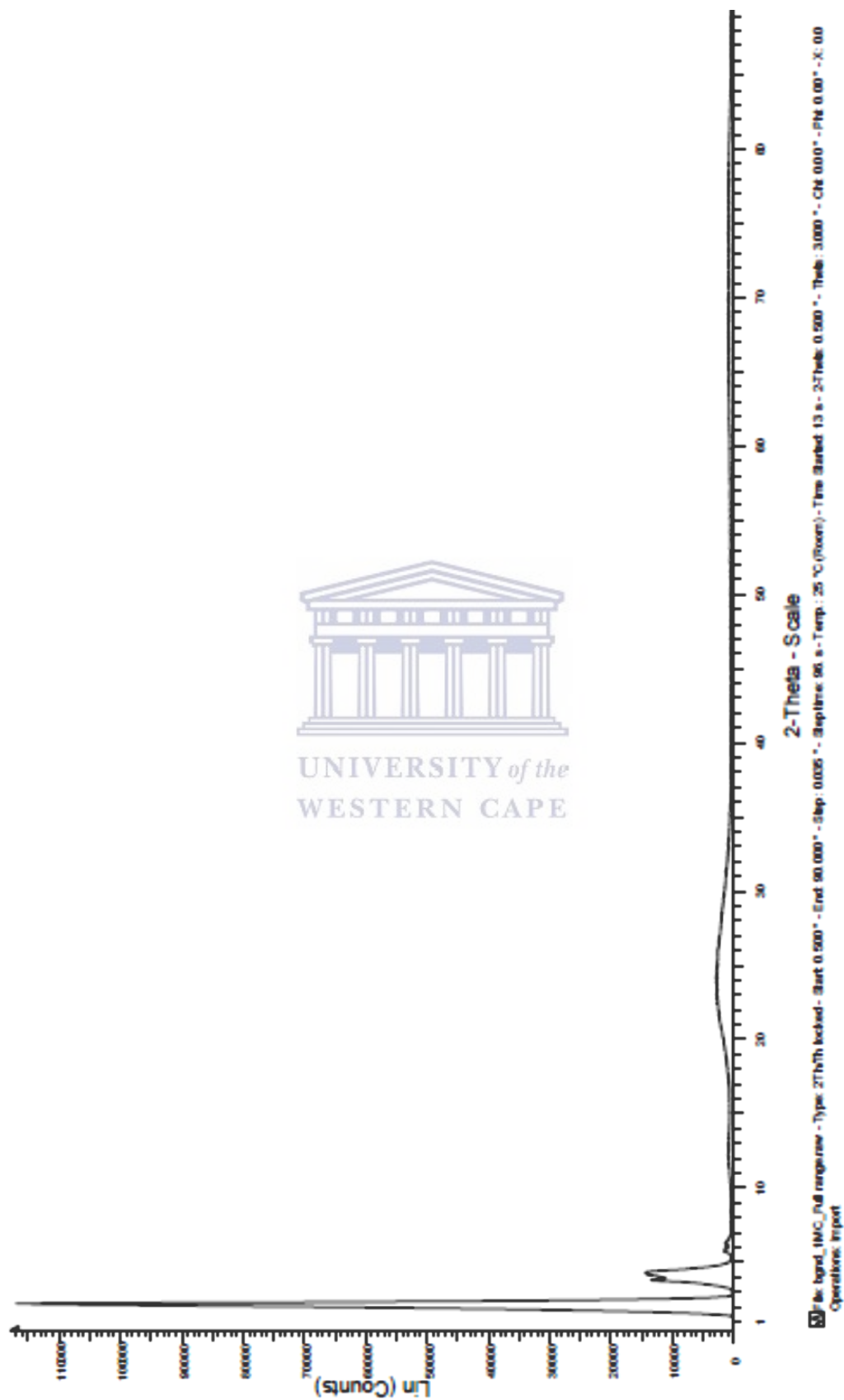
Appendix A1.3: XRD profile of sample 25AMW showing no peaks due to the Fe crystallites on the support material (MCM-41).

APPENDIX A2

Table A2.1: Inductively coupled plasma (ICP) analysis of elements present in the AMD feedstock used as metal solution precursor in the catalysts preparation.

Parameters	Units	AMD sample
pH	n/a	2.14±0.03
Electrical conductivity (EC)	mS/cm	15.4±0.01
Total dissolved solids (TDS)	mg/L	5266±448
Sulphate	mg/L	4959.86 ± 59
Chloride	mg/L	53.53±9
Nitrate	mg/L	ND
Al	mg/L	11.41 ± 3.66
As	mg/L	0.06 ± 0.01
B	mg/L	0
Ba	mg/L	0.03 ± 0.01
Be	mg/L	0.15 ± 0.01
Ca	mg/L	530.04 ± 78.63
Cd	mg/L	0.30 ± 0.05
Co	mg/L	0.35 ± 0.62
Cr	mg/L	0.23 ± 0.07
Cu	mg/L	0.58 ± 0.07
Fe	mg/L	1041.65± 26.46
Hg	mg/L	4.08 ± 1.39
K	mg/L	2.81 ± 0.31
Li	mg/L	0.03 ± 0.08
Mg	mg/L	189.89 ± 10.42
Mn	mg/L	55.45 ± 3.30
Mo	mg/L	0.50 ± 0.07
Na	mg/L	296.73 ± 40.32
Ni	mg/L	668.77 ± 68.95
Pb	mg/L	0.003 ± 0.000068
Se	mg/L	0.43
Si	mg/L	50.52 ± 4.8
Sr	mg/L	1.76 ± 0.18
Th	mg/L	14.33 ± 3.83
Ti	mg/L	0
V	mg/L	0
Y	mg/L	2.89 ± 0.31
Zn	mg/L	17.90 ± 1.81
Zr	mg/L	0.443 ± 0.03

APPENDIX A3
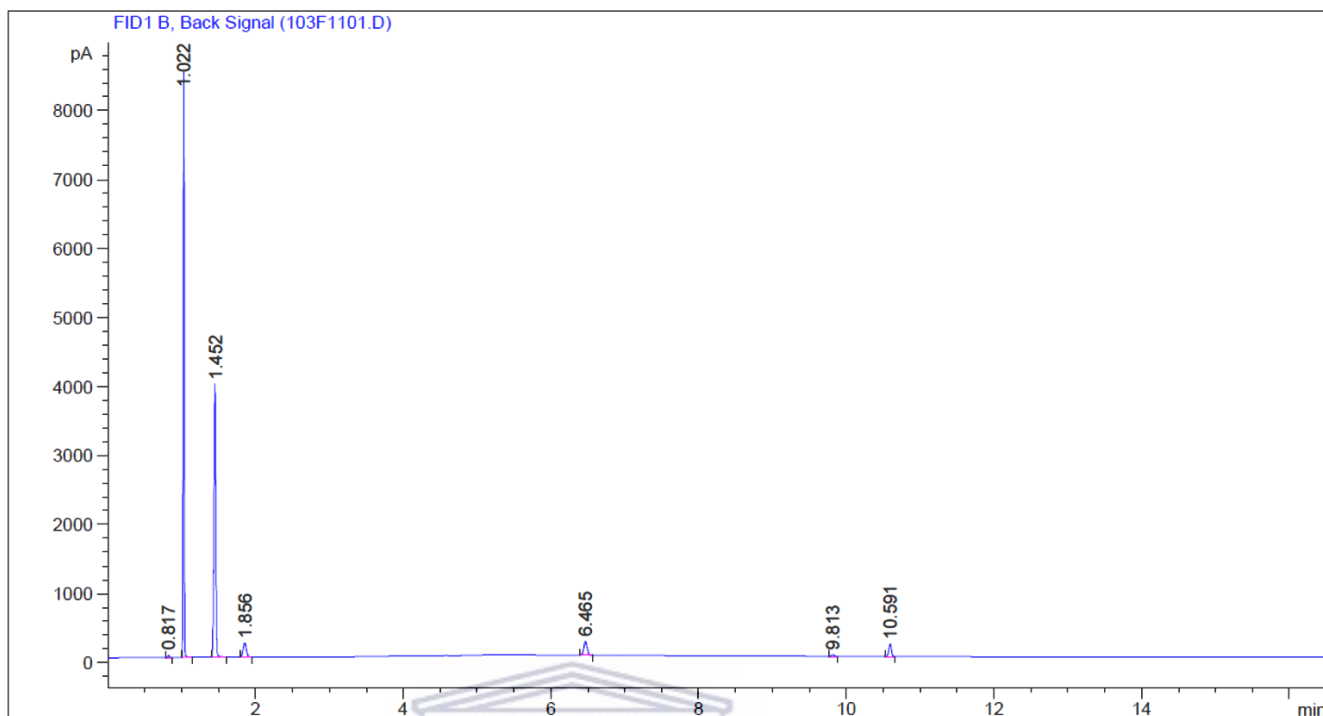
Appendix A3.1: Typical GC chromatogram obtained on the analysis of the Friedel-Crafts alkylation of benzene with t-butyl chloride at 45 0C using a benzene to t-butyl chloride volume ration of 10:1.

Table A3.1: Reactants and products retention times (GC analysis)

sample	sample code	retention time/min
tert butyl chloride	tBC	0.817
acetone	Ac	1.022
benzene	B	1.452
nonane	Non	1.856
tert butyl benzene	tBB	6.465
1,3 di tert butyl benzene	1,3 dtBB	9.813
1,4 di tert butyl benzene	1,4 dtBB	10.591
*tri tert butyl benzene	ttBB	11.463

note the tri tertiary butyl benzene was not detected in the product mixture over the series of catalysts tested.

APPENDIX A4

A 4: Calculation for metal loading via wet impregnation/ion exchange

A typical calculation used to determine the volume of Fe precursor solution added to the support in order to prepare a catalyst of Fe wt % loading of 3.5.

Worked example

The precursor solution was adjusted to 1 000 ppm for both FeAsh and AMD prior to use.

In order to prepare 1 g of catalysts with Fe wt % loading of 3.5, then 0.035 g should be Fe and 0.965 g should be the support.

Since the precursor solution concentration was 1 000 ppm, it follows that there are 1000 g of Fe in 1 000 000 mL of solution.

25 mL of precursor solution was used:

$$\frac{25}{1000000} \: x \: 1000 = 0.025 \: g$$

Thus to determine the solid amount appropriate to prepare 3.5 % Fe on support: 0.025 g is in 25 mL of metal precursor solution.

Again 0.965 g of support goes with 0.035 g of Fe

$$\frac{0.025}{0.035} \: x \: 0.965 = 0.6893 \: g$$

Thus 0.6893 g of support material should be mixed with 0.25 mL of precursor solution to prepare a catalyst with Fe wt % of 3.5.

The other catalysts with lower metal loading were prepared by dilution the precursor solution with lesser volume of the precursor and making the solution volume to 25 mL with deionised water to maintain the same liquid to solid ration in all catalyst preparation.
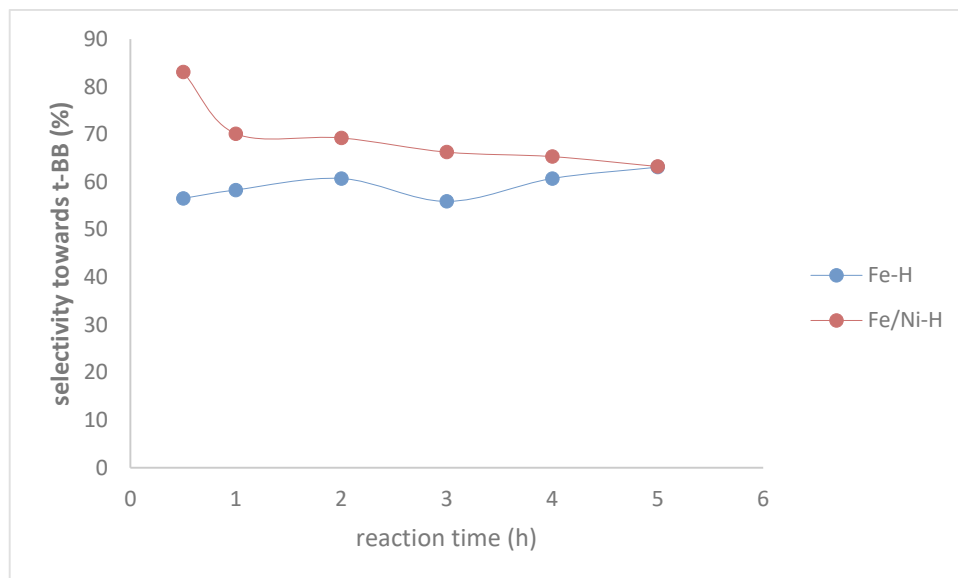
APPENDIX A5

Appendix A5: The effect of Ni doping on the catalytic activity of Fe supported on commercial HBEA.

The effect of Ni doping on the catalytic activity of Fe supported on commercial HBEA catalysts was investigated under the same condition and composition as in (10AHW). The conversion, selectivity and yield are presented in A5.1, A5.2 and A5.3 respectively.
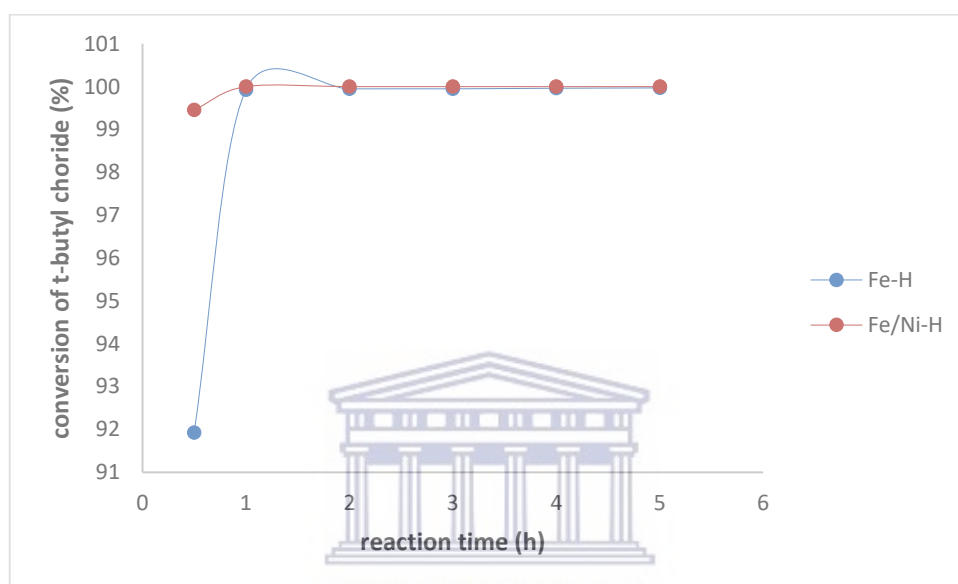
Appendix A5.1: Effect of Ni doping on the conversion of t-butyl chloride at 45 °C and benzene to t-BC ratio of 10:1.

Appendix A5.2: Effect of Ni doping on the selectivity of t-butyl benzene at 45 °C and benzene to t-BC ratio of 10:1.
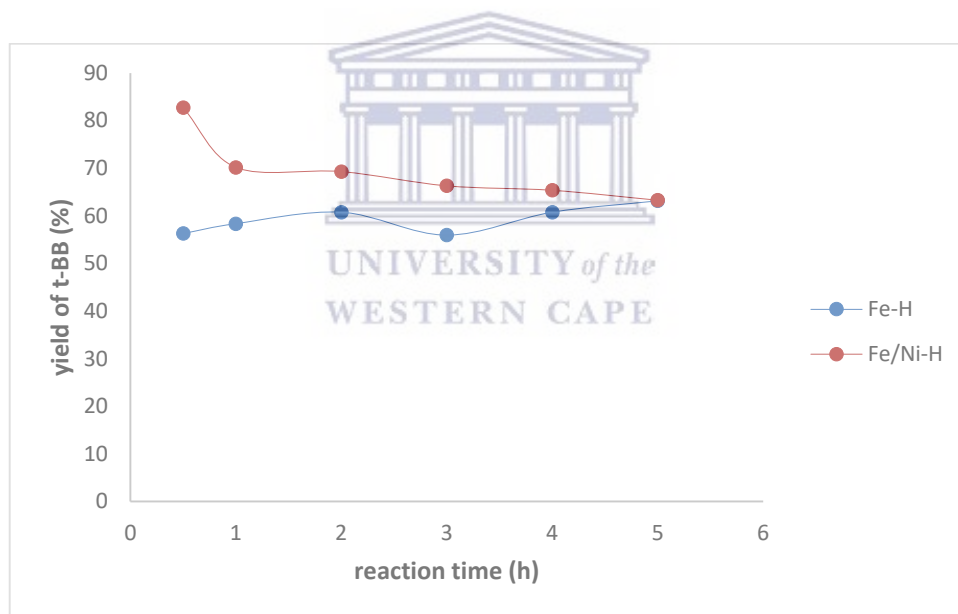
Appendix A5.3: Effect of Ni doping on the yield of t-butyl benzene at 45 °C and benzene to t-BC ratio of 10:1.